GEOCHEMICAL CONSTRAINTS ON THE ORIGIN OF MAFIC AND ULTRAPOTASSIC DYKES FROM THE SOUTHERN MANICOUAGAN AREA, GRENVILLE PROVINCE

CAROLINA VALVERDE CARDENAS

GEOCHEMICAL CONSTRAINTS ON THE ORIGIN OF MAFIC AND ULTRAPOTASSIC DYKES FROM THE SOUTHERN MANICOUAGAN AREA, GRENVILLE PROVINCE

by

Carolina Valverde Cardenas, B.Sc. (Hons)

A thesis submitted to the
School of Graduate Studies
in partial fulfilment of the
requirements for the degree of
Master of Science

Department of Earth Sciences
Memorial University of Newfoundland
2009

St. John's Newfoundland

Abstract

The Grenville Province has a long record of magmatic activity, including arc magmatism related to the pre-Grenvillian evolution of eastern Laurentia and magmatism during the final collision that shaped the orogen. This study focuses on recently identified mafic dykes exposed in the Gagnon Terrane and the Canyon Domain as well as late tectonic, ultrapotassic dykes exposed in the Canyon Domain, in the central part of the Province.

In the **Gagnon Terrane, mafic dykes** inferred to be ~1.74 Ga old, intrude Archean orthogneisses east of a major shear zone. These dykes are foliated and recrystallized under upper amphibolite to granulite facies conditions. These rocks have a geochemical signature of subalkaline tholeiitic basalts to andesites and, some, show primitive Mg#, Cr and Ni contents. Epsilon Nd values (at 1.75 Ga) range from + 1.1 to +2.1, to highly negative (-17.9). The geochemical data and presumed age suggest that the dykes represent mantle-derived melts variably contaminated by crust. The ~1.74 Ga magmatic event in Gagnon Terrane is coeval with late orogenic magmatism in the Makkovik Province and provides a hint for potentially widespread 1.7 Ga magmatism into the Laurentian margin.

In the **Canyon Domain, mafic dykes** intrude a ~1.4 Ga volcanoclastic sequence, inferred to represent remnants of an island arc, in the vicinity of a ~1.2 Ga bimodal sequence inferred to have formed in a back arc setting. These dykes are variably deformed and recrystallized under medium-P granulite facies conditions. These dykes have a geochemical signature of subalkaline tholeiitic basalts to andesites, similar REE patterns and $\varepsilon_{Nd}{}^{1300}$ values from +4.6 to +6.2. However, two groups have been

recognized based on the presence (*Group 2)* or absence *(Group 1*) of pronounced negative Nb anomalies. The dykes of *Group 2* have an arc geochemical signature and may have been emplaced during late stages of the development of the ~1.4 Ga arc. In contrast, the dykes of *Group 1* have a within-plate geochemical signature and may be correlative with the ~1.2 Ga (Elzevirian) bimodal meta-volcanic sequence exposed east of the Canyon Domain. It is therefore suggested that the ~1.2 Ga volcanic sequence developed in proximity to the Canyon Domain and that their juxtaposition is not the result of Grenvillian age tectonic transport.

A swarm of ~0.98 Ga late tectonic, **ultrapotassic dykes** occur in the **central and southern Canyon Domain.** These dykes crosscut the foliation, but have an internal fabric in the north. Farther south they are massive and display rims of granitic pegmatite. The ultrapotassic dykes consist of biotite-quartz-apatite ± K-feldspar ± plagioclase ± clinopyroxene ± orthopyroxene ± amphibole with highly variable proportions. Those lacking internal fabric preserve an igneous texture with large biotite and apatite in interstitial pools dominated by K-feldspar and quartz.

Some ultrapotassic dykes are characterized by primitive Mg#, Cr and Ni contents. They have extremely steep rare earth patterns and high concentrations of Ba (2000-9000 ppm) and Rb (65-260 ppm). However, concentrations of Nb and Ta are depleted relative to the Ba, Rb and La values on primitive mantle normalized plots. Th contents are variable, showing both enrichment and depletion relative to La. The dykes are characterized by low ε_{Nd} (-2.6 to -14.6) and ε_{Sr} (6.4 to 20.86) isotopic signatures (at T=1 Ga). Based on the geochemical data, the most likely source region would be a

metasomatized subcontinental lithospheric mantle. Ultrapotassic dykes emplaced within the age range of 990-970 Ma are also known in the ~1010 Ma Labrieville anorthosite to the south, and the Pinware and Lac Melville Terranes farther east. It is therefore suggested that a late orogenic (Grenvillian) magmatic event, involving a metasomatized subcontinental lithospheric mantle source, took place in the hinterland of the central eastern Grenville Province.

ACKNOWLEDGEMENTS

I would like to express my gratitude to all those who gave me the opportunity to work on this project and for the immense knowledge I have gained:

I am greatly indebted to Dr. Aphrodite Indares for her advice, assistance and encouragement at every stage of this project. For her infinite patience and guidance, I will always be grateful. Thank you to Dr. George Jenner for his advice and cooperation. He contributed special insight and detail to the geochemistry section of this thesis. I would also like to thank the School of Graduate Studies as well as both of my supervisors for their financial support.

Special thanks to Michael Shaffer, Danny Mulrooney and Wanda Aylward for their instruction and help with the mineral analyses using the electron microprobe and Alain Potrel for his training and assistance with the isotopic analyses. Thanks to Sherri Furey, Susan Strowbridge and Stephanie Lasalle for their suggestions and support during the preparation of this thesis. Finally, I would like to thank my family for their support and encouragement.

TABLE OF CONTENTS

LIST OF TABLES

CHAPTER 3

CHAPTER 4

CHAPTER 5

LIST OF FIGURES

CHAPTER 1

CHAPTER 3

CHAPTER 4

CHAPTER 5

CHAPTER 1: INTRODUCTION

1.1 Background and Aim

The Grenville Province records a Mesoproterozoic continental collision orogen that was formed on the Laurentia margin of the North American craton. This region has a long history of magmatic activity from the Archean to the Mesoproterozoic and includes: Archean magmatism linked to early development of the North American craton; several pulses of Proterozoic arc magmatism during the growth of SE Laurentia in an active continental margin setting (Rivers, 1997); and within-plate magmatism during the ~1.19-0.98 Ga final collision, *i.e.* Grenvillian orogeny (Corrigan and Hanmer, 1997). Distinction between different types of magmatism, in specific lithotectonic segments of the Grenville Province, provides first order constraints on their original setting and/or subsequent orogenic evolution. In addition, the presence of syn- to late-orogenic mafic dykes in parts of the province provides evidence for active involvement of the mantle during the development of the orogen.

Despite widespread high-grade metamorphic overprint(s) and deformation, application of igneous geochemistry in meta-igneous rocks combined with mapping and geochronology, has provided key constraints on the distribution and character of magmatic events in several parts of the Grenville Province (*e.g.* Culshaw and Dostal 2002; Blein *et al.*, 2004; Slagstad *et al.*, 2004; La Flèche *et al.*, 2005).

Determining the petrogenesis and tectonic significance of igneous rocks requires information about their composition. Interpretation of the geochemical data presumes that

the concentrations of elements under consideration remained unchanged during metamorphism and deformation. In general, low-field strength elements (Sr, K, Rb and Ba) are considered "mobile"; whereas, high-field strength elements (Y, Zr, Hf, Ti, Nb and P), the rare-earth elements (REE) and some transition metals (Ni, V and Cr) are considered relatively "immobile" (Rollinson, 1993) during weathering, hydrothermal alteration and greenschist to lower amphibolite-facies metamorphism (Pearce and Cann, 1973; Winchester and Floyd, 1976; Pearce and Norry, 1979; Pearce, 1982). In addition, Th, a low-field strength element, can generally be considered to behave in an immobile manner (Jenner, 1996). Successful geochemical studies in the Grenville Province (see above) and elsewhere suggest that relatively immobile trace elements may also provide useful constrains on the origin of higher grade (upper amphibolite and granulite facies) meta-igneous rocks. Thus, techniques involving the relatively immobile trace elements are extensively used in geochemical studies (Bernard-Griffiths *et al.*, 1985; Weber and Hecht, 2003) and are the most relevant for metamorphosed igneous rocks. In addition, certain isotopes (*e.g.* Sm-Nd) can be used as tracers to obtain information about the original source material from which a rock was derived and to provide age constrains (Hall, 1996; Dickin, 2005; O'Nions *et al.*, 1979).

This study focuses on recently discovered mafic and ultrapotassic dykes in the Gagnon Terrane and the Canyon Domain (Berthé Terrane) in the southern part of the Manicouagan reservoir (Central Grenville Province). The aim of this thesis is to determine the geochemical signature of these rocks in order to constrain their petrogenesis and tectonic environment of formation. The study involves detailed

petrography, major and trace element geochemistry as well use of Sm–Nd and Rb-Sr isotopic data.

The next sections discuss the general characteristics of the Grenville Province and study area, to provide background for the rationale of this study.

1.2 General Characteristics of the Grenville Province

The Grenville Province is defined as that part of the Grenville Orogen which is exposed in the southeastern Canadian Shield. It lies southeast of the Grenville Front, which is the limit of perceptible effects of Grenvillian deformation (Ludden and Hynes, 2000). In North America, the Grenville Orogen is known to extend, mainly in the subsurface, southwestward from the Canadian Shield to Texas and Mexico (Davidson, 1998).

The Grenville Province consists of lithologic units that range in age from Archean to Late Mesoproterozoic (Rivers, 1997), most of which were formed during the development of the SE Laurentian margin. Evidence suggests the existence of an active margin, with subduction-accretion and arc formation from the Late Paleoproterozoic to the Late Mesoproterozoic (Rivers, 1997; Gower and Krogh, 2002). The main crustal events recognized so far are the Labradorian (~1.71-1.62 Ga), Pinwarian (~1.50-1.45 Ga) and Elzevirian (~1.25-1.19 Ga) with the ages of major units being in general younger towards the southeast (Rivers, 1997). In addition, remnants of a ~1.45 Ga island arc (Montauban arc) and 1.40-1.32 Ga continental margin arc plutonics (La Bostonnais complex) are recognized in the central Grenville Province (Nadeau and van Breemen, 1994; Corrigan and van Breemen, 1997).

The Labradorian event in the NE Grenville Province is characterized by the formation of a magmatic arc, presumably over a south-dipping subduction zone and subsequent accretion, and closure of a back-arc basin (Rivers, 1997). During the Pinwarian event, it is inferred that subduction occurred under Laurentia and resulted in arc magmatism, compressional tectonics and high-grade regional metamorphism. The development of back-arc basins (mainly recognized in the SW part of the province) during the Elzevirian event is indicative of major extension. Their subsequent closure was followed by continent-continent collision and initiation of within plate plutonism during the Grenville orogeny (~1.19 and 0.98 Ga; Rivers, 1997).

The Grenville Province has been subdivided into belts, the configuration of which was achieved during the Grenvillian orogeny (Fig. 1-1). These belts are: a) a northwestern Parautochthonous belt tectonically under, to the southeast; b) a high-pressure belt; and c) an Allochthonous belt or hinterland (Rivers *et al.*, 1989; Ludden and Hynes, 2000). Units of the Parautochthonous belt can be lithologically correlated to the foreland and are characterized by Barrovian metamorphic signatures that were acquired during the final stages of the Grenvillian orogeny. The hinterland contains units that cannot be traced into the foreland, but which have Laurentian affinity (Rivers *et al.*, 1989). A large part of the hinterland is characterized by mid-P granulite facies metamorphic signatures acquired during the culmination of the Grenville orogeny, abundant Mesoproterozoic age anorthosites, and late Grenvillian magmatic activity (Interior Magmatic belt, Fig 1-1; Gower *et al.*, 1991). However there are also units that did not experience any perceptible Grenvillian metamorphism (Orogenic Lid, Fig 1-1; Rivers, 2008). Finally, the high-

pressure belt is characterized by eclogite and/or high-pressure granulite-facies Grenvillian metamorphism (Rivers *et al.*, 2002). The Parautochthonous and the high-pressure belts are interpreted to represent the orogenic front, whereas the hinterland likely represents the remnants of an eroded orogenic plateau (Rivers, 2008).

In addition, lateral variations are also documented across the hinterland. For instance, major features such as the Orogenic Lid and the Interior Magmatic belt do not occur along the full length of the province and the high-pressure belt is discontinuous. In that respect it is convenient to divide the Grenvillian hinterland into western, central and eastern segments, separated by NS-trending belts of Grenvillian-age anorthosites (Fig. 1-1; Dunning and Indares, pers. comm. 2008). For instance, the CRUML anorthosite belt (Dymek *et al.,* 2006), which separates the western from the central segment, marks the western boundary of the Interior Magmatic belt (Fig. 1-1).

The shoreline of the Manicouagan reservoir in the central Grenville Province provides excellent exposures of units belonging to the three major belts (*e.g.* Indares *et al.,* 2000; Indares and Dunning, 2004; Jordan *et al.,* 2006; Eaton *et al.,* 1995; Hynes *et al.,* 2000). The present study focuses on dykes observed in units of the Parautochtonous belt and the hinterland. These are exposed along the southern shore of the Manicouagan reservoir, and were identified only recently (Valverde, 2005; Dunning and Indares pers. comm. 2008). The following section presents: (a) an overview of mainly published information on Parautochthonous, high-P and hinterland units from the Manicouagan reservoir area (section 1.3); and (b) the regional geology of the recently identified units relevant to this study (section 1.4).

1.3 General geology of the Manicouagan Reservoir Area

The Grenville Province in the Manicouagan reservoir area consists of several complex lithotectonic packages (Fig. 1-2). From the presently lower structural levels towards higher levels, these packages are: the Parautochthonous Gagnon Terrane; the Manicouagan Imbricate Zone, which represents the high-pressure belt in this area; and the Hart Jaune and Berthé terranes, which are part of the hinterland (Indares and Dunning, 2004).

The structurally lowest **Gagnon Terrane** has been mainly studied northeast of the Manicouagan reservoir area in Labrador (Rivers *et al.*, 1993). It consists of the Knob Lake Group, a Paleoproterozoic sequence of supracrustal rocks including metapelite, semipelite, marble, quartzite, and iron formation, and its reworked Archean basement. In the Labrador area, the Gagnon Terrane was reworked at 1.0Ga into a fold-thrust and nappe belt, with metamorphic grade increasing southwards from greenschist to upper amphibolite and locally eclogite facies (River *et al.*, 1993, Indares and Rivers, 1995). The Gagnon Terrane has also been investigated along the western shore of the Manicouagan reservoir. In that area it is divided into two distinctive domains by a north-south trending subvertical shear zone (Southwestern Shear Zone, SWSZ; Fig. 1-2). West of the SWSZ anatectic metapelites in the paragneiss contain kyanite (Jordan *et al.*, 2006). The domain east of the SWSZ is characterized by sillimanite-bearing anatectic metapelites and by the presence of ultramafic rocks (Valverde, 2005; Valverde *et al.*, in prep.), metagabbro and mafic and granitic dykes that have not been observed elsewhere in the Gagnon Terrane. This domain will be further discussed in the next section.

The Manicouagan Imbricate Zone is a 1500 km^2 lobate assembly of imbricated Mesoproterozoic units with a distinctive high P-T (800-900°C and 1400-1800 MPa, metamorphic overprint acquired between ~1.05 and 1.03 Ga (Indares *et al.*, 2000). Its structurally lower component, the **Lelukuau Terrane**, consists mainly of an imbricated Labradorian (~1.65 Ga) anorthosite-mangerite-charnockite-granite (AMCG) suite. Structurally above is the **Tshenukutish Terrane**, which includes Pinwarian age crust (Baie du Nord segment), slivers of Labradorian AMCG rocks (Lac Espadon Segment), the 1.17 Ga Brien anorthosite and the 1.02 Ga Hart Jaune granite (Boundary Zone) (Indares *et al.*, 1998; Indares *et al.*, 2000). In addition, a strongly banded unit with plagioclase-rich components dated at ~1.21 Ga ("Baie du Nord anorthosite"; Indares *et al.*, 1998) is discontinuously exposed along the southern rim of the Baie du Nord segment, and was recently reinterpreted as of volcanic origin (Dunning and Indares, pers. comm. 2008). Finally, late-tectonic gabbro dykes with the geochemical signature of within plate basalts and with high-P granulite mineralogy occur in high strain zones of the upper Lelukuau Terrane (Termines dykes, Indares *et al.*, 2000).

To the southeast, the Manicouagan Imbricate Zone is structurally overlain by two hinterland units: the **Berthé and the Hart Jaune terranes**. The northern part of the Berthé Terrane, the **Gabriel Domain** (Hynes *et al.*, 2000), consists of migmatized tonalitic gneiss with sporadic rafts of anatectic metapelites (**Gabriel Complex**; Indares and Dunning, 2004) overlain to the south by ~1.2 Ga massive layers of granitic composition with concordant mafic sheets (**Banded Complex**; Indares and Dunning, 2004). The Banded Complex has been recently inferred to represent a bimodal sequence

of volcanic origin. This sequence, together with the similar age potentially metavolcanic rocks in the southern Baie du Nord segment, discussed earlier, provide for the first time evidence for Elzevirian-age magmatism, probably in an intra-continental setting, in the central Grenville Province (Dunning and Indares, pers. comm. 2008). Rocks of the Gabriel Complex were metamorphosed at high-T and mid-P granulite facies conditions (800-900°C, 1000-1100 MPa at ~ 1.04-1.05 Ga). In contrast, rocks of the Banded Complex display evidence for lower-P granulite-facies metamorphism (~ 800°C, 800MPa, Indares and Dunning, 2004). West of the Banded Complex, the Berthé Terrane is represented by the Canyon Domain (Hynes *et al.,* 2000), which mainly consists of supracrustal rocks. This domain will be discussed in the next section.

The structurally highest Hart Jaune Terrane is dominated by Mesoproterozoic mafic granulites and anorthosite bodies (Gobeil, 1997a, b; Hynes *et al.*, 2000). There is an earlier two-pyroxene (low-P) granulite-facies event dated at 1.47 Ga (Pinwarian event). Except for local development of garnet near the boundaries of the terrane that has been attributed to a 0.99Ga metamorphic event (Hynes *et al.*, 2000), Grenvillian age metamorphic signatures and deformation are lacking (Indares and Dunning, 2004).

Based on the metamorphic conditions for each lithotectonic unit it can be established that: the Manicouagan Imbricate zone and the Gabriel Domain of the Berthé Terrane represent deep and intermediate Grenvillian crustal levels, respectively, both of which underwent high-T metamorphism during the culmination of the Grenvillian orogeny. In contrast, the Hart Jaune Terrane represents the highest crustal levels, which

remained relatively cold throughout the Grenvillian orogeny (Indares and Dunning, 2004) and is included in the Orogenic Lid (Rivers, 2008).

High metamorphic temperatures as well as the presence of the late-tectonic mafic dykes in parts of the Manicouagan Imbricate zone suggest that extrusion was possibly triggered by collapse of the thickened crust following replacement of lithospheric mantle by asthenospheric material (Indares *et al.*, 1998; Indares and Dunning, 2004).

1.4 Local Geology

1.4.1 Gagnon Terrane east of the SWSZ and the Island Domain

In this area, the Gagnon Terrane (Fig. 1-3) consists of: variably granitized tonalitic gneiss interlayered with amphibolite, locally grading to metagabbro, and ultramafic rocks mainly occurring as layered bodies; tectonic slivers of supracrustal rocks including metapelite, quartzite and iron formation; and structurally late mafic and granitic dykes intruding tonalitic and granitic gneiss. The metagabbro is thoroughly amphibolitized and the metapelite is anatectic and contains sillimanite, suggesting mid-P upper amphibolite to granulite facies metamorphism. West of the SWSZ, metapelitic rocks contain kyanite (high-P) instead of silliminate (medium-P) and ultramafic rocks, as well as recognizable metagabbro, and late mafic and granitic dykes are absent (Valverde, 2005; Valverde *et al.*, in prep.).

The ultramafic rocks display geochemical signatures of primitive mantle and are interpreted to be Archean in age (Valverde, 2005; Valverde *et al.*, in prep.). Similar rocks occur in Archean greenstone belts that extend into the Parautochthonous belt farther to

the west (Chibougamau area, Rivers and Chown, 1986; Val d'Or area, La Flèche *et al.*, 2005), but have not been observed elsewhere in Gagnon Terrane. Therefore, the Gagnon Terrane in this area is interpreted to represent the extension of an Archean greenstone belt in the Grenville Province.

The area is affected by multiphase deformation that resulted in the development of prominent tectonic layering and, in most cases, obliteration of original igneous relationships. The latest deformation episode is expressed by deca- to hecto-metric scale upright folding with north-south trending axial planes and fold axes gently plunging to the south. Both the mafic and granitic dykes however are less deformed than their country rock and cut its foliation at variable angle, it is therefore inferred that they postdate part of the deformation.

The crystallization age of one granitic dyke located in the Gagnon Terrane has been constrained at 1741+/-32 Ma (U-Pb zircon, sample 04-289, Fig. 1-3; Indares and Dunning, pers. comm. 2008). Because granitic and mafic dykes in Gagnon Terrane east of SWSZ have similar field relations, it is suggested that they may also have broadly similar ages.

The age of the granitic dyke is coeval with monazite ages in anatectic metapelites from Gagnon Terrane west of the SWSZ (Jordan *et al.*, 2006) and with plutonic rocks found further to the southwest in Georgian Bay – Killarney area (Davidson *et al.*, 1992; Corrigan *et al.*, 1994), implying that a ~1.7 Ga thermal event was important in southern Gagnon Terrane, and, potentially on the southeastern margin of Laurentia at that time. Indeed, this thermal event in the Gagnon Terrane is coeval with late orogenic magmatism

(1.74-1.70 Ga) in the Makkovik Province (Culshaw *et al.*, 2000; Ketchum *et al.*, 2002), which was developed on the continental margin of the Nain Craton, father to the NE, and truncated at the Grenville Front (Fig. 1-1). This magmatic event is characterized by the emplacement of A-type plutons and linked with possible crust–mantle detachment and incursion of mafic magmas into the crust.

The Gagnon Terrane is tectonically overlain to the east by the **Island Domain** along a km-scale annealed shear zone (Fig. 1-3). This domain consists of variably recrystallized megacrystic granitoids and a gabbro-anorthosite complex with a minor ultramafic component. A metagabbro from the igneous complex was dated at 1694 +52/-45 Ma (U-Pb zircon; sample 04-277; Dunning and Indares, pers. comm. 2008). Near the boundary with the Gagnon Terrane these rocks grade into banded gneisses. The occurrence of metamorphic plagioclase-orthopyroxene-clinopyroxene-garnet ± quartz assemblages in the metagabbro and gneiss units implies that the Island Domain experienced medium-P granulite-facies metamorphism.

In addition, a tectonic klippe of megacrystic granitoids (Fig. 1-3), locally rimmed by ultramafic rocks and intruded by granite dykes has been identified on top of the Gagnon Terrane and has been considered as part of the Island Domain (Valverde, 2005; Valverde *et al.*, in prep.). Ultramafic rocks of the Island Domain (including those of the tectonic klippe) have arc-geochemical signatures (Valverde *et al.,* in prep.). Because these ultramafic rocks are an integral part of the igneous complex in which they occur, the Island Domain is inferred to represent a remnant of an early Labradorian arc system (Valverde *et al.,* in prep.). In the central-eastern Grenville Province, the 1.71-1.60 Ga

Labradorian event is characterized by early (1.68-1.65 Ga) arc related calc-alkaline magmatism and late (1.65-1.62 Ga) emplacement of AMGC suites (Gower and Krogh, 2002).

Ultramafic rocks of the klippe are also intruded by granitic dykes, one of which yielded a crystallization age of 1747 +7/-5 Ma (U-Pb zircon, sample 04-251, Fig 1-3; Dunning and Indares, pers. Comm. 2008), similar to that of the granitic dyke (and presumably the mafic dykes) in the Gagnon Terrane. It is therefore suggested that the units of the klippe may be older than the rest of the Island Domain and that the klippe and the Gagnon Terrane were linked during the ~1.7 Ga event.

1.4.2 Canyon Domain (Southern Berthé Terrane)

This domain was originally defined, together with the Gabriel Domain as part of the so-called Berthé Terrane (Hynes *et al.,* 2000; Fig 1-3). It tectonically overlays the Island Domain to the NW and is separated from the Gabriel Domain to the NE by an ill-defined high strain zone (Berthé shear zone; Fig. 1-3). The **Canyon Domain (CD)** mainly consists of a supracrustal package dominated by a banded quartzo-feldspathic unit and a layered mafic to intermediate unit.

The banded quartzo-feldspathic unit consists of massive layers showing variations in the proportion of quartz versus K-feldspar and plagioclase, with local intercalations of mafic layers and sillimanite-bearing anatectic metapelite. This unit has been interpreted as a partially silicified felsic volcanoclastic sequence (Dunning and Indares, pers. comm. 2008).

The mafic to intermediate sequence consists of mafic layers and pods alternating with (or included in) layers of intermediate compositions. The mafic layers contain the granoblastic assemblage plagioclase + hornblende + garnet ± orthopyroxene ± clinopyroxene ± quartz as well as sweats of garnet + orthopyroxene-bearing leucosome. This sequence has been interpreted as volcanic (or hypabyssal) in origin. The mafic component occurs sporadically as layers or tectonic lenses, in the banded quartzo-feldspathic unit, in which case it probably represents either flows or sills (Dunning and Indares, pers. comm. 2008). In addition: (a) mafic migmatite, rusty aluminous gneiss, quartzite and calcsilicate rocks occur locally and are interpreted to be parts of the same package; and (b) augen granitoid gneiss with rafts of supracrustal rocks were observed mainly in the northern and southern parts of the domain. Finally, abundant late-tectonic ultrapotassic and granite pegmatite dykes are exposed on the central-southern part of the domain; whereas, mafic dykes are less common and were mainly observed farther north (Fig. 1-3).

Diagnostic mineral assemblages identified in anatectic metapelites and mafic rocks indicate mid-*P* granulite facies metamorphism. The foliation in the Canyon Domain consistently dips moderately to the SE in the northern part of the domain, parallel to the contact with the Island Domain, towards the east in the central part of the domain and to the SW in the southern part of the domain defining a large scale, inclined south plunging fold (Fig. 1-3; Dunning and Indares, pers. comm. 2008).

Available U-Pb dates constrain the age of: (a) deposition of (at least part of) the supracrustal package at 1418 +31/-23 Ma; (b) the intrusion of an augen granitoid in the

northern part of Canyon Domain at 1403 +32/-25 Ma; (c) the age of granulite facies metamorphism at ~1080-1040 Ma; and (d) the intrusion of one ultrapotassic and one granite pegmatite dyke at 980+/- 3 Ma and 995 +/-3.5 Ma, respectively (Dunning and Indares, pers. comm. 2008).

In terms of lithology and age, the supracrustal sequence of the Canyon Domain is correlative with the ~1.44 Ga Montauban Group (Nadeau and Van Breemen 1994; Corrigan and Van Breemen 1997), which is exposed ~ 450 km to the SE (Fig. 1-1), and is inferred to have formed in an island arc setting. In addition, late Grenvillian ultrapotassic dykes have also been identified in the Interior Magmatic belt of the eastern Grenville Province; in the Labrieville anorthosite to the SE (Owens and Tomascak, 2002), and in the Pinware Terrane, farther east (Gower and Krogh, 2002).

1.5 Rationale for the thesis and structure

This study aims to constrain the nature of dyke forming magmatic events in the Gagnon Terrane and the Canyon Domain of the Manicouagan reservoir area by investigating two types of dykes: (a) undated mafic dykes from both lithotectonic units, which are deformed and metamorphosed, and therefore likely predate the Grenvillian orogeny, and (b) late-Grenvillian ultrapotassic dykes from the Canyon Domain.

The mafic dykes from the Gagnon Terrane intrude the SE rim of exposed Archean rocks in the Manicouagan reservoir area and may preserve record of early Meso-Proterozoic stages of the development of the Laurentian margin. The mafic dykes from the Canyon Domain intrude ~1.4 Ga volcanoclastic rocks presumably formed in an island

arc setting. However the Canyon Domain is bounded to the east by ~1.2 Ga units (*e.g.* Banded Complex) inferred to have formed in a back-arc setting. Therefore, depending on their geochemical character, these dykes may provide constraints on either the ~1.4 Ga evolution of the Canyon Domain, or on its relationship with the 1.2 Ga back-arc units.

In contrast, the ultrapotassic dykes from the Canyon Domain document magmatic activity during the late stages of the Grenvillian orogeny. Thus they may provide some insight on the nature of magma sources during late stages of orogenic evolution.

The thesis is organized as follows: Chapter 2 presents the approach followed for the geochemical study of the dykes and analytical techniques. Then, the mafic dykes from the Gagnon Terrane, those from the Canyon Domain, and the ultrapotassic dykes from the Canyon Domain are discussed separately in Chapters 3 to 5. Finally, Chapter 6 provides a summary and the general conclusions.

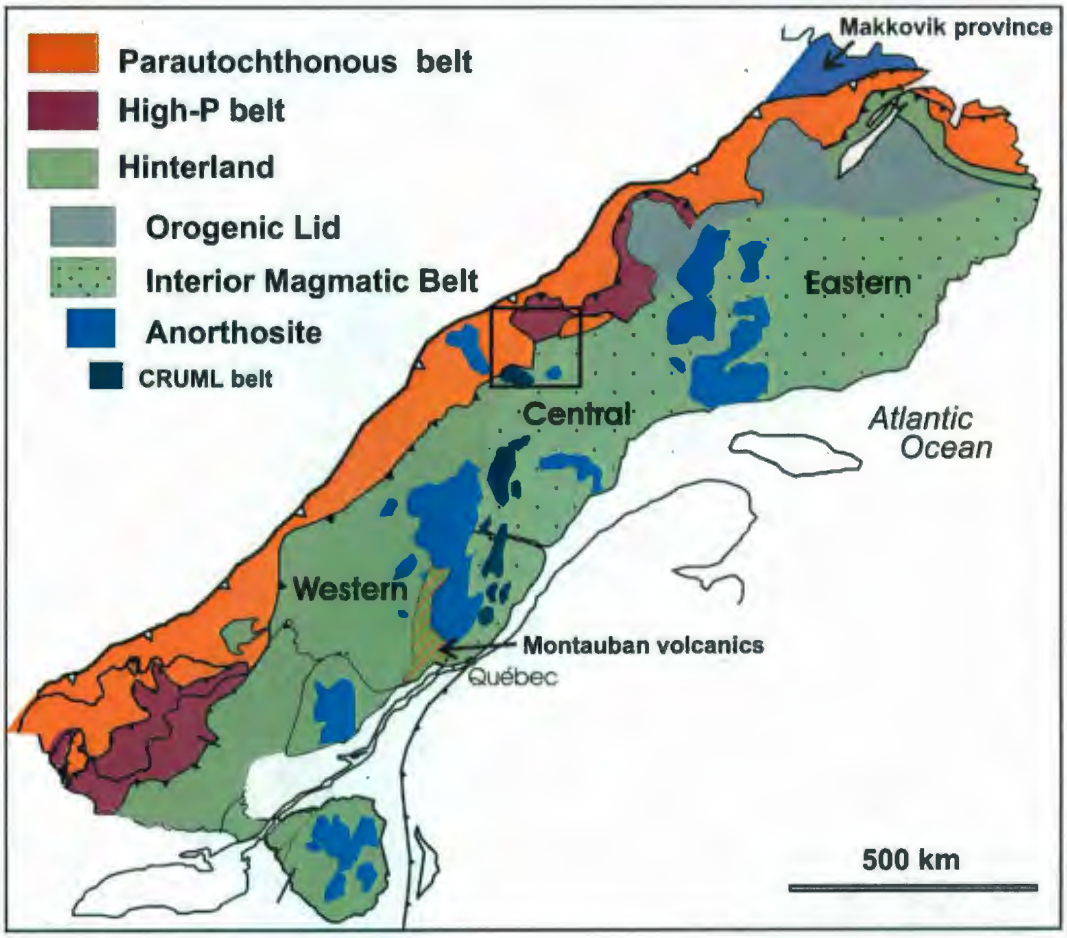

Figure 1-1: General framework of the Grenville Province showing its main divisions and the distribution of Grenvillian age anorthosites. Box shows the Manicouagan Reservoir area (location of Figure 1-2).

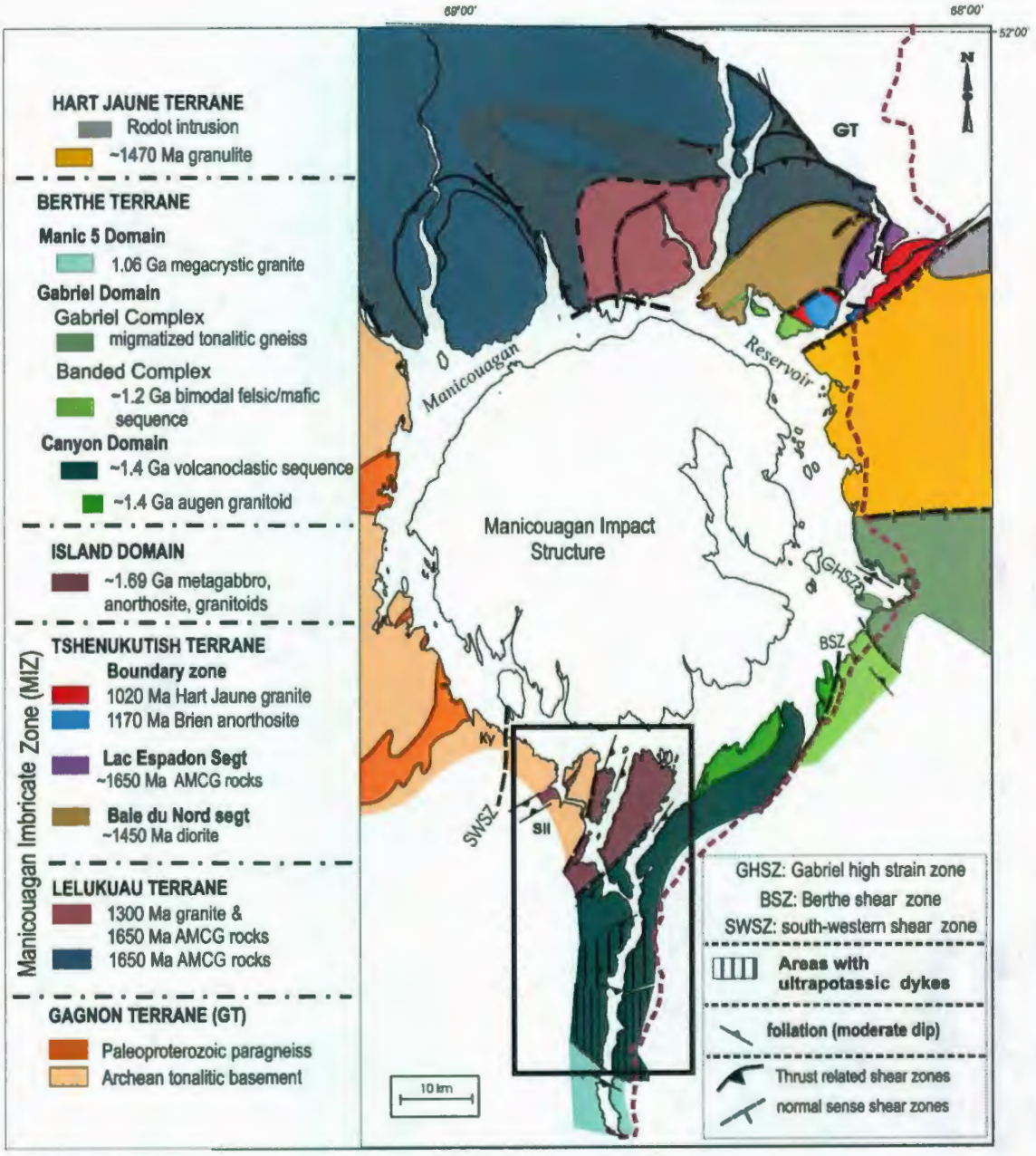

Figure 1-2: General framework of the Manicouagan reservoir area. Box shows the study area (location of Figure 1-3).

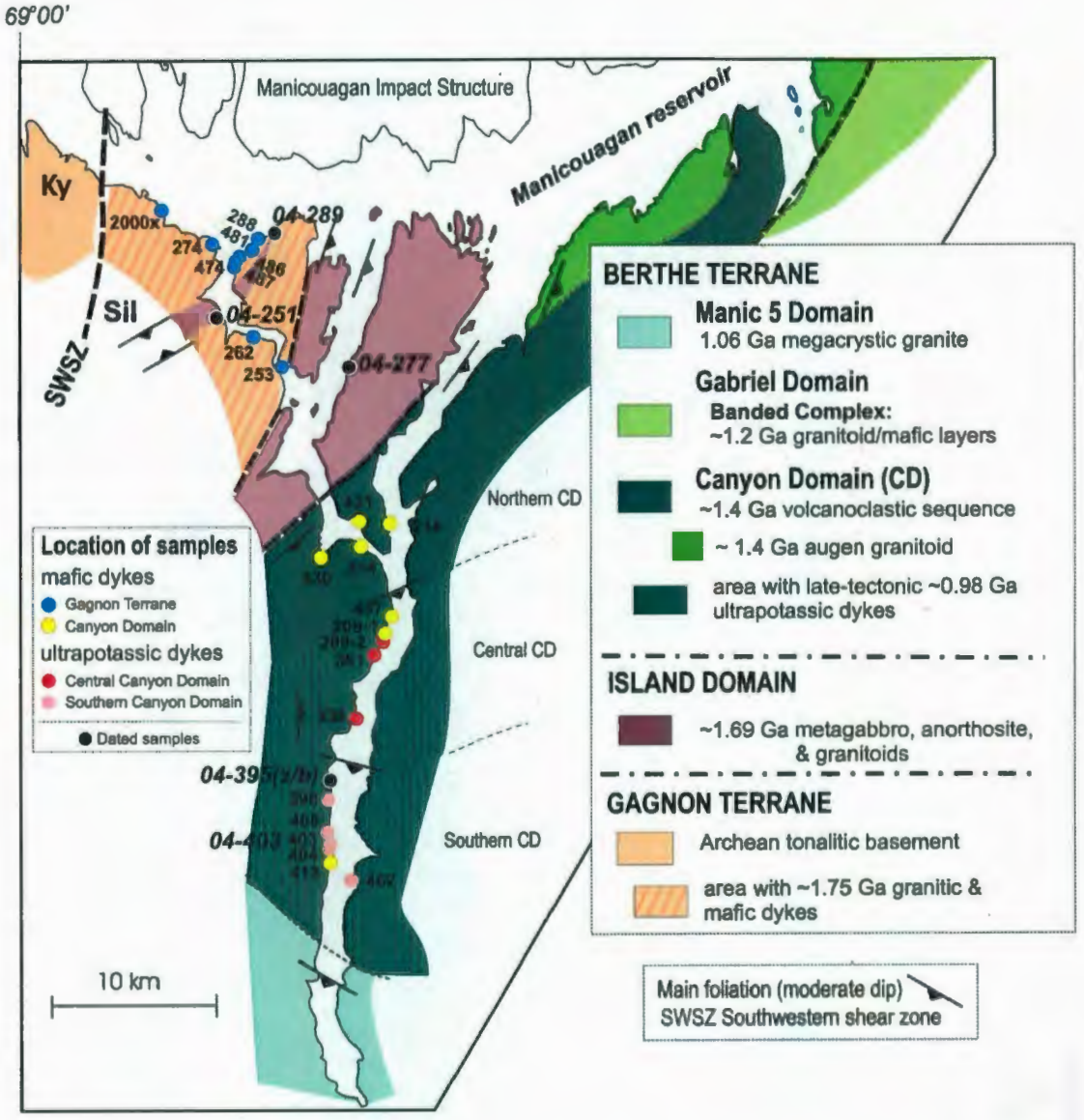

Figure 1-3: Geological map of the south shore of the Manicouagan reservoir showing location of samples in this study, and of dated samples after Dunning and Indares (pers. comm. 2008). Dated samples include: two granite dykes from the Gagnon Terrane (04-289) and klippe (Island Domain; 04-251); a metagabbro from the igneous complex of the Island Domain (04-277); an ultrapotassic dyke (04-403) and a felsic pegmatite (04-395b) from the Canyon Domain; and a component of the layered mafic to intermediate unit of the Canyon Domain (04 395z).

CHAPTER 2: APPROACH AND ANALYTICAL TECHNIQUES

2.1 General Approach

Samples of 12 mafic dykes from the Gagnon Terrane, and 8 mafic and 9 ultrapotassic dykes from the Canyon Domain were the subject of this study. The samples were collected in 2003 and 2004 by A. Indares. The approach used was:

(a) a detailed petrographic examination was undertaken to characterize these rocks in terms of texture, mineralogy and mineral chemistry. This was done by means of: (i) detailed description and interpretation of mineral assemblages and textures in thin-section using an optical microscope as well as textural maps of thin sections obtained by a scanning electron microscope (SEM); and (ii) chemical analysis of major minerals by an electron microprobe. The results of the petrographic examination were used to determine whether (and if so, to what extent) igneous textures and minerals are preserved, and to evaluate the degree of metamorphic recrystallization.

(b) the samples were characterized geochemically to identify patterns or signatures that can be linked to tectonic environment and/or petrogenetic processes and to constrain the nature of the (mantle) source (s). This was achieved by means of: (i) whole rock geochemical analysis to determine the major, trace and rare-earth element compositions of the rocks, and (ii) Sm-Nd

and, in some cases, Rb-Sr isotopic analysis to determine the isotopic signatures of the (mantle) source (s) and possibly to provide age constraints.

2.2 Major and Trace Element Geochemistry

Geochemical classification of the elements can be based on a number of different criteria, including concentration (*e.g.*, majors > 1 wt. % oxide), field strength (ionic radius/ionic charge) or mobility during alteration (immobile versus mobile) (Jenner, 1996). Here, we subdivide the trace elements (<0.1 wt. % oxide) into groups based on field strength: low-field-strength elements (LFSE: Rb, Sr, Ba, U, Th); high-field-strength elements (HFSE: Nb, Ta, Y, Zr, Hf, Ti); rare earth elements (REE: La□Lu) and transition elements (TE: Cr, Ni, Sc, V). The REE may be further subdivided into light and heavy groups (LREE – La, Ce, Pr, Nd, Sm; and HREE – Gd, Dy, Er, Yb, Lu, respectively).

The LFSE are considered "mobile" during metamorphism and alteration and may be ambiguous in terms of identifying the original igneous geochemical signature of the rocks. The HFSE; Th, a LFSE; the rare earth elements (REE) and some transition metals (Ni, V and Cr) are generally "immobile" during weathering, hydrothermal alteration and low-grade metamorphism (Rollinson, 1993; Pearce and Cann, 1973; Winchester and Floyd, 1976; Pearce and Norry, 1979; Pearce, 1982) and therefore form the basis for most of our interpretations.

The dykes were grouped on the basis of common geochemical characteristics, including:

(a) The presence or absence of negative Nb anomalies. These anomalies are defined by the primitive mantle normalized abundance of Nb, relative to Th and La on extended REE plots. The negative Nb anomaly is a characteristic signature from island arc volcanic rocks (Hofmann, 1988; Condie, 1986) and calc-alkaline rocks from other destructive plate margins, such as continental margins (Pearce, 1983; Thompson *et al.,* 1984). Thus, it is considered a major geochemical signature, which is generally used to discriminate arc from non-arc related rocks. However, it should be noted that mafic volcanic rocks and their differentiates, erupted through continental crust in non-destructive margin settings, may acquire a similar signature by assimilation or bulk contamination by continental crust;

(b) Similar rare-earth element ratios. As the REE are approximately equally incompatible during fractional crystallization, the slope on a REE diagram (as represented by normalized REE ratios such as $(La/Yb)_N$ should remain relatively constant. The total REE should increase until the latest stages of fractionation, and suites derived from the same source and related by fractionation, should yield parallel profiles (see Rollinson, 1993). Variations in the REE patterns can, therefore, indicate that other processes (*e.g.* crustal contamination; degree of partial melting) have played a role; and

(c) Similar concentrations of the HFSE in discrimination diagrams. A number of trace element discrimination diagrams use the known HFSE concentrations (e.g. Ti, Zr and Y) of basalts from island arcs, mid-ocean ridges and within-

plate environments to discriminate their tectonic setting (*e.g.* Pearce and Norry, 1979; Pearce and Gale, 1977; Wood, 1980).

2.3 Sm-Nd and Rb-Sr isotopes

Sm-Nd and Rb-Sr isotopic variations in the mafic and ultrapotassic dykes were employed as a geochronological tool, as well as a tracer of geochemical provenance. The utility of the Rb-Sr isotope system for dating results from the fact that ^{87}Rb decays to ^{87}Sr. Rocks derived from the same magma source have the same initial $^{87}Sr/^{86}Sr$. Differences in their present-day $^{87}Sr/^{86}Sr$, therefore, result from their differing amounts of Rb. The more Rb, the greater the enrichment in ^{87}Sr since the time of crystallization. The isotopic compositions of rock samples can be plotted on a diagram of $^{87}Sr/^{86}Sr$ against $^{87}Rb/^{86}Sr$. On this diagram, a suite of rocks will define a line termed an "isochron" when having the same age and initial $^{87}Sr/^{86}Sr$ ratio. The slope of this line is a measure of the age of the rocks (Hall, 1996; Dickin, 2005; O'Nions *et al.,* 1979).

Similarly, the Sm-Nd isotope system can be use for dating as a result of the decay of the long-lived isotope ^{147}Sm to ^{143}Nd. When a magma is formed, it will have the same ^{143}Nd /^{144}Nd ratio as its source material, though it's Sm/Nd ratio will be different (a consequence of Nd being more incompatible and partitioning more into the melt than Sm). The age of a suite of rocks can be determined by plotting their $^{143}Nd/^{144}Nd$ ratios against $^{147}Sm/^{144}Nd$ on an isochron diagram analogous to that used in the Rb-Sr system (Hall, 1996; Dickin, 2005; O'Nions *et al.,* 1979).

The measurements of initial ratios provide a way of constraining whether a particular magma was derived from a mantle or a crustal source. In a simplistic way the mantle has a relatively uniform and low $^{87}Sr/^{86}Sr$ ratio, and the continental crust has a much more variable, and, on average, higher ratio. In contrast, the $^{143}Nd/^{144}Nd$ ratio is generally higher in the mantle than in the crust. Although Nd-and/or Sr-isotope compositions alone can place important constraints on the petrogenetic relationships of many rocks, they have been particularly useful where considered together (Hall, 1996; Dickin, 2005; O'Nions *et al.,* 1979).

If we know the present-day Sm/Nd and $^{143}Nd/^{144}Nd$ ratio of a rock we can estimate its age or the time the rock has spent in the crust (*i.e. "model age"* or *"crustal residence time"*; Hall, 1996; Dickin, 2005; O'Nions *et al.,* 1979). This assumes we know how the mantle $^{143}Nd/^{144}Nd$ ratio has been evolving with time. Model ages were calculated with respect to: a) a depleted mantle isolated from the chrondite uniform reservoir (CHUR) since 4.55 Ga, following a linear evolution and with a present day ϵ_{Nd} value of +10 (T_{DM2}); and b) De Paolo's mantle model (De Pal; De Paolo, 1981). In this model, the mantle has undergone a non-linear evolution with steadily increasing depletion since the Achaean. In both scenarios, the model age is calculated by extrapolating the $^{143}Nd/^{144}Nd$ of a rock back to the intersection with the mantle growth curve.

Both the Sm-Nd and Rb-Sr isotopic systems may be disturbed during metamorphism. Since both Rb and Sr are LFSE, it is easier to reset this system then the Sm-Nd system, where the REE are more immobile. Thus there is a need to be aware of the effects of alteration and metamorphism when using these isotopic systematics. It is

preferable, but not always possible to use U-Pb geochronology on robust accessory phases to establish the original igneous age of formation. With this "age" or "date", it is easy to calculate initial isotopic ratios in the Rb-Sr and Sm-Nd system.

2.4 Methodology – Petrography

Twenty-five polished thin sections were examined under an optical microscope; thin-section mineral maps for 9 samples were obtain by scanning electron microscopy (SEM) analysis; and mineral analyses with an electron microprobe were carried out for 15 representative samples. In addition, the SEM was used to identify minor minerals in 3 samples from the Canyon Domain.

2.4.1 Scanning Electron Microscope (SEM) Based Mineral Liberation Analysis

Mineral maps and modal mineralogy were obtained using the scanning electron microscope (*FEI Quanta 400* environmental SEM) at Memorial University. This SEM is equipped with an energy dispersive x-ray (EDX) analytical system (Roentec XFlash 3001 SDD; silicon drift detector) and mineral liberation analysis (MLA) software. The on-line program of the MLA software package controls the SEM, captures sample images, performs necessary image analysis and acquires EDS x-ray spectra, while the off-line processing program transforms raw data into particle mineral maps and calculates bulk and liberation data from particle mineral maps (Gu, 2003, 2004). In this case we used the MLA X-ray Modal Analysis or "point count" mode (XMOD), in which the mineral identification is determined by one x-ray analysis at each counting point. These x-ray

spectra are collected and saved for off-line classification, which for this method is limited to modal mineralogy information (Gu, 2003).

Initially, a backscattered electron image is acquired (256x256 pixels) for each sample and it is then used to discriminate particle matter from background (Gu, 2003). There is a greyscale cut-off for determining what is considered part of the sample and what is not. Usually this cut-off is a low (near black) value for removing epoxy from consideration. Once the sample is identified, a grid is overlaid and an x-ray spectrum is acquired from each grid point (dwell time for the spectrum was 20 milliseconds). In this case the grid was for every 8^{th} pixel, which means a 32x32 grid on a 2x2mm area, implying a spectrum was acquired every 62.5 microns.

We acquired similar spectra from minerals we identified from their chemistry (*i.e.* each mineral grain shown in the BSE image can be identified with single x-ray analysis positioned inside the grain). These spectra provided a list of standard spectra for comparing with the unknowns. The last steps were the *classification,* which provided modal analysis, and joining of all the frames to acquire the maps (images) of the thin-sections, in which different types of minerals appear with different colours.

2.4.2 Electron Microprobe Analysis

Mineral analyses were obtained using a CAMECA SX50 electron microprobe at Memorial University. The mineral analyses were performed using Link energy dispersive (ED) and Cameca wavelength dispersive (WD) spectrometers. The minerals analyzed were: amphibole, biotite, feldspars, pyroxenes, apatite, magnetite and spinel. For each

major mineral, five grains including their core and rim were analyzed. For large grains, a set of points across the grains ware analyzed. Minor phases were identified using the IDFix program (acquisition and quantitative EDS package; www.samx.com) that is part of the microprobe software, and/or two to four grain cores were analyzed. The IDFix program is used to generate full spectra (electron volt (eV) vs. intensity) of the minerals in real time. The program database allows us to identify elements, which generate peaks at various energies and, therefore, identify mineral phases.

Each mineral was analysed for the following elements: Si, Al, Ca, Na, Mg, Ni, Cr, F, and Cl (WD) and K, Ti, Mn and Fe (ED) in amphibole and biotite; Si, Al, Ca, Mg, Mn, Ti, Cr and Ni (WD) and Fe (ED) in pyroxenes; Si, Al, Ca, Na, K and Fe in feldspars; and Si, Al, Mg, Cr and Mn (WD), Ti and Fe (ED) and, in some cases Ni, were analyzed in oxides and spinels; Si, Al, Ca, Na, Mg, Mn, Cr, Ti and Fe (ED) in garnet; and Si, Ca, P, Sr, F and Cl (WD) in apatite.

Analyses were performed with a beam current of 20 μA, at a beam size of 1μm and an accelerating voltage of 20 kV. Counting times varied from 6 to 30 seconds; 6 seconds for Si and Al in amphibole and biotite and 30 seconds for Ni.

Structural formula calculations for all the minerals were done using the software Formula 1, integrated in the microprobe computer system, which follows the procedure described in "The rock-forming minerals" (Deer *et al.,* 1992). In addition, pyroxenes formulas were re-calculated using the excel spreadsheet PX-NORM (Sturm, 2002), which estimates Fe^{3+} based on the method by Droop (1987) and uses the classification scheme of Morimoto (1988). Here we present Formula 1 calculated analyses, which were identical

to those using the spreadsheet, and mineral names acquired using the PX-NORM spreadsheet. Amphibole formulas were re-calculated using the spreadsheet AMP-CLASS (Esawi, 2004), which estimates Fe^{3+} based on the method described by Stout (1972) and uses the classification scheme of Leake *et al.* (1997, 2004). Here we present the Formula 1 calculated analyses, which were identical to those using AMP-CLASS, and the mineral names acquired using the AMP-CLASS spreadsheet. For oxides, cations were recalculated based on 4 oxygen and using the Droop (1987) method for the calculation of Fe^{3+}. The complete chemical data of the analysed minerals are shown in the Appendix 1.

2.5 Methodology - Geochemistry

A total of 29 samples were analysed for major and trace elements. A subset of 16 samples were analysed for Sm-Nd and 9 samples, all from the ultrapotassic dykes of the Canyon Domain, were analysed for Rb-Sr. Representative samples were crushed into a fine-grained powder, for bulk composition and isotope analysis, using an agate ring mill to minimize contamination. It is important to note that care was taken during the entire process in order to obtain reliable results. Weathered surfaces on the hand samples were removed in order to ensure the use of fresh material only. For the primary crushing, the samples were sawn (water-cooled, non-recycling) into thin pieces and crushed by wrapping the material in plastic bags and using a hammer on a metal plate.

2.5.1 Whole Rock Analysis

Whole-rock analyses of the selected suite of samples were obtained from

ACTLABS (Ancaster, Ontario.). The techniques used were inductively coupled plasma-mass spectrometry (ICP-MS) and inductively coupled plasma-optical emission spectrometry (ICP-OES). For both the ICP-OES and ICP-MS techniques, Actlabs employs a lithium tetraborate fusion, which ensures that all phases are dissolved.

Transition elements (V, Co, Cu, Ni, Sc, and Zn); low field strength elements (Ba, Ga, Ge, Rb, Sr, Th, U); high field strength elements (Zr, Hf, Nb, Ta, Y) and REE elements were determined using ICP-MS. Major elements (Si, Al, Fe, Mn, Mg, Ca, Na, K, Ti and P) and a few selected trace elements (Ba, Sr, Y, Sc, Zr and V), many of which are also provided in the ICP-MS data, were determined using ICP-OES. The values for V, Sr, Y and Zr are an average of both sets of results (ICP-MS/OES) while the values for Sc are from ICP-OES results only.

2.5.2 Sm-Nd Isotope Analysis

Sm□Nd isotope determinations were performed by thermal ionization mass spectrometry (TIMS) at MUN. A mixed $^{150}Nd/^{149}Sm$ spike was added to approximately 0.1 g of each rock powder. The samples were then dissolved in Savilex Teflon containers using a mixture of concentrated HF and HNO_3. After five days of digestion, the solution was evaporated to dryness and then dissolved in 6N HCl for a minimum of two days. The solution was then dried overnight and taken up in 2.5N HCl and loaded on cation exchange chromatography columns containing AG50W – X8 resin. The bulk REE fraction from the first columns was subsequently loaded on a secondary column loaded with Eichrom Ln resin, in order to produce separate Nd and Sm fractions. All reagents are

purified in order to ensure a low contamination level. The average total chemical blank is below 60 pg of Nd and is considered negligible.

Isotopic data were obtained using a multicollector Finnigan Mat 262 mass spectrometer in static mode. Nd isotopic ratios are normalized to $^{146}Nd/^{144}Nd = 0.7219$. During the course of data acquisition replicates of the Jndi-1 standard gave a mean value of $^{143}Nd/^{144}Nd = 0.512135 \pm 10$ (n = 47). All reported values for the samples were adjusted based on the known value of the Jndi-1 standard ($^{143}Nd/^{144}Nd_{certified} = 0.512115 \pm 7$, Tanaka *et al.,* 2000). The in-run precision for Nd isotope ratios are given at the 95% confidence level. Errors on Nd isotopic compositions are <0.002% and errors on the $^{147}Sm/^{144}Nd$ ratio are estimated to be lower than 0.1%. ε_{Nd} values were calculated using $^{147}Sm/^{144}Nd = 0.1967$ and $^{143}Nd/^{144}Nd = 0.512638$ for the present-day chondrite uniform reservoir (CHUR). The ^{147}Sm decay constant is $6.54\ 10^{-12}\ y^{-1}$ (Steiger and Jäger, 1977).

2.5.3 Rb-Sr Isotopic Analysis

Rb-Sr isotope determinations were performed by thermal ionization mass spectrometry (TIMS) at MUN. Depending on the Sr content of the sample 0.05 to 0.2 g of rock powder was dissolved in Savilex Teflon beakers using a mixture of concentrated HF – HNO_3 acids. After five days of acid digestion the solution was evaporated to dryness and then taken up in 6 N HCl for two days. The solution was then dried and taken up in 1 mL of 2.5N HCl, centrifuged and loaded on cationic exchange chromatography using AG50W – X8 resin. The main part of major and trace elements were eluted using 7 mL of 2.5N HCl. A first Sr concentrated fraction was collected with 2 mL of 6N HCl,

evaporated to dryness on a hot plate and loaded on 1 mL Sr resin (Eichrom®) column in 3M HNO_3 media. Rb and all the remaining elements were eluted with 2 mL of 3M HNO_3, Sr is collected with 0.5 mL H_2O nanopure. All reagents are purified in order to ensure a low contamination level. The measured chemical blank is below 0.7 ng and is considered negligible.

For each sample, the Sr fraction was loaded on a previously out-gassed single W filament together with 1 μL of Sr activator (Tantalum fluoride) and analyzed using a multicollector Finnigan Mat 262 mass spectrometer in static mode. Sr isotopic ratios were normalized to $^{88}Sr/^{86}Sr = 8.375209$. ^{87}Rb interferences are carefully checked by measuring ^{85}Rb peak intensity. The reported values are adjusted to the NBS 987 Sr standard ($^{87}Sr/^{86}Sr = 0.71034$). The mean value obtained on this standard is 0.710288 ± 28 (2σ, n = 37). The in-run precisions on Sr isotopic ratio are given at 95% confidence level. Errors on Sr isotopic compositions are <0.002%.

CHAPTER 3: MAFIC DYKES IN THE GAGNON TERRANE

3.1 Introduction and field occurrence

Granitic and mafic dykes cut Archean tonalitic and granitic gneisses of the Gagnon Terrane east of the SWSZ (Fig. 3-1). The two types of dykes appear less deformed than their country rock and cut its foliation at variable angle; therefore, it is inferred that they postdate part of the deformation.

Initially, these dykes were considered to be of Grenvillian age; however, one granitic dyke yielded an age of 1741+/-31Ma (sample 04-289; Dunning and Indares, pers. comm. 2008). Since the mafic dykes generally have similar field relationships as the granitic dykes, we infer they may be of a similar age and that the main fabric in the tonalitic gneiss is pre-Grenvillian.

The age of the granitic dyke, together with similar inherited monazite ages from anatectic metapelites sampled west of the SWSZ (Jordan *et al.,* 2006), suggest that a ~1.7Ga thermal event was important in southern Gagnon Terrane, which represents the southeasternmost (presently) exposed margin of Laurentia at that time. Such ages are not known elsewhere in the central-eastern Grenville Province, but this event has been tentatively correlated by Jordan *et al.* (2006) with late orogenic magmatism (1.74-1.7 Ga) in the Makkovik Province (Culshaw *et al.,* 2000; Ketchum *et al.,* 2002), farther NE, on the other side of the Grenville front (see section 1.4.1). Therefore, a geochemical investigation of the mafic dykes from southern Gagnon Terrane may provide constraints

on the, less well known, ~1.7 Ga stage of the evolution of the Laurentian margin that is now part of the Grenville Province.

Samples from seven mafic dykes (Fig. 3-1; locations #253, 487, 262, 274, 2000x, 288, 474, 481 and 486) were selected for detailed study. These dykes are about 10-30 cm wide, have sharp boundaries and cut the foliation at low to high angle (Fig. 3-2). In addition, one dyke at location #288 has unusual irregular (wobbly) contacts (Fig. 3-2d).

3.2 Mineralogy, textures and mineral chemistry

The dyke samples have a mineralogy dominated by hornblende and plagioclase, with lesser amounts of clinopyroxene (Table 3-1). Hornblende defines a weak foliation. Clinopyroxene forms isolated grains dispersed in the matrix (Fig. 3-3a-b). In some cases, clinopyroxene is corroded by hornblende along rims and cleavage (samples 288d and 2000x; Fig. 3-3c) and, in sample 2000x, it mainly occurs as relics partially enclosed in hornblende and locally replaced by carbonates (Fig. 3-3d). Quartz, K-feldspar, biotite, scapolite and opaques are present in minor and trace amounts in some samples (Table 3-1). K-feldspar and quartz are interstitial phases. Biotite usually occurs as small laths along hornblende rims. Opaques (magnetite and ilmenite) are interstitial or form blebs, locally included in plagioclase and amphibole. One sample (487) shows abundant chlorite and alteration of plagioclase to sericite. Overall the texture is equigranular. All the minerals have curved to straight boundaries and triple junctions are common (Fig. 3-3).

In contrast to the other samples, 474d consists mainly of equigranular plagioclase with much less hornblende, more quartz (Fig. 3-3e) and with clinopyroxene commonly

forming discontinuous rims around plagioclase (Fig. 3-3e) and hornblende. In addition, aggregates of biotite and hornblende intergrown with quartz, frequently around opaques, are common (Fig. 3-3f). Opaques are large relative to those in the other samples and are interstitial or form inclusions in plagioclase and quartz.

3.2.1 Mineral Compositions

Hornblende, feldspars and pyroxenes were analyzed in 5 representative samples (2000x, 288d1*, 481d, 474d and 486d; Table 3-2 and Figure 3-4; mineral analyses are listed in Appendix 1). Based on the amphibole classification scheme of Leake *et al.* (1997, 2004) the hornblende is magnesiohastingsite-tschermakite-edenite with XMg_{69-73} in sample 474d, pargasite with XMg_{68-73} in sample 2000x and magnesiohastingsite with XMg_{61-79} in the remaining samples (Fig. 3-4a). Plagioclase is chemically homogeneous oligoclase (An_{15-16}; Fig. 3-4b) in sample 474d and andesine (An_{31-38}; Fig. 3-4b) in the remaining samples. K-feldspar is orthoclase with Or_{87-93} (Fig. 3-4b). Clinopyroxene is chemically homogeneous based on the pyroxene nomenclature of Morimoto (1988) and it has the composition of diopside-augite (sample 474d) and diopside (remaining samples) (Fig. 3-4c). Opaques, when present, were identified as magnetite and/or ilmenite.

The compositions of minerals are correlated with the bulk chemistry of the samples (Table 3-3). For instance, sample 474d, which has one of the lowest whole rock Mg-numbers and the highest Na contents, contains the clinopyroxene with the lowest XMg and the plagioclase richest in albite. In contrast, the sample with the highest whole rock Mg-number (sample 288d1) contains the most magnesian pargasite and diopside.

3.2.2 Interpretation of textures

The foliation and equigranular texture of the samples are consistent with pervasive metamorphic recrystallization. In addition, observed mineral assemblages (*i.e.* plagioclase + hornblende ± clinopyroxene) are characteristic of upper amphibolite to lower granulite facies conditions (Pattison, 2003). Both clinopyroxene and hornblende are clearly part of the main assemblage and in most cases appear stable. The presence of some clinopyroxene grains corroded by or enclosed by hornblende (samples 288d and 2000x) indicates that part of the hornblende postdates the clinopyroxene, consistent with fluid infiltration (retrograde metamorphism) after the formation of clinopyroxene.

In sample 474d, textural evidence (*i.e.* clinopyroxene grains replacing hornblende along its rims) suggests that clinopyroxene formed later than hornblende, indicating a typical transition along a prograde P-T path. The aggregates of biotite and hornblende inter-grown with quartz and opaques are likely the result of small degrees of partial melting, which might have been facilitated by the presence of fluids (Pattison, 2003). The granoblastic/equigranular texture of this sample suggests that these intergrowths are not original igneous textures, since it is unlikely that such texture could have survived the recrystallization process.

3.3 Geochemistry

The mafic dykes of the Gagnon Terrane have experienced metamorphism at upper amphibolite to lower granulite facies. Owing to the possibility of element mobilization during metamorphism and late hydration, we have focused our geochemical interpretation

mainly on the immobile elements (see section 2-1). These elements include the rare earth elements (REE), Th (a low field strength element, LFSE) and the high field strength elements (HFSE). Because of the metamorphic grade, caution is needed in assessing element mobility/immobility.

Given that all the samples are depleted in Nb relative to La, they have been divided into groups based on: a) Nb/Th, which illustrates the variable enrichment of Th relative to Nb; and b) normalized rare earth element ratios (see section 2-1). Note that these groups form the basis for discussion of other aspects of the geochemistry.

Group 1 consists of samples that have Nb/Th > 5 and includes 2000x, 288d, -d1, 481d, 274d, 253-2, 262-1a, and 262-2a (Fig. 3-5). ***Group 2*** consists of samples that exhibit a negative Nb anomaly (*i.e.* these are depleted in Nb relative to both La and Th; Nb/Th < 5) and includes 474d, 486d and 487 (Fig. 3-5). These two groups were further subdivided into samples with *very low* (VL; <4), *low* (L; 4-8), *intermediate* (I; 8-11) and *high* (H; >11) primitive mantle normalized $(La/Yb)_N$ ratios (Table 3-3).

3.3.1 Major and trace element composition

Major and trace element abundances are listed in Table 3-3. According to the Winchester and Floyd (1977, 1978) diagrams of Zr/TiO_2-Nb/Y and Zr/TiO_2-SiO_2 (Fig. 3-6a-b) the dykes are dominantly subalkaline basalts-andesites. In addition, the variation of TiO_2 with FeO*/MgO (after Miyashiro, 1974; Fig. 3-6c) and/or TiO_2 with Mg# (Mg# =[molar MgO/(MgO + FeO*)] x100; Fig. 3-7) is consistent with a tholeiitic character. The samples of *Group 1* have SiO_2 contents between 47–49 wt.%, with Mg# in the range of

52 to 69 (Fig. 3-7). In these rocks, FeO ranges from 8.8 to 10.8 wt. %, CaO from 8.8 to 13.5 wt. %, Al_2O_3 from 12.4 to 17.9 wt.% and K_2O+Na_2O from 3.7 to 6.0 wt.%. The samples of *Group 2* are generally similar to those of *Group 1*, with the exception of SiO_2, which is slightly higher (~50 wt. %) in samples 487 and 486d and much higher (~57 wt.%) in sample 474d. In general, the Mg# shows a moderate positive correlation with CaO and CaO/Al_2O_3 ratios and a slight to moderate negative correlation with Na_2O (Fig. 3-7).

All the samples are characterized by low TiO_2 (0.7–1.3 wt. %) contents and some show Cr and Ni as high as 1088 ppm and 240 ppm, respectively. Ni and Cr show a crude correlation with Mg# suggesting they represent a range from primitive to fractionated compositions (Fig. 3-7). Note that the content of Cr in samples 274d and Ni in samples 274d and 474d are below detection.

3.3.2 Extended REE plots

The immobile element data are illustrated in primitive mantle normalized plots (Fig. 3-8 a-b, REE; c-d, all). Figures 3-8 e and f show a more complete spectrum of trace element data, including other potentially mobile LFSE like Rb, Ba, U, and Sr. All the samples are characterized by enrichment of the light REE (LREE; La_N ~12-60) and low concentrations of the heavy REE (HREE; Yb_N= 2-4).

Group 1 (*i.e.* samples with Nb/Th > 5; Fig 3-5) includes: (a) samples with *low* $(La/Yb)_N$ ratios and weak positive Eu anomalies (288d, -d1, 481d and 274d); (b) samples with *intermediate* $(La/Yb)_N$ (2000x and 262-1a); and (c) samples with *high* $(La/Yb)_N$

ratios (253-2 and 262-2a) (Fig. 3-8a). These rocks exhibit weak to strong negative Zr and Ti anomalies and are depleted in Nb and Th relative to La (Fig. 3-8c). The concentrations of Ba, K and, in some cases, Rb are elevated while the concentrations of other LFSE (U and Th) are generally depleted relative to the adjacent LREE. In addition, strong positive Sr anomalies are also visible, except in sample 262-1a (Fig. 3-8e).

Group 2 (*i.e.* samples with Nb/Th < 5; Fig 3-5) consists of three samples with distinctive $(La/Yb)_N$ ratios: sample 486d (*very low* $(La/Yb)_N$ ratio); sample 487d, (*low* $(La/Yb)_N$ ratio); and sample 474d (*high* $(La/Yb)_N$ ratio; Fig. 3-8b). These rocks exhibit negative Nb anomalies relative to Th and La, have weak negative Ti anomalies, and samples 486d and 487 have negative Zr anomalies (Fig. 3-8d). Samples 487 and 486d are enriched in Ba and K, and sample 487 in Rb relative to the adjacent LREE. In addition, sample 486d has a positive Sr anomaly. Sample 474d, shows a smoother extended pattern with strong depletion of Rb and enrichment in Ba relative to the adjacent LREE (Fig. 3-8f). The large $(La/Yb)_N$ ratio of sample 474d, coupled with its distinctive extended REE pattern, indicates that is not related to the other samples in *Group 2*.

3.3.3 Sm-Nd isotopic data

Sm-Nd isotopic data for three samples from *Group 1* (2000x, 288d, 262-1a) and two samples from *Group 2* (486 and 474d) are presented in Table 3-4. When the data are plotted on a $^{143}Nd/^{144}Nd$ versus $^{147}Sm/^{144}Nd$ diagram, the scatter is obviously too great to represent an isochron (Fig. 3-9a). Model ages were calculated with respect to a depleted

mantle model (T_{DM2}) and the De Paolo's mantle model (De Paolo, 1981) (see section 2-1) and are listed in Table 3-4.

Although no precise ages of intrusion are available for the dykes due to their low zirconium content, the crystallization age of one granitic dyke at 1741 +/-32 Ma (U-Pb on zircon; Dunning and Indares, pers. Comm. 2008), with the same field relationships as the mafic dykes, suggest emplacement during the time interval 1700-1800Ma. Thus, measured Nd isotope ratios were calculated back to 1750 Ma and expressed as the deviation from a chondritic uniform reservoir at that time ($\varepsilon_{Nd}{}^{1750}$). This information is illustrated in a ε_{Nd} versus time diagram (Fig. 3-9b). The samples of *Group 1* have $\varepsilon_{Nd}{}^{1750}$ values ranging from a positive ($\varepsilon_{Nd}{}^{1750}$ = + 1.1 to +2.1) to highly negative ($\varepsilon_{Nd}{}^{1750}$ = -17.9) character. Samples of *Group 2* have negative $\varepsilon_{Nd}{}^{1750}$ = -2.3 to -2.6, indicating derivation from a source with time integrated LREE-enrichment.

3.4 Interpretation and Discussion

The mafic dykes of the Gagnon Terrane have experienced pervasive metamorphism under upper amphibolite to lower granulite facies, indicated by their textures and mineral assemblage. In addition they contain abundant hornblende, suggesting that they experienced hydration at some stage of their post-crystallization evolution. An important consideration in the study of rocks metamorphosed at granulite facies conditions is the possibility of partial melting, especially when the melt is extracted from the rock. The mafic dykes of the Gagnon Terrane show no evidence of melting at the outcrop scale. At the thin-section scale sample 474d contains millimetric-size aggregates of biotite and

hornblende intergrown with quartz and opaques, which can be attributed to small degrees of melting. However, if it was melting then it remained localized and *"in situ"*.

The mafic dykes from the Gagnon Terrane are subalkaline tholeiitic basalts to andesites. They have remarkably similar LREE enriched patterns and low HREE concentrations (Fig. 3-8). Given that all the samples are depleted in Nb relative to La, they have been divided into groups based on Nb/Th, which illustrates the variable enrichment of Th relative to Nb (Fig. 3-5). *Group 2* consists of samples which exhibit negative Nb anomalies relative to both Th and La (Nb/Th < 5) while *Group 1* consists of samples, which although depleted in Nb relative to La, lack the enrichment of Th (Nb/Th >5).

In general, Nb depletion is typical of all island arc volcanic rocks (Hofmann, 1988; Condie, 1986) and calc-alkaline rocks from other destructive plate margins such as continental margins (Pearce, 1983; Thompson *et al.,* 1984). However it can also be found in many continental within-plate basalts (Duncan, 1987). Thus, the enrichment of LREE and LFSE relative to Nb and Ta can be considered to reflect either crustal contamination (Wilson, 1989; Hofmann and Stein, 1994) and/or production of mafic magmas in a mantle that has been enriched in LFSE and LREE by fluids from a subducted plate (Gill, 1981; Pearce, 1983; Condie, 1990; McCulloch and Gamble, 1991; Saunders *et al.*, 1991).

There are two possible scenarios for the formation of the mafic dykes that can explain their geochemical features as a group: 1) the dykes could represent mantle derived melts contaminated by crustal material and be related by different degrees of contamination or 2) the dykes could represent rocks formed in an arc setting.

3.4.1 Scenario #1: Contaminated mantle-derived magmas

Rare earth element data

Some samples from *Groups 1* and *2* (e.g. 288d1 and 487) have compositional features indicative of a mantle origin, including relatively high Mg#, Ni, and Cr (Perfit *et al.*, 1980; Table 3-3 and Fig. 3-7). However, their REE patterns and the depletion of some HFSE, especially Nb, suggest that these rocks did not originate from typical MORB or ocean island basalt (OIB) source regions, unless the parental melts were significantly modified (Figure 3-10).

A possible explanation for the compositional features of the mafic dykes is that they represent mantle-derived melts contaminated by upper crustal material, and related by different degrees of contamination. To evaluate this possibility, REE patterns for an N-MORB and OIB component contaminated by 10, 20 and 30% crust material were plotted and shown in Figures 3-11. Crust material is represented by: a) average upper continental crust (UCC; Taylor and McLennan, 1981); and b) average Archaean (3-3.5 Ga) tonalite–trondhjemite–granodiorite (TTG; Martin, 1994; Martin and Moyen, 2002). It is clear from the REE patterns that the average Archaean tonalite–trondhjemite–granodiorite represents a better candidate for the crustal material that may have mixed with a mantle-derived magma. In addition, an Archean TTG-like crust is consistent with the mafic dykes intruding Archaean rocks of the Gagnon Terrane.

The REE patterns in Figure 3-11 indicate that up to 50% contamination of the N-MORB magma by a TTG-like crust is required to account for the REE concentrations found in the mafic dykes, except for sample 474d. Figure 3-12 illustrates the

concentrations of Nb and Th for the two magma sources (*i.e.* N-MORB and OIB) contaminated with a TTG-like crust and indicates that ~50% bulk contamination of an N-MORB magma could account for the depletion of Nb in the mafic dykes. Figure 3-12b suggests that sample 474d could have been the result of an OIB magma contaminated with a TTG-like crust. This further indicates that sample 474d is not related to the other dykes.

Sm-Nd data

An old crust (~3Ga) that could have evolved to have a ε_{Nd} at ~1.8Ga of at least −20, is necessary to account for the highly negative ε_{Nd}^{1750} (-17.9) of sample 288d1. Such highly negative values have been reported for Archean TGG suites (De Paolo, 1981). However, the remaining samples have ε_{Nd}^{1750} of –2.6 to +2.1, which would require a TTG-like crust, with a ε_{Nd} 1750 of about –7. For instance, New Quebec and North Quebec crustal composites are interpreted to have formed at ~2.5-2.7Ga (McCulloch and Wasserburg, 1978; De Paolo, 1981), and would have ε_{Nd} at ~1.8Ga of about -7 to –9. A possible explanation would therefore be that we are seeing localized contamination by a very negative old crust and a more regionally representative average crust to account for the variable ε_{Nd}^{1750} of the mafic dykes. Since the crust is heterogeneous, this would be a reasonable explanation. It can be concluded that an N-MORB source with ~50% bulk contamination by a heterogeneous TTG-like crust could result in REE patterns and Nb concentrations comparable to those in the mafic dykes.

3.4.2 Scenario #2: Arc-related magmas

Figure 3-13 shows the REE and HFSE concentrations of the mafic dykes and a range of island arc basalts (IAB) from the Aeolian islands (calc-alkaline and potassic basalts; Ellam *et al.,* 1988) and the Kermadec islands (tholeiitic basalt; Ewart *et al.,* 1977). In addition, a field for the ultramafic rocks of the Island Domain, which have arc-signatures, have been added for comparison (Valverde, 2005; Valverde *et al.,* in prep.).

Island arc rocks have trace element characteristics that are markedly different from those of N-MORB and OIB, especially lower HFSE abundances relative to the REE and the LFSE (*i.e.* they have high ratios of LFSE to HFSE; Gill, 1981). The most distinctive feature on primitive mantle-normalized diagrams, such as Figure 3-13, is the negative anomaly at Nb (Ta) relative to adjacent REE and the HFSE.

Among arc-type rocks, low-K oceanic arc tholeiites and those forming in back-arc basins are considerably different from those calc-alkaline and high-K suites forming in both continental margin and evolved oceanic-arc environments (Pearce and Cann, 1973; Baker, 1982). The former (*e.g.* Kermandec, Tonga, Marianas, South Sandwich) vary from flat to LREE depleted REE patterns and are only slightly enriched in the LFSE (Sr, K, Rb, Ba, Th) and depleted in most of the other elements. The latter, on the other hand, are typically enriched in LREE in addition to the LFSE (*e.g.* Aeolian, Lesser Antilles). In other words, the LFSE/HFSE ratios are highest in the more depleted, low-K rocks (Hawkesworth *et al.,* 1993; Pearce and Peate, 1995).

The mafic dykes of the Gagnon Terrane have REE concentrations resembling those of calc-alkaline arc rocks (*e.g.* Aeolian calc-alkaline basalt; Fig 3-13). In addition,

the samples of *Group 1* and samples 486d and 487 from *Group 2* are enriched in the Sr, K, Ba, and Th and are depleted in Zr and Ti (Hf), consistent with an arc-signature (Fig. 3-14). It must be noted that the LFSE are susceptible to remobilization during alteration and metamorphism and their implications for tectonic settings may not be reliable. However, the arc type signatures of samples 486d and 487 from *Group 2* are still reflected by the patterns of the immobile elements (HFSE, Th and REE; Fig. 3-14), especially their negative Nb anomaly relative to both Th and La. The samples of *Group 1* have low concentrations of Th compared to La so that their patterns do not show a significant Nb anomaly with respect to Th (Fig. 3-14; Fig 3-5). The depletion of Th with respect to other incompatible elements may be due to removal in fluids during granulite-facies metamorphism (Weaver and Tarney, 1980, 1981). If this is the case, the samples of *Group 1* can still be interpreted as arc-related.

However, there are two shortcomings with this scenario: a problem with interpreting the (tholeiitic) mafic dykes of the Gagnon Terrane as having an arc signature is that they resemble calc-alkaline arc basalts as supposed to arc tholeiitic basalts, which have relatively flat to LREE depleted REE patterns. However, the enrichment of TiO_2 with Mg#, indicative of a tholeiitic trend, is not strong in the mafic dykes of the Gagnon Terrane, thus, the dykes could represent more transitional compositions (*i.e.* between tholeiitic and calc-alkaline trends).

Arc related rocks have $^{143}Nd/^{144}Nd$ ratios of a wide range, but generally lower than those reported for MORB. Although the studied mafic dykes have trace element concentrations similar to those reported in many arc basalts, their measured $^{143}Nd/^{144}Nd$

ratios are lower (*e.g.* Ellam and Hawkesworth, 1988). The extremely negative ε_{Nd} values of sample 288d1 could be attributed to some type of residence contamination in Archean gneisses as reflected by their irregular (wobbly) contacts.

3.5 Regional correlations and conclusions

3.5.1 ~1.7 Ga mantle-derived magmas linked to the Makkovik Orogeny

The mafic dykes in Gagnon Terrane east of SWSZ are inferred, based on field relations, to be of broadly similar age to the ~1750 Ma granitic dykes that are common in the same area. This ~1750 Ma magmatic event in Gagnon Terrane is coeval with late orogenic magmatism (1740-1700Ma) in the Makkovik Province (Culshaw *et al.,* 2000; Ketchum *et al.,* 2002). This magmatic event, developed on the continental margin of the Nain Craton and truncated at the Grenville Front farther east, is characterized by A-type plutons. However the plutons are interpreted to have been generated during mafic underplating likely related to crust-mantle detachment and could be linked to possible intrusion of mafic magmas into the crust (Kerr and Fryer, 1993; 1994; Culshaw *et al.,* 2000a). If the mafic dykes from the Gagnon Terrane represent mantle-derived magmas, contaminated by crustal material, then they may be linked to this event.

3.5.2 Arc related magmatism

Units with arc related signatures have been identified in the klippe and the Island Domain, both of which overlie the Gagnon Terrane in the area east of the SWSZ, and have been interpreted as remnants of an early arc system developed during the

Labradorian event (Valverde *et al.*, in prep.). In the central-eastern Grenville Province, the 1710-1600 Ma Labradorian event is characterized by early (1680-1650Ma) arc related calc-alkaline magmatism and the late (1650-1620Ma) emplacement of AMGC suites (Gower and Krogh, 2002). If the mafic dykes of the Gagnon Terrane are interpreted to have arc-signatures, then their presumed age (~1750 Ma) suggests that arc-magmatism in the central segment of the Grenville Province may have been initiated well within Geon 1.7. Alternatively, the mafic dykes could be younger and related to the Labradorian event.

3.5.3 Conclusions

In conclusion, both hypotheses seem to be geochemically reasonable; however, the presumed age of the mafic dykes at ~1750Ma as well as the inconsistency of the arc scenario, discussed above, favour Scenario #1 (crustal contaminated mantle-derived magmas linked to the Makkovik orogeny). South of Makkovik Province and within the eastern segment of the Grenville Province, ~1.7 Ga ages are rare (Corrigan *et al.*, 1994; Davidson *et al.*, 1992; Gower and Krogh, 2002). The Gagnon Terrane east of the SWSZ is the southernmost exposed part of the New Quebec orogen in the Grenville Province. Therefore, it may represent a rare window into potentially widespread 1.7 Ga magmatism into the Laurentian margin, evidence of which is obscured, for the most part, elsewhere in the province owing to subsequent Labradorian and Grenvillian events.

Table 3-1: Observed mineralogy of the mafic dykes from the Gagnon Terrane (xx- highly abundant, x- abundant, v- minor and vv- traces). Hbl: hornblende, Pl: plagioclase, Ksp: K-feldspar, Qtz: quartz, Cpx: clinopyroxene, Scp: scapolite, Bt: biotite, Ap: apatite, Phy: pyrrothite, Cal: carbonates and Chl: chlorite.

Sample	Hbl	Pl	Ksp	Qtz	Cpx	Scp	Bt	Ap	Opaques/ Sulphides		Other
2000x	x	x		vvv	x	v		vv	vvv	Phy	Cal
288d	xx	x			v	v	vv		vv		
288d1*	xx	x			vv	x	vv	vv	vv		Cal
288d1	xx	x			v	v	vv				
474d	x	xx	vv	x	x		vv	vv	vv		
481d	x	x	vv		x	v	vv		vv	Phy	
486d	xx	x	vv	vv	x	v	vv	vv	vv		
487	xx	x						vv			Chl

Table 3-2: Summary of mineral compositions in terms of XMg, where XMg = $[Mg/(Mg+Fe^{2+})]$ x 100, % of end-members in feldspars and mineral names for representative mafic dykes from the Gagnon Terrane (An = anorthite, Or = orthoclase, - = not present). Tschermakite has $(Na+K)_A < 0.5$ and $Ca_A < 0.5$ while pargasite, magnesiohastingsite and edenite have $(Na+K)_A \geq 0.5$ and Ti <0.5. Pargasite and magnesiohastingsite have the same Si (5.5-6.5), but $^{VI}Al > Fe^{3+}$ and $^{VI}Al < Fe^{3+}$, respectively and edenite has higher Si (6.5-7.5).

Sample	Plagioclase	K-feldspar	Clinopyroxene	Hornblende	Opaques
2000x	Andesine (An 34–36)	-	Diopside XMg (78–80) Ti (0.002-0.003) Al (0.07-0.11)	Pargasite XMg (68–73)	Magnetite
288d1*	Andesine (An 31–33)	-	Diopside XMg (77–80) Ti (0.001-0.003) Al (0.07-0.12)	Magnesiohastingsite XMg (75–79)	Magnetite - ilmenite
474d	Oligoclase (An 15–16)	Orthoclase (Or 91–93)	Diopside-Augite XMg (65–69) Ti (0.004-0.006) Al (0.09-0.10)	Magnesiohastingsite-Tschermakite - edenite XMg (69–73)	Ilmenite
481d	Andesine (An 36–38)	Orthoclase (Or 87–89)	Diopside XMg (67–73) Ti (0.002-0.008) Al (0.07-0.018)	Magnesiohastingsite XMg (61–65)	Magnetite
486d	Andesine (An 31–32)	Orthoclase (Or 89)	Diopside XMg (71–73) Ti (0.003-0.004) Al (0.12-0.15)	Magnesiohastingsite XMg (71–75)	Ilmenite

Table 3-3: Major and trace element data for the mafic dykes from the Gagnon Terrane. Major elements are reported in wt.% and trace elements in ppm; missing values are below detection. Major elements are recalculated volatile free with total Fe as FeO* and Mg# = [molar MgO/(MgO + FeO*)] x 100. Group 1 = samples that lack negative Nb anomalies and Group 2 = samples with negative Nb anomalies relative to La and Th. *VL = very low* (<4); *L = low* (4-8); *I = intermediate* (8-11) *and H = high* (>11) primitive mantle normalized $(La/Yb)_N$ ratios. N = normalized using the primitive mantle values of Sun and McDonough (1989).

SAMPLE	274d	288d	288d1	481d	2000x	262-1a	253-2	262-2a	486d	487	474d
Group	*1-L*	*1-L*	*1-L*	*1-L*	*1-I*	*1-I*	*1-H*	*1-H*	*2-VL*	*2-L*	*2-H*
SiO2	48.24	47.68	47.32	49.27	48.71	49.25	49.04	48.32	50.12	50.13	57.10
TiO2	1.29	0.71	0.74	0.95	0.67	0.97	0.89	0.70	0.75	0.76	0.98
Al2O3	17.85	15.96	14.54	17.53	13.88	12.41	15.41	13.35	15.98	13.71	14.54
FeO*	10.75	9.17	9.41	9.78	8.87	10.45	10.14	9.69	9.08	9.26	8.22
MnO	0.18	0.16	0.17	0.18	0.18	0.22	0.17	0.19	0.16	0.16	0.16
MgO	6.60	9.31	11.71	6.71	10.54	10.12	8.49	10.29	8.51	11.84	5.62
CaO	8.80	12.78	12.24	10.53	13.14	12.22	11.18	13.59	10.48	9.59	6.78
Na2O	4.07	2.94	2.65	3.83	2.64	3.01	3.20	2.74	3.63	3.06	5.02
K2O	1.68	1.09	1.07	0.97	1.16	1.11	1.25	0.92	1.07	1.17	1.01
P2O5	0.54	0.21	0.17	0.26	0.21	0.24	0.24	0.22	0.24	0.31	0.58
LOI	0.76	2.62	1.77	1.12	1.87	1.08	1.05	2.77	1.50	2.46	0.61
Mg#	***52***	***64***	***69***	***55***	***68***	***63***	***60***	***65***	***63***	***69***	***55***
Co	108	70	81	93	77	91	121	89	94	124	100
Cr		221	281	51	826	1060	249	821	402	1089	205
Cu				61.7	21.2		12.9		41.2	20.9	
Ni		126	187	62	124	72.1	90.8	148	113	241	
Sc	28.9	31.5	35.4	28.8	45.0	36.0	30.0	35.0	38.1	39.8	24.6
V	210	221	216	220	229	237	219	224	200	183	167
Zn	134.0	63.0	93.6	82.3	80.8	101.1	111.8	81.9	82.4	73.3	110.0
Ba	923	468	420	349	357	255	424	391	488	379	916
Ga	19.6	14.7	14.6	17.5	15.2	16.8	19.1	15.7	16.5	15.7	19.0
Rb	35.0	13.7	14.6	8.2	16.5	6.8	9.9	9.8	12.4	27.2	6.0
Sr	809	845	617	707	645	551	720	811	422	357	748
Th	0.52	0.63	0.62	0.62	0.97	1.31	0.94	0.95	0.72	1.47	3.80
U	0.31	0.11	0.10	0.21	0.33	0.56	0.33	0.24	0.31	0.42	1.50
Zr	78.3	22.1	18.7	45.3	25.5	68.2	53.7	33.3	51.5	56.5	171
Hf	2.27	0.84	0.94	1.44	0.84	1.92	1.49	0.98	1.65	1.88	4.50
Nb	6.18	4.20	4.16	6.17	6.47	9.77	8.64	9.07	3.09	3.14	18.0
Ta	0.31	0.21	0.21	0.31	0.24	0.54	0.39	0.31		0.21	1.20
Y	22.7	12.6	11.4	16.5	13.3	17.2	13.7	13.7	16.5	16.7	21.0
La	21.0	9.8	8.4	10.7	15.0	19.7	19.7	19.7	8.8	14.3	34.9
Ce	48.2	19.1	17.6	24.9	32.9	47.3	46.5	43.0	20.1	30.0	72.6
Pr	6.25	2.52	2.42	3.34	3.91	5.81	5.40	5.02	2.61	3.89	8.58
Nd	25.6	10.3	10.3	13.6	16.0	25.6	23.3	20.3	11.0	15.2	34.6
Sm	5.36	2.52	2.50	2.98	3.16	5.73	4.53	3.93	2.68	3.25	6.50
Eu	2.01	1.09	1.06	1.18	1.10	1.65	1.51	1.20	0.99	1.06	1.99
Gd	5.05	2.52	2.50	3.09	2.86	4.73	3.68	3.17	2.78	3.14	5.40
Tb	0.72	0.42	0.42	0.51	0.45	0.65	0.54	0.47	0.51	0.52	0.70
Dy	4.02	2.21	2.18	2.67	2.35	3.35	2.58	2.53	2.78	2.93	3.80
Ho	0.82	0.42	0.42	0.51	0.44	0.59	0.45	0.47	0.62	0.63	0.70
Er	2.27	1.26	1.25	1.54	1.29	1.72	1.22	1.38	1.75	1.78	2.00
Tm	0.33	0.17	0.17	0.24	0.19	0.25	0.17	0.20	0.26	0.26	0.28
Yb	2.06	1.05	1.04	1.44	1.18	1.57	1.09	1.21	1.65	1.67	1.80
Lu	0.31	0.17	0.16	0.22	0.17	0.22	0.15	0.17	0.25	0.26	0.27
W					96	136	200	142			595
Pb					7.17	6.11	6.25				10.0
Ge					1.55	1.75	1.85	1.43			
$(La/Ce)_N$	1.1	1.3	1.2	1.1	1.2	1.1	1.1	1.2	1.1	1.2	1.2
$(La/Sm)_N$	2.5	2.5	2.2	2.3	3.1	2.2	2.8	3.2	2.1	2.9	3.5
$(La/Yb)_N$	7.3	6.7	5.8	5.3	9.2	9.0	13.0	11.7	3.8	6.1	13.9
$(Dy/Yb)_N$	1.3	1.4	1.4	1.2	1.3	1.4	1.6	1.4	1.1	1.2	1.4

Table 3-4: Sm–Nd isotopic data for the mafic dykes from the Gagnon Terrane. Model ages were calculated with respect to a depleted mantle model (T_{DM2}) and De Paolo's mantle model (De Pal; De Paolo, 1981). The T_{DM2} model uses a mantle isolated from the CHUR (chondrite uniform reservoir) since 4.55 Ga following a linear evolution and with a present day ε_{Nd} value of +10. 2SE (M) = standard error of the mean (G1 = Group 1and G2 = Group 2; see Table 3-3).

Sample	Nd (ppm)	Sm (ppm)	$^{147}Sm/^{144}Nd$	$^{143}Nd/^{144}Nd$	2SE(M)	$\varepsilon_{Nd}(0)$	$\varepsilon_{Nd}(1750)$	De Pal (Ma)	T_{DM2} (Ma)
288d1 (G1)	9.09	3.28	0.2181	0.511973	5	- 13.0	- 17.9	-	-
2000x (G1)	15.56	2.90	0.1125	0.511777	5	- 16.8	+ 2.1	1905	2063
262-1a (G1)	25.63	5.34	0.1260	0.511881	5	- 14.8	+ 1.1	2019	2199
486d (G2)	11.62	2.65	0.1378	0.511841	5	- 15.5	- 2.3	1765	2618
474d (G2)	34.58	6.47	0.1131	0.511543	5	- 21.4	- 2.6	2277	2426

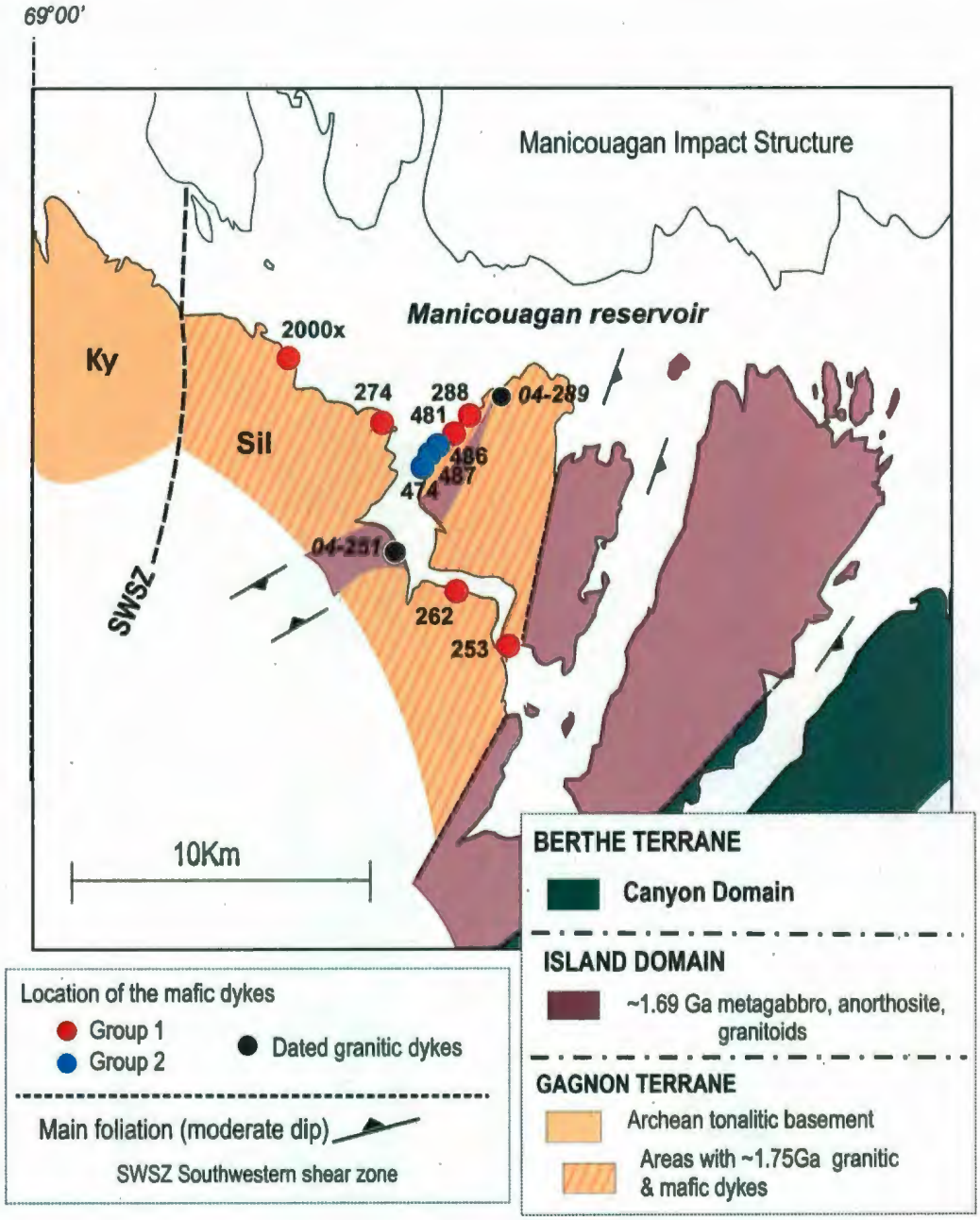

Figure 3-1: Geological map of the south shore of the Manicouagan reservoir showing the location of the mafic dykes from the Gagnon Terrane. Geochemical groups: Group 1 = samples that lack negative Nb anomalies; Group 2 = samples with Nb anomalies. Data for the dated granite dykes (Gagnon Terrane; 04-289 and klippe/Island Domain; 04-251) is from Dunning and Indares (pers. comm. 2008).

(a) 253

(b) 262

(c) 274

(d) 288

(e) 474

(f) 486

Figure 3-2: Outcrop photos of characteristic mafic dykes in the Gagnon Terrane. These dykes are variably attenuated and cut the main foliation of the country rock at variable angles.

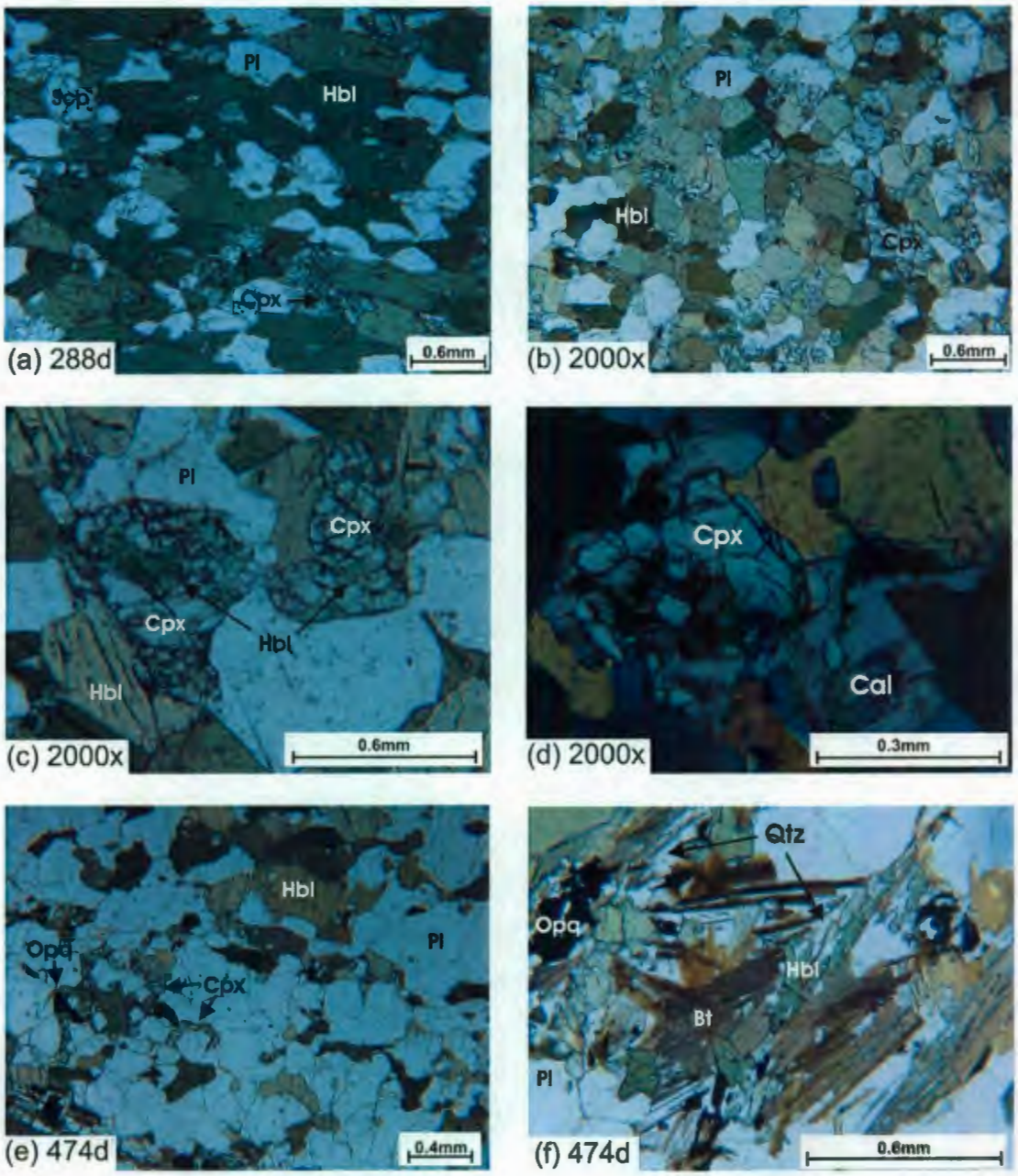

Figure 3-3: Microphotographs showing typical textures of the mafic dykes from the Gagnon Terrane (d taken under cross polarized light; remaining under plane polarized light). Hbl: hornblende, Pl: plagioclase, Bt: biotite, Cpx: Clinopyroxene, Qtz: quartz, Cal: carbonates, Opq: opaques and Scp: scapolite. (a) equigranular plagioclase, hornblende and minor clinopyroxene and scapolite; (b) equigranular hornblende and plagioclase with interstitial clinopyroxene; (c) clinopyroxene corroded by hornblende along rims and interior; (d) clinopyroxene partially replaced by carbonates; (e) equigranular plagioclase and hornblende with clinopyroxene along plagioclase rims; and (f) aggregates of biotite, hornblende and opaques inter-grown with quartz

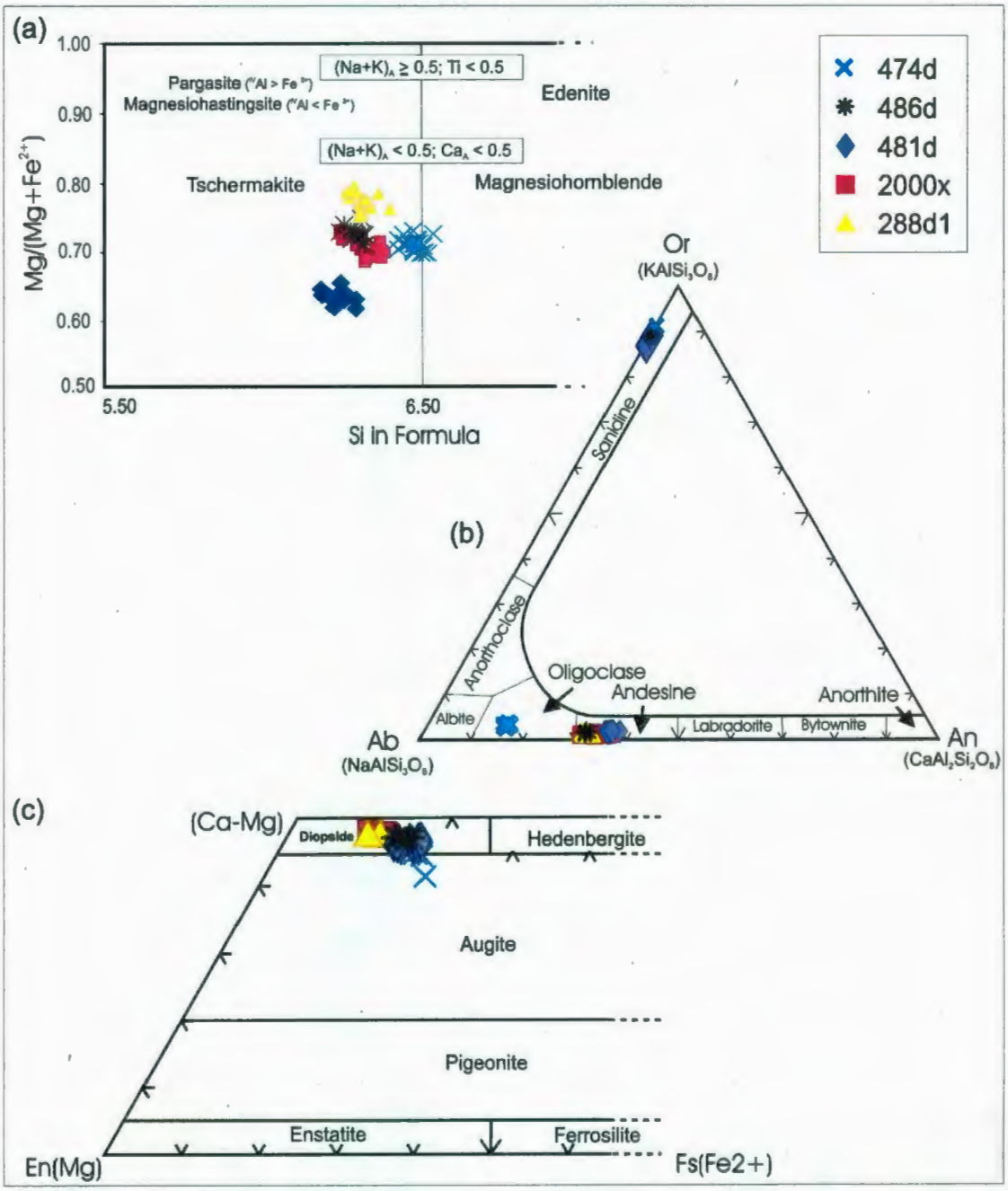

Figure 3-4: Composition/classification diagrams for major minerals in the mafic dykes from the Gagnon Terrane (a) amphibole (after Leake et al. 1997, 2004); (b) feldspars; and (c) pyroxene (after Morimoto et al. 1988). The standard amphibole formula is $AB_2^{VI}C_5^{IV}T_8O_{22}(OH)_2$, where A, B, C, T, O and OH are crystallographic sites. All the amphiboles are calcic ($(Mg, Fe^{2+}, Mn^{2+}, Li)_B \leq 0.50$; $(Ca, Na)_B \geq 1.0$ and Na_B between 0.5-1.50 and, usually, $Ca_B \geq 1.50$ (atoms per formula unit). Those with $(Na + K)_A \geq 0.5$ and $Ti < 0.5$ are classified as pargasite/magnesiohastingsite or edenite while those with $(Na+K)_A < 0.5$ and $Ca < 0.5$ are classified as magnesiohornblende or tschermakite based on Si in the formula.

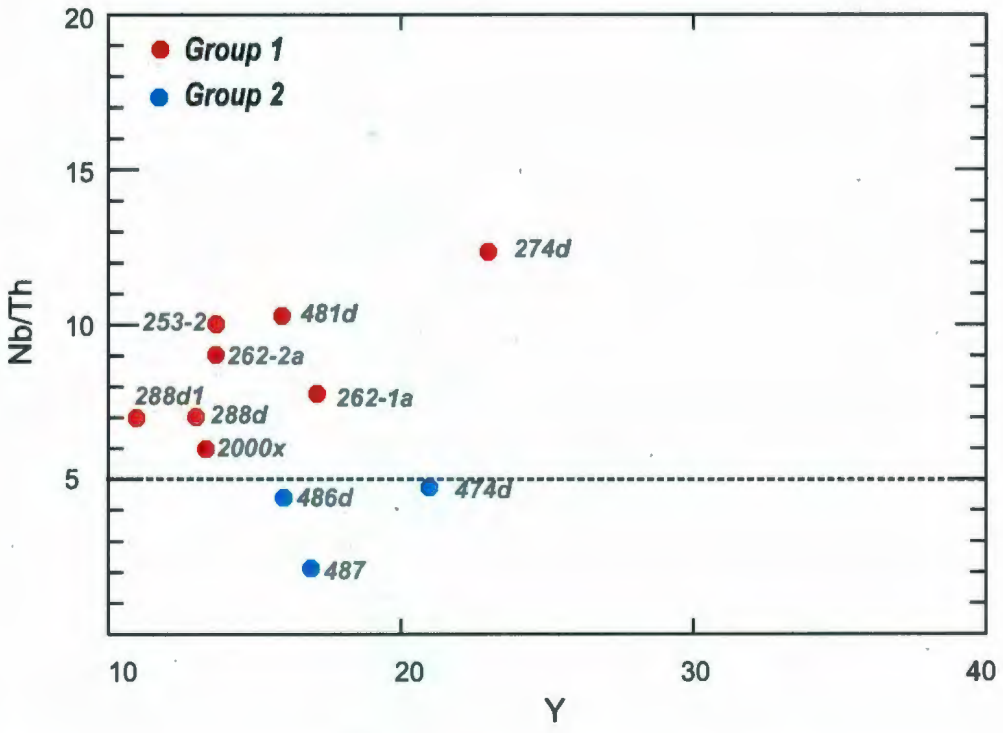

Figure 3-5: Y versus Nb/Th diagram of Swinden et al., (1997) for the mafic dykes from the Gagnon Terrane. Geochemical groups: Group 1 = samples with Nb/Th > 5; Group 2 = samples with Nb/Th < 5.

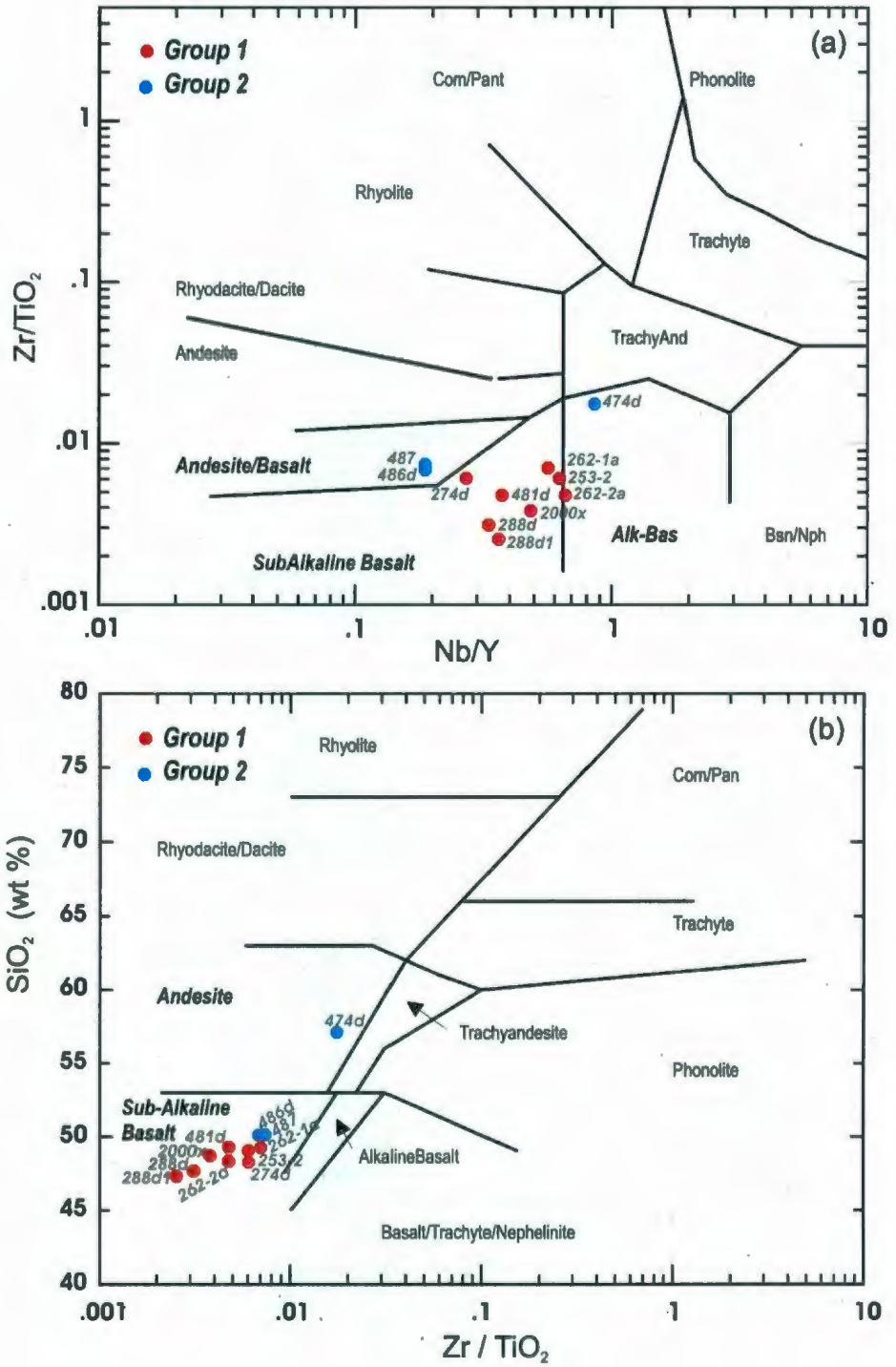
(a)
Group 1
Group 2
Com/Pant
Phonolite
Rhyolite
Trachyte
Rhyodacite/Dacite
TrachyAnd
Andesite
474d
Andesite/Basalt
487
486d
274d
481d
262-1a
253-2
262-2a
2000x
288d
288d1
Alk-Bas
Bsn/Nph
SubAlkaline Basalt
Zr/TiO2
Nb/Y
.001
.01
.1
1
10
(b)
Group 1
Group 2
Rhyolite
Com/Pan
Rhyodacite/Dacite
Trachyte
Andesite
474d
Trachyandesite
Phonolite
Sub-Alkaline Basalt
AlkalineBasalt
Basalt/Trachyte/Nephelinite
SiO2 (wt %)
Zr / TiO2
40
45
50
55
60
65
70
75
80

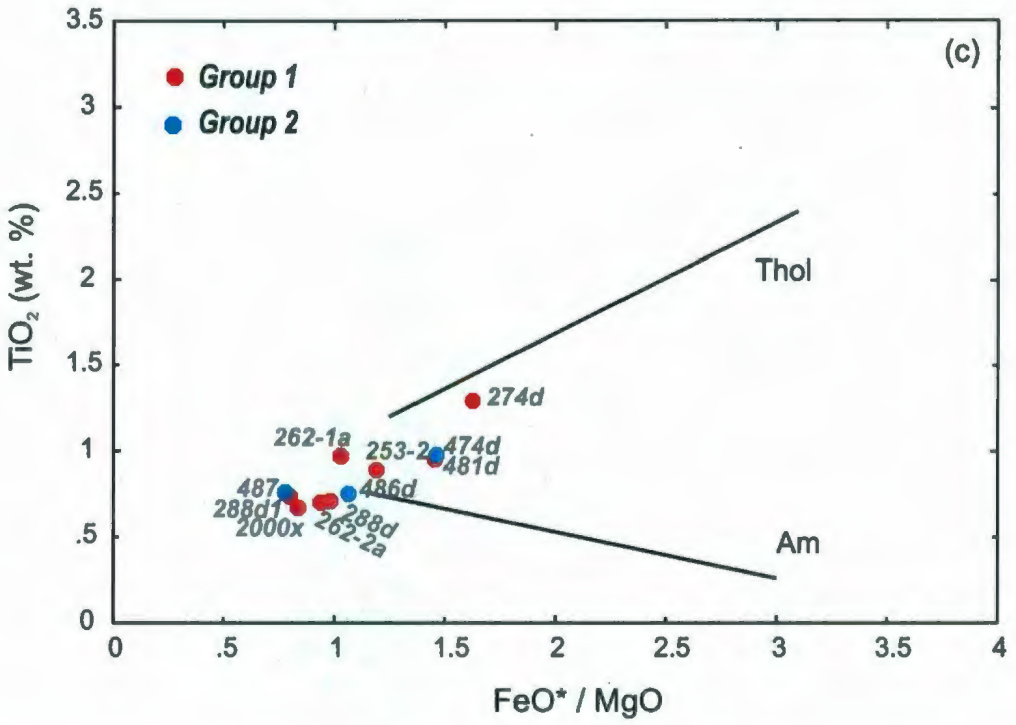

Figure 3-6: Plots of (a) Nb/Y vs. $Zr/TiO_2 \times 10000$ diagram (the Nb/Y ratio acts as an alkalinity index and the Zr/TiO_2 ratio acts as a differentiation index); (b) Zr/TiO_2 vs. SiO_2 (Winchester and Floyd, 1977 and 1978); and (c) TiO_2 - FeO*/MgO diagram of Myashiro (1974) for mafic dykes from the Gagnon Terrane. Geochemical groups as defined in Figure 3-5.

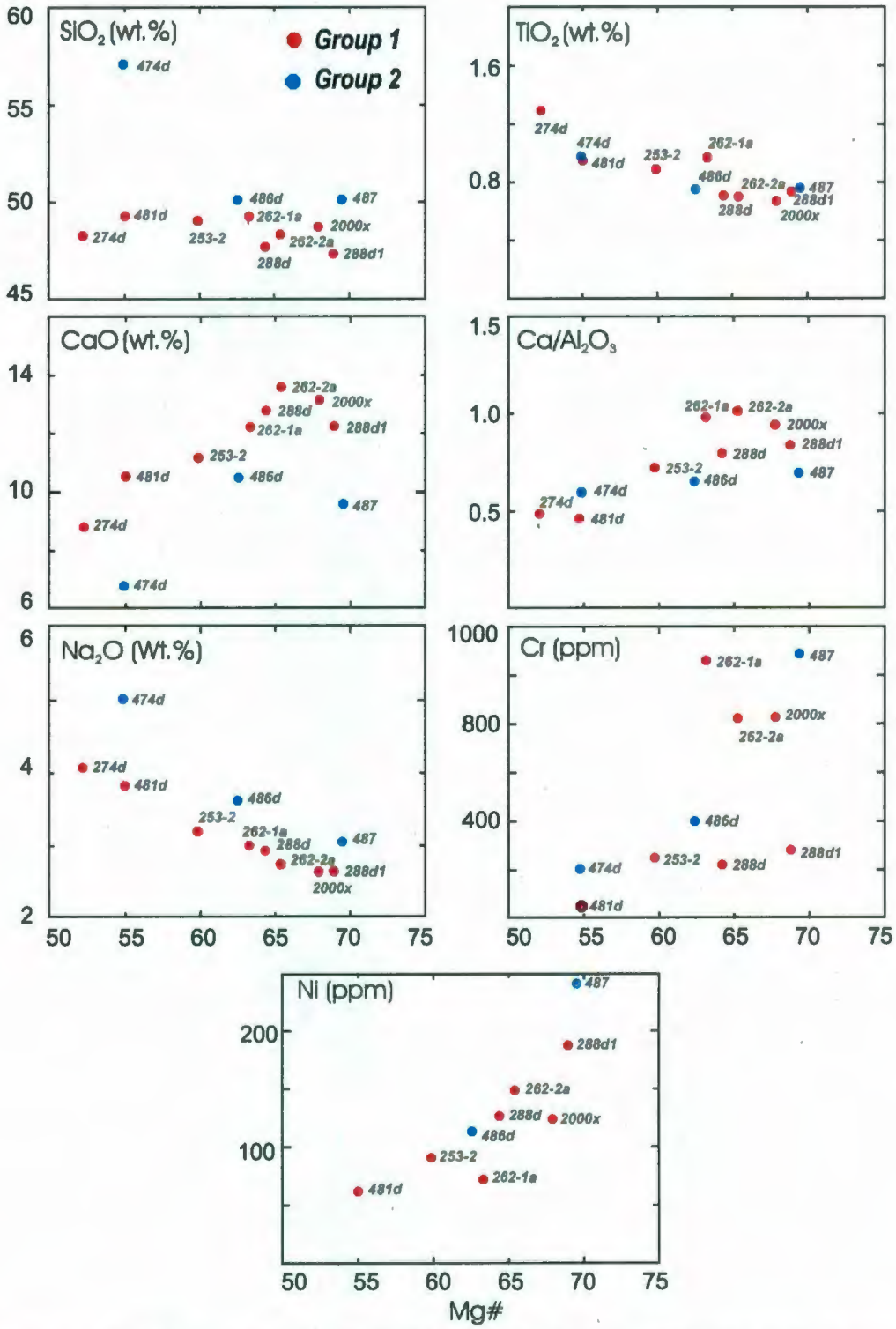

Figure 3-7: Variation of SiO_2, CaO, CaO/Al_2O_3, Na_2O, Cr and Ni with Mg#, where Mg# = [molar (MgO/MgO+FeO)] x 100 for mafic dykes from the Gagnon Terrane. Groups as defined in Figure 3-5.

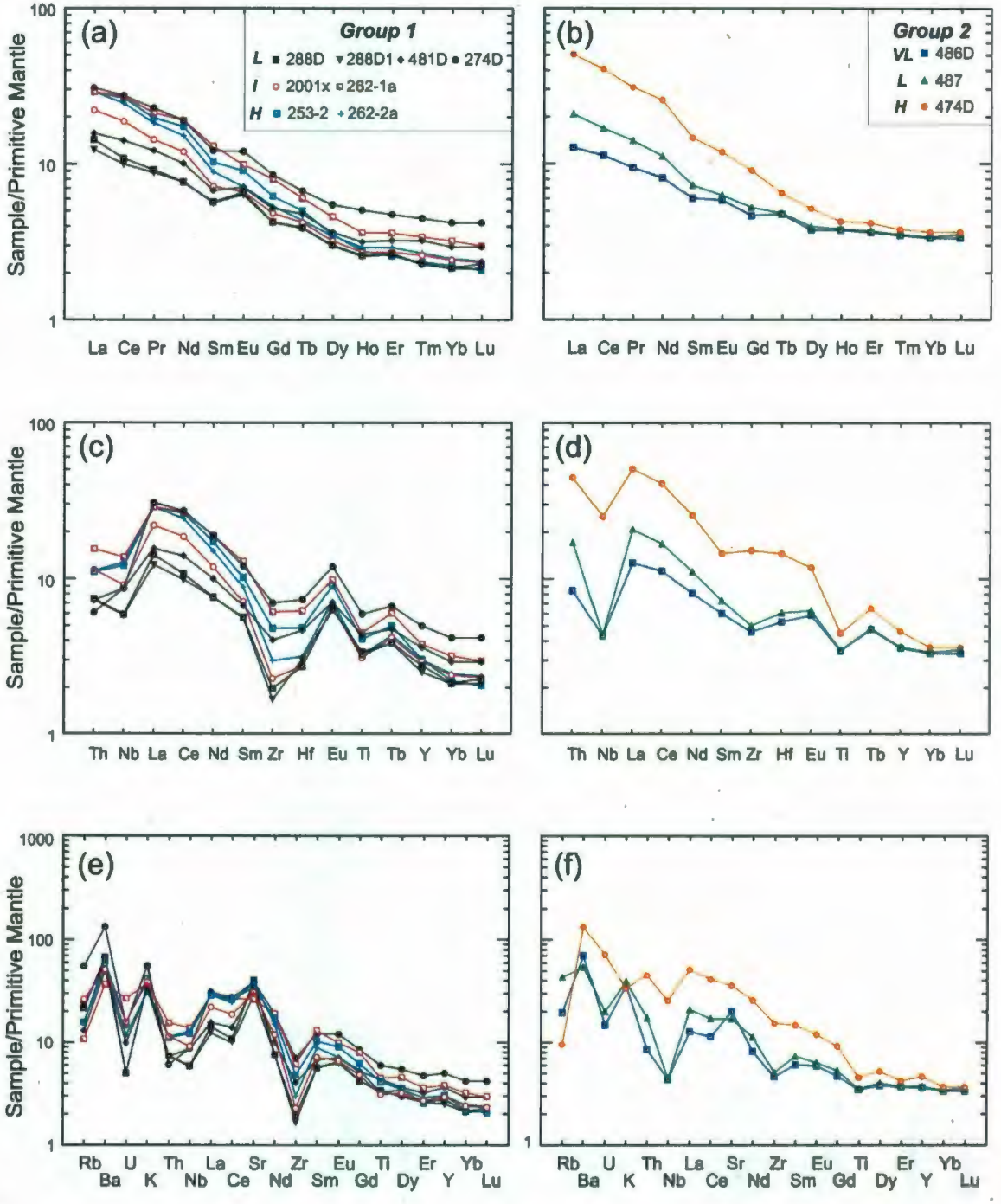

Figure 3-8: a-b) Primitive mantle normalized REE; c-d) extended (REE, HFSE, Th); and e-f) complete REE, HFSE & LFSE plots for the mafic dykes from the Gagnon Terrane. ***VL*** = very low (<4); ***L*** = low (4-8); ***I*** = intermediate (8-11) and ***H*** = high (>11) primitive mantle normalized $(La/Yb)_N$ ratios. Normalizing values after Sun and McDonough (1989).

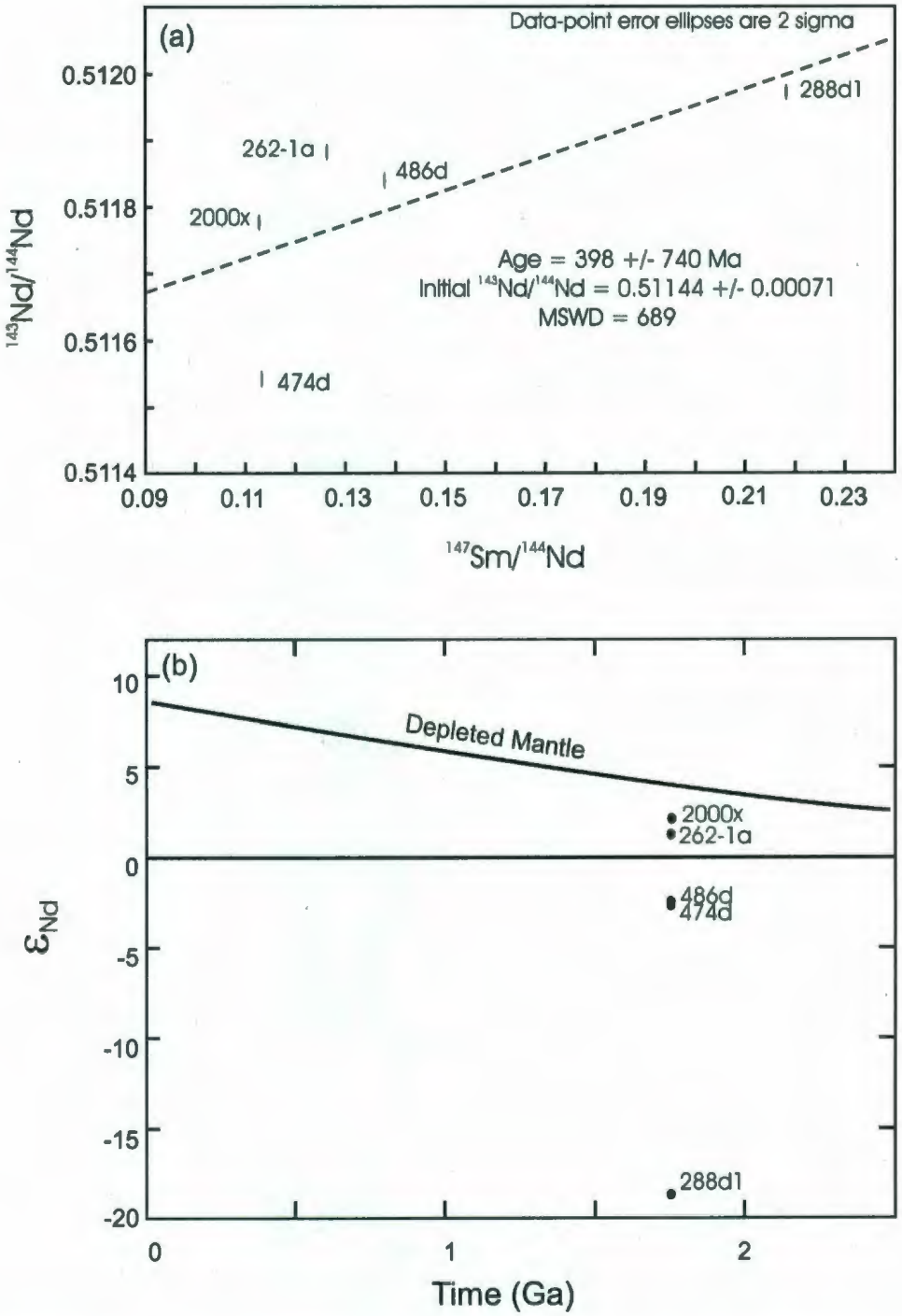

Figure 3-9: (a) $^{143}Nd/^{144}Nd$ versus $^{147}Sm/^{144}Nd$ diagram and (b) plot of initial ε_{Nd} versus age (T=1750Ma) for mafic dykes from the Gagnon Terrane. The depleted mantle curve is from De Paolo (1981).

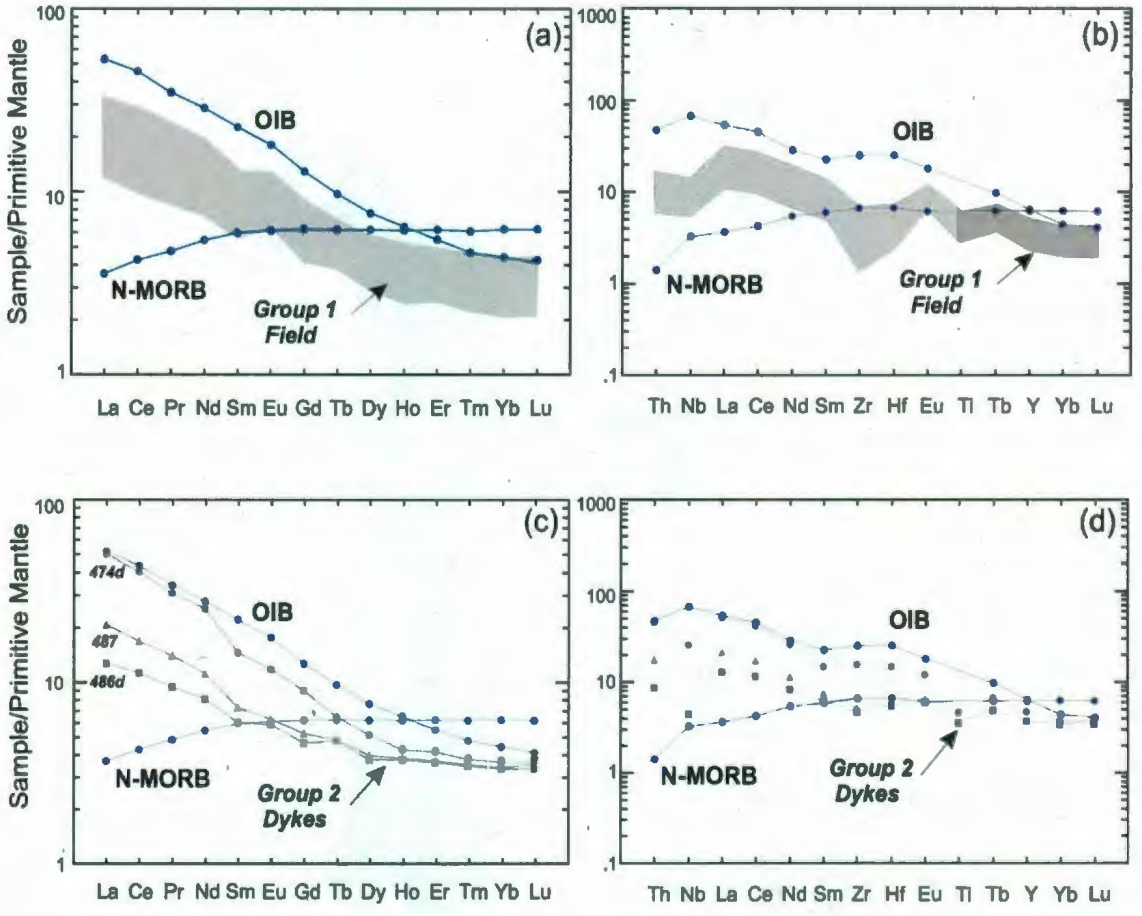

Figure 3-10: Primitive mantle normalized diagrams showing REE and selected HFSE concentrations for typical OIB, N-MORB basalts and mafic dykes from the Gagnon Terrane. (a-b) shows the field for the dykes of Group 1 and (c-d) the dykes of Group 2. OIB, N-MORB concentrations and normalizing values after Sun and McDonough (1989).

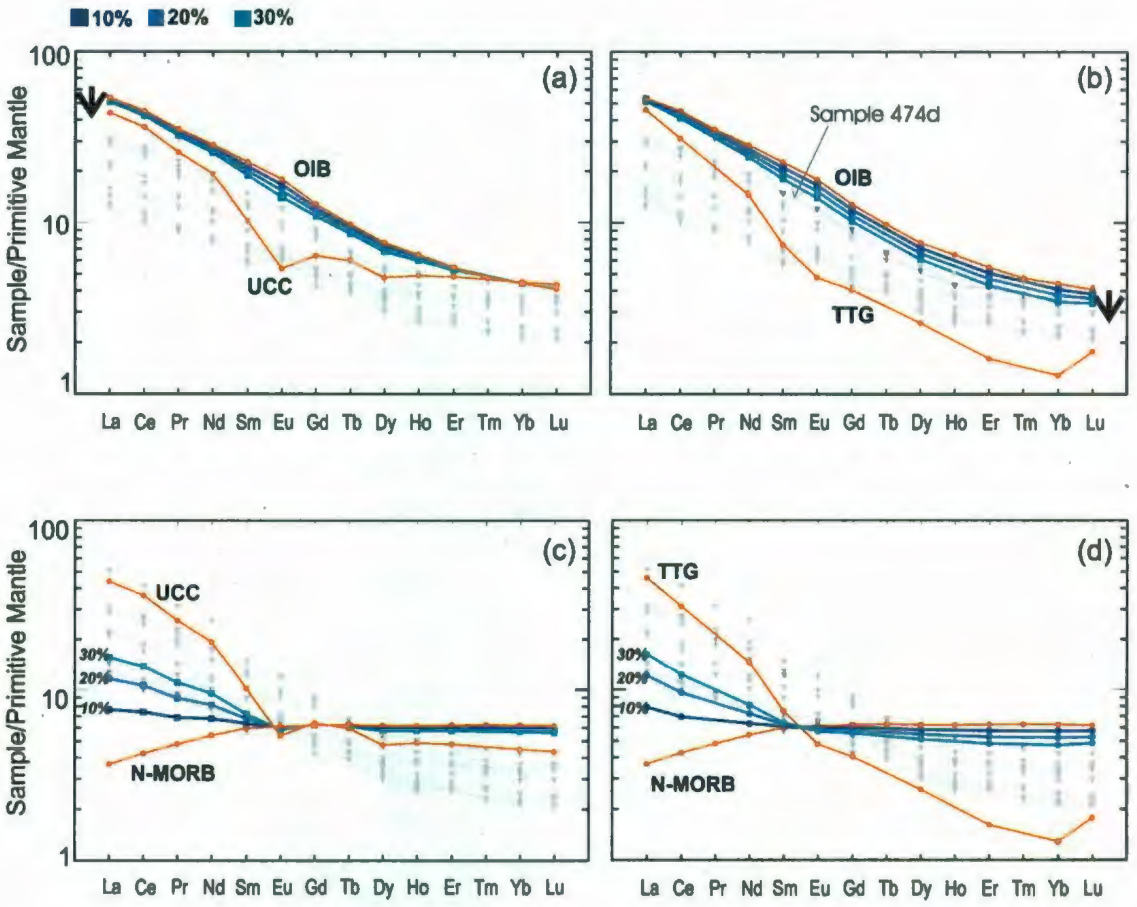

Figure 3-11: Primitive mantle normalized REE concentrations calculated for an (a-b) OIB and a (c-d) N-MORB component with 10, 20 and 30% contamination by average upper continental crust (UCC; Taylor and McLennan, 1981) and Archaean (3 -3.5Ga) tonalite-trondhjemite-granodiorite (TTG; Martin, 1994; Martin and Moyen, 2002). The mafic dykes from the Gagnon Terrane are shown in grey for comparison. Arrows indicate the direction of increasing contamination. Normalizing values after Sun and McDonough (1989).

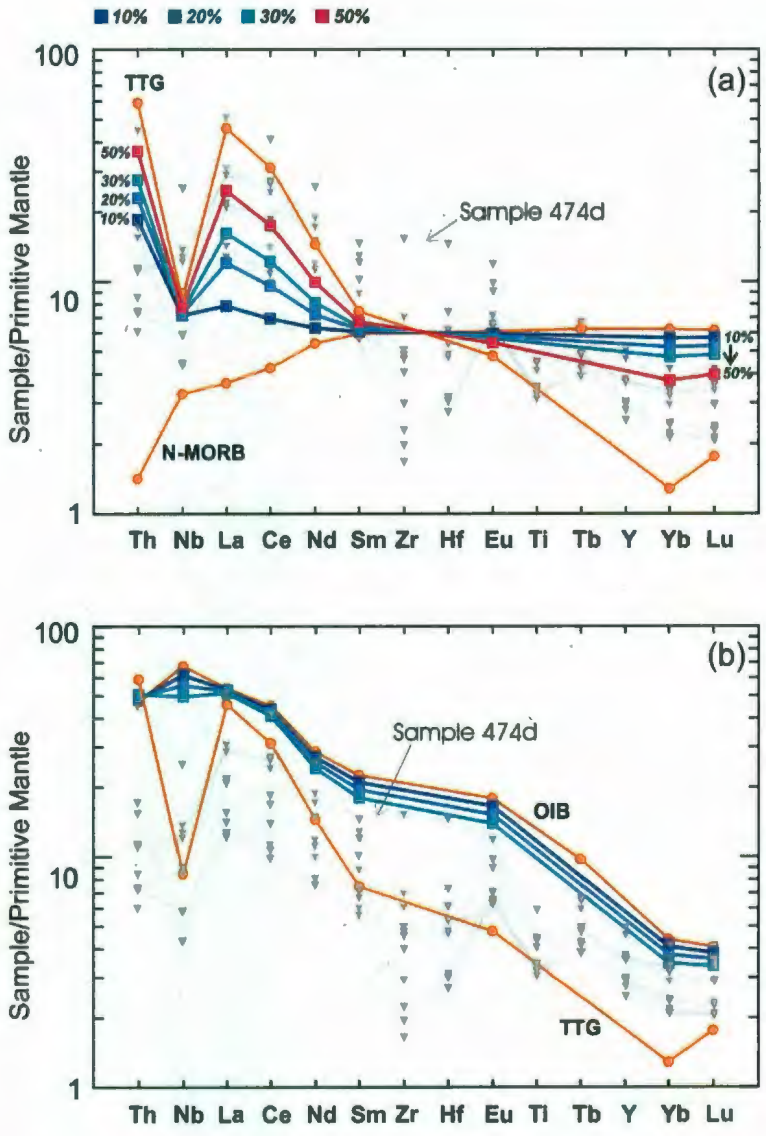

Figure 3-12: Primitive mantle normalized REE and HFSE concentrations calculated for an (a) N-MORB and (b) OIB component with 10, 20, 30 and 50% contamination by an average Archaean tonalite-trondhjemite-granodiorite (TTG; Martin, 1994; Martin and Moyen, 2002). Mafic dykes from the Gagnon Terrane are shown in grey for comparison. Normalizing values after Sun and McDonough (1989).

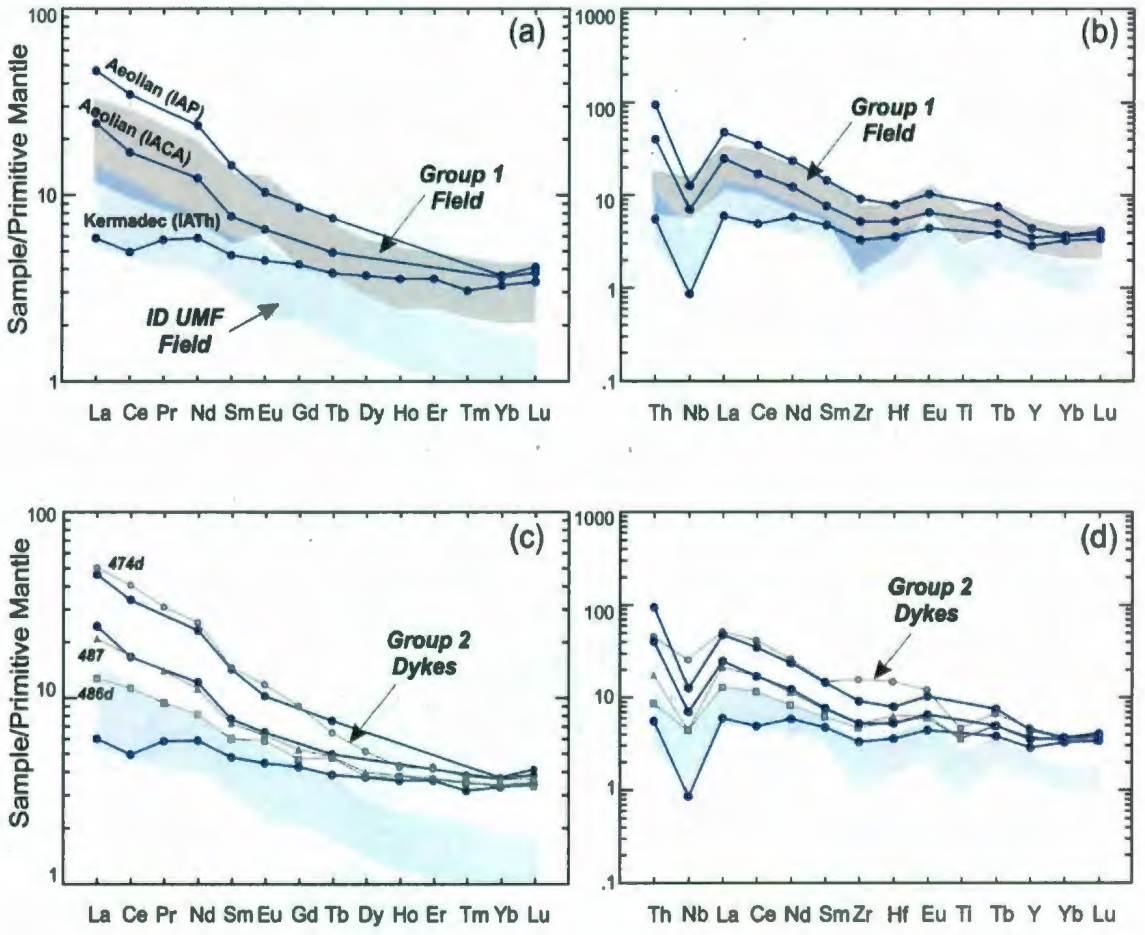

Figure 3-13: Primitive mantle normalized plots showing REE and selected HFSE concentrations of selected island arcs, the field for the ultramafic rocks (UMF) from the Island Domain and the mafic dykes from the Gagnon Terrane. (a-b) shows the field for the dykes of Group 1 and (c-d) the dykes of Group 2. IACA: calc-alkaline basalt (Salinas; sample ESAL14) and IAP: potassic basalt (Volcano older series; sample EVUL17) from the Aeolian Islands (Ellam et al., 1988). IATh: tholeiite basalt (Macouley Is. Sample 10380) from the Kermadec Islands (Ewart et al., 1977). Normalizing values after Sun and McDonough (1989).

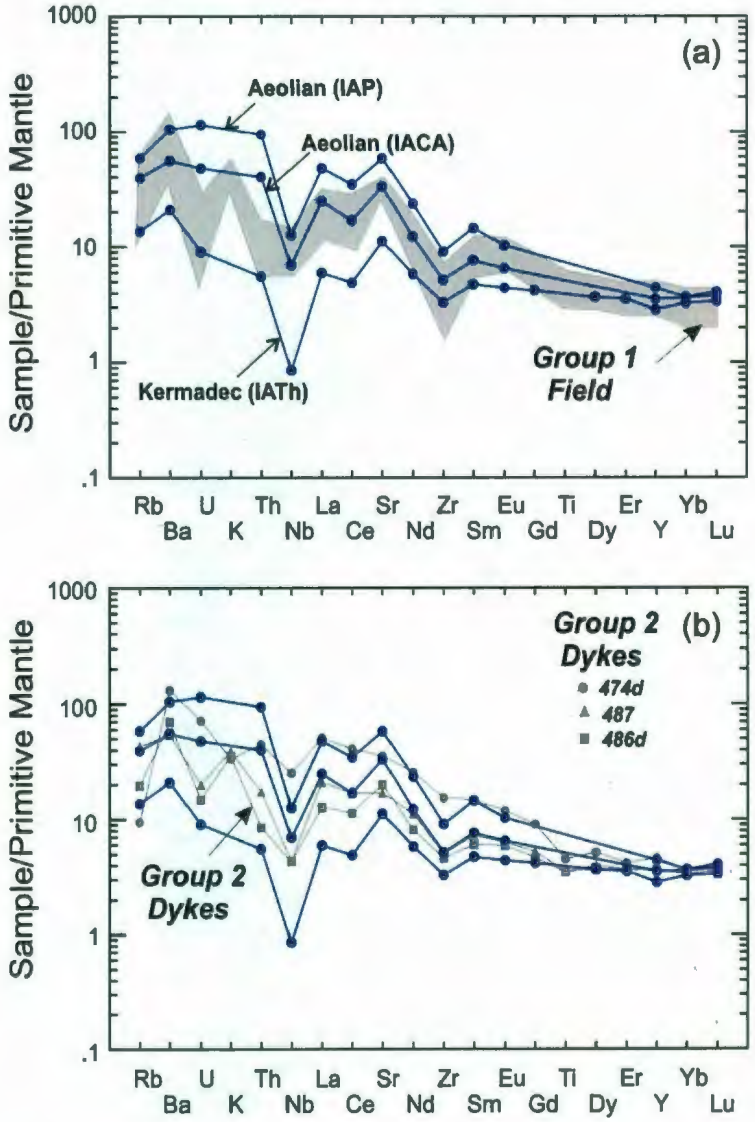

Figure 3-14: Primitive mantle normalized plots showing the REE, HFSE and LFSE concentrations of selected island arc basalts and the mafic dykes from the Gagnon Terrane. (a) Shows the field for the dykes of Group 1 and (b) the dykes of Group 2. IACA: calc-alkaline basalt (Salinas; sample ESAL14) and IAP: potassic basalt (Volcano older series; sample EVUL17) from the Aeolian Islands (Ellam et al. 1988). IATh: tholeiite basalt (Macouley Is.; Sample 10380) from the Kermadec Islands (Ewart et al. 1977). Normalizing values after Sun and McDonough (1989).

CHAPTER 4: MAFIC DYKES IN THE CANYON DOMAIN

4.1 Introduction

Mafic dykes occur in the Canyon Domain, mainly in the northern part near the boundary with the Island Domain, but also elsewhere (Fig. 4-1). The age of these dykes is unknown; however, they intrude the ~1.4Ga volcanoclastic sequence of Canyon Domain (Indares and Dunning, pers. Comm. 2008) and, although they locally crosscut the foliation of the country rock, they are in general deformed and metamorphosed. Therefore, they must have been emplaced in the time interval between the ~1.4 Ga deposition of the country rock and the Grenvillian metamorphism and deformation. In addition, because the dykes are variably deformed, field relations that could be indicative of two or more generations of dykes have not been preserved.

The 1.4 Ga rocks are correlative in terms of age and setting with those of the Montauban arc, identified further to the SSW, and inferred to represent remnants of an island arc (Corrigan and van Breemen, 1997). In addition, ~1.2 Ga metavolcanic rocks, interpreted to have been formed in a back-arc setting, were recently recognized between the Canyon Domain and the Gabriel Complex (Banded Complex; Fig. 4-1) and at the southern margin of the Tshenukutish Terrane (Dunning and Indares, pers. comm. 2008). It is, therefore, possible that the mafic dykes are related to (and depending on their geochemical signature they have the potential to provide further constraints) either one of these two events.

More specifically, the study of the mafic dykes in the Canyon Domain may constrain the original relationship between the ~1.2 Ga units of the Banded Complex and the ~1.4 Ga crustal edifice of the Canyon Domain, which is unknown, as their present juxtaposition may result from tectonic transport during the Grenvillian orogeny. For instance if the mafic dykes bear a geochemical signature consistent with a back arc setting of emplacement, it would suggest that the 1.2 back-arc basin developed in proximity to the Canyon Domain units.

4.2 Field occurrence

The mafic dykes in the northern portion of the Canyon Domain (Fig. 4-1 and Fig. 4-2) are of three types based on field relations. The first type consists of 20-30 cm wide mafic layers with sharp boundaries in banded granitic gneiss (locations #430, 431; Fig. 4-2a-b). These are located along a major NE-trending lineament that is parallel (and is located close) to the NW boundary of the Canyon Domain. The relation between deformation and the emplacement of these layers is not conclusive (*i.e.* they could either be emplaced late as sills, along the tectonic layering, or as dykes before the main deformation, in which case they got transposed together with the country rock).

The second type consists of dykes (maximum width 20-30 cm) in banded quartzo-feldspathic gneiss (location #214; Fig. 4-2c-d) that cut the main fabric of the country rock at low angle and are "pinched out". Finally, a mafic dyke in mafic migmatite (location #314; Fig. 4-2e) that has clear contacts with the country rock, but has irregular

width (dm to cm); this is consistent with emplacement in a ductile environment. In addition, this dyke is cut by ± folded felsic material and displays an internal fabric.

Further south, in the central Canyon Domain (Fig. 4-1 and Fig. 4-2), two ~10 cm wide mafic dykes intrusive into banded quartzo-feldspathic gneiss were identified (locations #209-1 and #457; Fig. 4-2f-g). These dykes have internal fabric that cuts the main fabric of the country rock, but they are attenuated, boudinaged and folded. Finally, in the southern part of the domain, there is a 10-20 cm wide mafic dyke with sharp boundaries crosscutting the main fabric in banded quartzo-feldspathic gneiss (location #413; Fig 4-1 and Fig. 4-2h).

4.3 Mineralogy, textures and mineral chemistry

The mafic dykes have a mineralogy dominated by hornblende and plagioclase ± orthopyroxene ± clinopyroxene ± garnet. Biotite, apatite, quartz and opaques are present in minor and trace amounts (Table 4-1; Fig 4-3 and Fig 4-4). One sample, 431, is highly altered and contains a vein of scapolite and quartz. Overall the texture is equigranular (Fig. 4-3a-d). All the minerals have curved to straight boundaries and triple junctions are common. Hornblende and, when present, biotite define the foliation.

Clinopyroxene and orthopyroxene usually occur isolated or as aggregates (Fig. 4-3b-c). In sample 209-1, clinopyroxene is corroded by hornblende (Fig. 4-3d). In sample 431, clinopyroxene is commonly rimed by hornblende and biotite and contains numerous worm-like inclusions of quartz and opaques (Fig. 4-3e-f). Clinopyroxene, in sample 314, is restricted to a vein/layer that also contains plagioclase and orthopyroxene. This

clinopyroxene is partially replaced by hornblende along its rims and cleavage. Garnet forms isolated grains and contains inclusions of feldspar, apatite and opaques (Fig. 4-3g).

Biotite forms ubiquitous dark brown flakes (Fig. 4-3h); however, in sample 431, it has an irregular shape and corrodes hornblende and opaques (Fig. 4-3e). In addition, both biotite and hornblende in sample 431 locally contain worm like inclusions of quartz and opaques. Opaques (magnetite and ilmenite) occur as blebs, locally included in plagioclase and hornblende, and as an interstitial phase (Fig. 4-3). Quartz is generally interstitial and is concentrated in a plagioclase-rich band in sample 209-1 (Fig. 4-4).

4.3.1 Mineral compositions

Feldspars, hornblende, pyroxenes, opaques, biotite and garnet (sample 457) were analysed in three representative samples (Table 4-2 and Figure 4-5; mineral analyses are listed in Appendix 1). Based on the amphibole classification scheme of Leake *et al.*, (1997, 2004) hornblende is pargasite-magnesiohastingsite with XMg_{63-66} in sample 430, ferro-pargasite with XMg_{47-49} in sample 457 and edenite-pargasite-tschermakite with XMg_{69-66} in sample 209-1 (Fig. 4-5a). Plagioclase has a wide range of anorthite contents in sample 430 (An_{53-68}; labradorite); is homogeneous and rich in anorthite in sample 209-1 (An_{75-80}; bytownite); and is relatively poor in anorthite in sample 457 (An_{36-38}; andesine; Fig. 4-5b). Based on the pyroxene nomenclature described by Morimoto (1988), orthopyroxene falls in the compositional field of enstatite (samples 209-1 and 430) and ferrosilite (sample 457) while clinopyroxene falls in the field of diopside and extends into the field of augite in sample 209-1 (Fig. 4-5c). In sample 457, garnet is rich

in almandine (Al_{65-67}) and biotite has an XMg of 47-50. Opaques were identified as ilmenite and magnetite.

4.3.2 Interpretation of textures

The foliation and equigranular texture exhibited by the samples are consistent with these rocks having experienced pervasive metamorphism and deformation. In addition, they exhibit mineral assemblages (*i.e.* plagioclase + hornblende ± clinopyroxene ± orthopyroxene ± garnet) characteristic of medium-P granulite facies conditions (Pattison, 2003). In all the samples, orthopyroxene, clinopyroxene and (except for sample 431) hornblende are clearly part of the peak assemblage and in most cases they appear stable. However, extensive replacement of clinopyroxene by quartz - opaque intergrowths and hornblende, with, locally, biotite (sample 431), and local replacement of clinopyroxene by hornblende (sample 209-1) indicates that part of the hornblende postdates the clinopyroxene, consistent with fluid infiltration (retrograde metamorphism) after the formation of clinopyroxene. Note that the granulite facies metamorphism in the Canyon Domain is dated at ~1080-1060 Ma (Dunning and Indares, pers. comm. 2008) and places a lower age limit on the mafic dykes.

4.4 Geochemistry

The mafic dykes of the Canyon Domain have experienced metamorphism at granulite facies. Owing to the possibility of element mobilization during metamorphism and late hydration, we concentrate on elements that are relatively immobile. These elements

include the rare earth elements (REE), Th (a low field strength element, LFSE) and the high field strength elements (HFSE; see section 2-1). Because of the metamorphic grade, we are aware that care is needed in assessing element mobility /immobility.

The samples can be divided into groups based on the presence or absence of pronounced negative Nb anomalies relative to Th and La (see section 2-1). ***Group 1*** consists of samples that lack a negative Nb anomaly and includes 457, 214b, 430 and 431. Sample 413, also lacks a negative Nb anomaly; however, it has a much higher $(La/Yb)_N$ ratio than all of the other samples. Thus, it will be treated as *Group 1a*. ***Group 2*** consists of samples that exhibit a pronounced negative Nb anomaly (relative to La and Th) and includes 209-1, 214a and 314.

4.4.1 Major and trace element composition

Major and trace element abundances are listed in Table 4-3. The Zr/TiO_2-Nb/Y and ZrTiO2-SiO_2 diagrams (Fig. 4-6) of Winchester and Floyd (1977; 1978) suggest that the mafic dykes are sub-alkalic basalts to andesite-basalts. In addition, the variation of TiO_2 with FeO*/MgO (Myrashiro, 1974; Fig 4-7) and/or TiO_2 with Mg# (Mg# =[molar MgO/(MgO + FeO*)]; Fig. 4-8) indicate a tholeiitic nature for these rocks.

Samples of *Group 1* and *2* have SiO_2 of ~46 to 53 wt.%, with those in *Group 2* having the highest values, and a wide range of Mg# (39–61; Fig. 4-8). In these rocks, FeO ranges from 10.7 to 15.8wt %, CaO from 7.8 to 11wt%, Al_2O_3 from 15 to 17% and K_2O+Na_2O from 0.98 to 4.94 wt.%. *Group 1a* (sample 413), has the highest SiO_2 (57 wt.%) and the lowest MgO, FeO, CaO and Al_2O_3 of all the samples (Table 4-3). In

general, the Mg# shows a weak to moderate positive correlation with CaO and CaO/Al_2O_3 ratios and a weak negative correlation with Na_2O. In addition, there is a general decrease in the REE with increasing Mg-number.

The samples are characterized by a low to high TiO_2 (0.89 to 3.21wt%) contents. Ni and Cr concentrations exhibit a wide range; with sample 431 having extremely high Ni (756ppm) and Cr (514ppm) compared to the other samples. Ni shows a weak positive correlation with Mg#, except for sample 431, while Cr shows considerable scatter when plotted against Mg# (Fig. 4-8). Note that Ni in samples 413 and 457 is below detection.

4.4.2 Extended REE plots

The immobile element data are illustrated in primitive mantle normalized plots (Fig. 4-9 a-b, REE; c-d, all). Figures 4-9 e and f show a more complete spectrum of trace element data including other potentially mobile LFSE like Rb, Ba, U, and Sr. The samples display smoothly decreasing abundances of the REE from enriched LREE to slightly depleted HREE. The samples from both *Group 1* and *2* display low $(La/Yb)_N$ ratios (2.1-4), while sample 413 (*Group 1a*) has a much higher $(La/Yb)_N$ ratio (10.8). In addition, sample 209-1 displays a strong negative Eu anomaly (Fig. 4-9a-b).

Samples of *Group 1* display "smooth" extended patterns (REE and HFSE) and lack negative Nb anomalies (Fig 4-9c). Only two samples (457 and 431) are enriched in some LFSE (K, Rb and Ba) relative to the adjacent REE. In addition, samples 457 and 214b are depleted in Sr and sample 430 is enriched in this element (Fig. 4-9e). Sample 413 (*Group 1a*), has low concentrations of Nb and Th compared to La, so that its pattern

do not show a significant Nb anomaly with respect to Th (Fig. 4-9d). This sample is depleted in Sr, Th, K and U and enriched in Ba and Rb relative to the adjacent REE.

The samples of *Group 2* display negative Nb anomalies, are weakly to strongly depleted in Zr and sample 209-1 is depleted in Ti (Fig. 4-9d). Samples 214a and 314 are variably enriched in Ba, K, Rb and Sr. Sample 209-1 displays a distinctive pattern, with depletions of all the HFSE and LFSE relative to the REE, with the exception of U and Th, which are enriched relative to La (Fig. 4-9f).

4.4.3 Sm-Nd isotopic data

Sm-Nd isotopic data for three samples from *Group 1* (431, 430 and 214b) and one sample from *Group 2* (241a) are presented in Table 4-4. When the data is plotted on a $^{143}Nd/^{144}Nd$ versus $^{147}Sm/^{144}Nd$ diagram the scatter is obviously too great to represent an isochron (Fig. 4-10a). The errorchron "age" is 1330 +/- 780 Ma, with an initial $^{143}Nd/^{144}Nd$ ratio of 0.51121 ± 0.00077. The excess scatter may indicate that the samples are not all the same age or that they did not originate from the same source region. Model ages were calculated with respect to a depleted mantle model (T_{DM2}) and De Paolo's mantle model (De Paolo, 1981) (see section 2-1) and are listed in Table 4-4.

As indicated previously, the age of the mafic dykes is bracketed between 1.4 and 1.08 Ga. In addition, they are potentially related to either one of two events recognized at ~1.4Ga and at ~1.2 Ga. Thus, measured Nd isotope ratios were calculated back to 1300 Ma and expressed as the deviation from a chondritic uniform reservoir at that time ($\varepsilon_{Nd}{}^{1300}$). This data is illustrated in a ε_{Nd} versus time diagram (Fig. 4-10b). The $\varepsilon_{Nd}{}^{1300}$ values

of the samples range from +4.6 to +6.2, with those of *Group 1* slightly higher (+ 6.1 to 6.2) than those of *Group 2* (+ 4.6 to 5.4), indicating derivation from a source that has a time-integrated depletion in the LREE.

4.5 Interpretation and Discussion

The mafic dykes of the Canyon Domain have experienced pervasive metamorphism under granulite facies conditions as indicated by their mineral assemblage and texture. Therefore, our interpretation focuses on the relatively immobile HFSE and REE (see section 2-1).

The mafic dykes of the Canyon Domain are sub-alkaline tholeiitic basalts to andesites. The dykes represent relatively evolved mafic magmas with Mg# and contents of compatible trace elements such as Ni and Cr that are too low to have been derived directly from a mantle reservoir (Perfit *et al.*, 1980). These evolved mafic dykes must, therefore, represent magmas that have fractionated since segregating from their mantle source. Although there are a few samples (*e.g.* 314 and 430) with high Mg contents and Mg# (60-61), their low concentrations of Ni and Cr (173–210ppm and 93-184ppm, respectively) indicate that they too are unlikely to be primary melts of a mantle source.

The mafic dykes have remarkably similar REE patterns characterized by slight enrichment of the LREE and a progressive increase of the overall concentration of the REE (La_N = 8-50 and Yb_N = 3.9-9.2). The dykes have $(La/Yb)_N$ = 2-4, with the exception of sample 413, which has an $(La/Yb)_N$ = 10. Three groups have been recognized: the dykes of *Group 2* exhibit negative Nb anomalies relative to Th and La; those of Group *1*

and 1a lack such anomalies and sample 413 *(Group 1a)* has a high $(La/Yb)_N$ ratio compared to all the other samples.

The correlation of Mg# with some major elements and REE as well as the almost parallel REE patterns of the dykes suggest that they could be related to each other by fractional crystallization. However, the presence of negative Nb anomalies in some dykes (*Group 2*) indicates that for the dykes to be related, crustal contamination must have played a role. In the following section we discuss whether fractional crystallization and crustal contamination may be the mechanisms responsible for the observed geochemical trends in the mafic dykes of the Canyon Domain.

4.5.1 Fractional crystallization and crustal contamination

The ability of fractional crystallization to reproduce the trace-element variations within the mafic dykes as a group, except for sample 413, was modeled using the composition of the most magnesium rich dyke (sample 314) and the following proportions of fractionated phases: olivine: 20, clinopyroxene: 30 and plagioclase: 50. It is clear from Figure 4-11a-c that this model cannot account for the extent of variation in trace elements observed within the dykes nor the variation in the range of highly incompatible-element ratios such as La/Sm and Nb/Zr (Fig. 11d-e).

The extent of crustal interaction in the petrogenesis of these rocks is not easily determined. However, Th/Nb ratios, a proxy for the extent of crustal contamination, appear to decrease with increasing Zr contents (Fig. 4-12a), the opposite of what would be expected if the more differentiated melts were the products of assimilation or

contamination processes. This is corroborated by the decrease of La/Nb with Zr (Fig 4-12b).

The above observations suggest that the dykes of *Group 1* and *2* are not related by different degrees of contamination or by fractional crystallization and that the variations in trace elements are the result of two or more magma sources. However, the similar REE patterns (i.e. slopes) suggest that they are derived from similar sources. In addition, the above observations do not preclude the dykes from *Group 1* (*i.e.* rocks with low Th/Nb) from having been contaminated by crustal material. In the following sections we discuss each group separately in terms of magma sources and tectonic setting.

4.5.2 Dykes of Group 1: within-plate basalts?

The lack of Nb anomalies for the dykes of *Group 1*, suggests that these rocks have not been contaminated by crustal material. In addition, assuming the age of the dykes is ~1.3Ga, the positive ε_{Nd} values at that age (+2.4-5.1) also indicate that assimilation of crustal material was insignificant.

Several discrimination diagrams have been proposed to determine tectonic setting of magmatism. High-field strength elements such as Zr, Y and Ti, which are less susceptible to alteration, are found to be particularly useful in determining the tectonic setting of magma generation. Pearce and Norry (1979) showed that the basalts from island arcs, mid-ocean ridges and within-plate environments contain different levels of Zr contents and ratios of Zr/Y (Fig. 4-13a). In this diagram the mafic dykes of *Group 1* have Zr contents and Zr/Y ratios comparable with within-plate basalts. Pearce and Gale (1977)

demonstrated that Nb is typically high in within-plate basalts compared to arc volcanic rocks and MORB basalts. The mafic dykes of *Group 1* contain Nb contents comparable to basalts from within plate setting (Fig. 4-13b). In the diagram of Pearce and Cann (1973), involving Ti, Y and Zr, the dykes also plot in the within-plate basalts field (Fig 4-13c). Finally, in the diagrams of Wood (1980) involving Th, Zr and Nb, most of the dykes of *Group 1* plot as E-type MORB and tholeiitic within plate basalts (Fig. 4-13d).

The above discrimination diagrams suggest that some of the mafic dykes (*Group 1)* of the Canyon Domain are within-plate basalts. Distinction between continental and oceanic within-plate basalts is difficult. However, the REE patterns of these dykes fall in the range of E-MORB to continental flood basalts (*e.g.* Columbia River flood basalts; USGS standard rock BCR-1 from Washington, U.S.A; Govindaraju, 1994; Fig. 4-14) and do not resemble typical oceanic within-plate basalts (*e.g.* OIB).

Sample 413 (*Group 1a)* plots in the within plate basalts field in most of the discrimination diagrams (Fig. 4-13). However, its distinctive REE pattern, comparable to that of OIB basalts, suggests that it was derived from a different source than the dykes of *Group 1.* This sample is also the only one located in the southern portion of the domain (Fig. 4-1), which further indicates that it is not related to the dykes of *Group 1 and 2.*

4.5.3 Dykes of Group 2: arc basalts?

In general, Nb depletions, like those of *Group 2*, are typical of all island arc volcanic rocks (Hofmann, 1988; Condie, 1986) and calc-alkaline rocks from other destructive plate margins such as continental margins (Pearce, 1983; Thompson *et al.*,

1984). In these settings, mafic magmas have been interpreted as derived from a mantle that has been enriched in LFSE and LREE by fluids from a subducted plate (Gill, 1981; Pearce, 1983; Condie, 1990; McCulloch and Gamble, 1991; Saunders *et al.*, 1991). In addition, Nb depletions can also be found in many continental within-plate basalts (Duncan, 1987).

In these settings, enrichment of LREE and LFSE relative to Nb and Ta is considered to reflect either crustal contamination (Wilson, 1989; Hofmann and Stein, 1994) or derivation of the mafic magmas from a metasomatically enriched sub-continental lithospheric mantle (Dostal *et al.*, 1989; Boily and Ludden, 1991; Zhao and McCulloch, 1993; Baker *et al.*, 2000; Amdt and Christensen, 1992; Amdt *et al.*, 1993; Turner and Hawkesworth, 1995). Crustal contamination can be ruled out on the basis of Nd isotopes. Assuming that the mafic dykes were formed at ~1.3Ga, the positive ε_{Nd} at that age (+3.2) indicate an insignificant assimilation of crustal material.

In the discrimination diagrams of Fig. 4-13, the mafic dykes of *Group 2* generally plot in arc (destructive plate margin) settings. Samples 209-1 and 314 have Zr and Zr/Y ratios comparable to those island arc basalts (Fig. 4-13a; Pearce and Norry, 1979) and Nb similar to those of arc volcanics (Fig. 4-13b; Pearce and Gale, 1977). In the discrimination diagram of Pearce and Cann (1973), samples 209-1 and 314 plot in the field of ocean floor, low-K and calc-alkaline basalts (Fig. 4-13c). Finally, in the diagram of Wood (1980) all the samples of *Group 1* plot in the field of destructive plate-margin basalts and differentiates (Fig. 4-13d).

4.6 Conclusions

Based on geochemistry, the mafic dykes of Canyon Domain have characteristics for which two distinct types of tectonic setting of emplacement are suggested: one with arc-related geochemical signature (*Group 2*) and one with a within-plate geochemical signature (*Group 1 and Group 1a*).

The country rock of the mafic dykes is a ~1.4 Ga meta-volcanoclastic package (Dunning and Indares, pers. comm. 2008) that may be part of the Montauban arc, for which an island arc setting has been suggested (Nadeau and Van Breemen 1994). Therefore it is likely that the dykes of *Group 2*, which have geochemical signatures similar to those in arc-related rocks, may have been emplaced during late stages of the development of the ~1.4 Ga arc. Also note that dyke #314, which belongs to *Group 2*, is an irregularly shaped dyke/body in mafic migmatites of the Canyon Domain (Fig. 4-2) that appears to be an integral part of this package.

In contrast, the dykes of *Group 1* and *1a* have the geochemical signature of within plate basalts, therefore they may be correlative with the ~1.2 Ga (Elzevirian) bimodal meta-volcanic sequence of the Banded Complex (east of the Canyon Domain; Fig. 4-1), and with banded units of similar age in southern Tshenukutish Terrane (Dunning and Indares, pers. comm. 2008), all of which are inferred to have developed in a ~1.2 Ga intra-continental rift setting. It is therefore suggested that the ~1.2 Ga volcanic sequences developed in proximity to the Canyon Domain and that their juxtaposition is not result of Grenvillian age tectonic transport.

Table 4-1: Observed mineralogy of the mafic dykes from the Canyon Domain (xx- highly abundant, x- abundant, v- minor and vv- traces *v = vein). Hbl: hornblende, Pl: plagioclase, Qtz: quartz, Opx: orthopyroxene, Cpx: clinopyroxene, Bt: biotite, Grt: garnet, Ap: apatite, Tit: titanite, Opq: opaques, Mag: magnetite, Ilm: ilmenite, Ms: muscovite and Chl: chlorite.

Sample	Hbl	Pl	Qtz	Opx	Cpx	Bt	Grt	Ap	Tit	Opq	Other
214a	x	x				vv		vv		vv	
214b	x	x	vv			vv		vv		Ilm, mag	Carbonates
430	x	x	v	x	v			vv		Ilm, mag	Carbonates
431	x	x	v	vv	v	v		vv		Ilm, mag	Muscovite
314	x	x		x	x(*v)					vv	
209-1	9	46	13 (*v)	25	2				v	Ilm	Ms, Chl Allanite
457	x	x		x		v	x	v		Ilm	
413	v	x		x							Allanite Zircon

Table 4-2: Summary of mineral compositions in terms of XMg, where XMg = $[Mg/(Mg+Fe^{2+})]$ x 100, % of end-members in plagioclase and mineral names for representative mafic dykes from the Canyon Domain (An = anorthite, - = not present). Pargasite, magnesiohastingsite and edenite have $(Na+K)_A \geq 0.5$ and Ti <0.5 while tschermakite and magnesiohornblende have $(Na+K)_A < 0.5$ and $Ca_A < 0.5$. Pargasite and magnesiohastingsite have the same Si in formula (5.5-6.5), but $^{VI}Al > Fe^{3+}$ and $^{VI}Al < Fe^{3+}$, respectively, while edenite has higher Si (6.5-7.5). Ferropargasite has the same characteristics as pargasite, but lower XMg (<0.5). Tschermakite has lower Si (5.5-6.5) than magnesiohornblende (Si = 6.5-7.5).

Sample	Plagioclase	Clinopyroxene	Orthopyroxene	Hornblende	Opaques	Garnet
430	Labradorite (An 53-68)	Diopside Xmg (69-73) Ti (0.015-0.018) Al (0.16-0.19)	Enstatite Xmg (63) Ti (0.005) Al (0.08)	Pargasite-Magnesiohanstingsite Xmg (63-66)	Magnetite-Ilmenite	-
209-1	Bytwonite (An 16-24)	Diopside-Augite Xmg (67-74) Ti (0.003-0.012) Al (0.03-0.095)	Enstatite Xmg (55-57) Ti (0.001-0.003) Al (0.03-0.04)	Edenite-Pargasite-Tschemakite-Magnesiohornblende Xmg (59-66)	Ilmenite	-
457	Andesine (An 36-38)	-	Ferrosilite Xmg (42-43) Ti (0.002-0.004) Al (0.03-0.04)	Ferropargasite Xmg (47-49)	Ilmenite	Almandine Al65-67

Table 4-3: Major and trace element data for the mafic dykes from the Canyon Domain. Major elements are reported in wt.% and trace elements in ppm; missing values are below detection. Major elements are recalculated volatile free with total Fe as FeO* and Mg# = [molar MgO/(MgO + FeO*)] x 100. Group 1 = samples that lack negative Nb anomalies, Group 2 = samples with negative Nb anomalies and Group 3 = sample depleted in Nb and Th and with a high $(La/Yb)_N$ ratio. N = normalized using the primitive mantle values of Sun and McDonough (1989).

SAMPLE	214b	314	430	457	209-1	431	214a	413
Group	*1*	*2*	*1*	*1*	*2*	*1*	*2*	*1a*
SiO2	46.37	49.33	47.88	46.81	53.61	47.27	47.28	57.52
TiO2	2.95	0.89	1.32	3.21	0.95	2.30	1.78	2.22
Al2O3	15.42	15.16	17.10	15.74	16.03	15.07	16.62	14.91
FeO	14.44	11.03	10.77	15.78	11.69	15.13	11.97	9.95
MnO	0.21	0.18	0.18	0.23	0.194	0.26	0.21	0.13
MgO	6.35	9.78	8.96	5.66	8.23	6.62	7.66	5.33
CaO	8.84	9.66	11.01	7.87	8.25	8.38	9.47	7.33
Na2O	3.90	3.34	2.39	3.14	0.75	3.26	3.68	1.00
K2O	1.04	0.58	0.25	1.04	0.23	1.19	1.05	0.91
P2O5	0.47	0.05	0.13	0.53	0.07	0.52	0.29	0.70
Na2O+K2O	4.94	3.92	2.65	4.18	0.98	4.45	4.73	1.92
CaO/Al2O3	0.57	0.64	0.64	0.50	0.51	0.56	0.57	0.49
LOI	1.20	1.77	0.60	0.29		1.47	0.87	0.95
Mg#	*44*	*61*	*60*	*39*	*56*	*44*	*53*	*49*
Co	90.2	320	134	217	168	106	90.9	273
Cr	62.2	93.0	184	71.9	288	514	62.0	217
Cu	31.1	60.0	51.0	41.1	33.9	31.5	20.7	10.3
Ni	31.1	210	173		80.9	756	51.7	
Sc	31.1	32.0	34.7	29.8	37.0	34.6	33.1	22.7
V	214	209	216	200	229	267	263	142
Zn	93.4	110	71.4	164	161	168	93.0	134
Ba	228	147	73.4	435	62.7	544	132	884
Ga	21.8	19.0	18.4	22.6	20.6	22.0	20.7	23.7
Rb	12.4	9.00	5.10	18.5	9.6	27.3	9.30	36.1
Sr	278	245	236	283	132	369	403	472
Th	2.39	0.60	0.61	1.54	3.16	0.94	1.34	1.44
U	0.62	0.20	0.20	0.41	1.60	0.42	0.41	0.41
Zr	225	49.0	78.5	228	56.8	115	74.4	234
Hf	5.81	1.40	2.24	6.16	1.95	3.25	2.38	6.50
Nb	20.7	3.00	6.12	16.4	3.69	8.40	3.10	14.4
Ta	1.45	0.10	0.41	1.13	0.34	0.31	0.21	1.03
Y	38.4	20.0	20.4	49.3	28.0	35.7	21.7	28.9
La	20.3	5.50	5.61	21.1	12.6	10.8	9.71	34.1
Ce	49.7	12.3	14.4	51.0	34.2	28.5	23.2	76.7
Pr	6.72	1.68	2.04	7.00	4.66	4.27	3.20	10.0
Nd	28.0	8.10	9.79	30.4	20.8	19.6	14.4	41.8
Sm	7.26	2.40	2.75	7.81	5.39	5.46	3.93	9.29
Eu	2.55	1.02	1.12	2.73	1.10	2.11	1.56	2.77
Gd	7.68	3.10	3.26	8.63	5.37	5.98	4.24	8.46
Tb	1.24	0.60	0.61	1.44	0.99	1.05	0.72	1.24
Dy	7.16	3.40	3.47	8.53	5.52	6.09	4.03	5.99
Ho	1.45	0.70	0.71	1.75	1.09	1.26	0.83	1.03
Er	4.05	2.00	2.04	4.93	3.30	3.57	2.17	2.89
Tm	0.58	0.30	0.30	0.72	0.50	0.52	0.32	0.37
Yb	3.63	1.90	1.94	4.52	2.99	3.36	1.96	2.27
Lu	0.57	0.26	0.29	0.71	0.40	0.50	0.29	0.33
W		125			378			
Pb								
Ge					1.55			
(La/Ce)N	1.1	1.2	1.0	1.1	1.0	1.0	1.1	1.1
(La/Sm)N	1.8	1.5	1.3	1.7	1.5	1.3	1.6	2.4
(La/Yb)N	4.0	2.1	2.1	3.3	3.0	2.3	3.6	10.8
(Dy/Yb)N	1.3	1.2	1.2	1.3	1.2	1.2	1.4	1.8

Table 4-4: Sm–Nd isotopic data for the mafic dykes from the Canyon Domain. Model ages were calculated with respect to a depleted mantle model (T_{DM2}) and De Paolo's mantle model (De Pal; De Paolo, 1981). The T_{DM2} model uses a depleted mantle separated from the CHUR (chondrite uniform reservoir) since 4.55 Ga following a linear evolution and having a present-day Epsilon value of +10. 2SE (M) = standard error of the mean (G1 = Group 1and G2 = Group 2; see Table 4-3).

Sample	Nd (ppm)	Sm (ppm)	$^{147}Sm/^{144}Nd$	$^{143}Nd/^{144}Nd$	2SE(M)	$\varepsilon_{Nd}(0)$	$\varepsilon_{Nd}(1300)$	DePal (Ma)	T_{DM2} (Ma)
430 (G1)	10.3	2.88	0.1696	0.512723	5	+ 1.7	+ 5.1	1105	1477
214a (G2)	14.2	3.76	0.1599	0.512560	5	- 1.5	+ 3.2	1362	1671
214b (G1)	28.0	6.83	0.1475	0.512532	7	- 2.1	+ 4.2	1176	1423
431 (G1)	27.3	5.35	0.1185	0.512248	4	- 7.6	+ 2.4	1270	1443

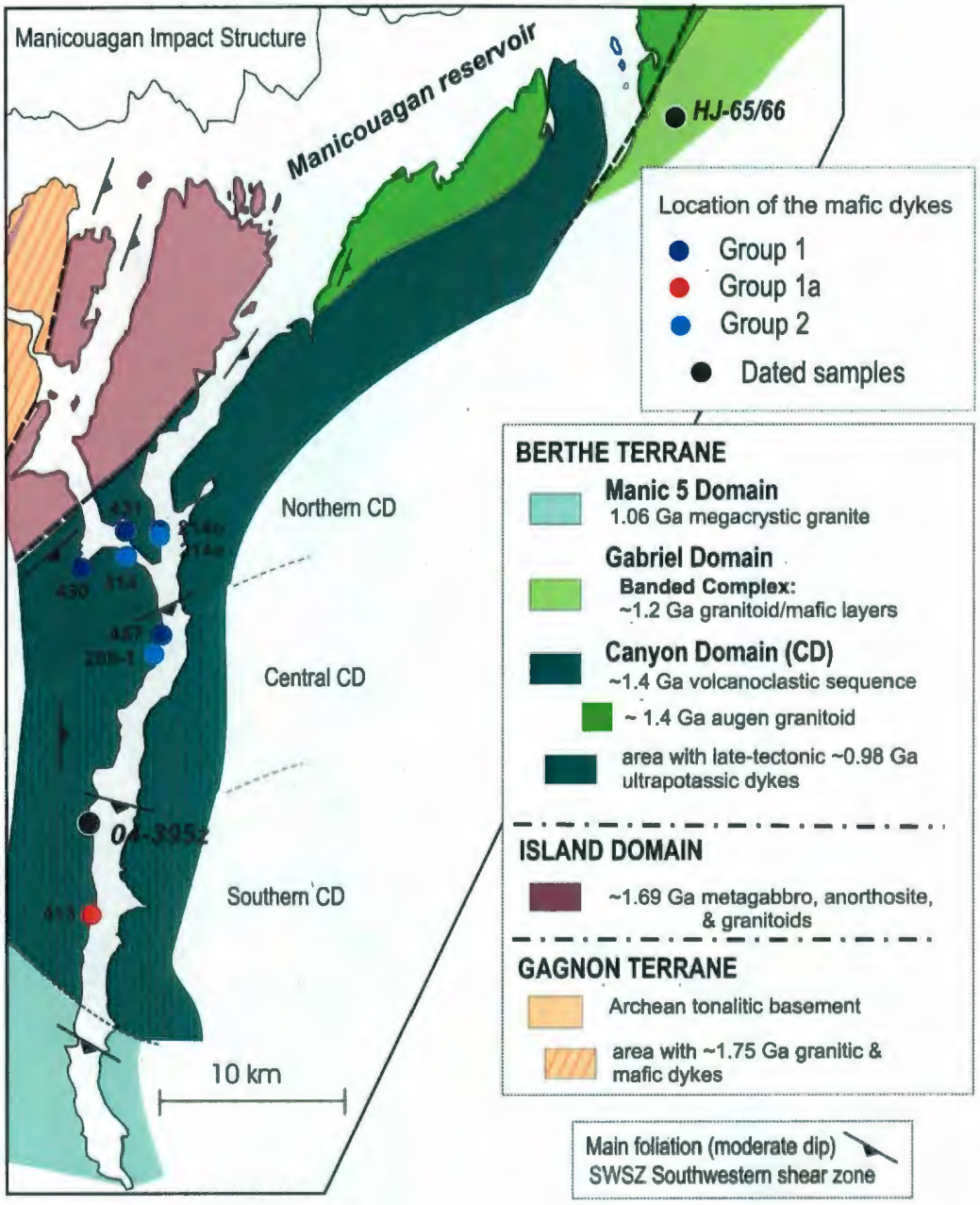

Figure 4-1: Geological map of the south shore of the Manicouagan reservoir showing the location of the mafic dykes from the Canyon Domain. Geochemical groups: Group 1 = samples that lack negative Nb anomalies, Group 1a = sample that also lack a negative Nb anomaly, but has a $(La/Yb)_N$ ratio much higher than all the other samples; and Group 2 = samples with pronounced Nb anomalies. Dated rocks (Indares and Dunning, 2004 and Dunning and Indares, pers. comm. 2008): ~1.2Ga massive granite layer (HJ-65), a granite dyke (HJ-66) from the Banded Complex and a ~1.4Ga component of layered mafic to intermediate unit of the Canyon Domain (04-395z).

(a) 430

(b) 431

(c) 214a

(d) 214b

(e) 314

(f) 209-1

(g) 457

(h) 413

Figure 4-2: Outcrop photos of characteristic mafic dykes from the (a-e) northern, (f-g) central and (h) southern Canyon Domain.

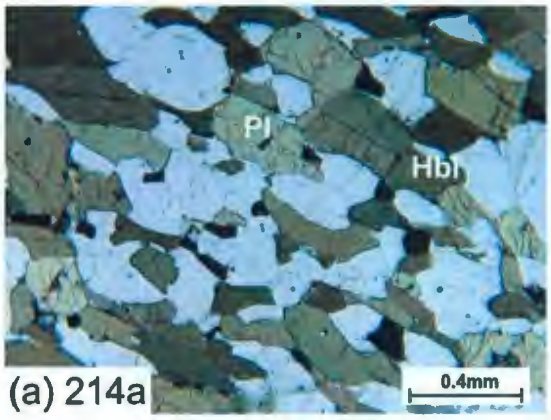

(a) 214a

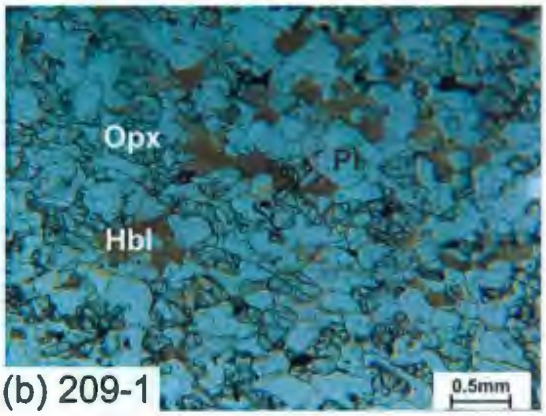

(b) 209-1

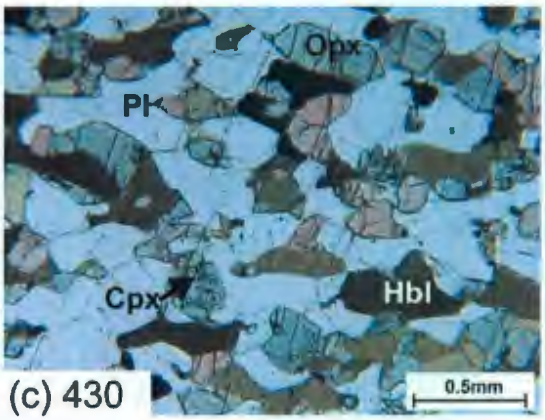

(c) 430

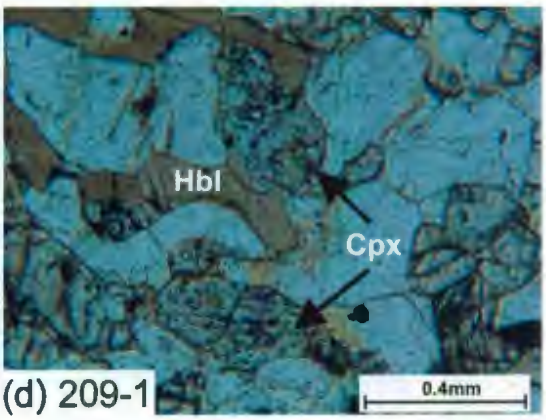

(d) 209-1

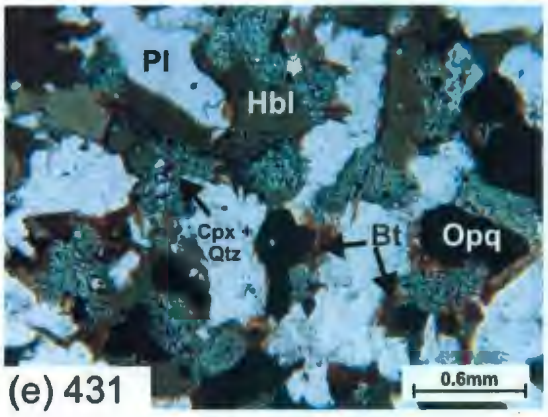

(e) 431

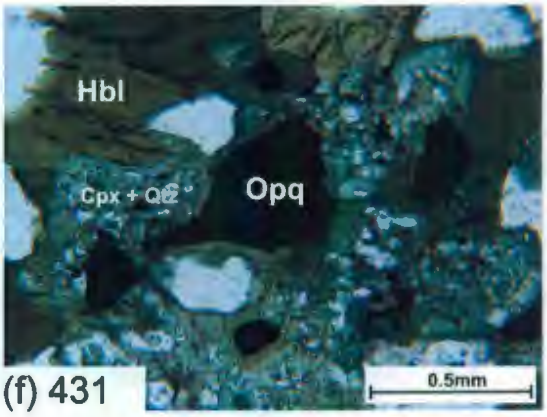

(f) 431

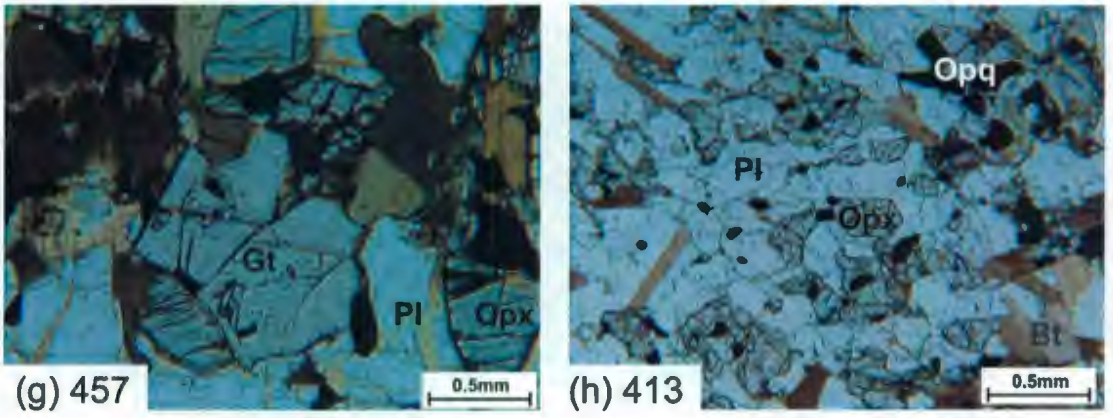

Figure 4-3: Microphotographs (taken under plane polarized light) showing typical textures of the mafic dykes from the Canyon Domain. Hbl: hornblende, Pl: plagioclase, Bt: biotite, Cpx: clinopyroxene, Opx orthopyroxene; Opq: opaques and Grt: garnet. (a) foliated equigranular hornblende and plagioclase; (b) granoblastic plagioclase and orthopyroxene; (c) isolated or aggragates of pyroxenes; (d) clinopyroxene corroded by hornblende along its rims and cleavage; (e) clinopyroxene rimed by hornblende and biotite; (f) clinopyroxene with numerous worm-like inclusions of quartz and opaques; (g) garnet with small inclusions of feldspar and opaques; and (h) dark brown flakes of biotite.

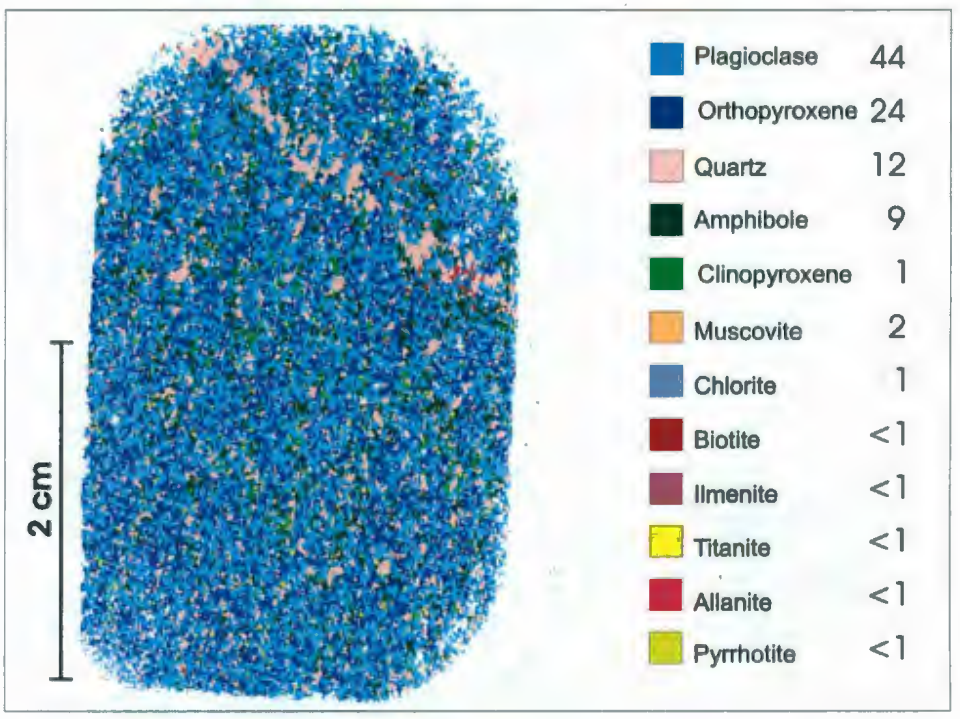

Figure 4-4: SEM false color mineral map, showing mineral modes (%), for sample 209-1 from the central Canyon Domain.

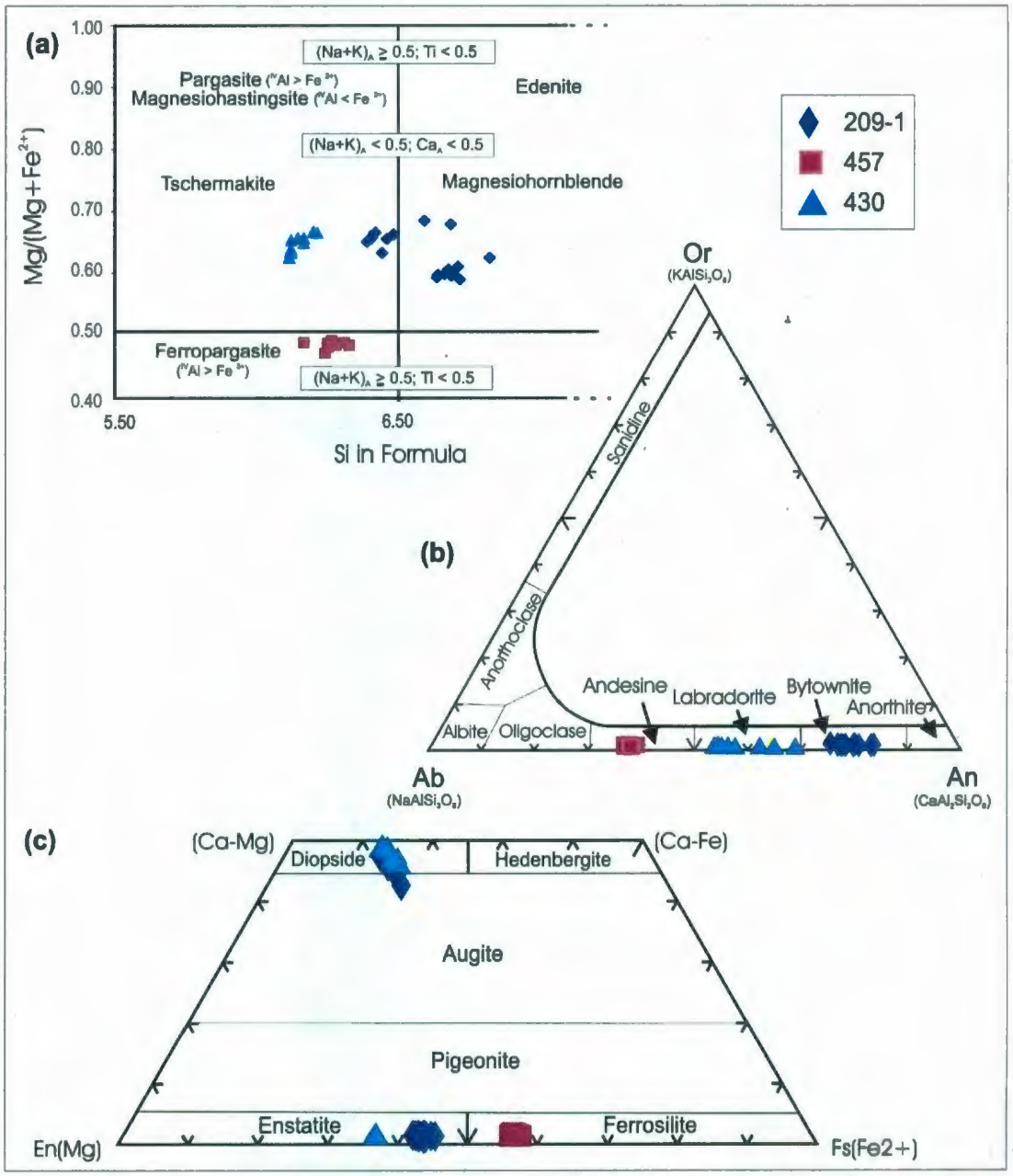

Figure 4-5: Composition/classification diagrams for major minerals in the mafic dykes from the Canyon Domain. (a) amphibole (after Leake et al. 1997, 2004); (b) feldspars; and (c) pyroxene (after Morimoto et al. 1988). The standard amphibole formula is $AB_2^{VI}C_5^{IV}T_8O_{22}(OH)_2$, where A, B, C, T, O and OH are crystallographic sites. All the amphiboles are calcic ($(Mg, Fe^{2+}, Mn^{2+}, Li)_B \leq 0.50$; $(Ca, Na)_B \geq 1.0$ and Na_B between 0.5-1.50 and, usually, $Ca_B \geq 1.50$ (atoms per formula unit). Those with Mg# >0.5 are subdivided into those with $(Na + K)_A \geq 0.5$ and $Ti < 0.5$ (pargasite/magnesiohastingsite or edenite) and those with $(Na+K)_A < 0.5$ and $Ca < 0.5$ (tschermakte or magnesiohornblende); while those with Mg# < 0.5 are classified as ferropargasite.

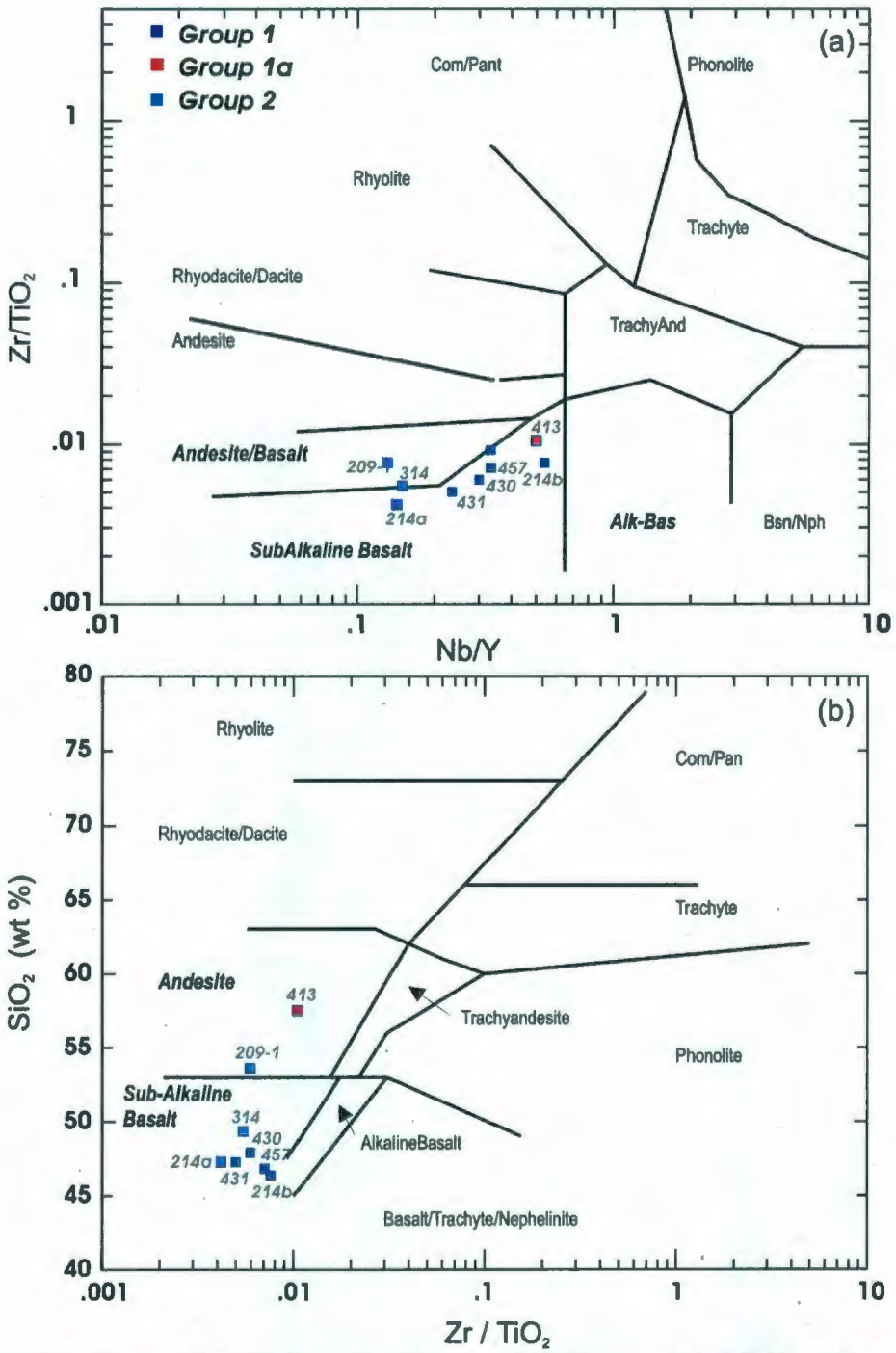

Figure 4-6: Plots of (a) Nb/Y vs. $Zr/TiO_2 \times 10000$ diagram (the Nb/Y ratio acts as an alkalinity index and the Zr/TiO_2 ratio acts as a differentiation index) and; (b) Zr/TiO_2 vs. SiO_2 (Winchester and Floyd, 1977 & 1978) for mafic dykes from the Canyon Domain. Geochemical groups: Group 1 = samples that lack negative Nb anomalies, Group 2 = samples with Nb anomalies and Group 3 = sample depleted in Nb and Th and with the highest (La/Yb) ratio.

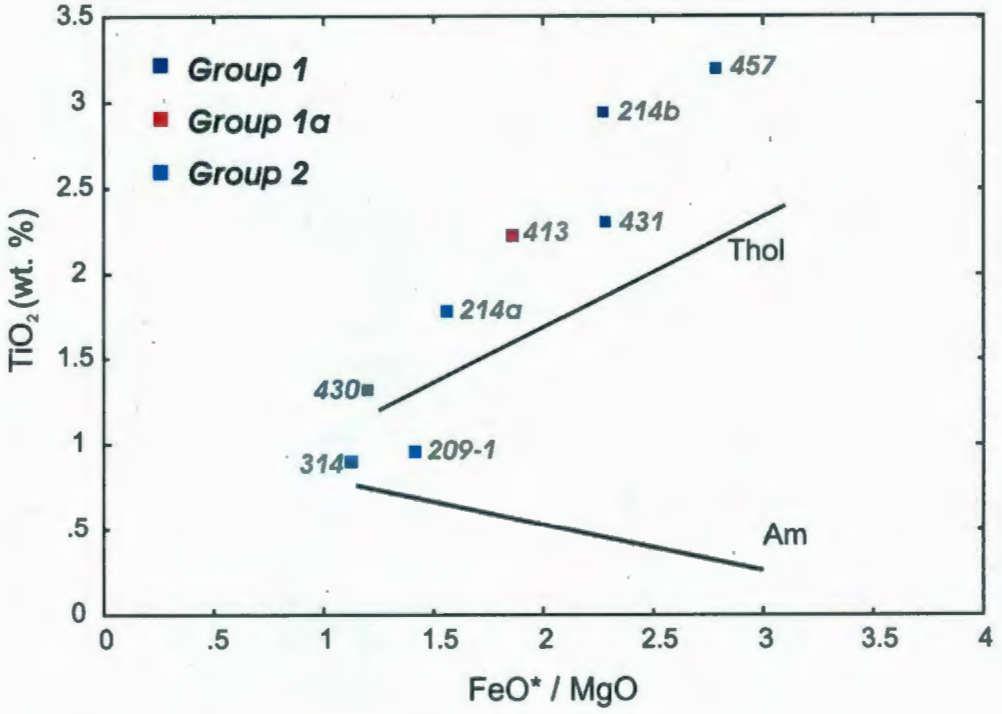

Figure 4-7: TiO_2 - FeO*/MgO diagram of Myashiro (1974) for mafic dykes from the Canyon Domain. Groups as defined in Figure 4-6.

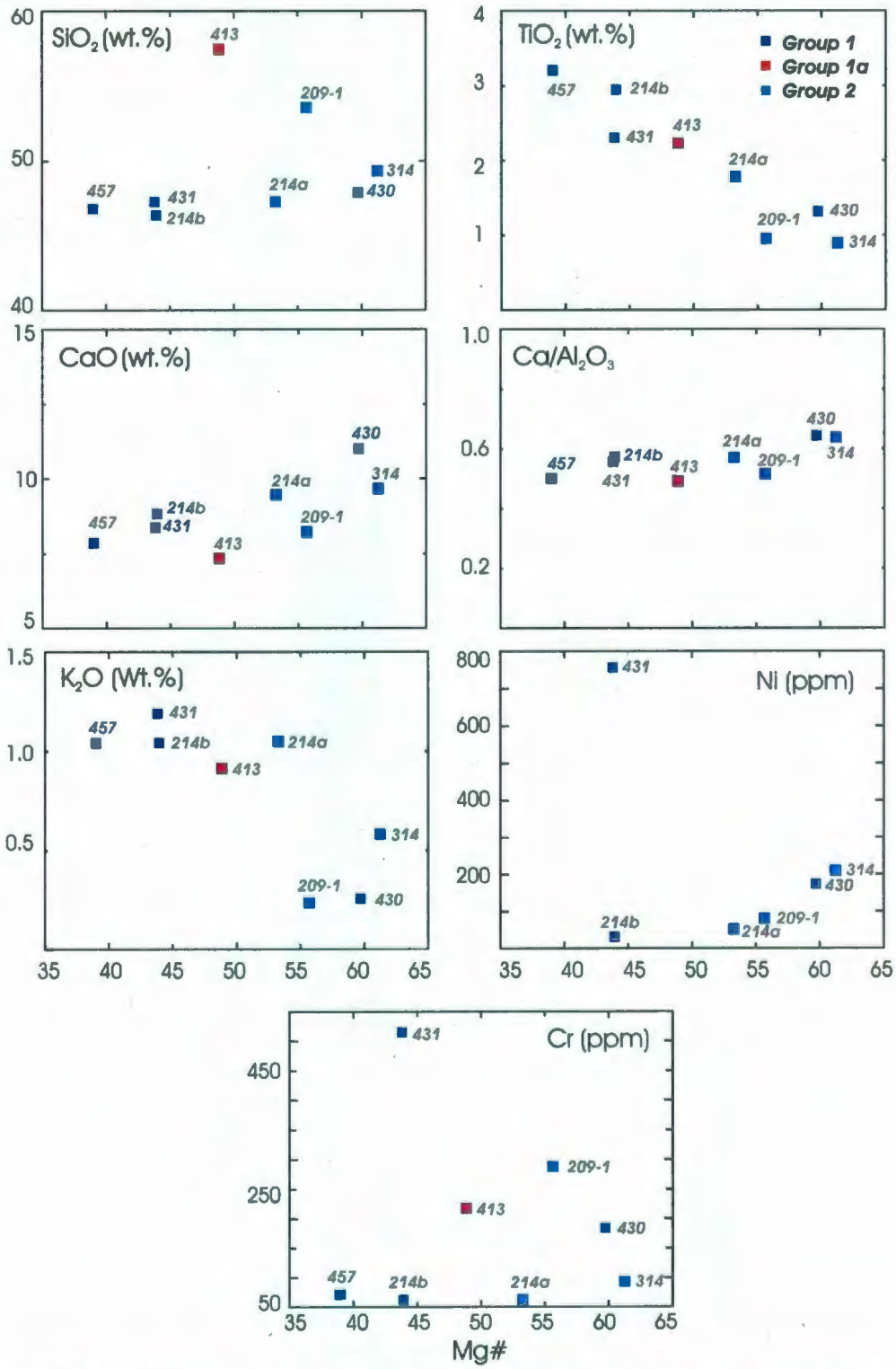

Figure 4-8: Variation of SiO_2, CaO, CaO/Al_2O3, Na_2O, Cr and Ni with magnesium number (Mg#), where Mg# = [molar (MgO/MgO+FeO*)] x 100 for mafic dykes from the Canyon Domain. Groups as defined in Figure 4-6.

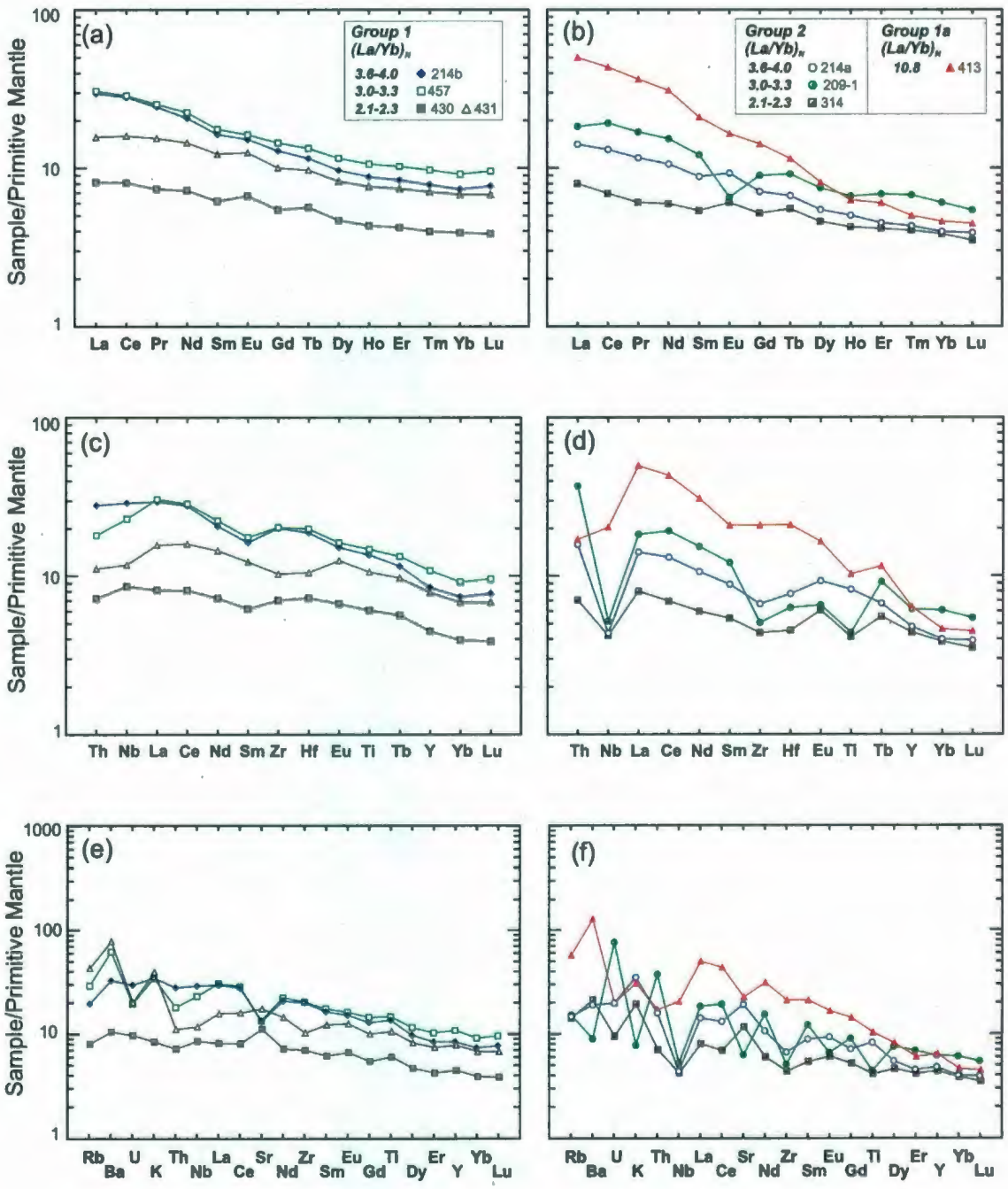

Figure 4-9: a-b) Primitive mantle normalized REE; c-d) extended (REE, HFSE, Th); and e-f) complete REE, HFSE & LFSE plots for the mafic dykes from the Canyon Domain. Normalizing values after Sun and McDonough (1989).

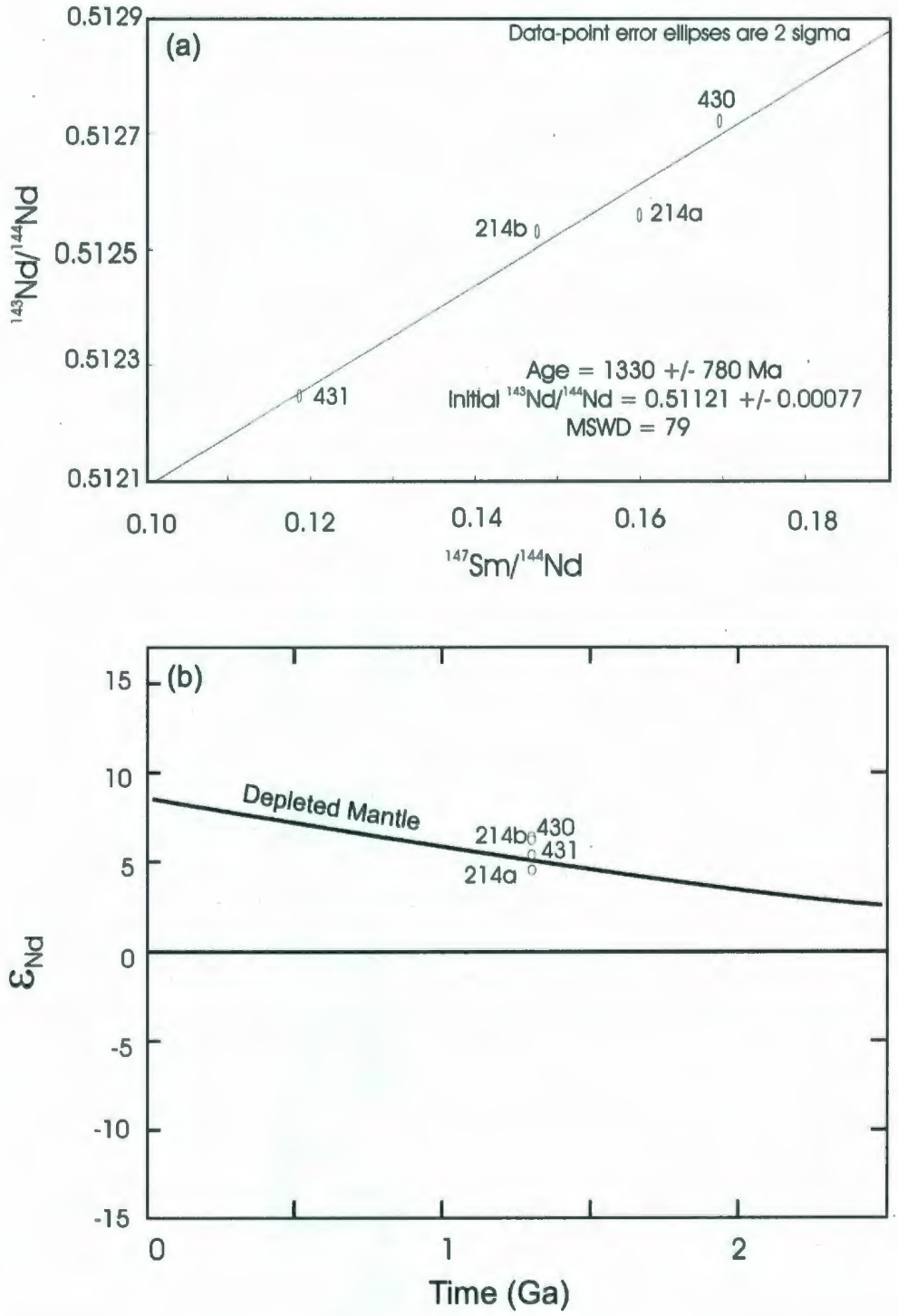

Figure 4-10: (a) $^{143}Nd/^{144}Nd$ versus $^{147}Sm/^{144}Nd$ diagram and (b) plot of initial ε_{Nd} versus age (T=1300Ma) for the mafic dykes from the Canyon Domain. The depleted mantle curve is from De Paolo (1981).

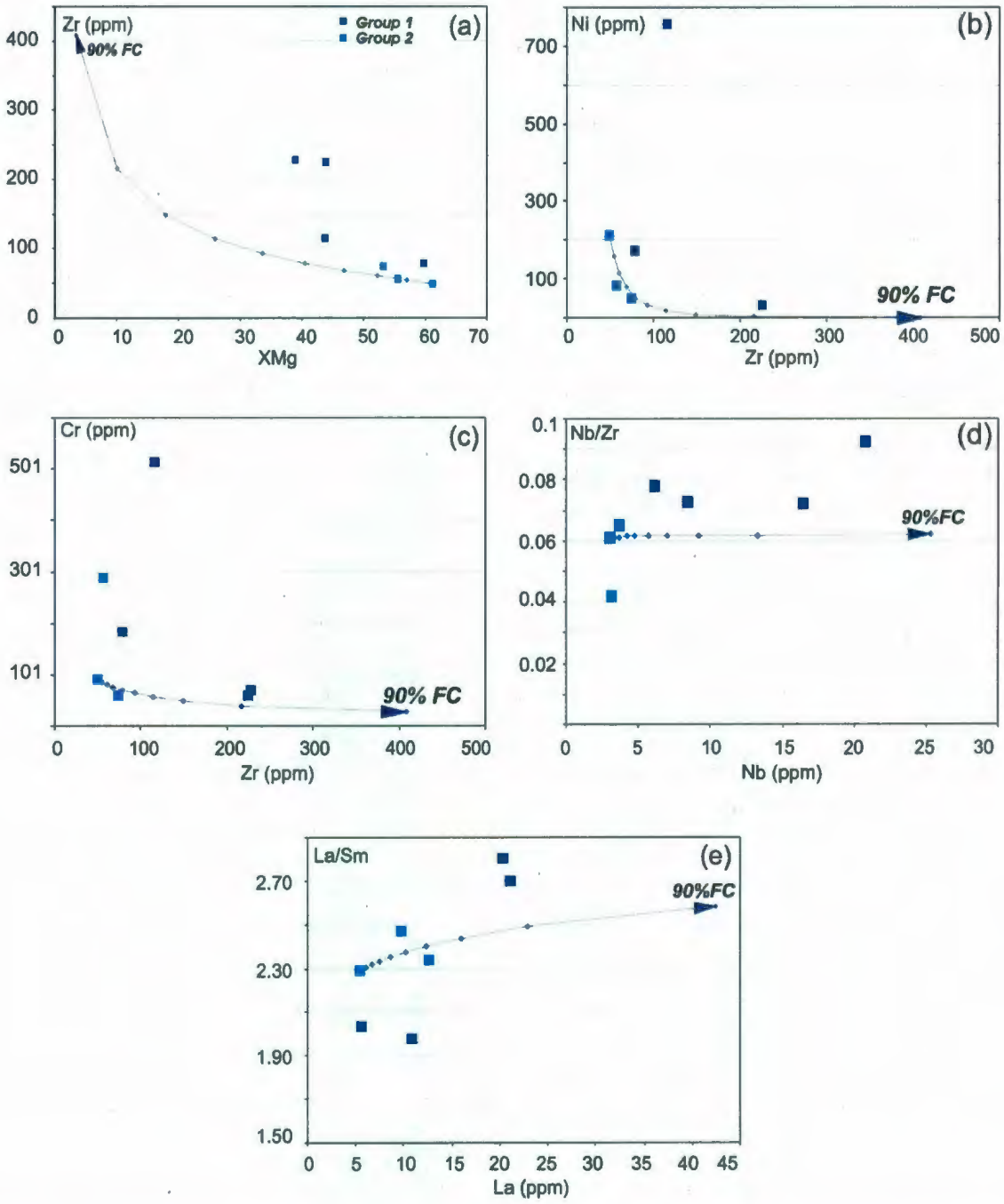

Figure 4-11: Plots of (a) Zr versus Mg#; (b) Ni versus Zr; (c) Cr versus Zr; (d) Nb/Zr versus Nb; and (e) La/Sm versus La for the mafic dykes of the Canyon Domain. Shown in all plots are the fractional crystallization lines for a melt with the composition of the sample with the highest XMg (#314). The proportions of fractionated phases used were: 20% olivine, 30% clinopyroxene and 50% plagioclase.

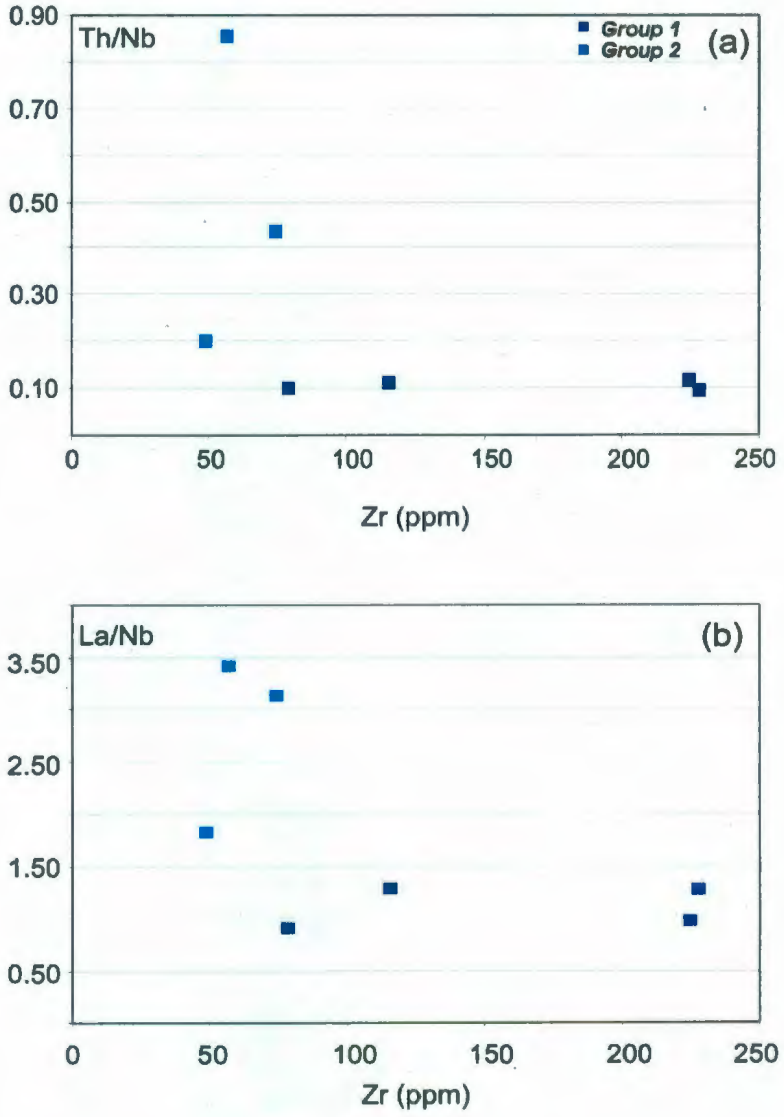

Figure 4-12: Plots of (a) Th/Nb and (b) La/Nb versus Zr for the mafic dykes of the Canyon Domain.

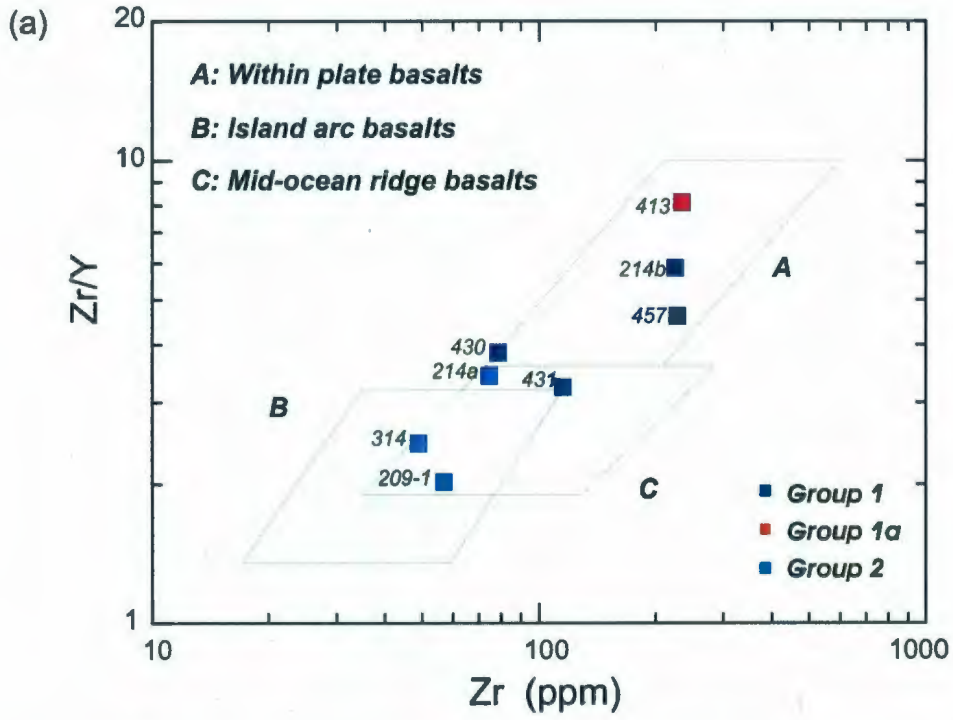
(a)
A: Within plate basalts
B: Island arc basalts
C: Mid-ocean ridge basalts
413
214b
457
430
214a
431
314
209-1
A
B
C
Group 1
Group 1a
Group 2
Zr/Y
Zr (ppm)
20
10
1
10
100
1000

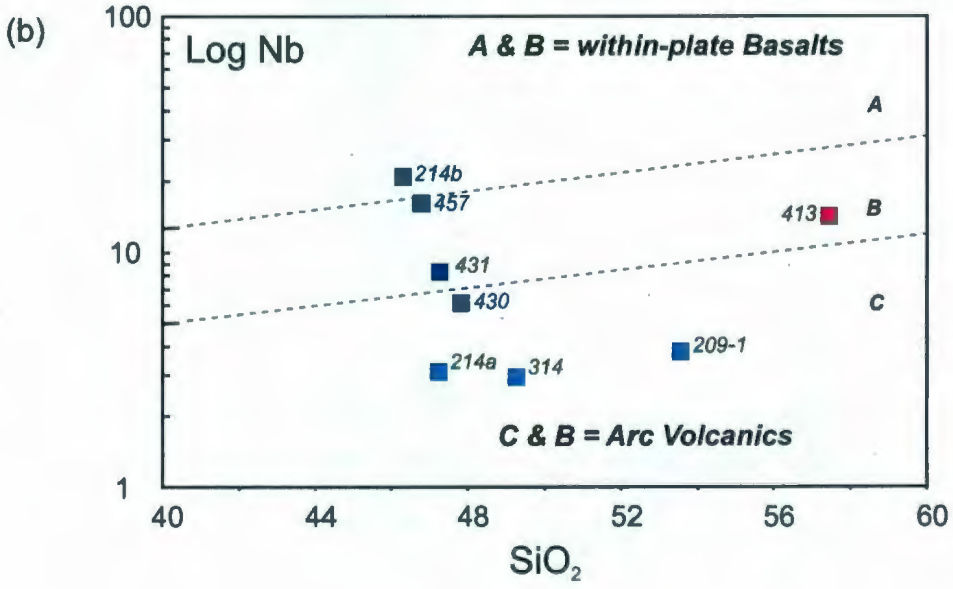
(b)
Log Nb
A & B = within-plate Basalts
A
B
C
214b
457
413
431
430
209-1
214a
314
C & B = Arc Volcanics
100
10
1
40
44
48
52
56
60
SiO2

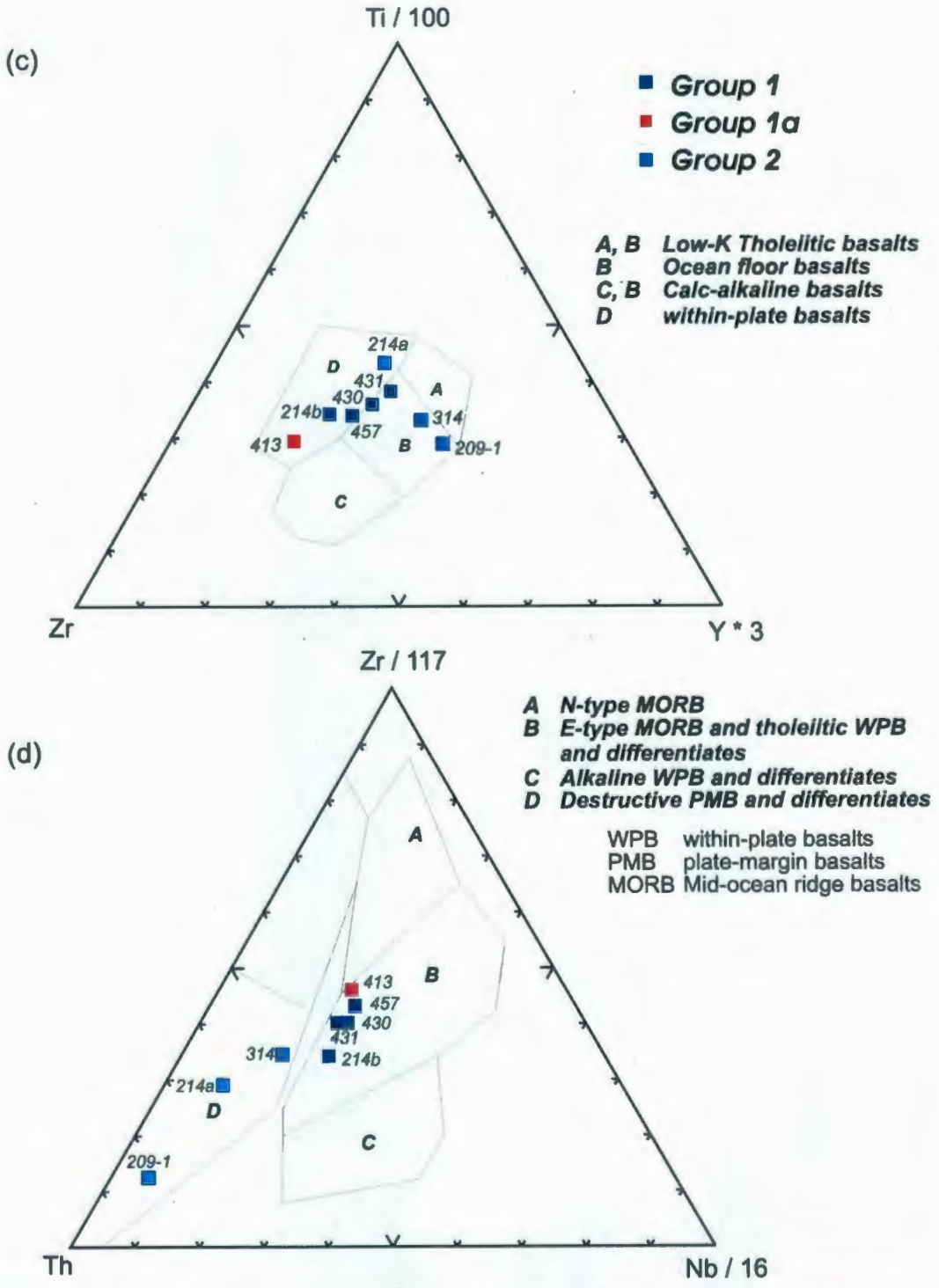

Figure 4-13: Discrimination diagrams for the characterization of the tectonic setting of magma generation for the mafic dykes of the Canyon Domain. a) Zr content and Zr/Y ratios (Pearce and Norry, 1979); b) Nb (Pearce and Gale, 1977); c) Zr-Ti-Y (Pearce and Cann, 1973); and d) Th-Zr-Nb (Wood, 1980).

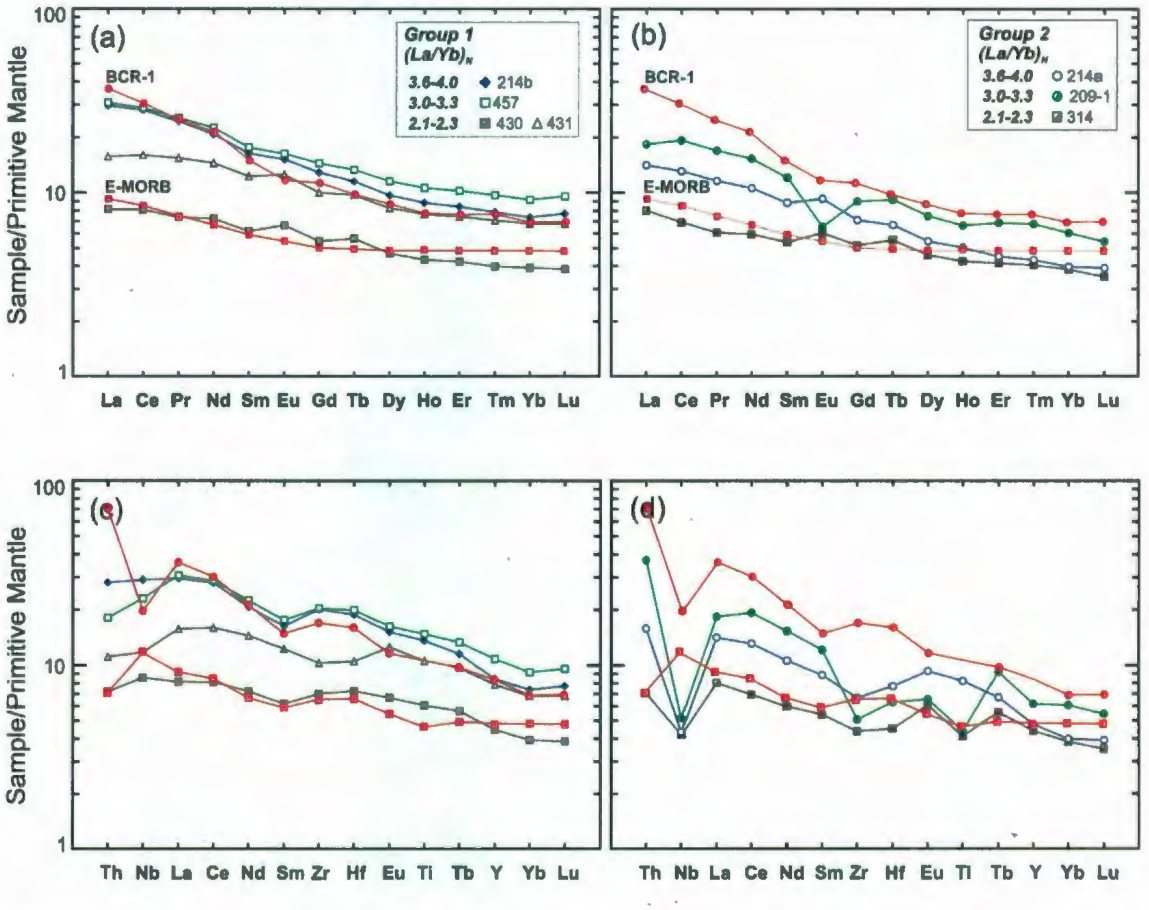

Figure 4-14: a-b) Primitive mantle normalized rare earth element; c-d) extended (REE, HESE, Th) for the mafic dykes from the Canyon Domain and typical E-type MORB and USGS standard rock BCR-1 from Washington, U.S.A (continental flood basalt). E-type MORB data and normalizing values after Sun and McDonough (1989) and BCR-1 data after Govindaraju (1994). (a and c) show the mafic dykes from Group 1 and (b and d) those of Group 2.

CHAPTER 5: ULTRAPOTASSIC DYKES OF THE CANYON DOMAIN

5.1 Introduction

A compositionally and mineralogically diverse suite of dykes intrudes the central and southern Canyon Domain (Fig. 5-1). These dykes range from biotite-rich to more typical granitoid mineralogies and can form composite bodies. Field terms used to describe these rocks were lamprophyres and granitic pegmatites.

These dykes are a key element in understanding the evolution of this area, since their mode of occurrence indicates they intruded late, they proved amenable to age-dating and they can have unusual compositions. To simplify the presentation and discussion of the data obtained from these dykes, we refer to them as late tectonic, ultrapotassic to felsic pegmatoid dykes. The basis for these terms is provided below.

The age, geochemistry and isotopic composition of these dykes, in conjunction with data from other studies, suggest that there is a late orogenic (Grenvillian) magmatic event that taps a distinct metasomatized mantle source. The regional tectonic implications are discussed.

5.2 Field relationships and age

In the central Canyon Domain, the ultrapotassic dykes are ~10-20 cm wide, biotite-rich and cut the main foliation and compositional layering of the country rock (banded quartzo-feldspathic unit) at consistently high angles (#209-2, #338z, #361 and #361z; Fig.

5-2a-d). These dykes have an internal fabric nearly parallel to their rims and locally have a rim of felsic pegmatite of variable width.

In the southern part of the Canyon Domain, the ultrapotassic dykes are either undeformed or are the focus of ~south dipping decimetric to metric late shear zones that deflect the main foliation. They are ~5-30 cm wide, biotite-rich dykes that cut the main foliation and compositional layering of the country rock at high angle, are consistently steeply dipping, and have variable width rims of felsic pegmatite (# 398a, 403, 404; Fig. 5-2e-g). In addition, dyke #408 locally follows the foliation and compositional layering of the country rock and then cuts across. Dyke #398a is the locus of an incipient late shear zone (Fig. 5-2h). Dyke #462z is attenuated and has diffuse margins (Fig. 5-2i).

One felsic pegmatite (outcrop #04-395b) from the central Canyon Domain and the ultrapotassic component of a composite dyke (outcrop #04-403) from the southern part of the domain yielded crystallization ages of 995±3.5 and 980±3 Ma, respectively (Fig. 5-1 and Fig 5-3; Dunning and Indares, pers. Comm. 2008).

5.3 Mineralogy, Textures and Mineral Chemistry

The samples of the central (samples 209-d2, 338z, 361z and 361) and the southern (samples 403, 404, 408, 398a, 462-z) Canyon Domain are characterized by the predominance of biotite in the mineral assemblage and amounts of apatite as high as 10% (Table 5-1 and Fig. 5-4). The proportions of other phases (plagioclase, K-feldspar, quartz, clinopyroxene and orthopyroxene) are highly variable. Accessory minerals include allanite, zircon, monazite, titanite, rutile and opaques.

Based on general texture, the investigated samples may be divided into: (a) strongly foliated, generally fine to medium grained; and (b) weakly foliated to massive, coarse grained. These two types will be described separately below.

5.3.1 Strongly foliated samples (#209-2, 361, 361z, 404 and 398a)

These samples are characterized by a strongly foliated, biotite-rich matrix, which consists mainly of plagioclase and quartz (#209-2, 404 and 398a; Fig. 5-4a-c) or plagioclase and K-feldspar (#361 and 361z; Fig. 5-4d). Plagioclase and K-feldspar are usually free of inclusions and are variably altered to sericite. In addition, myrmekitic texture (vermicular or wormy intergrowth of quartz in plagioclase Fig. 5-5a) and biotite with worm-like inclusions of quartz are locally present (#361).

Additional phases include: relatively large semi-rounded clinopyroxene crystals with a pronounced cleavage, and sporadic feldspar and opaque inclusions (sample 361z; Fig 5-5b); aggregates of clinopyroxene and hornblende (sample 404, 361 and 398a; Fig 5-5c), in which clinopyroxene is highly corroded by hornblende along its rims and cleavage; and small aggregates of hornblende (sample 209-2). In addition, a large K-feldspar with numerous quartz inclusions and partially rimmed by a quartz ribbon (xenolith; Fig. 5-5d; Fig. 5-4d) occurs in sample 361z.

5.3.2 Weakly foliated to massive samples (#338z, 403, 462z and 408)

These samples are coarse grained and their general texture ranges from weakly foliated (#338z) to massive (samples #403, 408, 462z). Samples 338z, 403 and 462z lack

pyroxenes and contain minor or no plagioclase (Fig. 5-4e-f).

Sample 338z has a distinctive texture characterized by pods of biotite, K-feldspar and apatite with interstitial quartz and relics of large quartz crystals (Fig. 5-5e; Fig. 5-4e). Plagioclase is a minor phase and contains exsolution lamellae of K-feldspar.

Sample 403 is the most coarse-grained and heterogeneous. It consists of two textural domains: a) biotite, K-feldspar and quartz intergrowths; and b) quartz pods ± biotite rimmed by biotite (Fig. 5-5f; Fig. 5-4f). K-feldspar is anhedral and has exsolutions of plagioclase (Fig. 5-5g) as well as inclusions of quartz and biotite. Large apatites are abundant in both domains.

Sample 462z has a distinctive texture characterized by large biotite and K-feldspar with interstitial quartz (Fig. 5-5h). Large apatites are also abundant. Finally, sample 408, is homogeneous and consists mainly of plagioclase with interstitial biotite and subordinate orthopyroxene, hornblende and clinopyroxene (Fig. 5-5i; Fig. 5-4g). Pyroxenes are corroded by hornblende along their rims and cleavage (Fig. 5-5j). Biotite and amphibole locally contain worm-like inclusions of quartz.

5.3.3 Mineral chemistry

Biotite, feldspars, pyroxenes, hornblende, apatite and opaques were analyzed in seven samples (Table 5-2 and Fig. 5-6; mineral analyses are listed in Appendix 1). Biotite is chemically homogeneous at the sample scale (Fig. 5-6a), with XMg ranging from 50 to 80. The more magnesian biotites (phlogopites), in samples 338z and 403, typically contain TiO_2 of 2.0-5.5 wt.%. Plagioclase is homogeneous within each sample; however,

overall there is a large range of anorthite contents in the samples (An_{32-84}; Fig. 5-6b). The most anorthite-rich plagioclase (bytownite) occurs in samples lacking K-feldspar (e.g. 404 and 209-2). K-feldspar is orthoclase (Or_{70-89}; Fig. 5-6b).

According to the pyroxene nomenclature of Morimoto (1988) clinopyroxene falls in the compositional fields of diopside to augite and has an XMg in the range of 60-73 (Fig. 5-6c). Orthopyroxene, in sample 408 only, falls in the compositional field of ferrosilite ($XMg_{0.45-0.48}$; Fig. 5-6c; Morimoto, 1988). Based on the amphibole classification scheme of Leake *et al.* (1997, 2004) hornblende (209-2, 404 and 408) falls in the compositional range of magnesiohornblende (not shown). Apatite is rich in Sr (SrO 4-4.5 wt.%) in sample 403. Opaques (samples 209-2, 404, 408) were identified as ilmenite.

There are strong correlations between the bulk chemistry and the minerals present in each sample (Tables 5-2 and 5-3). For instance, the samples with the highest bulk Mg# (samples 403 and 338z) contain the most magnesian biotites. These samples also have the highest P_2O_3 and K_2O contents, which correlate well with the high proportions of apatite (~8-10%) and K-feldspar present (17-30%) in these rocks. In addition, the highest Na_2O occurs in samples with high modal proportion of albite-rich plagioclase (*e.g.* 408 and 361z).

5.3.4 Interpretation of Textures and Classification based on mineralogy

The ultrapotassic dykes of the Canyon Domain have not experienced any metamorphism; however, the strongly foliated textures in some of the samples is

consistent with them having experienced some deformation. The samples with weak foliation to massive textures experienced little to no deformation. In addition, some of these samples display igneous texture with large biotite and apatite in interstitial pools dominated by K-feldspar+/-quartz.

Initially the dykes were identified in the field as lamprophyres. Lamprophyres are porphyritic igneous rocks consisting of biotite (or Fe-phlogopite) +/- amphibole and clinopyroxene, with feldspar restricted to groundmass and usually with a panidiomorphic texture. More specific names are applied to lamprophyres based on the proportions of plagioclase, K-feldspar, biotite and hornblende (kersantite or minette vs. spessartite or vogesite). For the general classification of these rocks, see Le Maitre (2002) and for detailed descriptions see Rock (1991). While the samples have a similar mineralogy to lamprophyres, their texture (*e.g.* lack of biotite/phlogopite phenocrysts and lack of panidiomorphic texture) precludes them from being called lamprophyres. Thus, the samples were classified based on their bulk composition (see below).

5.4 Geochemistry

Major and trace element compositions are listed in Table 5-3. There are no geochemical correlations/relationships indicating any difference between the ultrapotassic dykes from the central or the southern Canyon Domain. Thus, they are discussed together in the following sections.

5.4.1 Major and trace element composition

Major and trace element abundances are listed in Tables 5-3. The samples have bulk Mg# (Mg# =[molecular proportion MgO/(MgO + FeO*)] x 100) in the range of 42 to 75 and have a wide range of SiO_2 (49-60 wt.%) and MgO (3.8-10.8 wt.%) contents (Fig. 5-7a). Most of samples have K_2O and MgO > 3 wt. % and K_2O/Na_2O > 2 wt. % and (Fig. 5-7b-c), making them ultrapotassic rocks according to the definition of Foley *et al.* (1987). Contents of TiO_2 range for 1.5 to 3.8 wt. % and those of P_2O_5 from 1 to 4.3 wt.%.

The samples have concentrations of Cr and Ni ranging from below detection to 300 ppm and 150 ppm, respectively. One sample (398a) has over 600 ppm Cr and over 200 ppm Ni. Ni and Cr show a crude correlation with MgO suggesting they represent a range from primitive to fractionated compositions (Fig. 5-8a-b). Concentrations of other transition elements (Sc- 4–22 and V- 65–169) are highly variable amongst the samples.

Concentrations of Ba (2000–9000 ppm), Sr (1090–6500 ppm) and Rb (65–263 ppm are very high in all the samples (Table 5-3). In contrast, the concentrations of other low field strength elements (*e.g.* Th and U) are low. These elements show no correlation with MgO. Rb, U and Th show a slight positive correlation with K_2O.

5.4.2 Extended REE plots

The immobile element data are illustrated in primitive mantle normalized plots (Fig. 5-9 a-b, REE; c-d, all). Figures 5-9 e and f show a more complete spectrum of trace element data including potentially mobile LFSE like Rb, Ba, U and Sr. All the samples are characterized by high concentrations of the light REE (LREE; La_N ~100-400) and low

concentrations of the heavy REE (HREE; Yb_N= 3-8).

The ultrapotassic dykes were subdivided into samples with *low* (L; <25; samples 361z and 408), *intermediate* (I; 25-45; samples 361, 462z & 398a) and *high* (H; >45; samples 209-2, 338z, 403 and 404) primitive mantle normalized $(La/Yb)_N$ ratios (Table 5-3; Fig. 5-9a-b). In addition, samples 361 and 398a show slight positive Eu anomalies and sample 403 has a "concave" HREE pattern.

Samples with low and intermediate $(La/Yb)_N$ ratios are depleted in Nb(Ta) and Th and are slightly depleted in Ti relative to the adjacent REE (Fig. 5-9c). In addition, these samples show elevated Ba, K and Rb and are depleted in U relative to La. Some of these samples are also slightly depleted in Zr, and for samples 361z and 408 Sr (Fig. 5-9e).

Samples with high $(La/Yb)_N$ ratios are also depleted in Nb(Ta) and Th and are strongly depleted in Ti relative to the adjacent REE (Fig. 5-9d). In addition, samples 338z and 209-2 are strongly depleted in Zr (Hf). These samples show elevated Ba and Rb and are depleted in Th, U and K relative to La (Fig. 5-9f).

5.4.3 Rb-Sr and Sm-Nd isotopes

Rb-Sr and Sm-Nd isotopic data for representative samples are presented in Table 5-4. Measured $^{87}Sr/^{86}Sr$ ratios range from 0.7046 to 0.7107. The samples form a linear array when plotted on an isochron diagram (Fig. 5-10a), but the scatter is obviously too great to represent an isochron (see section 2-1). The errorchron "age" is 996 ± 180 Ma, with an initial $^{87}Sr/^{86}Sr$ ratio of 0.70421 ± 0.00058. The excess scatter may indicate that the samples are not all the same age or that they did not originate from the same source

region. The ultrapotassic component of a composite dyke from the southern Canyon Domain yielded a crystallization age of 980 ± 3 Ma (sample #403; Fig 5-3). Thus, an emplacement age of ~1 Ga seems reasonable for all samples and initial isotopic ratios have been calculated for this age. At 1 Ga, initial ratios for the samples are in the range of 0.7038–0.7048 ($\varepsilon_{Sr}{}^{1000}$ = 7-21; Table 5-4).

Measured $^{143}Nd/^{144}Nd$ ratios range from 0.511183 to 0.511853. The samples display considerable heterogeneity in initial ε_{Nd} values at 1 Ga, ranging from –14 to –2.6 (Table 5-4). These data are illustrated on a plot of ε_{Nd} vs. age in Fig. 5-10b, which also includes a field for "Quebecia" crust from Owens and Tomascak (2002) (based on the Nd-isotopic results of Dickin and Higgins (1992) and Dickin (2000)). It is clear from Figure 5-10b, that there are two discrete ranges in ε_{Nd} for the samples (-2.6 to -6.9 and -12 to -14.4). In general, samples with low (L; <25; sample 408) and intermediate (I; 25-45; samples 361 and 398a) primitive mantle normalized $(La/Yb)_N$ ratios (and one sample with high ratio 209-2) have ε_{Nd} values at 1 Ga ranging from -2.6 to -6.9; while those with high (H; >45; samples 338z and 403; and one sample with intermediate ratio 462z) have more negative values (- 12 to -14.4). Figure 5-11 (ε_{Sr} vs. ε_{Nd} at 1Ga) illustrates the low ε_{Nd} and low ε_{Sr} signature of the ultramafic dykes. The lack of correlation between Sr and Nd isotopic compositions suggests some decoupling of these systems. Model ages were calculated with respect to a depleted mantle model (T_{DM2}), and the De Paolo's mantle model (De Paolo, 1981) (see section 2-1) and are listed in Table 5-4.

5.5 Interpretation and Discussion

The K-rich dykes of the Canyon Domain are considered ultrapotassic in the sense of Foley *et al.* (1987). On primitive mantle-normalized spidergrams, the dykes show enrichment in low field strength elements (LFSE; Ba, K, Rb) and LREE (La_N ~100-400), and depletion in high field strength elements (HFSE; Th, Nb, Ta and Ti) and heavy rare earth elements (HREE; Yb_N= 3-8)). In addition, the dykes are characterized by low ε_{Nd} – low ε_{Sr} signatures.

The age of the ultrapotassic dykes is constrained by the 980±3 Ma crystallization age of an ultrapotassic dyke (sample #403) from the southern Canyon Domain (Dunning and Indares, pers. comm. 2008). Elsewhere in the central Grenville Province, late lamprophyre dykes are reported from within the ~1010 Ma Labrieville anorthosite (Owens and Tomascak, 2002). In addition alkalic mafic dykes are widespread in the Pinware Terrane and in the Gilbert river fault of the lake Melville Terrane (eastern Grenville; Gower and Krogh, 2002) where they were dated at 985±6 and 974±6 Ma, respectively (Wasteneys *et al.,* 1997). In contrast, alkalic magmatism of that age is apparently absent in the western Grenville Province.

5.5.1 Comparison with the Labrieville Lamprophyres

The lamprophyres of the Labrieville Anorthosite (Owens and Tomascak, 2002) are ultrapotassic as defined by Foley *et al.* (1987) (*i.e.* they have $K_2O/Na_2O > 2$ and MgO and $K_2O > 3$wt. %). In addition, other major element concentrations are within the range of the ultrapotassic dykes in this study and they also have high concentrations of Cr (278-

393 ppm) and Ni (101-180 ppm) and are highly enriched in Ba (4612-5583ppm), Rb (64-94) and Sr (2350-3110ppm).

In a primitive mantle-normalized multi-element plot (Fig. 5-12), the Labrieville lamprophyres show patterns similar to those of the ultrapotassic dykes of this study, especially those with low and intermediate $(La/Yb)_N$ ratios (Fig. 5-12a), with elevated Ba, Rb, and K and depletions in Th, Nb, Ta and U. Samples with high $(La/Yb)_N$ ratios (209-2, 338z, 404 and 403) show higher REE concentrations and a weak K peak (Fig. 5-12b).

Figure 5-13 shows ε_{Nd} vs. ε_{Sr} at 1Ga for the ultrapotassic dykes and a number of potassic and ultrapotassic rocks including the Labrieville lamprophyres. The latter have negative ε_{Nd} values (–10.2 to –4.0), similar to those of the ultrapotassic dykes and slightly lower ε_{Sr} values (*i.e.* close to bulk earth). The relatively unradiogenic Sr-isotopic signature of the Labrieville Lamprophyres and the ultrapotassic dykes of this study, combined with an enriched Nd-isotopic signature have also been reported for other potassic rocks (*e.g.* Leucite Hills). However, many other examples of potassic and ultrapotassic rocks display good correlations between these isotopic parameters and plot well within the "enriched" quadrant of Fig. 5-13 at much higher ε_{Sr}.

5.5.2 Magma source

Although some of the ultrapotassic dykes have the characteristics of moderately evolved magmas (relatively low MgO, Ni, Cr); some of the ultrapotassic dykes share many of the compositional features of other ultrapotassic rocks indicative of a mantle origin, including relatively high Mg#, Ni and Cr (Table 5-3; Perfit *et al.*, 1980). The high

concentrations of K, Ba, Sr, and REE, as well as high $(La/Yb)_N$, preclude an origin for these rocks from typical MORB or ocean island basalt (OIB) source regions, unless the parental melts were significantly modified (Fig. 5-14). The LREE and LFSE enrichment and HFSE depletion in the ultrapotassic rocks may reflect either a LFSE and LREE enriched mantle source (*i.e.* metasomatized) or continental crust contamination of a mantle derived magma during ascent and emplacement.

A possible explanation for the compositional features of the ultrapotassic dykes is that they represent significant contamination of mantle-derived melts by upper crustal material (e.g. Wang *et al.*, 2007). The strongest piece of evidence suggesting crustal contamination is the highly negative ε_{Nd} values at 1Ga for the dykes. Some of the samples (209-1, 361, 398a and 408) have ε_{Nd} values similar to those of "Quebecia" crust (Owens and Tomascak, 2002) at 1 Ga (Fig. 5-10b), which may reflect contamination by the local crust. The remaining samples (338z, 403 and 462z) have ε_{Nd} values lower than "Quebecia" crust at 1 Ga, which could reflect contamination by Archaean crust. However, crustal contamination can be ruled out on the basis of Sr isotopes and trace elements. First, the relatively unradiogenic Sr-isotopic signature of the dykes would preclude a significant upper crustal component. Secondly, concentrations of the LREE are very high compared to those of the upper crust or even those of older Archean crust (Fig. 5-14); and finally, concentrations of Ba, K and Sr, are also far greater than in typical upper crust. For instance, Sr abundances of 1000-6500 ppm in the ultrapotassic dykes versus 350 ppm typical for upper continental crust; Ba contents in the dykes are between 2000-9000 ppm versus 550 ppm, which characterizes the upper continental crust (Taylor

and McLennan, 1981). Thus, it is considered unlikely that crustal contamination had any significant effect on the composition and isotopic signatures of the magmas. These are both regarded to be source features.

If the source region for the ultrapotassic dykes was the mantle, then this mantle must have been enriched in the incompatible elements and in many LFSE. The most likely source region that fits these requirements is a subcontinental lithospheric mantle with an ancient and long-lived history of enrichment in incompatible and LFSE (metasomatized), as argued by many other investigators of similar potassic and ultrapotassic rocks (*e.g.,* Bachinski and Scott, 1979; McKenzie, 1989; Thompson *et al.*, 1989; Canning *et al.,* 1996; Owens and Tomascak, 2002). Although such magmas potentially could be derived solely within the lithosphere, they might also represent mixing of lithospheric and asthenospheric components. The origin of mantle enrichment remains much debated; however, there are two widely accepted models: 1) interaction between lithospheric mantle and volatile-rich, low density melts that have migrated from the asthenosphere and accumulated in the lithosphere (McKenzie, 1989; Gibson *et al.,* 1995; Olafsson and Eggler, 1983; Hawkesworth *et al.,* 1990; Sevigny and Theriault, 2003); and 2) metasomatism by melts/fluids released from a subducting slab (Maury *et al.*, 1992; Peccerillo, 1990, 1999; Foley and Peccerillo, 1992; Rogers, 1992; Nelson, 1992; Nelson *et al.*, 1986; van Bergen *et al.*, 1992).

The negative ε_{Nd} values in the ultrapotassic dykes, as well as those reported for other ultrapotassic rocks (*e.g.* Italy, Virunga, West Kimberley and Gaussberg), indicate that these magmas are derived from, or contain a contribution from, old sources enriched

in the light REE relative to heavy REE (*i.e.* long-term light-REE enrichment). In addition, the two discrete ranges in ε_{Nd} for the dykes (-2.6 to –6.9 & -12 to –14.4) may indicate that these groups come from two source regions, both of which had a history of light REE enrichment. The relatively unradiogenic Sr-isotopic signature of the ultrapotassic dykes of this study, suggest that the light REE enrichment of the source was not accompanied by a strong increase in Rb/Sr (McCulloch *et al.,* 1983). This contrasts with generally coupled LREE and Rb/Sr enrichment or depletion in mantle processes as inferred from the inverse Sr-Nd isotopic correlation for oceanic basalts (Dickin, 2005).

Low ε_{Nd} – low ε_{sr} isotopic signatures have been reported elsewhere (*e.g.* Labrieville Lamprophyres and Leucite Hills Lamproites) and have been thought to be a function of the nature of the metasomatizing agent. In some areas, for example, it has been explained by the introduction of CO_2-rich melts to the lithospheric mantle (*e.g.,* Menzies and Wass, 1983; Dudás *et al.*, 1987; Nelson, 1989; Meen *et al.,* 1989). Others have argued that it may result from a common tectonic factor (Nelson, 1989). Peterson *et al.* (1994) recognized similar isotopic features in Proterozoic ultrapotassic rocks from the Churchill Province and suggested the possible presence of a Laurentian ultrapotassic "superprovince" that is characterized by this distinctive juxtaposition of Nd and Sr isotopic compositions.

The above observations indicate that the mantle was locally highly enriched in alkalis and some incompatible trace elements, particularly Sr, Ba, and REE. However, levels of U and Th in the dyke are low. Thus, the metasomatic component that affected the lithospheric mantle here was not enriched in all incompatible elements. In contrast to

the evidence for long-term LREE enrichment, the relatively unradiogenic Sr isotope signature implies that the mantle was not similarly enriched in Rb.

The nature and timing of the enrichment in the mantle source of the ultrapotassic dykes of this study cannot be distinguished. In some cases the enrichment of the mantle source of some lamprophyres or ultrapotassic rocks formed in post-collisional settings has been interpreted as the result of early subduction processes (Wang *et al.,* 2007; Guo *et al.*, 2005). In other cases (*e.g* Sevigny and Theriault, 2003) the mantle enrichment has been attributed to volatile-rich, asthenospheric melt fractions accumulated in the sublithostheric mantle (model 1) during a continental rifting event that took place ~700Ma before the emplacement of the lamprophyres. Thus, the studied ultrapotassic dykes could have been derived from partial melting of a lithospheric mantle previously enriched by subduction processes or by interaction with volatile-rich, low density melts that have migrated from the asthenosphere.

In a post-tectonic setting, as that of the studied dykes, melting of the subcontinental lithospheric mantle can be triggered by detachment of some of the lithospheric root of the mountain belt via convective thinning (Houseman *et al.,* 1981), lithospheric delamination (Kay and Kay 1993) or slab 'breakoff'(Davies and von Blanckenburg 1995). In all scenarios, upwelling, hot asthenospheric mantle may be brought into contact with, and induce partial melting of, previously metasomatized lithospheric mantle.

5.6 Conclusions

The primitive geochemical signature (i.e. high Mg#, Cr and Ni), in some of the dykes, suggests that the dykes were derived from a mantle source. To explain the incompatible enrichment and highly negative epsilon Nd values, we could appeal to significant contamination of mantle-derived melts by upper crustal material. However, the relatively unradiogenic Sr isotopic signature, and the highly enriched incompatible and LFS element concentrations of the ultrapotassic dykes indicates that crustal involvement was insignificant.

If the ultrapotassic dykes were indeed derived from a mantle source, then this mantle must have an ancient and long-lived history of enrichment in incompatible and some LFS elements (*i.e.* metasomatized), to account for the highly enriched incompatible and LFS element concentrations and highly negative Epsilon Nd values of the dykes. The most likely source region that fits these requirements is a metasomatized subcontinental lithospheric mantle.

The age of the ultrapotassic dykes is constrained by the 980±3 Ma crystallization age of an ultrapotassic dyke from the southern Canyon Domain. Ultrapotassic and alkalic dykes emplaced within the age range of 990-970 Ma are also found in: (a) the ~1010 Ma Labrieville anorthosite and (b) the Pinware and lac Melville Terranes.

The age, geochemistry and isotopic composition of the ultrapotassic dykes, in conjunction with data from other studies (above), suggest that a late orogenic (Grenvillian) magmatic event, that taps a distinct metasomatized mantle source, took place in the hinterland of the central eastern Grenville Province.

Table 5-1: Modal mineralogy (in percent) from SEM analysis and observed mineralogy (xx- highly abundant, x- abundant, v- minor and vv- traces). Bt: biotite, Qtz: quartz, Pl: plagioclase, Ksp: K-feldspar, Cpx: clinopyroxene, Opx: orthopyroxene, Hbl: hornblende, Ms: muscovite, Chl: chlorite, Cal: carbonates, All: allanite, Ilm: ilmenite, Pyr: pyrrothite, Rut: rutile and Tit: titanite.

Sample	Bt	Qtz	Pl	Ksp	Cpx	Opx	Hbl	Ap	Ms	Chl	Cal	All	Ilm	Pyr	Rut	Tit
209-2	31	25	27				2	3	5	1	3	1	1	1		
404	35	19	23		5		8	4			2	1	2	1		
398a	51	8	11	4	13		4	3	2	4	1					
361	xx	x	xx	xx	v			vv								
361z	37	8	22	20	8		1	2				1				
338z	40	26	5	17				8	2	1	2					
403	35	22		30				10							1	2
462z	x	x		x				x							x	x
408	23	5	50		2	4	11	2		1		1	1			

Table 5-2: Summary of mineral compositions in terms of XMg, where XMg = $[Mg/(Mg+Fe^{2+})]$ x100, % end-members for feldspar and mineral names for representative ultrapotassic dykes from the Canyon Domain (An = anorthite, Or = orthoclase, n.a = not analyzed, - = not present in sample). Magnesiohornblende has $(Na+K)_A < 0.5$, $Ca_A < 0.5$ and Si = 6.5-7.5.

Sample	Bt	Pl	Ksp	Cpx	Opx	Hbl	Ap	Opq
209-2	XMg (0.52-0.55) Ti (0.48-0.56)	Bytownite (An 69-82)	-	-	-	Magnesio-hornblende XMg (65-70)	SrO 0.71-0.84 wt.%	Ilm
361z	XMg (0.55) Ti (0.49-0.60)	Andesine (An 39-44)	Orthoclase (Or 84-88)	Diopside XMg (60-67) Ti (0.001-0.008) Al (0.02-0.24)	-	n.a	n.a	-
338z	XMg (0.69-0.7) Ti (0.37-0.41)	Andesine (An 32-35)	Orthoclase (Or 77-79)	-	-	-	SrO 0.67-78 wt.%	-
403	XMg (0.76-0.79) Ti (0.21-0.29)	-	Orthoclase (Or 82-89)	-	-	-	SrO 4-4.5 wt.%	-
404	XMg (0.61-0.63) Ti (0.45-0.49)	Bytownite (An75-84)	-	Diopside-Augite XMg (68-73) Ti (0.002-0.008) Al (0.02-0.07)	-	Magnesio-hornblende XMg (75-77)	SrO <1 wt.%	Ilm
408	XMg (0.5) Ti (0.44-0.54)	Andesine (An 45-50)	-	Diopside-Augite XMg (61-64) Ti (0.002-0.009) Al (0.03-0.07)	Ferrosilite XMg (45-48) Ti (0.002-0.005) Al (0.02-0.03)	Magnesio-hornblende XMg (61-65)	n.a	Ilm
398a	XMg (0.65-0.66) Ti (0.41-0.44)	Andesine (An 44-50)	Orthoclase (Or 62-74)	Diopside XMg (71-73) Ti (0.001-0.005) Al (0.03-0.06)	-	n.a	n.a	-

Table 5-3: Major and trace element data for the ultrapotassic dykes from the Canyon Domain. Major elements are reported in wt.% and trace elements in ppm; missing values are below detection. Major elements are recalculated volatile free with total Fe as FeO*; Mg# = [molar MgO/(MgO + FeO*)] x 100. C= central and S= southern Canyon Domain; *L = low* (<25); I = *intermediate* (25-45) *and H = high* (>45) primitive mantle normalized $(La/Yb)_N$ ratios. Normalizing values after Sun and McDonough (1989).

SAMPLE	209-2	338-z	403	404	462-z	398A	361	361-z	408
Terrane	BT-C	BT-C	BT-S	BT-S	BT-S	BT-S	BT-C	BT-C	BT-S
Group	*H*	*H*	*H*	*H*	*I*	*I*	*I*	*L*	*L*
SiO2	53.01	56.27	54.95	49.09	60.05	49.52	56.44	52.12	50.86
TiO2	2.54	1.57	2.55	3.37	2.08	2.02	2.38	2.05	2.43
Al2O3	15.08	12.47	11.08	13.25	12.87	12.74	14.93	14.91	17.34
FeO	11.04	5.31	4.08	10.69	3.65	10.22	9.29	9.89	10.69
MnO	0.21	0.09	0.08	0.13	0.06	0.15	0.14	0.11	0.15
MgO	5.26	6.70	6.98	7.72	4.89	10.83	3.76	6.28	5.17
CaO	7.61	6.77	6.59	9.40	3.90	7.26	5.44	6.15	7.41
Na2O	0.61	0.58	0.20	0.30	0.91	0.98	1.39	1.35	2.77
K2O	2.68	5.99	8.55	3.67	9.21	4.86	4.77	5.95	2.27
P2O5	1.95	4.25	4.93	2.38	2.37	1.43	1.45	1.19	0.92
LOI	1.92	2.21	1.13	1.57	0.92	1.46	1.81	1.25	1.22
K2O/Na2O	4.36	10.25	43.79	12.21	10.12	4.96	3.42	4.41	0.82
Na2O+K2O	3.29	6.57	8.74	3.97	10.12	5.84	6.16	7.30	5.04
CaO/Al2O3	0.50	0.54	0.59	0.71	0.30	4.96	0.36	0.41	0.43
Mg#	***46***	***69***	***75***	***56***	***70***	***65***	***42***	***53***	***46***
Co	121	194	166	160	145	107	146	110	127
Cr	63.8	151	270	98.3	169	638	52.4	145	
Cu	42.5		27.9	26.0		41.9	41.9	35.4	
Ni	21.3	82.3	139	44.5	115	230		102	24.9
Sc	20.2	4.00	7.00	22.0	11.0	19.9	13.6	17.0	21.0
V	143	33.6	64.8	164	62.1	166	136	169	142
Zn	213	205	69.7	173	86.6	167	147	161	121
Ba	7621	4960	7117	4771	3642	9017	6156	5208	2098
Ga	23.4	22.3	21.8	22.1	24.1	18.8	23.0	21.2	22.1
Rb	76.5	245	193	96.6	263	153	103	216	65
Sr	4301	2701	6521	2456	2889	1918	2618	1415	1091
Th	6.06	11.6	16.2	6.13	10.8	2.62	3.04	5.13	3.40
U	1.28	2.46	5.20	1.65	2.75	0.73	0.94	1.46	0.92
Zr	391	191	911	709	382	348	330	408	355
Hf	9.03	6.18	19.3		12.1	8.79	7.85	10.2	8.76
Nb	20.2	12.8	27.8	29.5	37.5	16.7	20.9	23.2	17.5
Ta	1.06	0.94	1.00	1.24	2.12	0.84	1.15	1.31	0.80
Y	56.3	54.0	39.0	40.2	31.6	24.1	31.4	26.7	32.7
La	256	252	245	220	137	79.5	115	92.5	95.6
Ce	500	511	526	441	285	177	253	196	187
Pr	66.5	61.7	62.4	52.4	33.3	22.6	31.6	22.6	21.3
Nd	244	249	240	199	124	88.5	120	89.0	80.7
Sm	36.8	47.3	36.6	30.6	19.3	15.0	18.7	14.6	13.5
Eu	9.93	11.7	9.04	7.67	4.40	4.53	5.96	3.97	3.60
Gd	26.1	32.1	22.0	19.6	12.6	10.7	12.9	9.79	10.2
Tb	2.76	3.63	2.21	2.24	1.52	1.15	1.36	1.26	1.46
Dy	11.5	13.7	8.61	9.45	6.76	5.02	6.07	5.64	7.09
Ho	1.91	1.87	1.33	1.42	1.09	0.84	1.05	0.95	1.24
Er	4.78	4.59	3.65	3.53	3.00	1.99	2.62	2.69	3.45
Tm	0.63	0.54	0.52	0.45	0.39	0.25	0.35	0.37	0.47
Yb	3.93	3.30	3.74	2.79	2.30	1.46	2.09	2.45	2.90
Lu	0.57	0.46	0.65	0.37	0.30	0.20	0.29	0.35	0.40
W		587	467	406	413			230	310
Pb		20.6	35.9	17.9	30.4			14.6	18.6
Ge		1.24	1.31	1.07	1.47			1.04	1.15
(La/Ce)N	1.3	1.3	1.2	1.3	1.3	1.2	1.2	1.2	1.3
(La/Sm)N	4.5	3.5	4.4	4.7	4.6	3.5	4.0	4.1	4.6
(La/Yb)N	47.0	55.2	47.3	56.9	43.1	39.2	39.7	27.3	23.8
(Dy/Tb)N	2.0	2.8	1.5	2.3	2.0	2.3	1.9	1.5	1.6

Table 5-4: Sm–Nd isotope analyses for ultrapotassic dykes of the Canyon Domain. Model ages were calculated with respect to a depleted mantle (T_{DM2}) and De Paolo's mantle model (De Pal; De Paolo, 1981). The T_{DM2} model uses a mantle separated from the chondrite uniform reservoir (CHUR) since 4.55 Ga following a linear evolution and having a present-day Epsilon value of +10. 2SE (M) = standard error of the mean; (2) and (3) = duplicated analyses; - = not analysed. Groups as defined in Table 5-3.

Sample	Group (La/Yb_N)	Sr (ppm)	Rb (ppm)	$^{87}Rb/^{86}Sr$	$^{87}Sr/^{86}Sr$	2SE (M)	$(^{87}Sr/^{86}Sr)_0$	$\varepsilon_{Sr}(1000)$	Nd (ppm)	Sm (ppm)	$^{147}Sm/^{144}Nd$	$^{143}Nd/^{144}Nd$	2SE (M)	$\varepsilon_{Nd}(0)$	$\varepsilon_{Nd}(1000)$	De Pal (Ma)	T_{DM2} (Ma)
403	*H*	-	-	-	-	-	-	-	257	36.8	0.0868	0.511182	4	-28.4	-14.4	2213	2355
403(2)	*H*	-	-	-	-	-	-	-	260	38.3	0.0888	0.511183	4	-28.4	-14.6	2247	2391
403(3)	*H*	6521	193	0.085803	0.7055	10	0.7043	13.75	256	37.1	0.0875	0.511183	5	-28.4	-14.4	2252	2367
338z	*H*	2701	245	0.262639	0.7076	12	0.7038	6.64	259	46.6	0.1089	0.511450	5	-23.2	-12.0	2324	2463
209-2	*H*	4301	76.5	0.051458	0.7046	12	0.7039	8.06	261	37.0	0.0858	0.511560	5	-21.0	-6.9	1765	1891
404	*H*	2456	96.6	0.113749	0.7064	20	0.7048	20.86	-	-	-	-	-	-	-	-	-
462z	*I*	2889	263	0.263862	0.7080	16	0.7042	12.33	137	20.1	0.089	0.511224	5	-27.6	-13.8	2226	2345
361	*I*	2618	103	0.113393	0.7057	30	0.7041	10.91	122	18.4	0.0907	0.511672	5	-18.8	-5.3	1696	1828
398a	*I*	1918	153	0.230433	0.7071	9	0.7038	6.64	92.1	14.7	0.0967	0.511763	5	-17.1	-4.3	1663	1804
408	*L*	1091	65.4	0.181778	0.7072	9	0.7046	18.0	76.4	12.3	0.0972	0.511853	5	-15.3	-2.6	1554	1694
361z	*L*	1415	216	0.440777	0.7107	22	0.7044	15.17	-	-	-	-	-	-	-	-	-

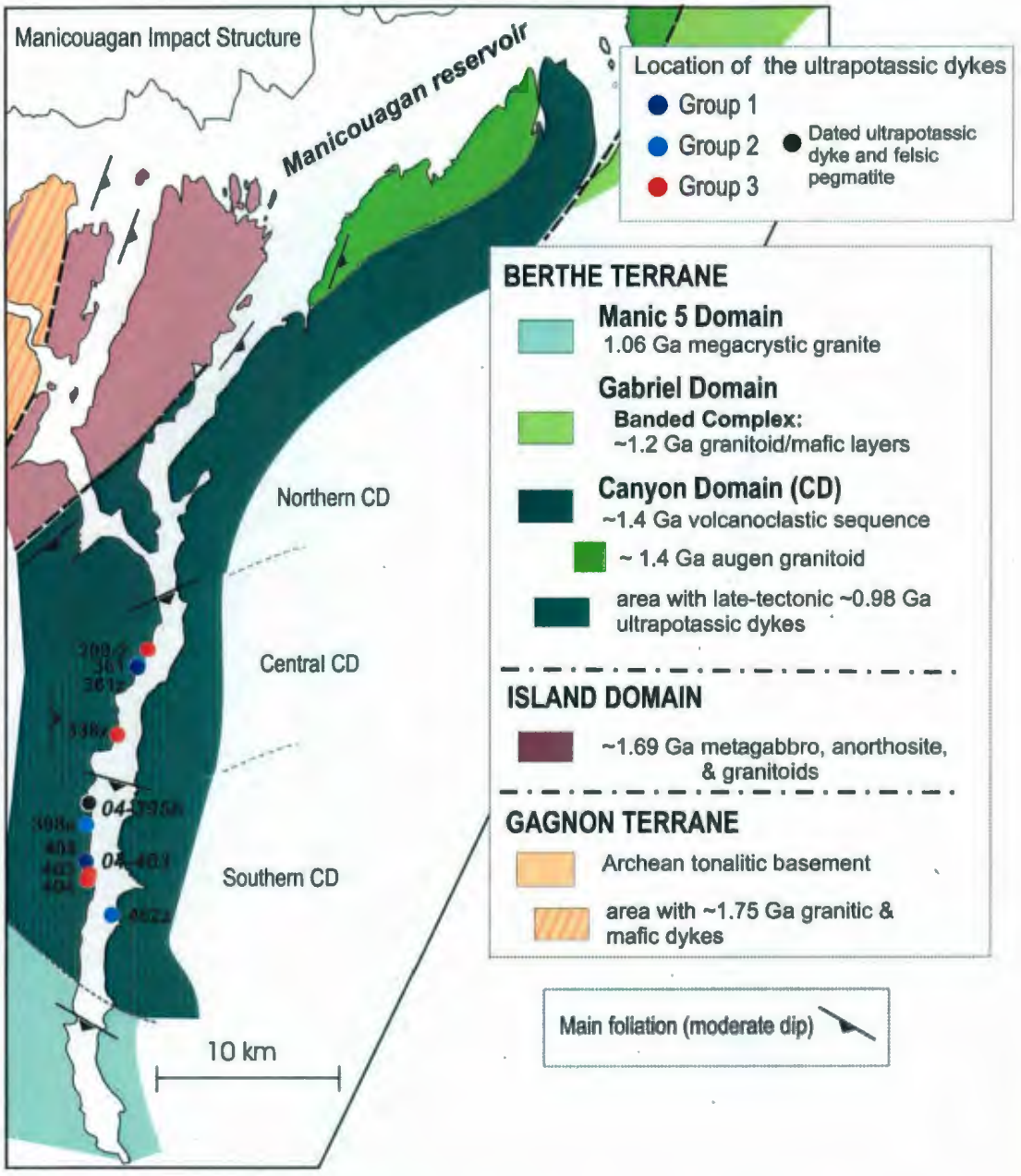

Figure 5-1: Geological map of the south shore of the Manicouagan reservoir showing the location of the ultrapotassic dykes from the Canyon Domain. Geochemical groups: Group 1, Group 2 and Group 3 = samples with low, intermediate and high $(La/Yb)_N$ ratios. The data for the dated ultrapotassic dyke (04-403) and the felsic pegmatite (04-395b) is from Dunning and Indares (pers. comm. 2008).

(a) 361

(b) 361

(c) 209-2

(d) 338z

(e) 413

(f) 403

(g) 412

(h) 398a

(i) 462z

Figure 5-2: Outcrop photos of characteristic ultrapotassic dykes from the central (a-d) and southern (e-i) Canyon Domain.

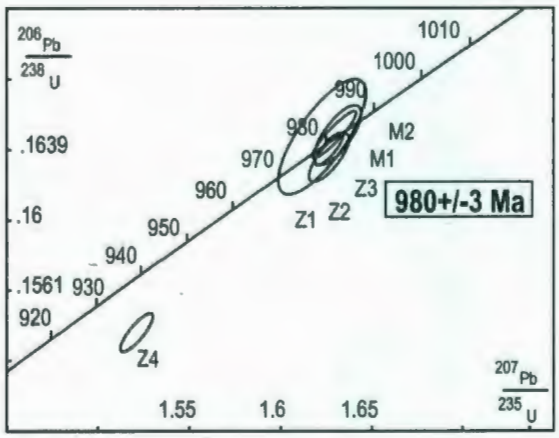

(a) 403

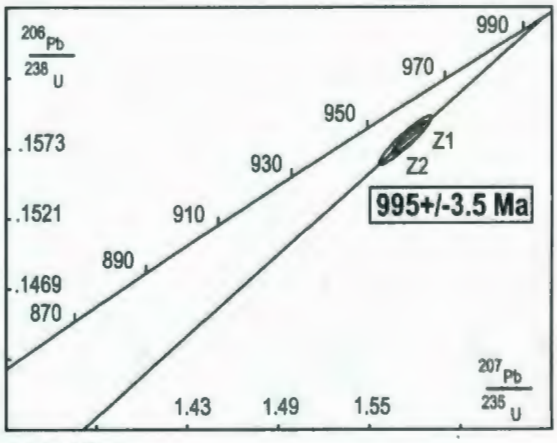

(b) 395b

Figure 5-3: U-Pb zircon ages; concordia diagrams for: a) an ultrapotassic dyke (403) and b) a felsic pegmatite dyke (395b) from the Canyon Domain (Dunning and Indares, pers. comm. 2008).

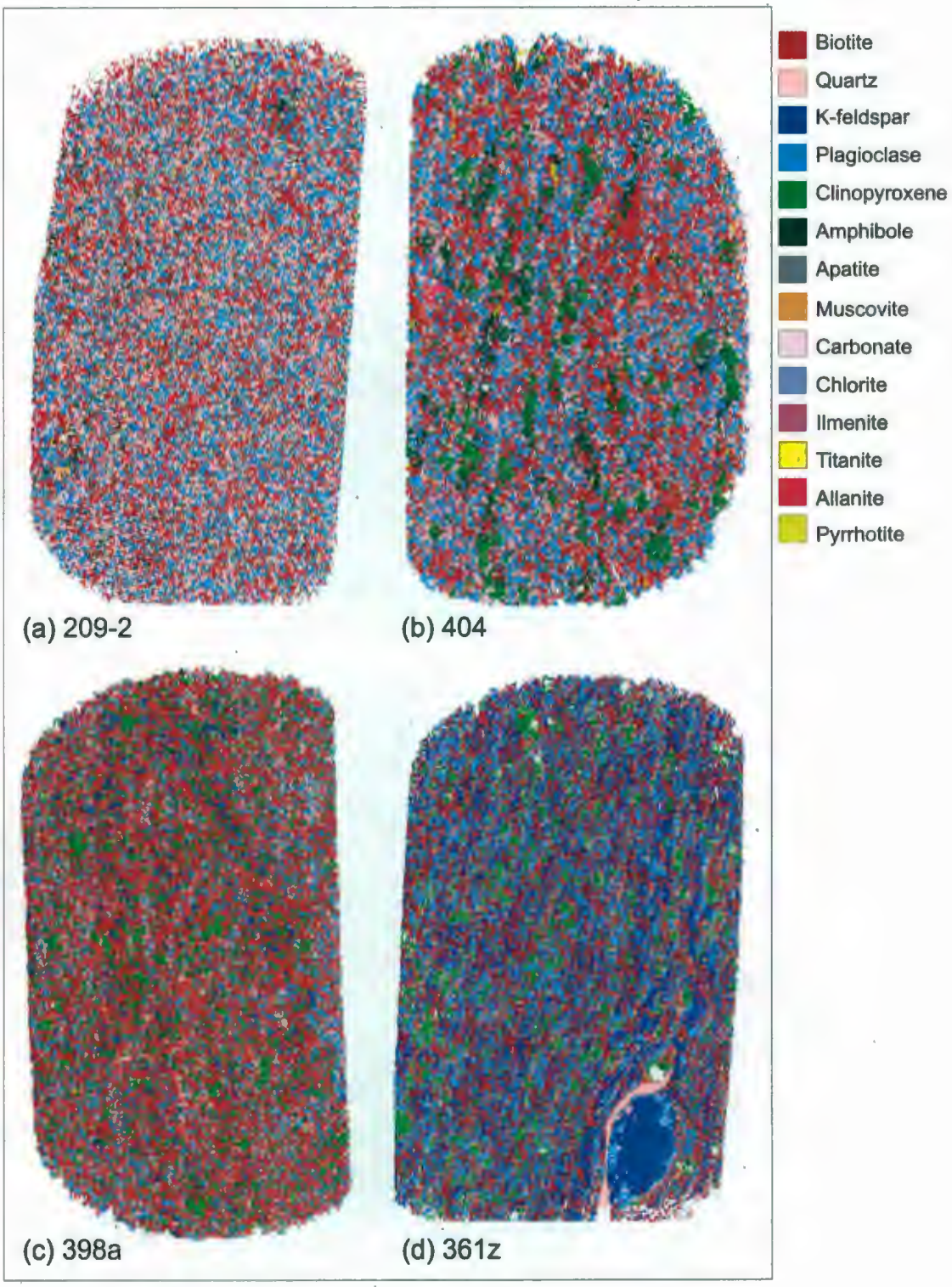
Biotite
Quartz
K-feldspar
Plagioclase
Clinopyroxene
Amphibole
Apatite
Muscovite
Carbonate
Chlorite
Ilmenite
Titanite
Allanite
Pyrrhotite
(a) 209-2
(b) 404
(c) 398a
(d) 361z

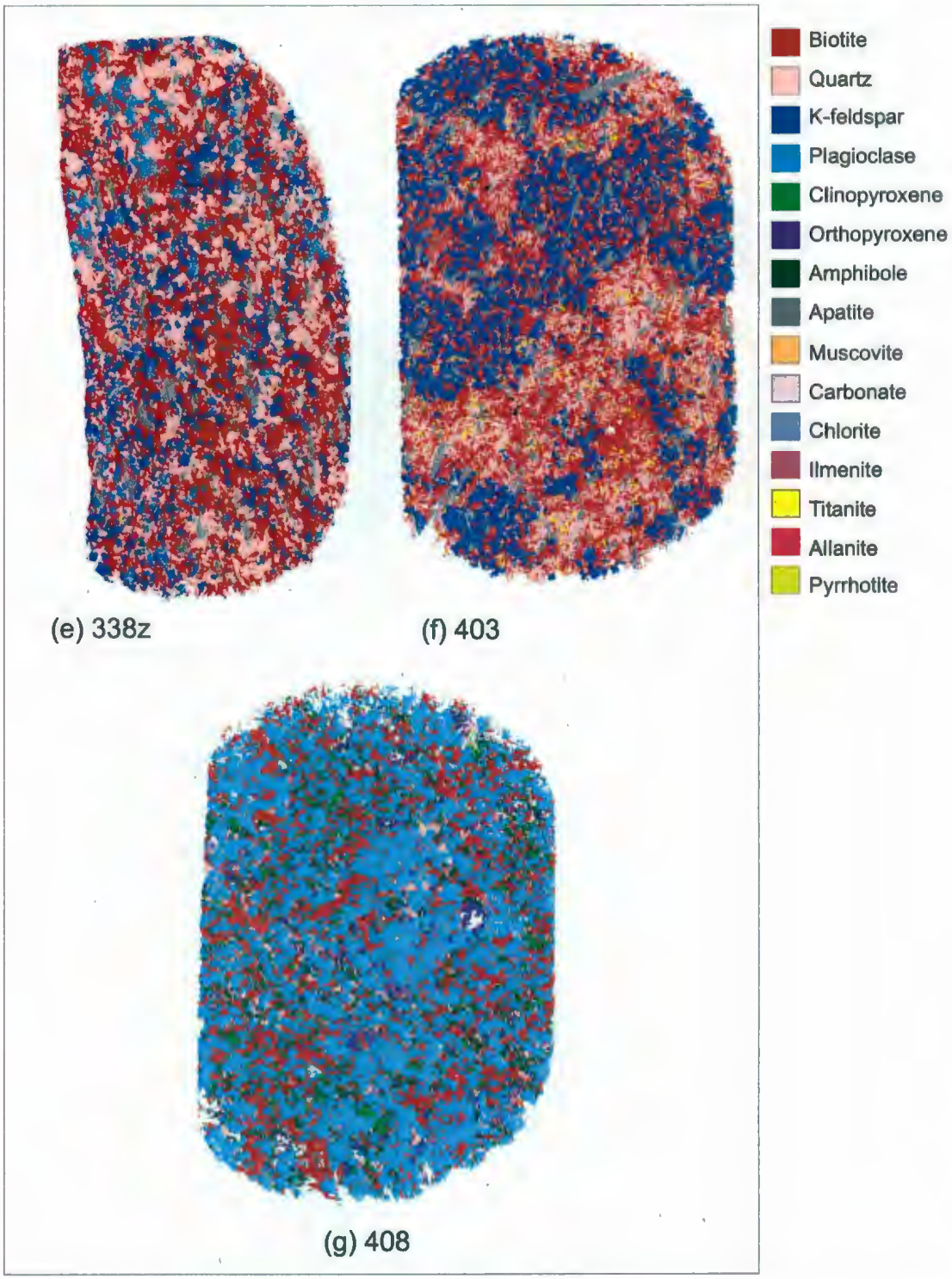

Figure 5-4: SEM false color mineral maps for the ultrapotassic dykes of the Canyon Domain. Each map is ~4cm in length (size of a standard thin-section).

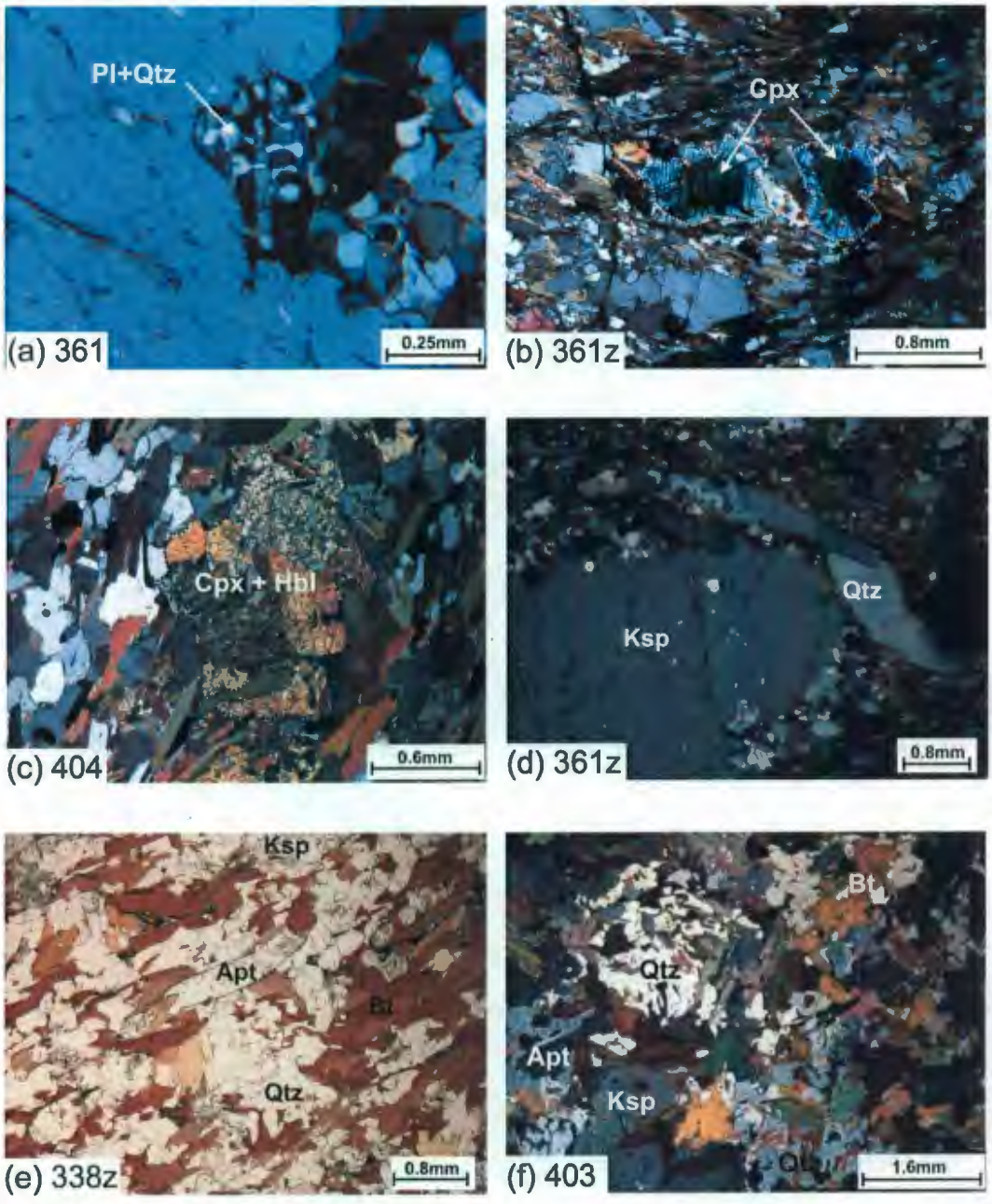
Pl+Qtz
0.25mm
(a) 361
Cpx
0.8mm
(b) 361z
Cpx + Hbl
0.6mm
(c) 404
Qtz
Ksp
0.8mm
(d) 361z
Ksp
Apt
Bt
Qtz
0.8mm
(e) 338z
Bt
Qtz
Apt
Ksp
1.6mm
(f) 403

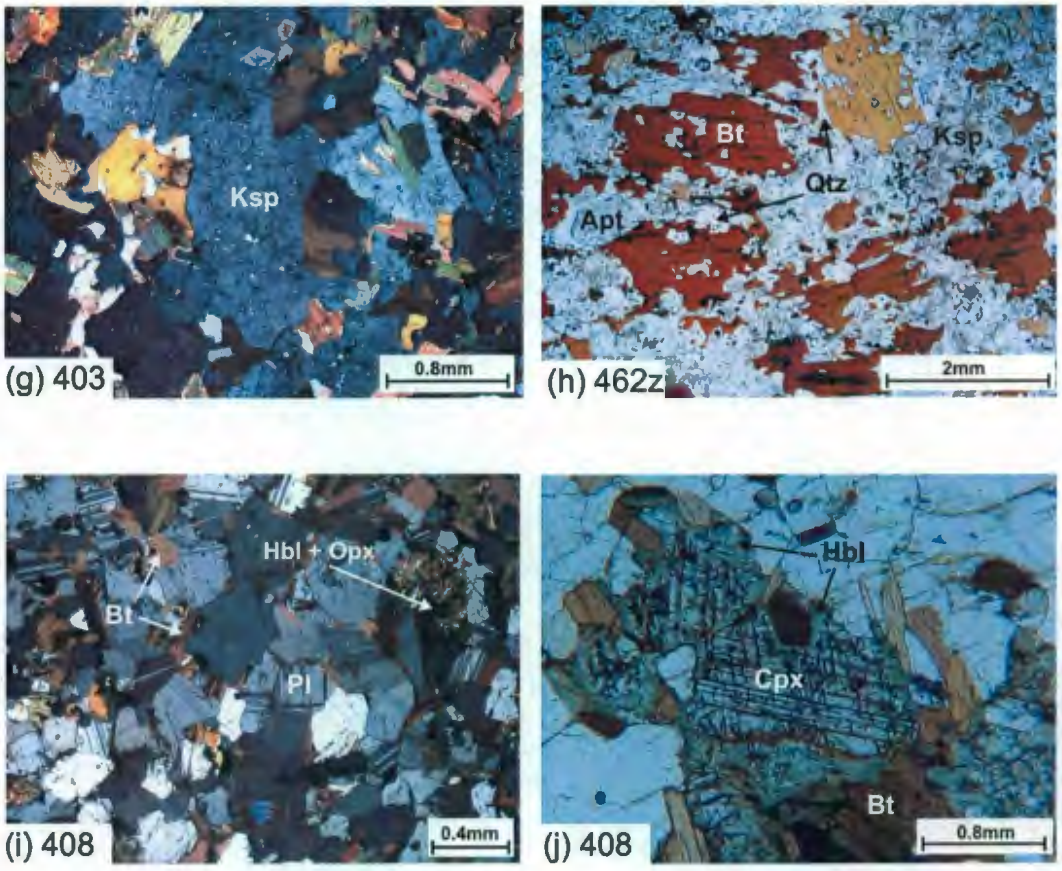

Figure 5-5: Microphotographs of typical textures of the ultrapotassic dykes from the Canyon Domain (e, h and j taken under plane polarized light; remaining under cross-polarized light). Cpx: clinopyroxene, Pl: plagioclase, Ksp: K-feldspar, Qtz: quartz, Bt: biotite, Apt: apatite, Hbl: hornblende. (a) myrmekite texture displayed by plagioclase and quartz; b) semi-rounded clinopyroxene with pronounced cleavage; (c) aggregates of clinopyroxene and hornblende in a biotite-rich feldspathic matrix; (d) recrystalized quartz ribbon around large K-feldspar xenocryst; (e) biotite, K-feldspar and apatite with interstitial quartz; (f) interstitial quartz in a biotite, K-feldspar and apatite matrix; (g) K-feldspar with exsolutions of plagioclase; (h) large biotite and K-feldspar with interstitial quartz; (i) plagioclase with interstitial biotite and subordinate orthopyroxene and hornblende; and (j) clinopyroxene corroded by hornblende and partially rimmed by biotite.

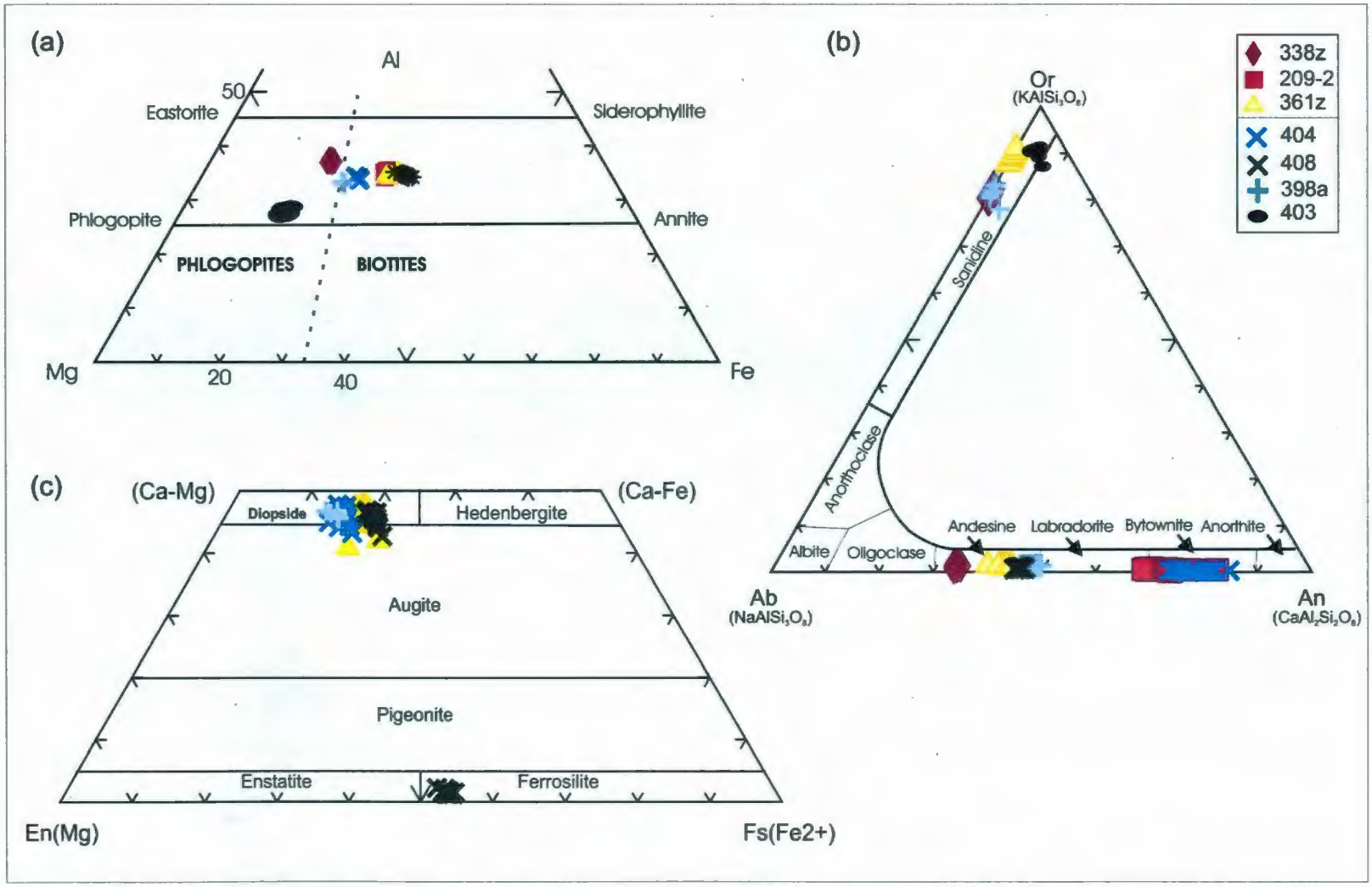

Figure 5-6: Composition/classification diagrams for: **a)** biotite in terms of Al-Mg-Fe (mole %); **b)** plagioclase (ternary classification diagram Ab-An-Or for feldspars) and; **c)** pyroxene (after Morimoto et al., 1988) in the ultrapotassic dykes of the central and southern Canyon Domain.

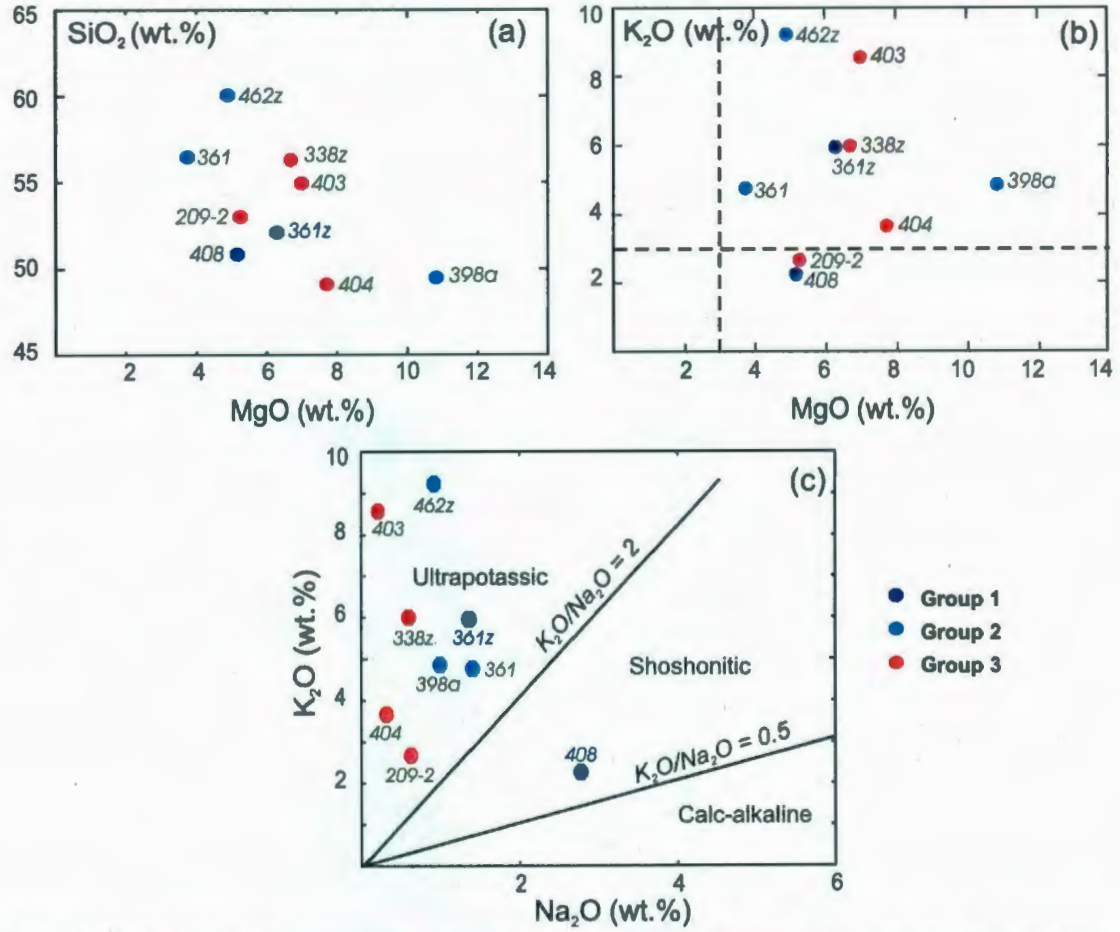

Figure 5-7: Variation diagrams of a) SiO_2 and b) K_2O versus MgO and c) K_2O versus Na_2O for the ultrapotassic dykes of Canyon Domain. Geochemical groups: Group 1 = samples with $(La/Nb)_N < 25$; Group 2 = samples with $(La/Nb)_N = 25$-45 and Group 3= samples with $(La/Nb)_N > 45$.

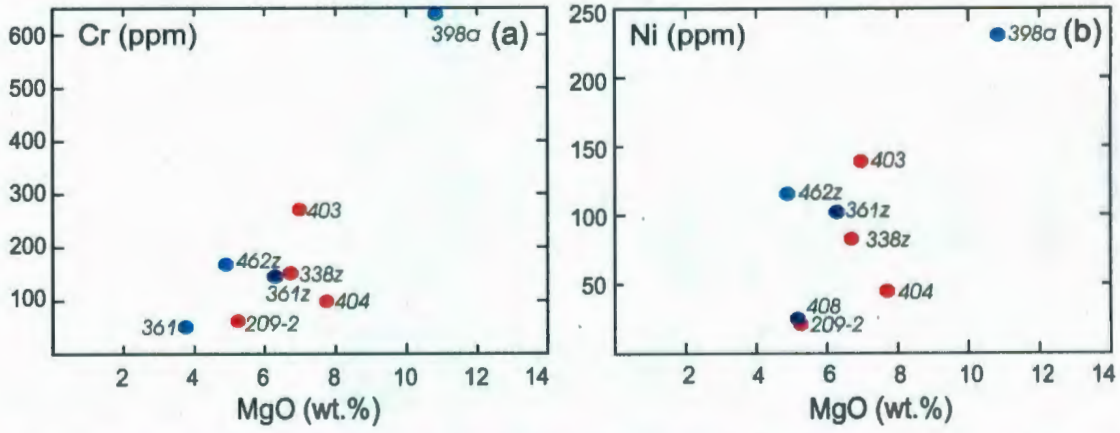

Figure 5-8: Variation diagrams of Cr and Ni versus MgO for the ultrapotassic dykes of Canyon Domain. Groups as defined in Figure 5-7.

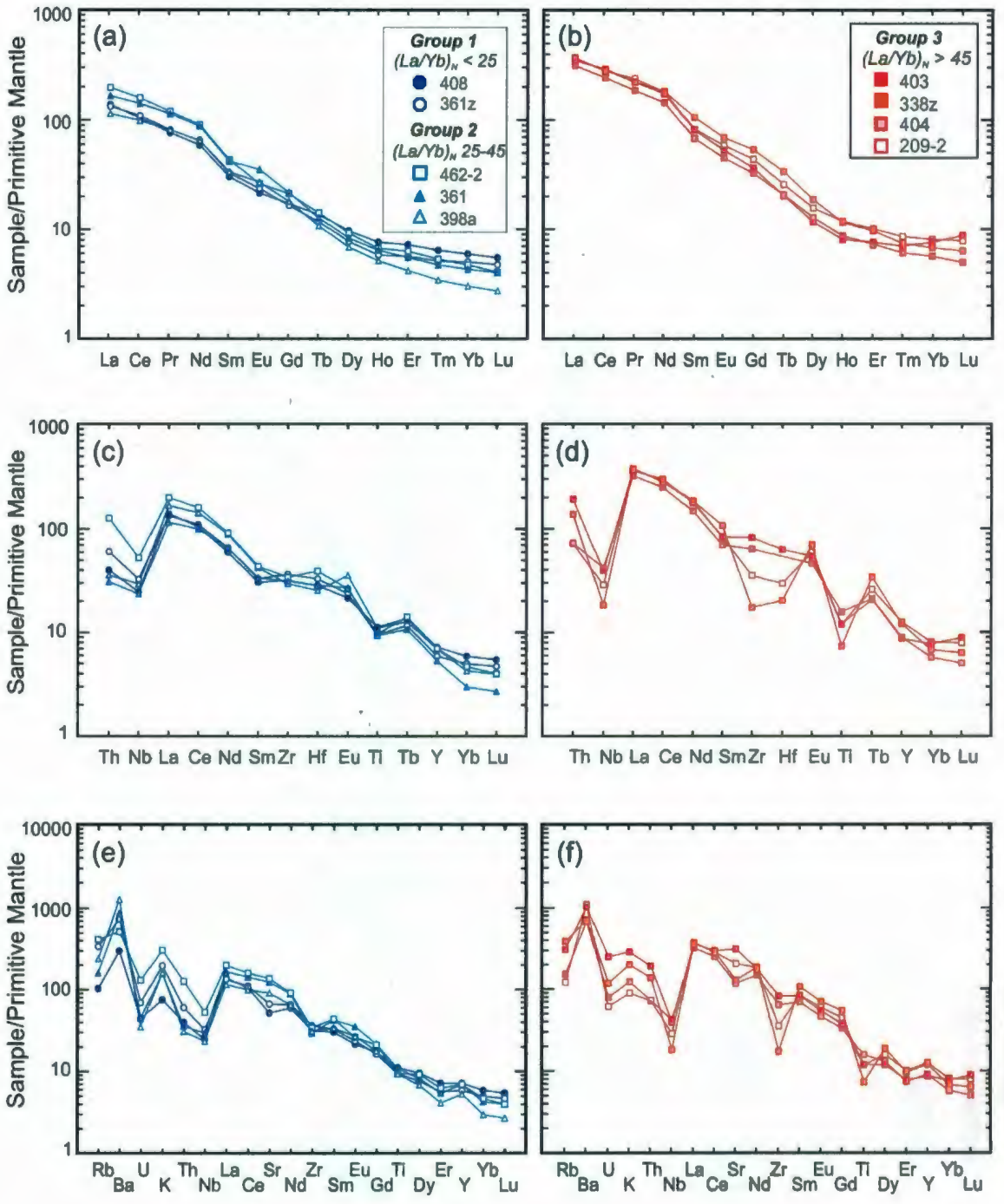

Figure 5-9: a-b) Primitive mantle normalized REE; c-d) extended (REE, HFSE, Th) and; e-f) complete REE, HFSE + LFSE plots for the ultrapotassic dykes of the central and southern Canyon Domain. Normalized values after Sun and McDonough (1989).

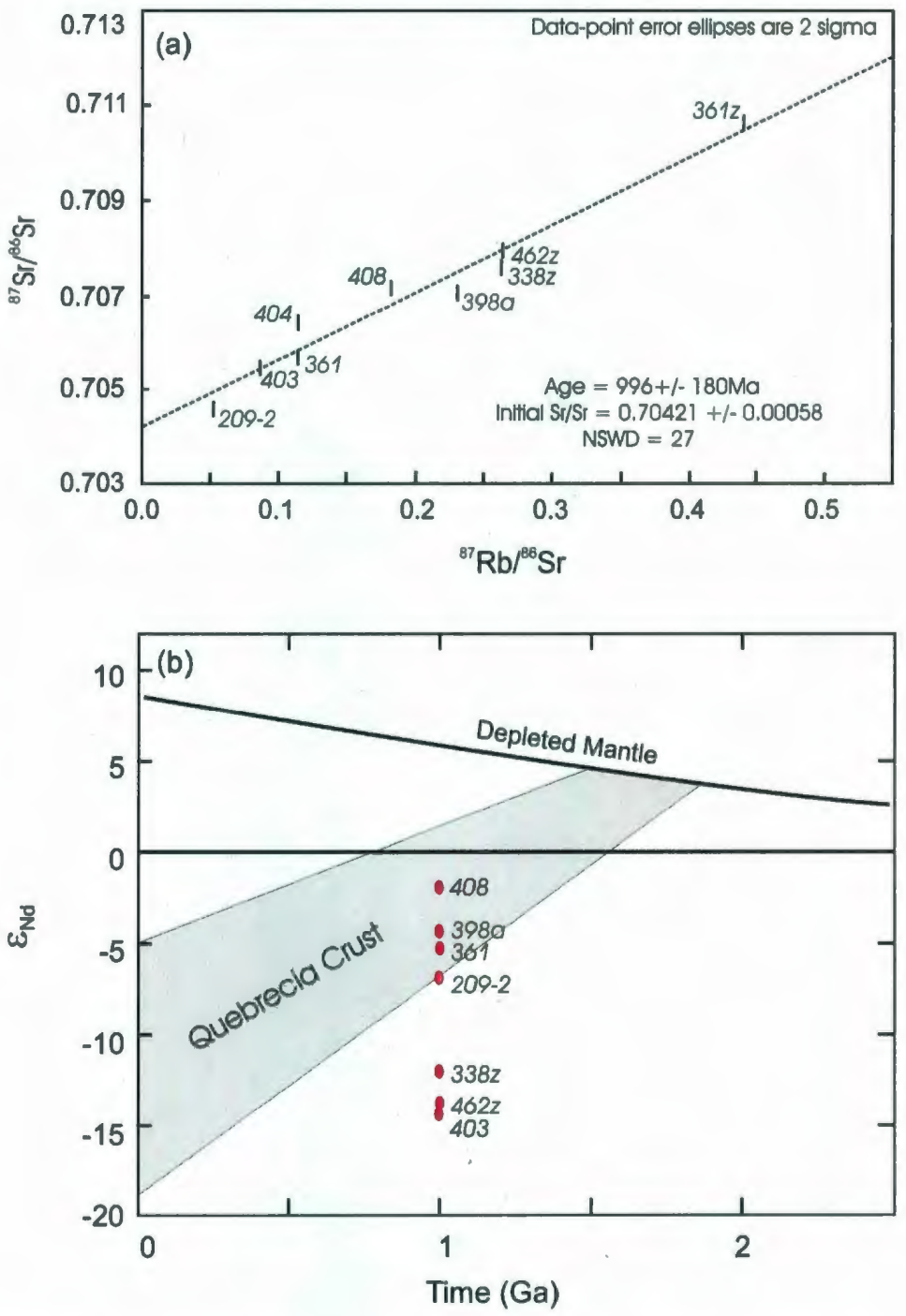

Figure 5-10: Plots of (a) $^{87}Sr/^{86}Sr$ versus $^{87}Rb/^{86}Sr$ and (b) initial ε_{Nd} versus age (T=1000Ma) for ultrapotassic dykes of the Canyon Domain. The depleted mantle curve is from De Paolo (1981). Data for Quebrecia Crust after Owens and Tomascak (2002).

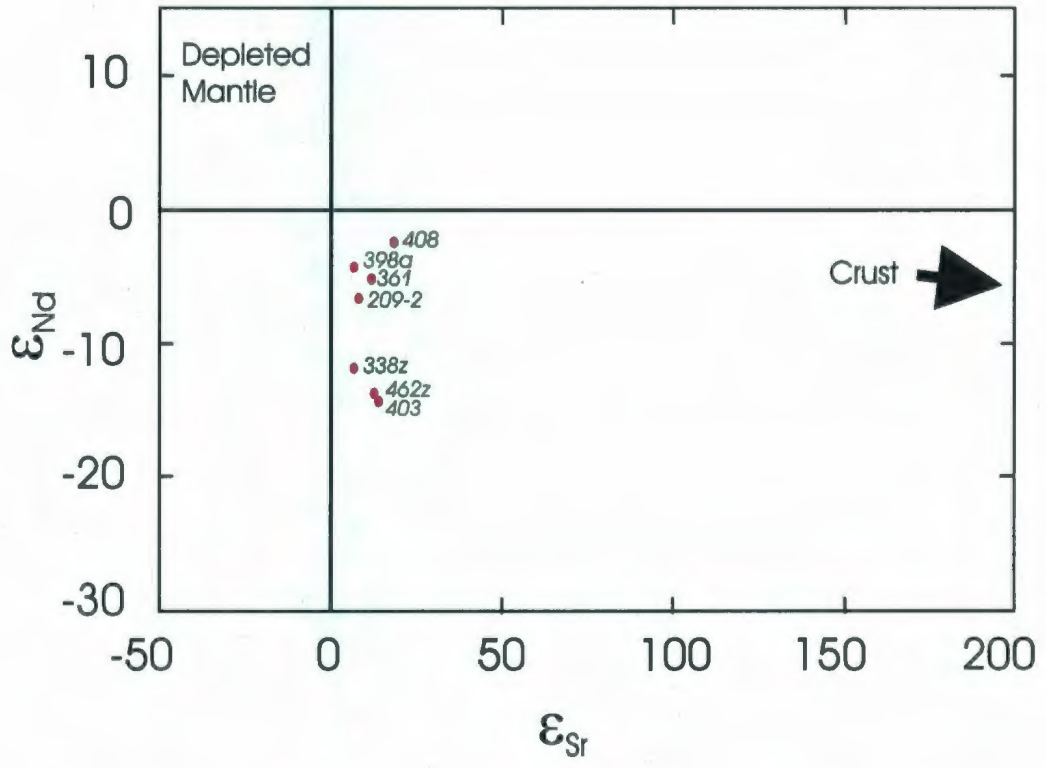

Figure 5-11: Plots of ε_{Nd} versus ε_{Sr} (T=1000Ma) for ultrapotassic dykes of the Canyon Domain.

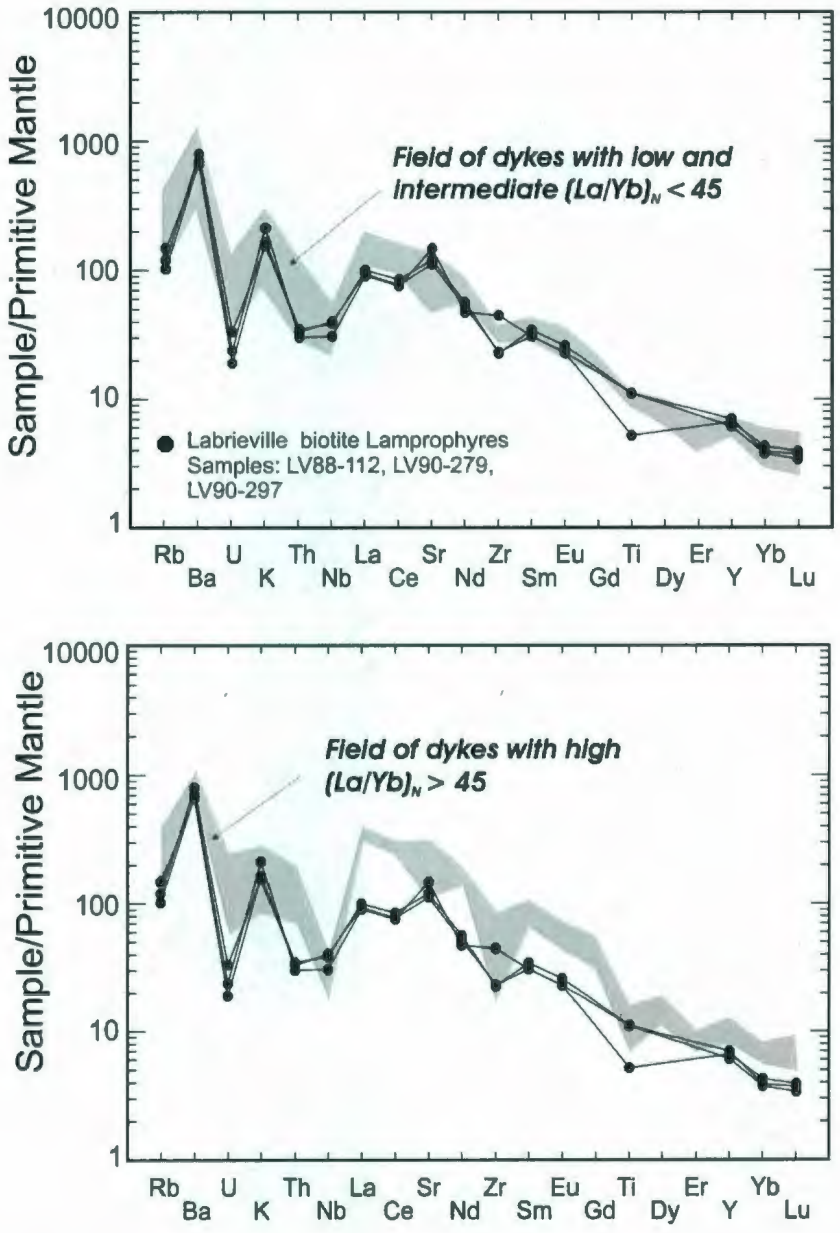

Figure 5-12: Primitive mantle-normalized multi-element plots for the Labrieville Lamprophyres (black; Owens and Tomascak, 2002) and fields for the ultrapotassic dykes of the Canyon Domain with a) low and intermediate and b) high $(La/Yb)_N$ ratios (grey). Normalized values after Sun and McDonough (1989).

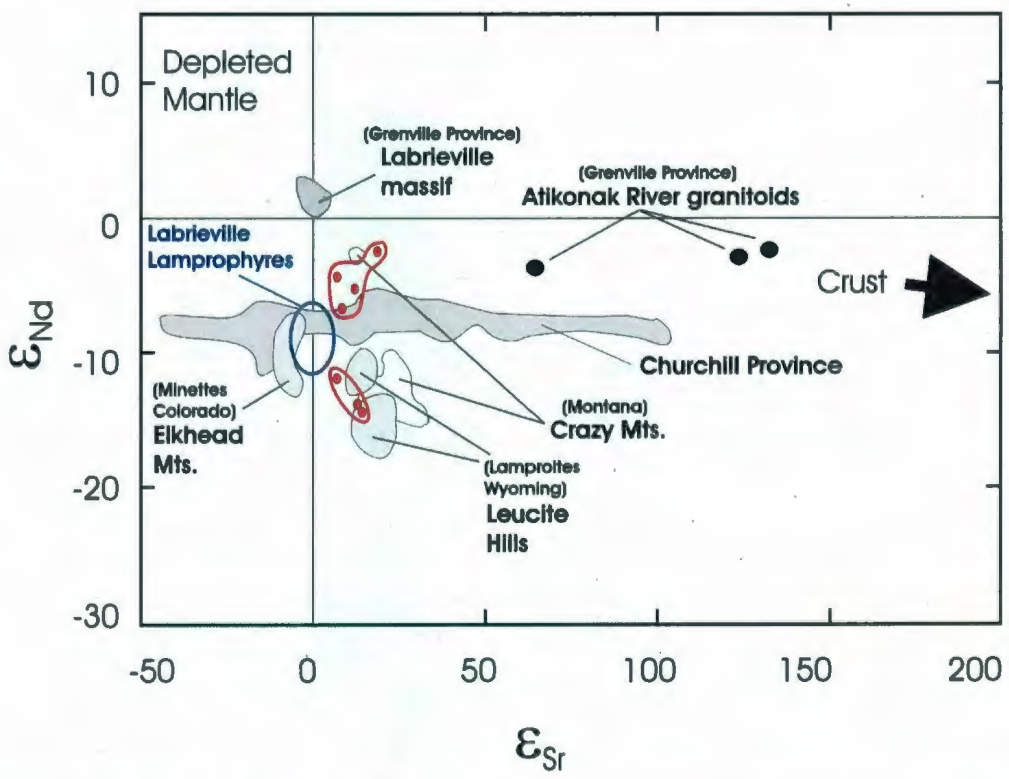

Figure 5-13: A plot of ε_{Nd} vs. ε_{Sr} for ultrapotassic samples (red), calculated for an age of 1 Ga. Also shown for comparison are fields for other potassic to ultrapotassic rocks that are isotopically similar to the lamprophyres of this study (Modified from Owens and Tomascak, 2002). Sources of data include Peterson et al., (1994; Churchill Province), Dudás et al., (1987; Crazy Mts.), Thompson et al., (1989; Elkhead Mts.), Vollmer et al. (1984; Leucite Hills), & Owens and Tomascak (2002; Labrieville Lamprophyres). Data for several other Grenville Province anorthosites and related rocks (Emslie and Hegner 1993 & Owens et al., 1994) are also shown.

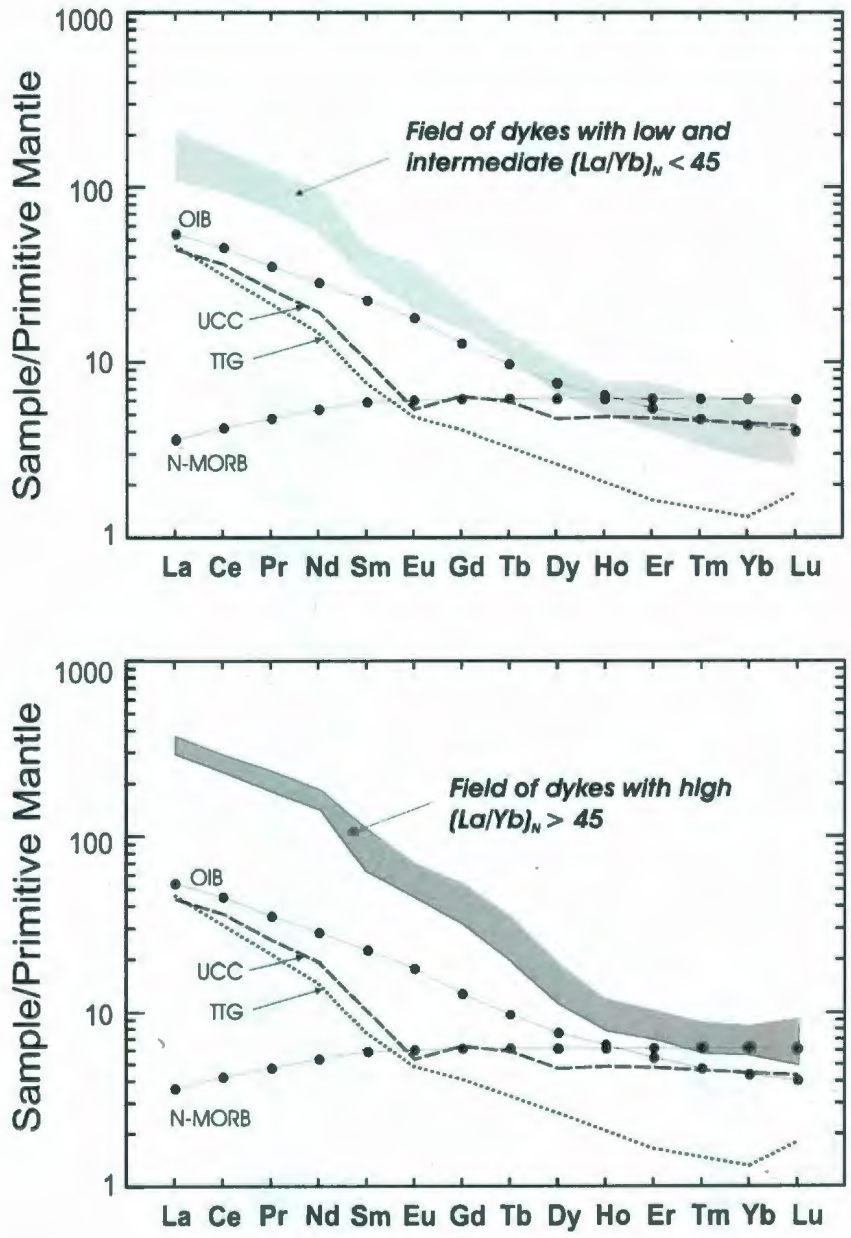

Figure 5-14: Primitive mantle normalized rare earth element plots showing the field for the ultrapotassic dykes of the Canyon Domain with a) low and intermediate and b) high $(La/Yb)_N$ ratios as well as typical patterns for ocean island (OIB) and mid-ocean ridge (N-MORB) basalt, average upper continental crust (UCC; Taylor and MacLennan, 1981) and average Archean tonalite-trondhjemite-granodiorite (TTG; Martin 1994; Martin and Moyen, 2002). Normalized values after Sun and McDonough (1989).

CHAPTER 6: SUMMARY AND CONCLUSIONS

The nature of dyke forming magmatic events in the Gagnon Terrane and the Canyon Domain (Manicouagan reservoir area; central Grenville Province) was investigated by means of detailed petrographic and geochemical study of (a): deformed and metamorphosed mafic dykes which intruded the two lithotectonic units most likely before the Grenvillian orogeny; and (b) late-Grenvillian ultrapotassic dykes from the Canyon Domain.

6.1 Mafic dykes from the Gagnon Terrane

In the Gagnon Terrane, mafic and granitic dykes sharing similar field relationships, and therefore inferred to be of similar age, intrude the SE rim of exposed Archean rocks in the Manicouagan reservoir area. Their time of intrusion is constrained by a 1741+/-31Ma age obtained from a granitic dyke (Dunning and Indares pers. comm. 2008). This age, together with similar inherited monazite ages from anatectic metapelites sampled farther west (Jordan *et al.,* 2006), suggests that a ~1.7Ga thermal event was important in southern Gagnon Terrane, which also represents the southeasternmost (presently) exposed margin of Laurentia at that time.

Mineral assemblages in the mafic dykes were pervasively recrystallized under upper amphibolite to lower granulite facies conditions. However, the geochemistry of these rocks preserves a record of their original character and is consistent with crystallization from subalkaline mafic to intermediate magmas. All the samples are

depleted in Nb relative to La, but only a subset of samples exhibit negative Nb anomalies (*i.e. Group 2*: Nb/Th < 5). However, the remarkably similar LREE enriched patterns and low HREE concentrations of the dykes, suggests that they are related to each other and derived from a common source.

The geochemical features of the dykes suggest that they could represent either considerably contaminated mantle-derived melts by crustal material and be related by different degrees of contamination or rocks formed in an arc setting. However, the presumed age the mafic dykes at ~1750Ma as well as some inconsistencies of the arc scenario (*i.e.* the low $^{143}Nd/^{144}Nd$ ratios compared to arc-related rocks and their similarity to calc-alkaline basalts as supposed to arc tholeiites) favors the mantle-derived scenario. An N-MORB like source with up to 50% bulk contamination by a heterogeneous TTG-like crust could account for the observed REE patterns and Nb concentrations.

The ~1750 Ma magmatic event in Gagnon Terrane is coeval with late orogenic magmatism (1740-1700Ma) in the Makkovik Province (Culshaw *et al.*, 2000; Ketchum *et al.*, 2002). This magmatic event, developed on the continental margin of the Nain Craton and truncated at the Grenville Front farther east, is interpreted to have been generated during mafic underplating likely related to crust-mantle detachment and could be linked to possible intrusion of mafic magmas into the crust (Kerr and Fryer, 1993; 1994; Culshaw *et al.*, 2000a). If the mafic dykes from the Gagnon Terrane represent mantle-derived magmas, contaminated by crustal material, then they may be linked to this event.

South of Makkovik Province and within the eastern segment of the Grenville Province, ~1.7 Ga ages are rare (Corrigan *et al.*, 1994; Davidson *et al.*, 1992; Gower and

Krogh, 2002). The Gagnon Terrane east of the SWSZ is the southernmost exposed part of the New Quebec orogen in the Grenville province. Therefore, it may represent a rare window into potentially widespread 1.7 Ga magmatism into the Laurentian margin, evidence of which is, for the most part, obscured elsewhere in the province owing to subsequent Labradorian and Grenvillian events.

6.2 Mafic dykes from the Canyon Domain

The mafic dykes from the Canyon Domain intrude ~1.4 Ga volcanoclastic rocks, presumably formed in an island arc setting, and metamorphosed under mid-pressure granulite facies conditions at ~1080-1060 Ma (Dunning and Indares, pers. comm. 2008). Although the mafic dykes locally crosscut the foliation of the country rock, they are in general deformed and metamorphosed at the same conditions as the country rocks suggesting that their intrusion predates the Grenvillian metamorphism in the Canyon Domain. In addition, ~1.2 Ga meta-volcanic units (*e.g.* Banded Complex) inferred to have formed in a back-arc setting are recognized east of the Canyon Domain (Dunning and Indares, pers. comm. 2008).

The mafic dykes are characterized by geochemical signatures of sub-alkaline tholeiitic basalts to andesites. They have REE patterns characterized by slight enrichment of the LREE and a progressive increase of the overall concentration of the REE. Two major groups were recognized based on the presence *(Group 2)* or absence *(Group 1)* of negative Nb anomalies relative to Th and La. In addition, one sample from *Group 1,* which has a very high $(La/Yb)_N$ ratio, was treated separately as *Group 1a.*

The variation in trace elements among the samples as a group cannot be explained by fractional crystallization or crustal contamination alone, which suggests that the dykes were derived from two or more magma sources. Based on this variation in compositions, including the Nb anomalies, distinct settings of emplacement were suggested for the two groups: one with an arc-related geochemical signature *(Group 2)* and one with a within-plate geochemical signature *(Group 1)*.

The ~1.4 Ga meta-volcanoclastic package (Dunning and Indares, pers. comm. 2008) the mafic dykes intrude may be part of the Montauban arc, for which an island arc setting has been suggested (Nadeau and Van Breemen, 1994). Therefore it is likely that the dykes of *Group 2*, may have been emplaced during late stages of the development of the ~1.4 Ga arc.

In contrast, the dykes of *Group 1* have the geochemical signature of within plate basalts; therefore, they may be correlative with the ~1.2 Ga (Elzevirian) bimodal meta-volcanic sequence of the Banded Complex (east of the Canyon Domain) and with banded units of similar age in southern Tshenukutish Terrane (Dunning and Indares, pers. comm. 2008), all of which are inferred to have developed in a ~1.2 Ga intra-continental rift setting. It is therefore suggested that the ~1.2 Ga volcanic sequences developed in proximity to the Canyon Domain and that their juxtaposition is not result of Grenvillian age tectonic transport.

6.3 Ultrapotassic dykes from the Canyon Domain

K-rich dykes, commonly associated with felsic pegmatite, are abundant in the

central and southern part of Canyon Domain, where they invariably crosscut the main foliation of the country rock at high angle. In addition, one of these dykes yielded a 980±3 Ma crystallization age (Dunning and Indares, pers. comm. 2008). These dykes, therefore, attest for magmatic activity during the late stages of the Grenvillian orogeny.

The K-rich dykes of the Canyon Domain are considered ultrapotassic in the sense of Foley *et al.* (1987). On primitive mantle-normalized spidergrams, the dykes show enrichment in low field strength elements and LREE and depletion in high field strength elements and heavy rare earth elements. In addition, the dykes are characterized low ε_{Nd} and low ε_{Sr} signatures.

The primitive signature (*i.e.* high Mg#, Cr and Ni) of the dykes suggests they are derived from a mantle source. To explain the incompatible enrichment and highly negative epsilon Nd values, we could appeal to significant contamination of mantle-derived melts by upper crustal material. However, the relatively unradiogenic Sr isotopic signature, and the highly enriched incompatible and LFS element concentrations of the ultrapotassic dykes indicates that crustal involvement was insignificant.

If the ultrapotassic dykes were indeed derived from a mantle source, then this mantle must have an ancient and long-lived history of enrichment in incompatible and some LFS elements, to account for the highly enriched incompatible and LFS element concentrations and highly negative Epsilon Nd values of the dykes. The most likely source region that fits the geochemical characteristics of the dykes is a metasomatized subcontinental lithospheric mantle.

The geochemical and isotopic signature of the dykes indicate that the mantle was locally highly enriched in alkalis and some incompatible trace elements, particularly Sr, Ba, and REE. In contrast to the evidence for long-term LREE enrichment, the relatively unradiogenic Sr isotope signature implies that the mantle was not similarly enriched in Rb.

The ultrapotassic dykes are, therefore, the result of partial melting of previously metasomatized lithospheric mantle in a post-tectonic setting. In such a setting, melting of the subcontinental lithospheric mantle can be induced by contact with upwelling, hot asthenospheric mantle generated by detachment of some of the lithospheric root of the mountain belt via convective thinning or lithospheric delamination.

Elsewhere in the central Grenville Province, late lamprophyre dykes are reported from within the ~1010 Ma Labrieville anorthosite (Owens and Tomascak, 2002). In addition alkalic mafic dykes are widespread in the Pinware Terrane and in the Gilbert river fault of the lake Melville Terrane (eastern Grenville; Gower and Krogh, 2002) where they were dated at 985±6 and 974±6 Ma, respectively (Wasteneys *et al.*, 1997). In contrast, alkalic magmatism of that age is apparently absent in the western Grenville Province.

REFERENCES

Amdt, N. T., and Christensen, U., 1992. The role of lithospheric mantle in continental flood volcanism: thermal and geochemical constraints. Journal of Geophysical Research, **97:** 10967–10981.

Amdt, N. T., Czamanske, G.K., Wooden, J.L., and Fedorenko, V.A., 1993. Mantle and crustal contributions to continental flood volcanism. Tectonophysics, **223:** 39–52.

Bachinski, S. W., and Scott, R. B., 1979. Rare-earth and other trace element contents and the origin of minettes (mica-lamprophyres). Geochimica et Cosmochimica Acta, **43:** 93–100.

Baker, P. E., 1982. Evolution and classification of orogenic volcanic rocks. In: Thorpe, R.S. (ed.) Andesites: Orogenic Andesites and Related Rocks. Chichester John Wiley, pp. 11–23.

Baker, J. A., Macpherson, C. G., Menzies, M. A., Thirlwall, M. F., Al-Kadasi, M., and Mattey, D. P., 2000. Resolving crustal and mantle contributions to continental flood volcanism, Yemen; constraints from mineral oxygen isotope data. Journal of Petrology, **41:** 1805–1820.

Bernard-Griffiths, J., Peucat, J., Iglesias Ponce de Leon, M., and Gil Ibarguchi, J. I., 1985. U–Pb, Nd isotope and REE geochemistry in eclogites from the Cabo Ortegal Complex, Galicia, Spain; an example of REE immobility conserving MORB-like patterns during high-grade metamorphism. Chemical Geology, **52:** 217–225.

Blein, O., Corriveau L, R., and La Flèche, M., 2004. Cordierite-orthopyroxene white gneiss: A key to unveiling premetamorphic hydrothermal activity in the Bondy gneiss complex, Grenville Province, Québec. Memoir 197: Proterozoic Tectonic Evolution of the Grenville Orogen in North America: **197 (0):** 19–33.

Boily, M., and Ludden, J. N., 1991. Trace-element and Nd isotopic variations in Early Proterozoic dyke swarms emplaced in the vicinity of the Kapuskasing structural zone: enriched mantle or assimilation and fractional crystallization (AFC) process? Canadian Journal of Earth Sciences, **28:** 26–36.

Canning, J. C., Henney, P. J., Morrison, M. A., and Gaskarth, J. W., 1996. Geochemistry of late Caledonian minettes from Northern Britain: implications for the Caledonian sub-continental lithospheric mantle. Mineralogical Magazine, **60:** 221–236.

Condie, K. C., 1990. Growth and accretion of continental crust: Inferences based on Laurentia. Chemical Geology, **93:** 183–94.

Condie, K. C., 1986. Geochemistry and tectonic setting of Early Proterozoic supracrustal rocks in the southwestern United States. J. Geol., **94:** 845–864.

Corrigan, D., Culshaw, N., G., and Mortensen, J.K., 1994. Pre-Grenvillian evolution and Grenvillian overprinting of the Parautochthonous Belt in the Key Harbour area, Ontario: U-Pb constraints. Canadian Journal of Earth Sciences, **31,** 160-175.

Corrigan, D., and Hanmer, S., 1997. Anorthosites and related granitoids in the Grenville orogen: a product of convective thinning of lithosphere? Geology, **25:** 61–64.

Corrigan, D., and van Breemen, O., 1997. U-Pb age constraints for the lithotectonic evolution of the Grenville Province along the Mauricie transect, Quebec. Canadian Journal of Earth Sciences: **34 (3):** 299–316.

Culshaw, N., and Dostal, J., 2002. Amphibolites of the Shawanaga Domain, Central Gneiss Belt, Grenville Province, Ontario: tectonic setting and implications for relations between the Central Gneiss Belt and Mid-continental USA. Precambrian Research, **113:** 65–85.

Culshaw, N. G., Ketchum, J. W. F., and Barr, S., 2000. Structural evolution of the Makkovik Province, Labrador, Canada: tectonic processes during 200 m.y at a Paleoproterozoic active margin. Tectonics, **19:** 961–977.

Davidson, A., 1998. An overview of Grenville Province geology, Canadian Shield. *In* Geology of the Precambrian Superior and Grenville provinces and Precambrian fossils in North America. *Coordinated by* S.B. Lucas and M.R. St-Onge. Geological Survey of Canada, Geology of Canada, **7(3):** 205–270. (Also Geological Society of America, The Geology of North America, Vol. C-1.)

Davidson, A., van Breemen, O., and Sullivan, R. W., 1992. ca. 1.75Ga ages for plutonic rocks from the Southern Province and adjacent Grenville Province: what is the expression of the Penokean Orogeny? In Radiogenic ages and isotopic studies: Report 6. Geological Survery of Canada, Paper **92,** 107-118.

Davies, J. H., and von Blanckenburg, F., 1995. Slab breakoff: a model of lithospheric detachment and its test in the magmatism and deformation of collisional orogens. Earth and Planetary Science Letters, **129:** 85–102.

Deer, W. A., Howie, R. A., and Zussman, J., 1992. An introduction to the rock-forming minerals. 2nd edition. Longman Scientific & Technical, Harlow, Essex, England, 696 p.

De Paolo, D. J., 1981. Neodymium isotopes in the Colorado Front Range and implications for crust formation and mantle evolution in Proterozoic. Nature, **291:** 193–197.

Dickin A. P., 2005. Radiogenic Isotope Geology, 2nd edition. Cambridge: Cambridge Univ. Press, 492 p.

Dickin, A. P., and Higgins, M., 1992. Sm/Nd evidence for a major 1.5 Ga crust-forming event in the central Grenville Province. Geology, **20:** 137–140.

Dickin, A.P., 2000. Crustal formation in the Grenville Province: Nd-isotope evidence. Canadian Journal of Earth Sciences, **37:** 165–181.

Dostal, J., Jackson, G. D., and Galley, A., 1989. Geochemistry of Neohelikian Nauyat plateau basalts, Borden rift basin, northwestern Baffin Island, Canada. Canadian Journal of Earth Sciences, **26:** 2214–2223.

Droop, G. T. R., 1987. A general equation for estimating Fe 3+ concentrations in ferromagnesian silicates and oxides from microprobe analyses, using stoichiometric criteria. Mineralogical Magazine, **51:** 431–437.

Dudás, F. Ö., Carlson, R. W., and Eggler, D. H., 1987. Regional Middle Proterozoic enrichment of the subcontinental mantle source of igneous rocks from central Montana. Geology, **15:** 22–25.

Duncan, A. R, 1987. The Karoo igneous province: a problem area for inferring tectonic setting from basalt geochemistry. Journal of Volcanology and Geothermal Research, **32:** 13–34.

Dymek R. F., Gromet, L. P., Icenhower, J. P., Owens, B. E., and Tucker, R. D., 2006. Ages of jotunite-mangerite plutonism in the Charlevoix region, Grenville Province, Quebec; implications for massif anorthosite development in the CRUML Belt. Abstract Volume (Geological Association of Canada), **31:** 44.

Eaton, D., Hynes, A., Indares, A., and Rivers, T., 1995. Seismic images of eclogites, crustal-scale extension and Moho relief in the eastern Grenville Province, Quebec. Geology, **23:** 855–858.

Ellam, R. M, and Hawkesworth, C. J., 1988. Elemental and isotopic variations in subduction related basalts: evidence for a three component model. Contributions to Mineralogy and Petrology, **98:** 72–80.

Ellam. R. M., Menzies, M. A., Hawkesworth, C. J., Leeman, W. P., Rosi, M., and Serri, G., 1988. The transition from calc-alkaline to potassic orogenic magmatism in the Aeolian Islands, Southern Italy. Bulletin of Volcanology, **50:** 386–398.

Esawi, E. K., 2004. AMPH-CLASS: an Excel spreadsheet for the classification and nomenclature of amphiboles based on the 1997 recommendations of the International Mineralogical Association. Computers and Geosciences, **30:** 753–760.

Ewart, A., Brothers, R. N., and Mateen, A., 1977. An outline of the geology and geochemistry, and the possible petrogenetic evolution of the volcanic rocks of the Tonga-Kermadec-New Zealand Island Arc. Journal of Volcanology and Geothermal Research, **2:** 205–250.

Foley, S., and Peccerillo, A., 1992. Potassic and ultrapotassic magmas and their origin. Lithos, **28:** 181–186.

Foley, S. F., Venturelli, G., Green, D. H., and Toscani, L., 1987. The ultrapotassic rocks: characteristics, classification, and constraints for petrogenetic models. Earth Science Reviews, **24:** 81–134.

Gibson, S. A., Thompson, R. N., Leonardos, O. H., Dickin, A. P. and Mitchell, J. G., 1995. The late Cretaceous impact of the Trindade mantle plume: evidence from large-volume, mafic, potassic magmatism in SE Brazil. Journal of Petrology, **36:** 189–229.

Gill, J. B., 1981. Orogenic Andesites and Plate Tectonics. Berlin: Springer-Verlag, 389 p.

Gobeil, A., 1997a. Géologie de la région du Lac Grandmesnil. Ministère des Ressources naturelles, Québec; RG 96–04, 10 p.

Gobeil, A., 1997b. Géologie de la région du Lac Lacoursière. Ministère des Ressources naturelles, Québec; RG 96–03, 14 p.

Govindaraju, K., 1994. 1994 compilation of working values and sample description for 383 geostandards. Geostandards Newsletter, **18:** 1-158

Gower, C. F., Heaman, L. M., Loveridge, W. D., Schärer, U., and Tucker, R. D. 1991. Grenvillian magmatism in the eastern Grenville. Province, Canada. Precambrian **51:** 315–336.

Gower, C. F. and Krogh, T. E., 2002. A U-Pb geochronological review of the Proterozoic history of the eastern Grenville Province. Canadian Journal of Earth Sciences, **39:** 795–829.

Gu, Y., 2003. Automoated scanning electron microscope based mineral liberation analysis - An introduction to JKMRC/FEI Mineral Liberation Analyser, Journal of Minerals and Materials Characterization and Engineering, **2:** 33–41.

Gu, Y., 2004. Rapid mineral liberation analysis with X-ray and BSE image processing, Applied Mineralogy, Pecchio et al. (eds) 2004 ICAM-BR. Sao Paulo, pp. 119–122.

Guo, Z., Hertogen, J., Liu, J., Pasteels, P., Boven, A., Punzalan, L., He, H., Lou, X., and Zhang, W., 2005. Potassic Magmatism in Western Sichuan and Yunnan Provinces, SE Tibet, China: Petrological and Geochemical Constraints on Petrogenesis. Journal of Petrology, **46 (1):** 33–78.

Hall, A., 1996. Igneous Petrology, 2nd. Addison Wesley, New York. 551 p.

Hawkesworth, C. J., Gallagher, K., Hergt, J. M., and McDermott, F., 1993. Mantle and slab contribution in arc magmas. Annual Reviews in Earth and Planetary Sciences, **21:** 175–204.

Hawkesworth, C.J., Kemptoon, P.D., Rogers, N.W., Ellam, R.M., and Van Calsteren, P.W., 1990. Continental mantle lithosphere and shallow level enrichment processes in the Earth's mantle. Earth and planetary Sciences Letters, **96:** 256–268.

Hofmann, A, W., 1988. Chemical Differentiation of the Earth: the relationship between mantle, continental crust, and oceanic crust. *Earth and Planetary Science Letters* **90**, 297–314.

Hofmann, A. W., and Stein, M., 1994. Episodic crustal growth and mantle evolution. Mineralogical Magazine, **58A**, 420–421.

Houseman, G.A., McKenzie, D.P., and Molnar, P., 1981. Convective instability of a thickened boundary layer and its relevance for the thermal evolution of continental convergent belts. Journal of Geophysical Research, **86:** 6115–6132.

Hynes, A., Indares, A., Rivers, T., and Gobeil, A., 2000. Lithoprobe Line 55: integration of out-of-plane seismic results with surface structure, metamorphism, and geochronology, and the tectonic evolution of the eastern Grenville Province. Canadian Journal of Earth Sciences, **37:** 341–358.

Indares, A., Dunning, G., Cox, R., Gale, D., and Connelly, J., 1998. High P-T rocks from the base of thick continental crust: geology and age constrains from the

Manicouagan Imbricate Zone, eastern Grenville Province. Tectonics, **17:** 426–440.

Indares, A., Dunning, G., and Cox, R., 2000. Tectono-thermal evolution of deep crust in a Mesoproterozoic continental collision setting: the Manicouagan example. Canadian Journal of Earth Sciences, **37:** 325–340.

Indares, A., and Dunning, G., 2004. Crustal architecture above the high-pressure belt of the Grenville Province in the Manicouagan area: new structural, petrologic and U-Pb age constraints. Precambrian Research, **130:** 199–228.

Indares, A., and Rivers, T., 1995. Textures, metamorphic reactions and thermobarometry of eclogitized metagabbros; a Proterozoic example. European Journal of Mineralogy, **7 (1):** 43–56.

Jenner, G.A., 1996, Trace element geochemistry of igneous rocks: geochemical nomenclature and analytical geochemistry, in Wyman, D., ed., Trace element geochemistry of volcanic rocks: applications for massive-sulphide exploration: Geological Association of Canada, Short Course Notes, **12:** 51–77.

Jordan S. L., Indares, A., and Dunning, G., 2006. Partial melting of metapelites in the Gagnon Terrane below the high-pressure belt in the Manicouagan area (Grenville Province): pressure-temperature (P-T) and U-Pb age constraints and implications. Canadian Journal of Earth Sciences, **38:** 1309–1329.

Kay, R.W., and Kay, S.M., 1993. Delamination and delamination magmatism. Tectonophysics, **219**: 177–189.

Ketchum, W.F, Culshaw, N. G., and Barr, S. M., 2002. Anatomy and orogenic history of a Paleoproterozoic accrecionary belt: the Makkovik Province, Labrador, Canada. Canadian Journal of Earth Sciences, **39:** 711–730.

Kerr. A., and Fryer, B.J., 1993. Nd isotopic evidence for crust-mantle interaction in the genesis of A-type granitoid suites in Labrador, Canada. Chemical geology, **104:** 39–60.

Kerr, A., and Fryer, B.J., 1994. The importance of late- and postorogenic crustal growth in the early Proterozoic: evidence from Sm–Nd isotopic studies of igneous rocks in the Makkovik Province, Canada. Earth and Planetary Science Letters, **125:** 71–88.

La Flèche, M. R., Birkett, T. C., and Corriveau, L., 2005. Crustal development at the pre-Grenvillian Laurentia margin: a record from contrasting geochemistry of mafic

and ultramafic orthogneisses in the Chochocouane River area, Quebec. Canadian Journal of Earth Sciences, **42:** 1653–1675.

Leake, B. E., Woolley, A. R., Arps, E. S., and 19 others, 1997. Nomenclature of amphiboles; Report of the Subcommittee on Amphiboles of the International Mineralogical Association, Commission on New Minerals and Mineral Names. American Mineralogist, **83:** 1019–1037.

Leake, B. E., Woolley, A. R., Birch, W. D., and 9 others, 2004. Nomenclature of amphiboles; additions and revisions to the International Mineralogical Association's amphibole nomenclature. American Mineralogist, **89:** 883–887.

Le Maitre, R.W. (Ed.), 2002. Igneous Rocks: A Classification and Glossary of Terms. Recommendations of the International Union of Geological Sciences Subcommission on the Systematics of Igneous Rocks. Cambridge Univ. Press, Cambridge. 252 p.

Ludden, J. and Hynes, A., 2000. The Lithoprobe Abitibi-Grenville transect: two billion years of crust formation and recycling in the Precambrian Shield of Canada. Canadian Journal of Earth Sciences, **37:** 459–476.

Martin, H., 1994. The Archean grey gneisses and the genesis of the continental crust. In: Condie, K.C. (Ed.), The Archean Crustal Evolution, Developments in Precambrian Geology. Elsevier, Amsterdam, pp. 205–259.

Martin, H., and Moyen, J. F., 2002. Secular changes in TTG composition as markers of the progressive cooling of the Earth. Geology, **30 (4):** 319–322.

Maury, Y. R., Defant, C., and Joron, M.J., 1992. Metasomatism of the sub-arc mantle inferred from trace elements in Philippines xenoliths. Nature, **360:** 661–663.

McCulloch, M. T., and Gamble, J. A., 1991. Geochemical and geodynamical constraints on subduction zone magmatism. Earth and Planetary Science Letters, **102:** 358-74

McCulloch, M. T., Jaques, A. L., Nelson, D. R., and Lewis, J. D., 1983. Nd and Sr isotopes in kimberlites and lamproites from western Australia: an enriched mantle origin. Nature, **302:** 400–403.

McCulloch, M. T., and Wasserburg, G. J., 1978. Sm-Nd and Rb-Sr chronology of continental crust formation. Science, **200:** 1003–1011.

McKenzie, D.P., 1989. Some remarks on the movement of small melt fractions in the mantle. Earth and Planetary Science Letters, **95:** 53–72.

Meen, J. K., Ayers, J. C., and Fregeau, E. J., 1989. A model of mantle metasomatism by carbonated alkaline melts: trace-element and isotopic compositions of mantle source regions of carbonatite and other continental igneous rocks. In Carbonatites. Edited by K. Bell. Unwin Hyman, London, 464–499.

Menzies, M. A., and Wass, S. Y., 1983. CO2- and LREE-rich mantle below eastern Australia: a REE and isotopic study of alkaline magmas and apatite-rich mantle xenoliths from the Southern Highlands Province, Australia. Earth and Planetary Science Letters, **65:** 287–302.

Miyashiro, A., 1974. Volcanic rock series in island arc and active continental margins. American Journal of Science, **274:** 321–357.

Morimoto, N., 1988. Nomenclature of pyroxene. American mineralogist, **73:** 1123–1133.

Nadeau, L., and van Breemen, O., 1994. Do the 1.45–1.39 Ga Montauban Group and the La Bostonnais complex constitute a Grenvillian accreted terrane? Geological Association of Canada - Mineralogical Association of Canada meeting, Program with abstracts, **19:** A81.

Nelson, D.R., 1992. Isotopic characteristics of potassic rocks: evidence for the involvement of subducted sediments in magma genesis. Lithos, **28:** 403–20.

Nelson, D.R., 1989. Isotopic characteristics and petrogenesis of the lamproites and kimberlites of central west Greenland. Lithos, **22:** 265–274.

Nelson, D.R., McCulloch, M., and Sun, S.S., 1986. The origins of ultrapotassic rocks as inferred from Sr, Nd and Pb isotopes. Geochimica et Cosmochimica Acta, **50:** 231–245.

O 'N ions, R. K., Carter, S. R., Evensen, N. M., and Hamilton, P. J., 1979. Geochemical and Cosmochemical Applications of Nd Isotope Analysis. Annual Reviews in Earth and Planetary Sciences, **7:** 11-38.

Olafsson, M., and Eggler, D.M., 1983. Phase relations of amphibole, amphibole-carbonate and phlogopite-peridotite: petrologic constraints on the asthenosphere. Earth and planetary Sciences Letters, **64:** 305–315.

Owens, B. E., and Tomascak, P. B., 2002. Mesoproterozoic lamprophyres in the Labrieville Massif, Quebec: clues to the origin of alkalic anorthosites? Canadian Journal of Earth Sciences, **39:** 983–997.

Pattison, D. R. M., 2003. Petrogenetic significance of orthopyroxene-free garnet + clinopyroxene + plagioclase ± quartz-bearing metabasites with respect to the amphibolite and granulite facies. Journal of metamorphic petrology, **21(1):** 21-34.

Pearce, J. A., 1982. Trace element characteristics of lavas from destructive plate boundaries. In: R.S. Thorpe (Editor), Andesites. Wiley, New York, pp. 525–548.

Pearce, J.A., 1983. Role of the sub-continental lithosphere in magma genesis at active continental margins. In: C.J. Hawkesworth and M.J. Norry (Editors), Continental Basalts and Mantle Xenoliths. Shiva Publishing, Nantwich, pp. 158–l 85.

Pearce, J. A., and Cann, J. R., 1973. Tectonic setting of basic volcanic rocks determined using trace element analyses. Earth and Planetary Science Letters, **19:** 290.

Pearce, J. A., and Gale, G.H., 1977. Identification of ore-deposition environment from trace-element geochemistry of associated igneous host rocks. Geological Society, London, Special Publications, **7:** 14–24.

Pearce, J. A., and Norry, M. J., 1979. Petrogenetic implications of Ti, Zr, Y, and Nb variations in volcanic rocks. Contributions to Mineralogy and Petrology, **69(1):** 33–47.

Pearce, J. A., and Peate, D. W., 1995. Tectonic Implications of the Composition of Volcanic ARC Magmas. Annual Review of Earth and Planetary Sciences, **23:** 251–285.

Peccerillo, A., 1990. On the origin of the Italian potassic magma-comments. Chemical. Geology, **85:** 183–96.

Peccerillo, A., 1999. Multiple mantle metasomatism in central–southern Italy: geochemical effects, timing and geodynamic implications. Geology, **27:** 315–18.

Peterson, T. D., Esperança, S., and LeCheminant, A.N., 1994. Geochemistry and origin of the Proterozoic ultrapotassic rocks of the Churchill Province, Canada. Mineralogy and Petrology, **51:** 251–276.

Perfit, M. R., Gust, D. A., Bence, A. E., Arculus, R. J., and Taylor, S. R., 1980. Chemical characteristics of island arc basalts: implications for mantle sources. Chem. Geol. **30:** 227–256.

Rivers T., 2008. Assembly and preservation of lower, mid, and upper orogenic crust in the Grenville Province-Implications for the evolution of large hot long-duration orogens. Precambrian Research, **167:** 237–259.

Rivers, T., 1997. Lithotectonic elements of the Grenville Province: review and tectonic implications. Precambrian Research, **86:** 117–154.

Rivers, T., and Chown, E. H., 1986. The Grenville orogen in eastern Quebec and western Labrador - Definition, identification and tectonometamorphic relationships of autochthonous, parautochthonous and allochthonous terranes. In The Grenville Province. *Edited by* J.M Moore, A. Davidson, and A.J. Bear. Geological Association of Canada, Special Paper, **31:** 31–50.

Rivers, T., Ketchum, J. W. F., Indares, A., and Hynes, A., 2002. The high-pressure belt in the Grenville Province; architecture, timing and exhumation. Canadian Journal of Earth Sciences, **39:** 867–893.

Rivers, T., Martignole, J., Gower, C.F., and Davidson, A. 1989. New tectonic divisions of the Grenville Province, southeast Canadian Shield. Tectonics, **8:** 63–84.

Rivers, T., van Gool, J., and Connelly, J., 1993. Contrasting styles of crustal shortening in the northern Grenville orogen. Geology, **21:** 1127–1130.

Rock, N. M. S., 1991. Lamprophyres. New York: Blackie and Son. Ltd., Glasgow, 285 p,

Rogers, N.W., 1992. Potassic magmatism as a key to trace element enrichment processes in the upper mantle. Journal of Volcanology and Geothermal Research, **50:** 85–99.

Rollinson, H. R., 1993. Using Geochemical Data: Evaluation, Presentation, Interpretation, Longman, UK. 352 p. [Co-published by J. Wiley & Sons. Inc. in the USA]. IBSN 0 582 0 6701 4. Reprinted 1994, 1995, 1996, 1998.

Saunders, A. D., Norry, M. J., and Tarney, J. 1991. Fluid influence on the trace element compositions of subduction zone magmas. Philosophical Transactions of the Royal Society of London, **335(A):** 377–92.

Sevigny, J.H., and Thériault, R.J., 2003. Geochemistry and Sr-Nd isotopic composition of Eocene lamphropyre dykes, southeastern British Columbia. Canadian Journal of Earth Sciences, **40:** 853–864.

Slagstad, T., Culshaw, N. G., Jamieson, R. A., and Ketchum, J. W. F., 2004a. Early Mesoproterozoic tectonic history of the southwestern Grenville Province, Ontario: constraints from geochemistry and geochronology of high-grade gneisses. In: Tollo, R. P., Corriveau, L., McLelland, J. & Bartholomew, M. J. (eds) Proterozoic Tectonic Evolution of the Grenville Orogen in North America. Geological Society of America, Memoir, **197:** 209–241.

Steiger, R. H., and Jäger, E., 1977. Subcommission on geochronology: convention on the use of decay constants in geo- and cosmo-chronology. Earth Planetary Science Letters, **36:** 359–362.

Stout, J. H., 1972. Phase petrology and mineral chemistry of coexisting amphiboles from Tidemark, Norway. Journal of Petrology, **13 (1):** 99–145.

Sturm, R., 2002. PX-NOM - an interactive spreadsheet program for the computation of pyroxene analyses derived from the electron microprobe. Computers & Geosciences, **28:** 473–483.

Sun, S.S., and McDonough, W.F. 1989. Chemical and isotopic systematics of oceanic basalts: implications for mantle composition and processes. In: Saunders, A.D., Norry, M.J. (Eds.), Magmatism in the Ocean Basins. Geological Society of London Special Publication 42. Geological Society of London, Blackwell Scientific Publications, Oxford, UK, pp. 313–345.

Swinden, H.S., Jenner, G.A., and Szybinski, Z.A., 1997, Magmatic and tectonic evolution of the Cambrian-Ordovician Laurentian margin of the Iapetus: Geochemical and isotopic constraints from the Notre Dame subzone, Newfoundland, *in* Sinha, A.K., et al., eds. The nature of magmatism in the Appalachian orogen: Geological Society of America Memoir **191**, 337–364.

Taylor S.R, and McLennan, S.M., 1981. The composition and evolution of the continental crust: rare earth evidence from sedimentary rocks. Philosophical Transactions of the Royal Society of London, **301(A):** 185–197.

Tanaka, T., Togashi, S., Kamioka, H., and 16 others, 2000. Jndi-1: a Neodymium isotopic reference in consistency with La Jolla Neodymium, Chemical Geology, **168:** 279–281.

Thompson, R. N, Hendry, G. L., and Parry, S. J., 1984. An assessment of the relative roles of crust and magma genesis: An elemental approach. Philosophical Transactions of the Royal Society of London, **310:** 549–90.

Thompson, R.N., Leat, P.T., Dickin, A.P., Morrison, M.A., Hendry, G.L., and Gibson, S.A. 1989. Strongly potassic mafic magmas from lithospheric mantle sources during continental extension and heating: evidence from Miocene minettes of northwest Colorado, U.S.A. Earth and Planetary Science Letters, **98:** 139–153.

Turner, S., and Hawkesworth, C. 1995. The nature of the sub-continental mantle: constraints from the major element composition of continental flood basalts. Chemical Geology, **120:** 295–314.

Valverde, 2005. Ultramafic rocks of the Gagnon Terrane and Long Island Domain, Manicouagan Area, Grenville Province, Quebec. Honours Thesis, Memorial University of Newfoundland, 103 p.

van Bergen, M. J., Vroon, P. Z., Varekamp, J.C., and Poorter, R.P.E., 1992. The origin of the potassic rock suite from Batu Tara volcano (East Sunda Arc, Indonesia). Lithos, **28:** 261–82.

Wang, X., Wang, T., Jahn, B., Hu, N., and Chen, W., 2007. Tectonic significance of Late Triassic post-collisional lamprophyre dykes from the Qinling Mountains (China) Geological Magazine, **144 (5):** 837–848.

Wasteneys, H.A., Kamo, S.L., Moser, D., Krogh, T.E., Gower, C.F., and Owen, J.V. 1997. U–Pb geochronological constraints on the geological evolution of the Pinware terrane and adjacent areas, Grenville Province, southeast Labrador, Canada. Precambrian Research, **81:** 101–128.

Weaver, B. L., and Tarney , J., 1980. Geochemistry of Lewisian Granulites-facies gneisses northwest Scotland: Implications for the petrogenesis of the Archean lower continental crust. Earth and Planetary Science Letters, **51:** 279–296.

Weaver, B. L. and Tarney, J., 1981. Lewisian gneiss geochemistry and Archaean crustal development models. Earth and Planetary Science Letters, **55(1):** 171–180.

Weber, B., and Hecht, L., 2003. Petrology and geochemistry of meta-igneous rocks from a Grenvillian basement fragment in the Maya block: the Guichicovi complex, Oaxaca, southern Mexico. Precambrian Research, **124:** 41–67.

Winchester, J. A and Floyd, P. A., 1976. Geochemical magma type discrimination: application to altered and metamorphosed basic igneous rocks. Earth and Planetary Science Letters, **28 (3):** 459-469.

Winchester, J. A and Floyd, P. A., 1977. Geochemical discrimination of different magma series and their differentiation products using immobile elements. Chemical Geology, **20(4):** 325–343.

Winchester, J. A and Floyd, P. A., 1978. Identification and discrimination of altered and metamorphosed volcanic rocks using immobile elements. Chemical Geology, **21(3-4):** 291–306.

Wilson, M., 1989. Igneous Petrogenesis: A Global Tectonic Approach. Unwin Hyman Ltd, London. 466 p.

Wood, D. A., 1980. The application of a Th-Hf-Ta diagram to problems of tectonomagmatic classification and to establishing the nature of crustal contamination of basaltic lavas of the British Tertiary volcanic province. Earth and Planetary Science Letters, **50:** 11–30.

Zhao, J., and McCulloch, M.T. 1993. Melting of a subduction-modified continental lithospheric mantle: evidence from Late Proterozoic mafic dyke swarms in central Australia. Geology, **21:** 463–466.

APPENDIX 1

MINERAL ANALYSES

List of abbreviations

CD = Canyon Domain

GT= Gagnon Terrane

C= core

R = rim

XMg = [Mg / (Mg + Fe^{2+})]

Amp = Amphibole

Mg-hast = Magnesiohastingsite

Tsch = Tschermakite

Mg-hbl = Magnesiohornblende

Fe-parg = Ferro Pargasite

Parg = Pargasite

Bt = Biotite

Pl = Plagioclase

Ksp = K-feldspar

Ab = Albite

An = Anorthite

Or = Orthoclase

Grt = Garnet

Cpx = Clinopyroxene

Opx = Orthopyroxene

Wo = Wollastonite

En = Enstatite

Fs = Ferrosilite

Ilm = Ilmenite

Apt = Apatite

Amphibole Analyses by sample (recalculated to 100%), cations based on 23 (O) Oxygens.

Terrane/ Sample	GT 2000x																		
Label	Amp1 C	Amp1 C	Amp1 C	Amp1 R	Amp2 C	Amp2 R	Amp2 R	Amp3 C	Amp3 R	Amp4 C	Amp4 R	Amp5 C	Amp5 R	Amp6 C	Amp6 R	Amp7 R	Amp7 C	Amp8 C	Amp8 R
SiO2	42.52	42.95	43.08	42.76	43.34	42.55	42.96	42.73	43.07	42.54	43.46	43.01	42.87	43.02	43.56	43.38	42.98	42.94	43.48
TiO2	1.10	1.07	1.13	1.12	1.12	1.09	1.14	1.10	1.14	1.09	1.04	1.16	1.10	1.15	1.06	1.07	1.10	1.10	1.07
Al2O3	12.82	12.51	12.36	12.64	12.39	12.83	12.45	12.73	12.62	12.85	12.21	12.84	12.80	12.57	12.34	12.16	12.73	12.65	12.21
Cr2O3	0.18	0.17	0.17	0.23	0.23	0.17	0.20	0.26	0.24	0.15	0.20	0.16	0.15	0.25	0.27	0.17	0.16	0.20	0.18
Fe2O3	4.20	2.23	2.65	4.67	3.17	4.73	2.14	4.48	4.22	4.67	4.13	4.40	3.79	3.15	3.11	2.87	3.75	3.65	3.48
FeO	9.01	10.53	10.22	8.55	9.68	8.48	10.36	8.80	8.80	8.60	9.15	8.94	9.34	10.07	9.82	10.23	9.48	9.55	9.72
MnO	0.23	0.22	0.22	0.26	0.19	0.22	0.21	0.17	0.25	0.25	0.20	0.17	0.21	0.22	0.16	0.20	0.21	0.22	0.22
MgO	12.63	12.66	12.66	12.70	12.68	12.75	12.83	12.61	12.65	12.69	12.65	12.42	12.53	12.37	12.58	12.63	12.45	12.48	12.57
CaO	11.82	12.23	12.03	11.75	11.85	11.74	12.23	11.65	11.62	11.75	11.77	11.50	11.80	11.88	11.89	12.05	11.79	11.77	11.70
Na2O	1.77	1.74	1.82	1.70	1.71	1.72	1.80	1.77	1.77	1.76	1.56	1.68	1.70	1.72	1.67	1.65	1.71	1.77	1.78
K2O	1.59	1.60	1.51	1.50	1.53	1.62	1.57	1.57	1.50	1.57	1.51	1.62	1.57	1.52	1.39	1.54	1.51	1.56	1.50
NiO	0.01	0.01	0.03	0.02	0.02	0.01	0.02	0.04	0.03	0.00	0.02	0.02	0.02	0.00	0.06	0.00	0.03	0.03	0.01
F	0.37	0.13	0.51	0.27	0.32	0.17	0.20	0.22	0.29	0.28	0.36	0.25	0.50	0.11	0.22	0.06	0.15	0.17	0.13
Cl	0.08	0.05	0.02	0.01	0.04	0.03	0.05	0.05	0.02	0.04	0.04	0.05	0.04	0.05	0.02	0.02	0.05	0.03	0.03
H2O	1.84	1.95	1.79	1.92	1.88	1.95	1.92	1.92	1.90	1.90	1.86	1.91	1.79	1.97	1.94	2.00	1.96	1.94	1.97
O=F	0.15	0.06	0.21	0.11	0.14	0.07	0.09	0.09	0.12	0.12	0.15	0.10	0.21	0.05	0.09	0.03	0.06	0.07	0.05
O=Cl	0.02	0.01	0.01	0.00	0.01	0.01	0.01	0.01	0.00	0.01	0.01	0.01	0.01	0.01	0.00	0.00	0.01	0.01	0.01
Sum Ox%	100	100	100	100	100	100	100	100	100	100	100	100	100	100	100	100	100	100	100
Si	6.258	6.331	6.345	6.279	6.364	6.251	6.328	6.279	6.318	6.252	6.378	6.311	6.303	6.333	6.392	6.381	6.317	6.316	6.386
Ti	0.122	0.119	0.126	0.124	0.124	0.120	0.126	0.121	0.126	0.121	0.115	0.128	0.121	0.127	0.117	0.118	0.122	0.122	0.119
Al/Al IV	1.742	1.669	1.655	1.721	1.636	1.749	1.672	1.721	1.682	1.748	1.622	1.689	1.697	1.667	1.608	1.619	1.683	1.684	1.614
Al VI	0.481	0.504	0.490	0.465	0.508	0.473	0.490	0.484	0.500	0.478	0.489	0.533	0.521	0.514	0.526	0.490	0.522	0.509	0.501
Cr	0.022	0.020	0.020	0.028	0.027	0.021	0.023	0.030	0.029	0.018	0.023	0.018	0.018	0.029	0.031	0.019	0.018	0.023	0.021
Fe3+	0.465	0.248	0.294	0.517	0.350	0.523	0.237	0.495	0.466	0.516	0.456	0.486	0.419	0.349	0.343	0.318	0.415	0.404	0.385
Fe2+	1.109	1.298	1.259	1.051	1.189	1.042	1.276	1.082	1.080	1.057	1.123	1.096	1.147	1.239	1.205	1.259	1.165	1.174	1.194
Mn2+	0.029	0.028	0.028	0.033	0.024	0.028	0.027	0.021	0.031	0.032	0.025	0.021	0.027	0.027	0.021	0.025	0.027	0.028	0.028
Mg	2.772	2.782	2.780	2.779	2.776	2.792	2.817	2.762	2.766	2.779	2.766	2.716	2.744	2.714	2.750	2.770	2.726	2.736	2.752
Ca	1.864	1.931	1.898	1.848	1.865	1.848	1.930	1.835	1.827	1.851	1.849	1.808	1.859	1.872	1.869	1.899	1.856	1.854	1.842
Na	0.506	0.497	0.519	0.485	0.487	0.492	0.515	0.505	0.503	0.500	0.444	0.478	0.483	0.492	0.475	0.470	0.486	0.505	0.506
K	0.298	0.299	0.284	0.281	0.286	0.303	0.294	0.295	0.280	0.293	0.281	0.303	0.296	0.284	0.261	0.287	0.285	0.292	0.281
Ni	0.002	0.001	0.004	0.003	0.002	0.001	0.003	0.005	0.003	0.000	0.002	0.003	0.003	0.000	0.007	0.000	0.004	0.004	0.001
F	0.170	0.063	0.236	0.126	0.152	0.083	0.096	0.103	0.138	0.129	0.168	0.116	0.237	0.052	0.104	0.030	0.069	0.082	0.061
Cl	0.020	0.012	0.006	0.002	0.010	0.008	0.012	0.013	0.005	0.010	0.009	0.012	0.009	0.011	0.006	0.006	0.013	0.008	0.008
OH	1.810	1.925	1.758	1.873	1.838	1.909	1.891	1.884	1.858	1.861	1.823	1.873	1.754	1.937	1.891	1.964	1.918	1.909	1.931
Sum Cat#	17.668	17.728	17.702	17.615	17.638	17.643	17.739	17.634	17.61	17.643	17.574	17.589	17.637	17.649	17.605	17.656	17.628	17.65	17.629
XMg	0.71	0.68	0.69	0.73	0.70	0.73	0.69	0.72	0.72	0.73	0.71	0.71	0.71	0.69	0.70	0.69	0.70	0.70	0.70
Name	Parg	Parg	Parg	Mg-hast	Parg	Mg-hast	Parg	Mg-hast	Parg	Mg-hast	Parg	Parg	Parg	Parg	Parg	Parg	Parg	Parg	Parg

Amphibole Analyses by sample (recalculated to 100%), cations based on 23 (O) Oxygens.

GT 288d1																			
Label	Amp1	Amp1	Amp2	Amp2	Amp3	Amp3	Amp4	Amp4	Amp4	Amp4	Amp5	Amp5	Amp5	Amp5	Amp6	Amp6	Amp6	Amp6	Amp7
	C	R	C	R	R	C	C	C	R	R	C	C	R	R	C	C	R	R	C
SiO2	43.14	43.30	43.35	43.69	43.33	43.39	42.95	42.95	43.24	43.36	42.97	43.08	43.13	43.29	43.18	43.20	42.86	42.79	43.28
TiO2	1.04	1.01	1.00	1.00	0.92	0.96	1.05	0.97	0.94	0.97	0.95	0.95	1.00	1.01	0.99	1.03	0.95	1.02	1.00
Al2O3	12.23	12.08	11.97	11.85	11.64	11.96	12.30	12.13	12.15	12.17	12.24	12.27	12.12	12.04	12.19	12.23	12.26	12.25	12.06
Cr2O3	0.01	0.06	0.05	0.02	0.08	0.00	0.04	0.00	0.05	0.07	0.01	0.05	0.02	0.05	0.03	0.03	0.05	0.01	0.06
Fe2O3	4.02	4.51	4.53	4.98	4.37	4.36	5.10	5.36	4.91	4.75	4.97	3.54	4.03	4.74	5.05	4.32	5.40	4.86	3.94
FeO	8.03	7.48	7.48	6.99	7.58	7.79	7.13	6.82	7.24	7.26	7.19	8.27	7.94	7.37	6.93	7.55	6.82	7.18	7.96
MnO	0.28	0.21	0.19	0.27	0.20	0.13	0.20	0.26	0.24	0.20	0.17	0.24	0.18	0.23	0.25	0.21	0.27	0.24	0.23
MgO	13.70	13.88	13.97	14.04	14.24	13.92	13.88	14.04	13.91	13.91	14.01	13.84	13.91	13.95	13.99	13.93	13.94	14.03	13.90
CaO	12.13	11.94	11.94	11.84	12.38	12.14	11.94	12.04	12.03	11.93	12.25	12.42	12.19	12.14	12.04	12.13	12.00	12.15	12.11
Na2O	1.77	1.83	1.85	1.77	1.71	1.68	1.83	1.80	1.73	1.82	1.65	1.70	1.84	1.64	1.69	1.76	1.79	1.84	1.87
K2O	1.46	1.47	1.46	1.41	1.35	1.46	1.42	1.40	1.43	1.36	1.41	1.44	1.41	1.41	1.41	1.40	1.44	1.41	1.41
NiO	0.03	0.05	0.03	0.01	0.03	0.01	0.01	0.03	0.00	0.02	0.02	0.03	0.05	0.00	0.04	0.04	0.04	0.04	0.00
F	0.28	0.56	0.39	0.28	0.38	0.49	0.22	0.46	0.18	0.22	0.42	0.53	0.29	0.15	0.57	0.45	0.46	0.41	0.52
Cl	0.14	0.16	0.19	0.12	0.18	0.20	0.14	0.21	0.15	0.19	0.16	0.17	0.15	0.13	0.16	0.14	0.15	0.15	0.14
H2O	1.88	1.75	1.82	1.89	1.82	1.76	1.91	1.79	1.92	1.90	1.81	1.75	1.87	1.94	1.74	1.80	1.79	1.81	1.76
O=F	0.11	0.24	0.16	0.12	0.15	0.20	0.09	0.19	0.08	0.09	0.18	0.23	0.12	0.06	0.24	0.19	0.19	0.18	0.23
O=Cl	0.03	0.04	0.04	0.03	0.04	0.05	0.03	0.05	0.03	0.04	0.03	0.04	0.03	0.03	0.03	0.03	0.03	0.03	0.03
Sum Ox%	100	100	100	100	100	100	100	100	100	100	100	100	100	100	100	100	100	100	100
Si	6.318	6.331	6.339	6.370	6.340	6.347	6.279	6.282	6.318	6.330	6.282	6.312	6.314	6.326	6.307	6.314	6.270	6.263	6.334
Ti	0.115	0.110	0.110	0.109	0.101	0.106	0.115	0.107	0.103	0.106	0.104	0.105	0.111	0.111	0.109	0.114	0.105	0.113	0.110
Al/Al IV	1.682	1.669	1.661	1.630	1.660	1.653	1.721	1.718	1.682	1.670	1.718	1.688	1.686	1.674	1.693	1.686	1.730	1.737	1.666
Al VI	0.429	0.413	0.401	0.405	0.348	0.409	0.400	0.373	0.410	0.424	0.392	0.430	0.406	0.397	0.405	0.420	0.383	0.377	0.413
Cr	0.002	0.007	0.006	0.002	0.010	0.000	0.004	0.000	0.005	0.008	0.001	0.006	0.002	0.006	0.004	0.003	0.006	0.001	0.007
Fe3+	0.443	0.496	0.498	0.546	0.481	0.480	0.561	0.590	0.540	0.522	0.547	0.390	0.445	0.522	0.555	0.475	0.594	0.535	0.434
Fe2+	0.983	0.916	0.914	0.852	0.928	0.953	0.872	0.835	0.885	0.887	0.880	1.014	0.973	0.901	0.847	0.923	0.835	0.879	0.974
Mn2+	0.034	0.025	0.024	0.033	0.024	0.017	0.025	0.032	0.029	0.025	0.020	0.030	0.023	0.028	0.031	0.026	0.033	0.030	0.029
Mg	2.990	3.026	3.043	3.051	3.104	3.035	3.022	3.060	3.029	3.025	3.053	3.022	3.035	3.036	3.045	3.034	3.039	3.060	3.033
Ca	1.902	1.871	1.869	1.849	1.941	1.901	1.871	1.886	1.883	1.867	1.919	1.950	1.912	1.900	1.884	1.899	1.880	1.906	1.898
Na	0.502	0.517	0.526	0.498	0.484	0.477	0.518	0.508	0.488	0.517	0.470	0.482	0.524	0.465	0.480	0.500	0.507	0.524	0.532
K	0.272	0.274	0.271	0.263	0.253	0.273	0.264	0.261	0.267	0.252	0.262	0.270	0.264	0.263	0.264	0.261	0.269	0.263	0.264
Ni	0.004	0.006	0.004	0.001	0.003	0.001	0.001	0.004	0.000	0.003	0.003	0.003	0.006	0.000	0.005	0.004	0.005	0.004	0.000
F	0.127	0.260	0.177	0.133	0.175	0.224	0.104	0.211	0.087	0.104	0.197	0.246	0.130	0.070	0.261	0.207	0.212	0.192	0.243
Cl	0.037	0.040	0.047	0.030	0.043	0.051	0.035	0.052	0.038	0.047	0.039	0.040	0.038	0.034	0.040	0.037	0.038	0.039	0.037
OH	1.837	1.700	1.776	1.837	1.782	1.725	1.861	1.737	1.875	1.849	1.764	1.714	1.831	1.896	1.699	1.756	1.749	1.768	1.720
Sum Cat#	17.677	17.662	17.667	17.61	17.678	17.651	17.654	17.656	17.638	17.636	17.65	17.702	17.7	17.628	17.628	17.66	17.657	17.692	17.693
XMg	0.75	0.77	0.77	0.78	0.77	0.76	0.78	0.79	0.77	0.77	0.78	0.75	0.76	0.77	0.78	0.77	0.79	0.78	0.76
	Mg-hast	Mg-hast	Mg-hast	Mg-hast	Mg-hast	Mg-hast	Mg-hast	Mg-hast	Mg-hast	Mg-hast	Mg-hast	Mg-hast	Mg-hast	Mg-hast	Mg-hast	Mg-hast	Mg-hast	Mg-hast	Mg-hast

Amphibole Analyses by sample (recalculated to 100%), cations based on 23 (O) Oxygens.

GT 474d																			
Label	Amp1	Amp1	Amp1	Amp2	Amp2	Amp2	Amp2	Amp3	Amp3	Amp3	Amp3	Amp3	Amp4	Amp4	Amp5	Amp5	Amp6	Amp5	Amp7
	R	R	C	C	C	R	R	C	C	R	R	R	C	R	R	R	C	R	C
SiO2	44.28	44.09	43.66	44.29	43.78	43.98	43.96	44.16	44.16	44.34	44.18	44.56	43.73	43.50	44.01	43.93	43.57	43.84	43.89
TiO2	1.49	1.83	1.93	1.67	1.83	1.76	1.73	1.68	1.74	1.91	1.62	1.48	1.90	1.96	1.59	1.73	1.82	1.69	1.86
Al2O3	10.15	9.82	9.90	10.04	10.03	9.75	9.86	9.97	10.02	9.91	10.14	9.73	9.71	9.84	9.79	9.89	9.88	9.89	9.62
Cr2O3	0.05	0.02	0.03	0.05	0.03	0.04	0.03	0.03	0.05	0.04	0.03	0.02	0.01	0.05	0.02	0.02	0.04	0.02	0.02
Fe2O3	5.28	5.21	6.14	5.63	6.13	5.70	5.13	6.03	6.16	4.94	5.87	5.99	7.17	6.14	6.29	5.65	6.48	5.92	5.85
FeO	9.73	9.79	9.15	9.33	9.11	9.30	9.82	9.09	8.92	9.79	8.96	8.78	8.52	9.38	8.61	9.57	8.96	9.22	9.24
MnO	0.17	0.33	0.44	0.28	0.30	0.38	0.26	0.31	0.31	0.34	0.25	0.27	0.40	0.43	0.36	0.29	0.30	0.29	0.42
MgO	12.54	12.54	12.46	12.56	12.56	12.70	12.69	12.59	12.56	12.52	12.74	12.95	12.54	12.37	12.95	12.57	12.61	12.72	12.70
CaO	11.31	11.23	10.89	11.02	10.99	11.15	11.30	10.99	10.92	11.12	12.74	11.32	10.80	11.09	11.22	11.15	11.10	11.22	11.22
Na2O	1.91	1.84	2.00	1.96	2.01	1.91	2.00	1.99	1.93	1.90	12.74	1.68	1.94	1.87	1.82	1.98	1.94	1.93	1.78
K2O	0.96	1.20	1.31	1.10	1.17	1.26	1.14	1.10	1.13	1.11	12.74	1.12	1.22	1.28	1.24	1.17	1.16	1.17	1.31
NiO	0.02	0.01	0.02	0.00	0.00	0.00	0.01	0.00	0.01	0.00	12.74	0.03	0.00	0.04	0.01	0.01	0.02	0.00	0.02
F	0.44	0.31	0.21	0.00	0.12	0.20	0.07	0.08	0.43	0.15	12.74	0.20	0.05	0.09	0.41	0.19	0.48	0.21	0.20
Cl	0.04	0.04	0.02	0.03	0.01	0.02	0.04	0.03	0.03	0.03	12.74	0.02	0.02	0.02	0.02	0.04	0.04	0.04	0.04
H2O	1.81	1.87	1.92	2.03	1.98	1.93	1.98	2.00	1.83	1.96	12.74	1.94	2.00	1.98	1.83	1.93	1.80	1.93	1.92
O=F	0.18	0.13	0.09	0.00	0.05	0.08	0.03	0.03	0.18	0.06	12.74	0.08	0.02	0.04	0.17	0.08	0.20	0.09	0.08
O=Cl	0.01	0.01	0.00	0.01	0.00	0.00	0.01	0.01	0.01	0.01	12.74	0.00	0.00	0.00	0.01	0.01	0.01	0.01	0.01
Sum Ox%	100	100	100	100	100	100	100	100	100	100	12.74	100	100	100	100	100	100	100	100
Si	6.515	6.502	6.448	6.512	6.452	6.486	6.485	6.496	6.494	6.525	6.489	6.540	6.448	6.433	6.478	6.480	6.432	6.465	6.479
Ti	0.164	0.203	0.214	0.185	0.203	0.194	0.191	0.186	0.192	0.211	0.180	0.164	0.212	0.218	0.176	0.192	0.202	0.188	0.207
Al/Al IV	1.485	1.498	1.552	1.488	1.548	1.514	1.515	1.504	1.506	1.475	1.511	1.460	1.552	1.567	1.522	1.520	1.568	1.535	1.521
Al VI	0.275	0.209	0.171	0.251	0.194	0.182	0.199	0.224	0.230	0.244	0.245	0.223	0.135	0.148	0.177	0.199	0.152	0.184	0.153
Cr	0.006	0.003	0.004	0.006	0.004	0.005	0.004	0.004	0.006	0.005	0.004	0.002	0.001	0.006	0.002	0.002	0.004	0.002	0.003
Fe3+	0.584	0.578	0.683	0.623	0.680	0.632	0.570	0.667	0.682	0.547	0.648	0.661	0.795	0.683	0.697	0.627	0.720	0.656	0.649
Fe2+	1.198	1.208	1.130	1.147	1.122	1.147	1.211	1.118	1.097	1.205	1.102	1.079	1.051	1.160	1.060	1.180	1.106	1.138	1.141
Mn2+	0.022	0.041	0.055	0.035	0.038	0.046	0.032	0.039	0.039	0.042	0.031	0.034	0.051	0.053	0.044	0.036	0.039	0.037	0.053
Mg	2.749	2.756	2.741	2.752	2.758	2.793	2.792	2.761	2.752	2.746	2.789	2.833	2.756	2.727	2.844	2.762	2.775	2.796	2.793
Ca	1.783	1.774	1.723	1.736	1.735	1.762	1.787	1.732	1.720	1.754	1.768	1.780	1.707	1.758	1.770	1.762	1.756	1.773	1.773
Na	0.543	0.527	0.573	0.560	0.575	0.545	0.571	0.565	0.551	0.541	0.526	0.477	0.555	0.536	0.521	0.564	0.557	0.552	0.510
K	0.181	0.225	0.247	0.206	0.218	0.238	0.215	0.207	0.212	0.208	0.192	0.209	0.228	0.242	0.233	0.220	0.219	0.219	0.247
Ni	0.002	0.001	0.003	0.000	0.000	0.000	0.002	0.000	0.002	0.000	0.002	0.003	0.000	0.004	0.001	0.001	0.002	0.000	0.002
F	0.204	0.144	0.100	0.000	0.058	0.094	0.034	0.038	0.197	0.069	0.074	0.093	0.022	0.041	0.190	0.089	0.222	0.099	0.093
Cl	0.011	0.009	0.004	0.009	0.002	0.005	0.011	0.008	0.007	0.008	0.009	0.004	0.004	0.005	0.006	0.010	0.010	0.010	0.011
OH	1.785	1.846	1.895	1.991	1.940	1.901	1.954	1.954	1.796	1.923	1.916	1.903	1.974	1.954	1.804	1.900	1.768	1.892	1.896
Sum Cat#	17.51	17.53	17.54	17.50	17.53	17.54	17.57	17.50	17.48	17.50	17.49	17.47	17.49	17.54	17.52	17.55	17.53	17.54	17.53
XMg	0.70	0.70	0.71	0.71	0.71	0.71	0.70	0.71	0.72	0.70	0.72	0.72	0.72	0.70	0.73	0.70	0.72	0.71	0.71
	Edenite	Edenite	Mg-hast	Edenite	Mg-hast	Mg-hast	Mg-hast	Mg-hast	Tsch	Edenite	Tsch	Mg-hbl	Tsch	Mg-hast	Mg-hast	Mg-hast	Mg-hast	Mg-hast	Mg-hast

Amphibole Analyses by sample (recalculated to 100%), cations based on 23 (O) Oxygens.

GT 481d													
Label	Amp1 C	Amp1 R	Amp2 C	Amp2 R	Amp3 C	Amp3 R	Amp4 R	Amp4 C	Amp5 C	Amp5 R	Amp6 C	Amp6 C	Amp6 R
SiO2	42.05	42.36	41.84	41.92	41.67	42.13	42.15	42.08	41.55	41.58	41.60	42.32	42.06
TiO2	1.67	1.63	1.69	1.64	1.68	1.72	1.58	1.65	1.65	1.56	1.63	1.72	1.68
Al2O3	12.37	12.27	12.70	12.73	12.43	12.36	12.26	12.42	12.38	12.33	12.84	12.35	12.45
Cr2O3	0.00	0.00	0.04	0.03	0.01	0.00	0.01	0.05	0.04	0.08	0.02	0.03	0.05
Fe2O3	4.62	4.37	4.07	4.93	5.23	5.65	4.86	4.53	6.04	5.28	5.26	3.08	5.25
FeO	11.48	11.50	11.90	11.15	11.13	10.44	11.18	11.44	10.70	11.06	11.02	12.29	10.90
MnO	0.32	0.28	0.20	0.29	0.26	0.26	0.29	0.26	0.21	0.28	0.25	0.28	0.26
MgO	10.78	10.89	10.72	10.65	10.84	11.00	10.97	10.81	10.85	10.98	10.72	10.95	10.83
CaO	11.26	11.31	11.42	11.27	11.33	11.21	11.35	11.23	11.28	11.57	11.21	11.54	11.28
Na2O	1.82	1.75	1.81	1.56	1.77	1.54	1.84	1.85	1.75	1.80	1.88	1.83	1.67
K2O	1.58	1.53	1.57	1.70	1.58	1.64	1.43	1.57	1.52	1.40	1.53	1.55	1.50
NiO	0.01	0.03	0.00	0.03	0.00	0.00	0.03	0.04	0.01	0.00	0.02	0.00	0.01
F	0.20	0.28	0.19	0.24	0.32	0.05	0.14	0.15	0.10	0.32	0.00	0.18	0.22
Cl	0.04	0.02	0.01	0.04	0.02	0.05	0.03	0.02	0.03	0.02	0.03	0.02	0.04
H2O	1.91	1.88	1.92	1.89	1.85	1.98	1.94	1.93	1.95	1.85	2.00	1.93	1.90
O=F	0.08	0.12	0.08	0.10	0.13	0.02	0.06	0.06	0.04	0.14	0.00	0.08	0.09
O=Cl	0.01	0.01	0.00	0.01	0.00	0.01	0.01	0.01	0.01	0.01	0.01	0.01	0.01
Sum Ox%	100	100	100	100	100	100	100	100	100	100	100	100	100
Si	6.261	6.298	6.232	6.238	6.211	6.252	6.268	6.262	6.190	6.200	6.192	6.298	6.249
Ti	0.186	0.183	0.189	0.184	0.188	0.191	0.176	0.185	0.185	0.175	0.183	0.193	0.187
Al/Al IV	1.739	1.702	1.768	1.762	1.789	1.748	1.732	1.738	1.810	1.800	1.808	1.702	1.751
Al VI	0.432	0.447	0.462	0.471	0.394	0.415	0.417	0.441	0.365	0.367	0.443	0.464	0.430
Cr	0.000	0.000	0.005	0.004	0.001	0.000	0.001	0.006	0.004	0.010	0.002	0.004	0.005
Fe3+	0.517	0.489	0.456	0.552	0.587	0.631	0.544	0.507	0.677	0.592	0.589	0.345	0.588
Fe2+	1.430	1.430	1.482	1.388	1.388	1.295	1.390	1.424	1.333	1.379	1.371	1.530	1.355
Mn2+	0.040	0.036	0.025	0.037	0.033	0.033	0.037	0.033	0.027	0.036	0.032	0.036	0.033
Mg	2.393	2.411	2.380	2.361	2.408	2.434	2.431	2.399	2.409	2.440	2.378	2.428	2.399
Ca	1.797	1.802	1.823	1.796	1.809	1.783	1.807	1.791	1.800	1.848	1.788	1.840	1.796
Na	0.524	0.504	0.522	0.452	0.512	0.443	0.532	0.533	0.506	0.518	0.543	0.528	0.479
K	0.299	0.292	0.299	0.323	0.300	0.310	0.272	0.299	0.288	0.266	0.290	0.294	0.283
Ni	0.001	0.003	0.000	0.003	0.000	0.000	0.003	0.005	0.001	0.000	0.003	0.000	0.002
F	0.094	0.133	0.091	0.116	0.149	0.026	0.064	0.073	0.047	0.155	0.000	0.086	0.103
Cl	0.010	0.006	0.002	0.011	0.005	0.012	0.007	0.006	0.009	0.006	0.009	0.006	0.010
OH	1.896	1.861	1.907	1.872	1.845	1.962	1.929	1.921	1.945	1.839	1.991	1.908	1.887
Sum Cat#	17.619	17.598	17.644	17.571	17.621	17.536	17.611	17.623	17.595	17.633	17.621	17.663	17.557
XMg	0.63	0.63	0.62	0.63	0.63	0.65	0.64	0.63	0.64	0.64	0.63	0.61	0.64
	Mg-hast	Mg-hast	Mg-hast	Mg-hast	Mg-hast	Mg-hast	Mg-hast	Mg-hast	Mg-hast	Mg-hast	Mg-hast	Parg	Mg-hast

Amphibole Analyses by sample (recalculated to 100%), cations based on 23 (O) Oxygens.

GT 486d												
Label	Amp1	Amp1	Amp2	Amp2	Amp2	Amp3	Amp3	Amp3	Amp4	Amp4	Amp5	Amp5
	C	R	R	C	R	C	R	R	R	C	R	C
SiO2	42.43	43.05	42.92	42.74	42.58	43.01	42.75	43.08	42.70	42.74	43.04	42.92
TiO2	1.28	1.31	1.18	1.30	1.31	1.19	1.34	1.26	1.35	1.14	1.34	1.29
Al2O3	12.43	12.06	12.12	12.02	12.21	12.18	12.21	12.14	12.30	12.39	12.28	12.08
Cr2O3	0.09	0.08	0.14	0.07	0.15	0.07	0.04	0.06	0.06	0.08	0.11	0.12
Fe2O3	5.61	5.32	5.01	5.37	5.95	5.19	4.94	5.97	4.66	5.25	4.52	4.57
FeO	8.37	8.57	8.75	8.45	8.02	8.59	8.78	7.75	8.91	8.43	9.18	9.24
MnO	0.27	0.26	0.30	0.32	0.31	0.22	0.23	0.25	0.29	0.19	0.23	0.24
MgO	12.54	12.57	12.63	12.69	12.66	12.68	12.66	12.80	12.62	12.75	12.46	12.53
CaO	11.57	11.44	11.62	11.56	11.51	11.56	11.68	11.44	11.69	11.72	11.59	11.69
Na2O	1.70	1.62	1.64	1.66	1.63	1.67	1.63	1.53	1.68	1.66	1.62	1.64
K2O	1.59	1.62	1.63	1.66	1.62	1.57	1.62	1.60	1.64	1.53	1.60	1.60
NiO	0.03	0.00	0.00	0.06	0.00	0.00	0.05	0.03	0.04	0.04	0.00	0.02
F	0.25	0.30	0.04	0.31	0.00	0.13	0.25	0.25	0.20	0.13	0.00	0.22
Cl	0.01	0.02	0.01	0.02	0.02	0.02	0.02	0.03	0.03	0.04	0.02	0.01
H2O	1.91	1.89	2.02	1.89	2.03	1.97	1.91	1.92	1.94	1.96	2.03	1.93
O=F	0.11	0.13	0.02	0.13	0.00	0.06	0.11	0.10	0.08	0.05	0.00	0.09
O=Cl	0.00	0.01	0.00	0.00	0.00	0.01	0.00	0.01	0.01	0.01	0.00	0.00
Sum Ox%	100	100	100	100	100	100	100	100	100	100	100	100
Si	6.246	6.326	6.314	6.293	6.261	6.319	6.291	6.315	6.286	6.280	6.327	6.322
Ti	0.141	0.145	0.130	0.144	0.145	0.132	0.147	0.139	0.149	0.127	0.148	0.142
Al/Al IV	1.754	1.674	1.686	1.707	1.739	1.681	1.709	1.685	1.714	1.720	1.673	1.678
Al VI	0.404	0.416	0.415	0.378	0.378	0.428	0.409	0.414	0.421	0.427	0.455	0.418
Cr	0.011	0.009	0.017	0.008	0.017	0.008	0.005	0.007	0.007	0.010	0.013	0.014
Fe3+	0.622	0.589	0.554	0.596	0.659	0.574	0.547	0.659	0.516	0.581	0.499	0.506
Fe2+	1.031	1.054	1.076	1.042	0.986	1.055	1.081	0.950	1.097	1.036	1.127	1.138
Mn2+	0.034	0.032	0.037	0.040	0.039	0.028	0.029	0.031	0.036	0.023	0.029	0.031
Mg	2.753	2.754	2.770	2.784	2.776	2.775	2.777	2.796	2.769	2.792	2.729	2.750
Ca	1.825	1.801	1.832	1.825	1.813	1.820	1.843	1.798	1.843	1.845	1.825	1.844
Na	0.487	0.462	0.469	0.474	0.465	0.473	0.464	0.433	0.479	0.474	0.461	0.469
K	0.298	0.305	0.307	0.312	0.303	0.295	0.303	0.298	0.307	0.286	0.300	0.300
Ni	0.004	0.000	0.000	0.007	0.000	0.000	0.006	0.004	0.004	0.004	0.000	0.002
F	0.117	0.142	0.019	0.144	0.000	0.061	0.118	0.116	0.094	0.060	0.000	0.103
Cl	0.001	0.006	0.003	0.004	0.005	0.006	0.005	0.008	0.007	0.009	0.004	0.003
OH	1.882	1.852	1.978	1.851	1.995	1.933	1.877	1.876	1.899	1.931	1.996	1.894
Sum Cat#	17.61	17.57	17.61	17.61	17.58	17.59	17.61	17.53	17.63	17.60	17.59	17.61
XMg	0.73	0.72	0.72	0.73	0.74	0.72	0.72	0.75	0.72	0.73	0.71	0.71
	Mg-hast	Mg-hast	Mg-hast	Mg-hast	Mg-hast	Mg-hast	Mg-hast	Mg-hast	Mg-hast	Mg-hast	Mg-hast	Mg-hast

Amphibole Analyses by sample (recalculated to 100%), cations based on 23 (O) Oxygens.

Terrane / Sample	CD 430											
Label	Amp1	Amp1	Amp2	Amp2	Amp3	Amp3	Amp4	Amp4	Amp5	Amp5	Amp6	Amp6
	C	R	R	C	C	R	C	R	C	R	C	R
SiO2	41.32	41.17	41.26	41.30	41.74	41.63	41.23	41.95	41.58	42.10	41.89	41.86
TiO2	2.39	2.59	2.35	2.22	2.27	2.19	2.29	2.17	2.46	2.27	2.34	2.28
Al2O3	12.92	13.10	13.10	13.32	13.04	12.83	13.37	12.33	12.96	12.58	12.61	12.99
Cr2O3	0.08	0.06	0.09	0.09	0.01	0.03	0.07	0.07	0.06	0.04	0.04	0.06
Fe2O3	3.64	2.65	2.52	2.59	3.64	2.97	2.11	3.37	3.00	3.31	2.43	2.35
FeO	11.05	12.07	11.77	11.81	10.82	11.38	11.95	10.89	11.08	10.78	11.81	11.69
MnO	0.12	0.14	0.12	0.15	0.19	0.16	0.16	0.11	0.17	0.16	0.16	0.14
MgO	11.49	11.11	11.48	11.32	11.43	11.63	11.39	12.05	11.66	11.84	11.58	11.53
CaO	11.82	11.78	12.03	11.96	11.71	12.00	12.06	12.06	11.90	11.78	12.01	11.86
Na2O	2.17	2.25	2.25	2.27	2.12	2.17	2.26	2.09	2.17	2.14	2.14	2.24
K2O	0.82	0.91	0.83	0.81	0.79	0.80	0.88	0.78	0.79	0.78	0.79	0.82
NiO	0.07	0.04	0.05	0.03	0.11	0.05	0.09	0.00	0.04	0.05	0.07	0.03
F	0.31	0.37	0.37	0.45	0.29	0.49	0.34	0.20	0.33	0.47	0.33	0.28
Cl	0.12	0.11	0.12	0.13	0.13	0.12	0.13	0.12	0.14	0.14	0.14	0.14
H2O	1.84	1.81	1.81	1.77	1.86	1.76	1.83	1.90	1.83	1.77	1.83	1.86
O=F	0.13	0.15	0.15	0.19	0.12	0.21	0.14	0.08	0.14	0.20	0.13	0.12
O=Cl	0.03	0.02	0.03	0.03	0.03	0.03	0.03	0.03	0.03	0.03	0.03	0.03
Sum Ox%	100	100	100	100	100	100	100	100	100	100	100	100
Si	6.128	6.122	6.127	6.130	6.173	6.172	6.123	6.206	6.153	6.220	6.209	6.197
Ti	0.268	0.290	0.262	0.247	0.253	0.244	0.255	0.242	0.273	0.253	0.260	0.254
Al/Al IV	1.872	1.878	1.873	1.870	1.827	1.828	1.877	1.794	1.847	1.780	1.791	1.803
Al VI	0.385	0.418	0.420	0.462	0.445	0.413	0.464	0.357	0.414	0.410	0.413	0.465
Cr	0.010	0.008	0.011	0.011	0.002	0.004	0.009	0.009	0.007	0.005	0.004	0.007
Fe3+	0.406	0.297	0.282	0.289	0.405	0.330	0.236	0.375	0.334	0.368	0.270	0.262
Fe2+	1.370	1.500	1.461	1.465	1.339	1.411	1.485	1.348	1.371	1.332	1.464	1.447
Mn2+	0.015	0.018	0.016	0.019	0.024	0.021	0.020	0.014	0.022	0.020	0.020	0.017
Mg	2.538	2.464	2.542	2.503	2.519	2.570	2.520	2.656	2.573	2.607	2.560	2.544
Ca	1.878	1.877	1.915	1.903	1.856	1.907	1.920	1.911	1.887	1.866	1.908	1.882
Na	0.624	0.650	0.648	0.654	0.609	0.625	0.650	0.601	0.623	0.614	0.616	0.642
K	0.156	0.172	0.159	0.154	0.148	0.152	0.167	0.147	0.148	0.147	0.150	0.155
Ni	0.008	0.005	0.006	0.003	0.013	0.006	0.011	0.000	0.005	0.005	0.009	0.004
F	0.147	0.174	0.172	0.211	0.136	0.230	0.158	0.094	0.155	0.221	0.152	0.133
Cl	0.030	0.028	0.031	0.033	0.031	0.030	0.034	0.032	0.035	0.034	0.035	0.036
OH	1.824	1.798	1.796	1.756	1.833	1.741	1.808	1.874	1.810	1.745	1.812	1.830
Sum Cat#	17.658	17.698	17.721	17.711	17.613	17.685	17.737	17.659	17.658	17.626	17.674	17.679
XMg	0.65	0.62	0.64	0.63	0.65	0.65	0.63	0.66	0.65	0.66	0.64	0.64
Name	Mg-hast	Parg	Parg	Parg	Parg	Parg	Parg	Mg-hast	Parg	Parg	Parg	Parg

Amphibole Analyses by sample (recalculated to 100%), cations based on 23 (O) Oxygens.

CD 209-1																		
Label	Amp1	Amp1	Amp2	Amp2	Amp3	Amp3	Amp3	Amp4	Amp4	Amp4	Amp4	Amp4	Amp5	Amp5	Amp5	Amp6	Amp6	Amp6
	C	C	C	R	C	R	R	C	R	R	R	R	C	C	R	C	C	C
SiO2	46.01	44.64	44.61	44.95	44.27	44.68	43.73	43.35	44.67	43.62	44.82	45.18	44.63	43.93	44.07	43.52	44.81	45.76
TiO2	1.56	1.74	2.07	1.99	2.09	1.89	2.05	2.01	1.95	1.92	1.92	1.69	1.88	1.78	1.58	1.99	1.94	1.57
Al2O3	9.67	10.24	10.41	10.12	10.46	10.12	12.33	12.37	10.35	11.99	10.51	11.20	10.50	11.97	11.48	12.28	10.12	10.38
Cr2O3	0.31	0.38	0.44	0.38	0.32	0.29	0.35	0.33	0.31	0.31	0.22	0.21	0.40	0.35	0.30	0.28	0.32	0.22
Fe2O3	0.00	0.00	0.00	0.00	0.00	0.00	1.09	1.95	0.00	2.08	0.00	2.14	0.00	1.83	3.30	2.35	0.00	2.06
FeO	12.95	13.85	13.29	13.28	13.63	13.57	12.03	11.35	13.68	10.96	13.48	10.45	13.51	11.33	10.87	11.04	13.90	10.83
MnO	0.17	0.18	0.18	0.08	0.17	0.14	0.17	0.09	0.12	0.11	0.14	0.16	0.08	0.14	0.15	0.14	0.09	0.13
MgO	11.92	11.37	11.15	11.48	11.13	11.50	11.42	11.63	11.14	12.04	11.23	12.53	11.12	11.85	11.78	11.66	11.00	12.64
CaO	12.57	12.64	12.59	12.70	12.75	12.66	11.63	11.62	12.70	11.88	12.45	11.69	12.66	11.70	11.67	11.61	12.66	11.68
Na2O	1.22	1.25	1.31	1.22	1.31	1.27	1.24	1.26	1.23	1.17	1.34	1.17	1.27	1.31	1.17	1.18	1.22	1.22
K2O	1.35	1.48	1.67	1.55	1.57	1.59	1.65	1.71	1.59	1.53	1.60	1.35	1.59	1.52	1.39	1.62	1.57	1.22
NiO	0.00	0.00	0.00	0.00	0.04	0.00	0.04	0.05	0.01	0.05	0.01	0.00	0.02	0.02	0.00	0.03	0.09	0.01
F	0.83	0.59	0.63	0.55	0.78	0.72	0.78	0.86	0.79	1.06	0.71	0.51	0.98	0.69	0.63	0.77	0.83	0.82
Cl	0.29	0.32	0.35	0.32	0.34	0.35	0.32	0.33	0.32	0.36	0.35	0.26	0.37	0.33	0.27	0.33	0.34	0.28
H2O	1.56	1.66	1.63	1.69	1.56	1.58	1.58	1.54	1.56	1.44	1.60	1.74	1.46	1.62	1.67	1.58	1.54	1.60
O=F	0.35	0.24	0.27	0.23	0.32	0.31	0.33	0.36	0.33	0.45	0.30	0.21	0.41	0.29	0.27	0.32	0.35	0.35
O=Cl	0.06	0.07	0.08	0.07	0.07	0.08	0.07	0.08	0.07	0.08	0.08	0.06	0.08	0.08	0.06	0.08	0.07	0.06
Sum Ox%	100	100	100	100	100	100	100	100	100	100	100	100	100	100	100	100	100	100
Si	6.781	6.632	6.620	6.656	6.584	6.636	6.449	6.397	6.633	6.425	6.643	6.601	6.625	6.467	6.490	6.411	6.661	6.691
Ti	0.174	0.195	0.231	0.222	0.233	0.212	0.227	0.223	0.218	0.213	0.215	0.185	0.210	0.197	0.175	0.221	0.216	0.172
Al/Al IV	1.219	1.368	1.380	1.344	1.416	1.364	1.551	1.603	1.367	1.575	1.357	1.399	1.375	1.533	1.510	1.589	1.339	1.309
Al VI	0.461	0.424	0.441	0.423	0.419	0.406	0.593	0.548	0.444	0.506	0.480	0.530	0.463	0.544	0.483	0.543	0.435	0.480
Cr	0.036	0.044	0.052	0.045	0.038	0.034	0.041	0.039	0.036	0.036	0.025	0.024	0.048	0.041	0.035	0.033	0.038	0.025
Fe3+	0.000	0.000	0.000	0.000	0.000	0.000	0.121	0.216	0.000	0.231	0.000	0.236	0.000	0.203	0.365	0.261	0.000	0.227
Fe2+	1.597	1.721	1.650	1.645	1.695	1.686	1.484	1.400	1.699	1.351	1.671	1.277	1.678	1.394	1.338	1.360	1.728	1.324
Mn2+	0.020	0.023	0.023	0.010	0.020	0.019	0.021	0.012	0.015	0.014	0.017	0.020	0.011	0.017	0.019	0.017	0.012	0.016
Mg	2.617	2.517	2.466	2.534	2.468	2.545	2.509	2.557	2.466	2.644	2.481	2.729	2.462	2.601	2.584	2.561	2.436	2.756
Ca	1.985	2.013	2.003	2.016	2.031	2.015	1.837	1.836	2.021	1.876	1.978	1.830	2.014	1.846	1.842	1.834	2.015	1.830
Na	0.348	0.360	0.379	0.350	0.376	0.366	0.355	0.361	0.354	0.335	0.385	0.331	0.368	0.373	0.332	0.336	0.350	0.346
K	0.252	0.279	0.317	0.293	0.298	0.301	0.311	0.321	0.299	0.288	0.303	0.250	0.302	0.285	0.261	0.306	0.298	0.227
Ni	0.000	0.000	0.000	0.000	0.005	0.000	0.004	0.006	0.001	0.006	0.002	0.000	0.002	0.002	0.000	0.003	0.011	0.001
F	0.387	0.277	0.295	0.255	0.365	0.341	0.365	0.401	0.370	0.492	0.330	0.232	0.460	0.324	0.295	0.356	0.390	0.382
Cl	0.073	0.078	0.088	0.080	0.086	0.089	0.080	0.084	0.080	0.089	0.088	0.064	0.094	0.084	0.068	0.083	0.085	0.068
OH	1.540	1.645	1.617	1.665	1.549	1.570	1.555	1.516	1.550	1.419	1.582	1.705	1.447	1.592	1.637	1.561	1.525	1.551
Sum Cat#	17.488	17.574	17.561	17.538	17.584	17.584	17.504	17.518	17.553	17.499	17.555	17.411	17.557	17.504	17.435	17.476	17.541	17.404
XMg	0.62	0.59	0.60	0.61	0.59	0.60	0.63	0.65	0.59	0.66	0.60	0.68	0.60	0.65	0.66	0.65	0.59	0.68
	Edenite	Edenite	Edenite	Edenite	Edenite	Edenite	Parg	Parg	Edenite	Tsch	Edenite	Mg-hbl	Edenite	Parg	Edenite	Tsch	Edenite	Mg-hbl

Amphibole Analyses by sample (recalculated to 100%), cations based on 23 (O) Oxygens.

	CD 457											Ultrapotassic 209-2						
	Amp1	Amp1	Amp2	Amp2	Amp3	Amp3	Amp4	Amp4	Amp5	Amp5		Amp1	Amp1	Amp2	Amp2	Amp2	Amp2	Amp2
Label	R	C	R	C	C	R	R	C	R	C	Label	C	C	R1	C1	C2	C3	R2
SiO2	41.47	41.43	41.50	41.86	41.28	40.58	41.77	41.35	41.28	41.16	SiO2	46.34	46.79	47.55	47.45	46.29	47.02	47.40
TiO2	1.97	2.40	2.19	2.22	2.26	2.35	2.13	2.26	2.24	2.24	TiO2	1.11	1.11	0.93	0.92	1.09	0.98	0.88
Al2O3	12.36	12.06	12.12	11.92	12.16	12.21	12.07	11.86	12.28	12.49	Al2O3	9.79	9.60	8.78	8.81	9.62	8.70	8.89
Cr2O3	0.02	0.00	0.05	0.03	0.03	0.01	0.03	0.03	0.03	0.00	Cr2O3	0.03	0.03	0.02	0.00	0.05	0.00	0.00
Fe2O3	2.15	2.61	2.20	1.32	2.01	2.00	2.34	2.18	1.79	1.87	Fe2O3	3.63	3.16	3.83	3.95	4.16	5.50	3.65
FeO	16.45	16.21	16.59	16.97	16.55	16.70	16.38	16.51	16.78	16.92	FeO	11.14	3.16	10.62	10.48	11.00	9.49	10.54
MnO	0.18	0.22	0.13	0.10	0.15	0.21	0.15	0.17	0.17	0.21	MnO	0.27	3.16	0.28	0.31	0.22	0.34	0.27
MgO	8.56	8.51	8.50	8.72	8.61	8.71	8.54	8.73	8.53	8.24	MgO	11.92	3.16	12.50	12.56	11.90	12.61	12.70
CaO	11.50	11.18	11.29	11.55	11.47	11.79	11.29	11.53	11.53	11.24	CaO	11.61	3.16	11.63	11.59	11.53	11.45	11.79
Na2O	1.73	1.82	1.82	1.72	1.80	1.85	1.75	1.75	1.77	1.98	Na2O	0.95	3.16	0.84	0.90	0.97	0.88	0.86
K2O	1.52	1.50	1.54	1.50	1.52	1.53	1.46	1.52	1.51	1.53	K2O	0.97	3.16	0.83	0.85	0.95	0.82	0.82
NiO	0.02	0.00	0.00	0.00	0.04	0.02	0.01	0.02	0.00	0.01	NiO	0.00	3.16	0.03	0.00	0.01	0.01	0.00
F	0.30	0.67	0.69	0.48	0.91	0.54	0.54	0.73	0.71	0.68	F	0.82	3.16	0.52	0.34	0.71	0.74	0.82
Cl	0.06	0.06	0.05	0.06	0.07	0.04	0.09	0.08	0.03	0.07	Cl	0.17	3.16	0.11	0.14	0.16	0.12	0.14
H2O	1.82	1.65	1.64	1.74	1.53	1.70	1.71	1.61	1.63	1.63	H2O	1.62	3.16	1.78	1.86	1.67	1.67	1.64
O=F	0.13	0.28	0.29	0.20	0.38	0.23	0.23	0.30	0.29	0.29	O=F	0.35	3.16	0.22	0.14	0.30	0.31	0.35
O=Cl	0.01	0.01	0.01	0.01	0.02	0.01	0.02	0.02	0.01	0.02	O=Cl	0.04	3.16	0.03	0.03	0.04	0.03	0.03
Sum Ox%	100	100	100	100	100	100	100	100	100	100	Sum Ox%	100	3.16	100	100	100	100	100
Si	6.280	6.276	6.289	6.335	6.262	6.177	6.319	6.276	6.261	6.249	Si	6.784	6.841	6.925	6.911	6.780	6.854	6.905
Ti	0.224	0.273	0.249	0.254	0.258	0.269	0.242	0.257	0.256	0.257	Ti	0.122	0.122	0.102	0.101	0.121	0.108	0.097
Al/Al IV	1.720	1.724	1.711	1.665	1.738	1.823	1.681	1.724	1.739	1.751	Al/Al IV	1.216	1.159	1.075	1.089	1.220	1.146	1.095
Al VI	0.487	0.428	0.455	0.461	0.436	0.368	0.471	0.397	0.456	0.485	Al VI	0.474	0.495	0.431	0.424	0.441	0.349	0.430
Cr	0.002	0.000	0.006	0.004	0.003	0.001	0.003	0.003	0.004	0.000	Cr	0.003	0.004	0.002	0.000	0.006	0.000	0.000
Fe3+	0.246	0.298	0.250	0.151	0.230	0.229	0.266	0.249	0.204	0.213	Fe3+	0.400	0.347	0.420	0.433	0.458	0.603	0.400
Fe2+	2.084	2.053	2.102	2.149	2.100	2.127	2.072	2.095	2.129	2.149	Fe2+	1.364	1.396	1.293	1.277	1.348	1.156	1.283
Mn2+	0.024	0.028	0.017	0.013	0.020	0.026	0.019	0.022	0.023	0.028	Mn2+	0.034	0.033	0.034	0.038	0.028	0.042	0.033
Mg	1.931	1.920	1.921	1.968	1.948	1.977	1.924	1.974	1.929	1.867	Mg	2.602	2.604	2.714	2.727	2.597	2.741	2.757
Ca	1.867	1.815	1.833	1.873	1.865	1.923	1.830	1.876	1.875	1.829	Ca	1.822	1.821	1.815	1.809	1.809	1.789	1.839
Na	0.509	0.533	0.537	0.506	0.529	0.544	0.514	0.513	0.520	0.584	Na	0.270	0.251	0.235	0.254	0.276	0.249	0.243
K	0.294	0.288	0.298	0.288	0.294	0.297	0.281	0.295	0.292	0.296	K	0.181	0.176	0.153	0.158	0.178	0.152	0.151
Ni	0.002	0.000	0.000	0.000	0.005	0.003	0.001	0.003	0.000	0.002	Ni	0.000	0.000	0.004	0.000	0.002	0.001	0.000
F	0.146	0.321	0.329	0.226	0.435	0.258	0.256	0.348	0.341	0.329	F	0.381	0.327	0.239	0.157	0.328	0.342	0.377
Cl	0.017	0.015	0.013	0.015	0.017	0.010	0.022	0.020	0.008	0.018	Cl	0.041	0.036	0.027	0.035	0.038	0.029	0.034
OH	1.837	1.664	1.658	1.759	1.547	1.732	1.722	1.632	1.651	1.653	OH	1.578	1.637	1.734	1.808	1.634	1.629	1.589
Sum Cat#	17.669	17.636	17.668	17.667	17.687	17.764	17.625	17.685	17.688	17.709	Sum Cat#	17.272	17.249	17.203	17.220	17.264	17.190	17.233
XMg	0.48	0.48	0.48	0.48	0.48	0.48	0.48	0.49	0.48	0.47	XMg	0.66	0.65	0.68	0.68	0.66	0.70	0.68
	Fe-parg	Fe-parg	Fe-parg	Fe-parg	Fe-parg	Fe-parg	Fe-parg	Fe-parg	Fe-parg	Fe-parg			Mg-hbl	Mg-hbl	Mg-hbl	Mg-hbl	Mg-hbl	Mg-hbl

Amphibole Analyses by sample (recalculated to 100%), cations based on 23 (O) Oxygens.

	Ultrapotassic 404					Ultrapotassic 408									
	Amp1	Amp1	Amp1	Amp1		Amp1	Amp1	Amp2	Amp2	Amp3	Amp3	Amp4	Amp4	Amp4	Amp4
Label	R	C	C	C	Label	C	C	C	C	C	C	C	C	C	C
SiO2	49.31	49.42	49.85	49.94	SiO2	46.56	46.74	47.26	46.76	45.39	46.00	47.62	46.69	46.30	46.72
TiO2	0.85	0.92	0.78	0.74	TiO2	0.83	0.88	0.68	0.76	1.09	1.05	1.02	0.89	0.99	1.08
Al2O3	7.31	7.12	6.81	6.60	Al2O3	9.34	9.29	8.57	9.10	10.42	9.73	8.06	9.49	9.79	8.91
Cr2O3	0.02	0.00	0.02	0.03	Cr2O3	0.00	0.01	0.03	0.01	0.00	0.00	0.02	0.00	0.01	0.02
Fe2O3	4.92	4.15	3.38	4.32	Fe2O3	6.40	5.67	6.38	5.28	5.74	4.88	5.18	5.42	5.36	5.09
FeO	7.77	8.30	8.73	8.23	FeO	10.60	11.12	10.86	11.68	11.63	12.11	11.07	11.23	11.33	11.77
MnO	0.27	0.25	0.20	0.24	MnO	0.30	0.24	0.24	0.24	0.29	0.28	0.30	0.25	0.24	0.24
MgO	14.41	14.53	14.77	14.71	MgO	11.19	11.20	11.33	11.14	10.40	10.76	11.84	11.14	10.98	11.14
CaO	11.52	11.80	11.90	11.74	CaO	11.04	11.17	11.14	11.28	11.03	11.13	11.26	11.16	11.16	11.18
Na2O	0.74	0.70	0.76	0.72	Na2O	1.06	0.97	0.86	1.00	1.14	1.23	0.93	1.04	1.04	1.00
K2O	0.66	0.63	0.61	0.55	K2O	0.57	0.61	0.57	0.66	0.76	0.71	0.59	0.58	0.64	0.71
NiO	0.00	0.01	0.00	0.01	NiO	0.00	0.00	0.00	0.01	0.03	0.00	0.01	0.00	0.01	0.00
F	0.82	0.67	0.65	0.52	F	0.41	0.36	0.23	0.32	0.28	0.38	0.28	0.40	0.51	0.46
Cl	0.08	0.06	0.05	0.05	Cl	0.06	0.04	0.04	0.04	0.08	0.08	0.06	0.05	0.07	0.09
H2O	*1.67	1.75	1.77	1.83	H2O	1.84	1.87	1.93	1.88	1.88	1.84	1.90	1.84	1.78	1.80
O=F	0.35	0.29	0.28	0.22	O=F	0.17	0.15	0.10	0.14	0.12	0.16	0.12	0.17	0.22	0.20
O=Cl	0.02	0.01	0.01	0.01	O=Cl	0.01	0.01	0.01	0.01	0.02	0.02	0.01	0.01	0.02	0.02
Sum Ox%	100	100	100	100	Sum Ox%	100	100	100	100	100	100	100	100	100	100
Si	7.084	7.103	7.161	7.169	Si	6.816	6.842	6.914	6.860	6.683	6.772	6.959	6.834	6.788	6.860
Ti	0.092	0.099	0.084	0.080	Ti	0.091	0.097	0.075	0.084	0.121	0.116	0.111	0.098	0.109	0.119
Al/Al IV	0.916	0.897	0.839	0.831	Al/Al IV	1.184	1.158	1.086	1.140	1.317	1.228	1.041	1.166	1.212	1.140
Al VI	0.321	0.310	0.314	0.285	Al VI	0.427	0.444	0.392	0.434	0.490	0.460	0.347	0.471	0.480	0.401
Cr	0.002	0.000	0.002	0.003	Cr	0.000	0.001	0.004	0.001	0.000	0.000	0.002	0.000	0.001	0.003
Fe3+	0.532	0.449	0.366	0.467	Fe3+	0.705	0.625	0.702	0.583	0.636	0.540	0.570	0.596	0.592	0.563
Fe2+	0.934	0.997	1.048	0.988	Fe2+	1.298	1.361	1.328	1.432	1.431	1.490	1.352	1.375	1.388	1.445
Mn2+	0.032	0.030	0.024	0.028	Mn2+	0.037	0.029	0.029	0.029	0.035	0.035	0.037	0.030	0.029	0.030
Mg	3.086	3.114	3.161	3.147	Mg	2.442	2.443	2.470	2.436	2.283	2.359	2.579	2.430	2.399	2.440
Ca	1.774	1.816	1.831	1.805	Ca	1.732	1.752	1.746	1.774	1.740	1.755	1.763	1.750	1.753	1.759
Na	0.207	0.194	0.213	0.202	Na	0.299	0.275	0.242	0.283	0.327	0.352	0.263	0.294	0.295	0.284
K	0.121	0.115	0.113	0.102	K	0.107	0.114	0.107	0.124	0.143	0.134	0.111	0.108	0.120	0.134
Ni	0.000	0.001	0.000	0.001	Ni	0.000	0.000	0.000	0.002	0.004	0.000	0.001	0.000	0.002	0.000
F	0.373	0.305	0.299	0.237	F	0.186	0.166	0.106	0.148	0.127	0.174	0.128	0.183	0.237	0.217
Cl	0.020	0.014	0.013	0.011	Cl	0.015	0.011	0.009	0.009	0.020	0.021	0.015	0.012	0.018	0.022
OH	1.607	1.681	1.688	1.752	OH	1.798	1.824	1.885	1.843	1.853	1.805	1.857	1.804	1.745	1.761
Sum Cat#	17.103	17.125	17.157	17.110	Sum Cat#	17.138	17.142	17.094	17.181	17.209	17.241	17.137	17.153	17.168	17.177
XMg	0.77	0.76	0.75	0.76	XMg	0.65	0.64	0.65	0.63	0.62	0.61	0.66	0.64	0.63	0.63
	Mg-hbl	Mg-hbl	Mg-hbl	Mg-hbl		Mg-hbl	Mg-hbl	Mg-hbl	Mg-hbl	Mg-hbl	Mg-hbl	Mg-hbl	Mg-hbl	Mg-hbl	Mg-hbl

Biotite Analyses by sample (recalculated to 100%), cations based on 22 (O) Oxygens.

Terrane/Sample	GT 457													
Label	Bt1 C	Bt2 C	Bt3 R1	Bt4 R1	Bt5 R1	Bt5 C	Bt5 R2	Bt1 R	Bt2 R	Bt3 C	Bt3 R2	Bt4 C1	Bt4 C2	Bt4 R2
SiO2	36.02	35.57	35.59	35.75	36.42	36.18	36.37	35.84	36.05	35.82	36.24	35.90	35.87	36.44
TiO2	4.68	5.03	4.94	5.10	5.19	5.20	5.04	4.39	4.97	4.93	5.00	5.00	5.12	4.63
Al2O3	14.23	13.80	13.83	13.96	13.83	13.75	13.92	13.88	13.84	13.69	13.85	14.10	13.77	14.07
Cr2O3	0.01	0.02	0.03	0.05	0.04	0.00	0.02	0.02	0.00	0.05	0.01	0.00	0.03	0.03
FeO	19.78	21.24	21.08	20.18	19.78	20.34	20.16	20.79	20.55	21.30	20.49	20.02	20.15	19.77
MnO	0.04	0.05	0.09	0.08	0.07	0.03	0.07	0.03	0.01	0.08	0.03	0.04	0.06	0.02
MgO	11.04	10.56	10.52	10.79	10.56	10.39	10.36	11.06	10.64	10.14	10.46	10.61	10.76	10.90
CaO	0.06	0.09	0.10	0.10	0.05	0.05	0.05	0.05	0.07	0.08	0.09	0.07	0.11	0.04
Na2O	0.09	0.14	0.18	0.22	0.14	0.13	0.18	0.09	0.10	0.16	0.19	0.19	0.15	0.15
K2O	9.96	9.41	9.50	9.63	9.76	9.83	9.73	9.73	9.65	9.65	9.56	9.94	9.85	9.80
NiO	0.01	0.02	0.05	0.03	0.05	0.04	0.01	0.04	0.01	0.02	0.00	0.00	0.00	0.04
F	1.11	1.31	1.18	1.35	1.33	1.00	1.10	1.34	1.29	1.09	0.99	1.52	1.52	1.25
Cl	0.08	0.07	0.09	0.10	0.11	0.08	0.11	0.06	0.11	0.10	0.10	0.10	0.16	0.11
H2O(c)	3.38	3.26	3.31	3.24	3.26	3.41	3.37	3.25	3.27	3.34	3.42	3.17	3.15	3.30
O=F	0.47	0.56	0.50	0.57	0.56	0.42	0.46	0.57	0.54	0.46	0.41	0.63	0.64	0.52
O=Cl	0.02	0.02	0.02	0.02	0.03	0.02	0.03	0.01	0.03	0.02	0.02	0.02	0.03	0.02
Sum Ox%	100	100	100	100	100	100	100	100	100	100	100	100	100	100
Si	5.511	5.475	5.480	5.484	5.567	5.547	5.565	5.509	5.529	5.522	5.551	5.506	5.507	5.567
Ti	0.539	0.582	0.572	0.589	0.597	0.599	0.581	0.508	0.573	0.571	0.575	0.578	0.591	0.532
Al/Al IV	2.489	2.502	2.511	2.516	2.433	2.453	2.435	2.491	2.471	2.478	2.449	2.494	2.492	2.433
Al VI	0.077	0.000	0.000	0.008	0.058	0.032	0.075	0.025	0.031	0.008	0.051	0.055	0.000	0.100
Cr	0.001	0.002	0.004	0.006	0.005	0.000	0.003	0.002	0.000	0.006	0.002	0.000	0.004	0.003
Fe2+	2.531	2.734	2.715	2.589	2.528	2.609	2.580	2.672	2.636	2.745	2.626	2.568	2.587	2.525
Mn2+	0.006	0.007	0.012	0.011	0.009	0.004	0.009	0.004	0.001	0.011	0.004	0.005	0.008	0.003
Mg	2.516	2.423	2.414	2.467	2.406	2.373	2.364	2.533	2.432	2.330	2.387	2.424	2.462	2.480
Ca	0.010	0.016	0.017	0.017	0.008	0.009	0.008	0.008	0.012	0.013	0.016	0.011	0.018	0.006
Na	0.027	0.043	0.055	0.064	0.042	0.038	0.055	0.028	0.032	0.050	0.056	0.057	0.043	0.045
K	1.943	1.848	1.866	1.884	1.902	1.923	1.900	1.908	1.888	1.897	1.867	1.946	1.929	1.910
Ni	0.001	0.003	0.006	0.004	0.006	0.005	0.001	0.005	0.001	0.003	0.001	0.000	0.000	0.005
F	0.538	0.637	0.576	0.658	0.641	0.487	0.530	0.653	0.630	0.533	0.479	0.734	0.736	0.606
Cl	0.021	0.018	0.024	0.026	0.029	0.020	0.029	0.015	0.031	0.028	0.027	0.027	0.042	0.028
OH	3.441	3.345	3.399	3.316	3.329	3.493	3.441	3.332	3.340	3.439	3.493	3.239	3.221	3.366
Sum Cat#	19.651	19.635	19.651	19.637	19.560	19.592	19.575	19.692	19.606	19.635	19.585	19.643	19.640	19.610
XMg	0.50	0.47	0.47	0.49	0.49	0.48	0.48	0.49	0.48	0.46	0.48	0.49	0.49	0.50

Biotite Analyses by sample (recalculated to 100%), cations based on 22 (O) Oxygens.

Ultrapotassic 338z													
Label	Bt1	Bt1	Bt1	Bt1	Bt2	Bt2	Bt2	Bt3	Bt3	Bt3	Bt4	Bt4	Bt4
	R1	C1	C2	R2	R1	C1	R2	R1	C	R2	R1	C1	C2
SiO2	37.91	38.34	38.14	37.83	38.26	38.02	37.96	38.17	38.09	37.44	37.83	38.00	37.86
TiO2	3.69	3.55	3.49	3.58	3.71	3.55	3.55	3.52	3.48	3.61	3.30	3.35	3.45
Al2O3	16.52	16.42	16.48	16.45	16.37	16.41	16.71	16.39	16.44	16.64	16.66	16.68	16.44
Cr2O3	0.09	0.00	0.10	0.06	0.06	0.07	0.04	0.04	0.06	0.14	0.03	0.09	0.05
FeO	11.83	11.77	11.87	12.13	11.89	12.14	11.76	11.91	11.78	12.06	12.20	11.98	11.99
MnO	0.13	0.15	0.12	0.08	0.11	0.09	0.11	0.11	0.13	0.15	0.06	0.07	0.07
MgO	15.23	15.13	15.12	15.27	15.11	15.17	15.34	15.42	15.61	15.41	15.20	15.23	15.44
CaO	0.00	0.00	0.01	0.02	0.00	0.00	0.00	0.04	0.03	0.02	0.01	0.03	0.02
Na2O	0.12	0.15	0.14	0.15	0.09	0.13	0.13	0.11	0.12	0.12	0.12	0.10	0.10
K2O	9.95	9.91	9.95	9.92	9.95	9.88	9.86	9.80	9.74	9.90	10.08	9.97	10.06
NiO	0.00	0.04	0.06	0.01	0.00	0.04	0.03	0.00	0.02	0.04	0.00	0.01	0.01
F	1.74	1.80	1.89	1.75	1.44	1.64	1.66	1.90	1.75	1.55	1.88	1.80	1.92
Cl	0.50	0.48	0.48	0.46	0.41	0.46	0.45	0.38	0.42	0.42	0.43	0.44	0.42
H2O(c)	3.13	3.12	3.07	3.13	3.30	3.19	3.19	3.09	3.16	3.23	3.08	3.11	3.06
O=F	0.73	0.76	0.79	0.73	0.61	0.69	0.69	0.81	0.74	0.65	0.79	0.76	0.81
O=Cl	0.11	0.11	0.11	0.10	0.09	0.10	0.10	0.09	0.10	0.09	0.10	0.10	0.09
Sum Ox%	100	100	100	100	100	100	100	100	100	100	100	100	100
Si	5.565	5.620	5.598	5.560	5.608	5.585	5.565	5.595	5.581	5.507	5.564	5.577	5.565
Ti	0.408	0.391	0.385	0.396	0.409	0.392	0.391	0.388	0.384	0.399	0.365	0.370	0.381
Al/Al IV	2.435	2.380	2.402	2.440	2.392	2.415	2.435	2.405	2.419	2.493	2.436	2.423	2.435
Al VI	0.423	0.457	0.449	0.409	0.436	0.426	0.452	0.427	0.420	0.393	0.452	0.462	0.412
Cr	0.010	0.000	0.012	0.007	0.007	0.008	0.005	0.005	0.007	0.016	0.004	0.010	0.006
Fe2+	1.452	1.444	1.457	1.491	1.457	1.491	1.442	1.459	1.443	1.484	1.501	1.471	1.473
Mn2+	0.016	0.019	0.015	0.011	0.013	0.011	0.014	0.014	0.016	0.019	0.008	0.009	0.008
Mg	3.334	3.306	3.309	3.345	3.301	3.321	3.350	3.367	3.408	3.379	3.332	3.331	3.383
Ca	0.000	0.000	0.001	0.003	0.000	0.000	0.001	0.006	0.005	0.003	0.002	0.004	0.003
Na	0.035	0.043	0.040	0.042	0.025	0.037	0.038	0.033	0.035	0.035	0.034	0.027	0.028
K	1.864	1.853	1.863	1.861	1.860	1.850	1.845	1.833	1.820	1.858	1.890	1.867	1.885
Ni	0.000	0.005	0.007	0.001	0.000	0.005	0.003	0.000	0.002	0.005	0.000	0.001	0.002
F	0.806	0.836	0.878	0.812	0.668	0.766	0.768	0.881	0.812	0.724	0.874	0.837	0.893
Cl	0.124	0.118	0.119	0.115	0.103	0.115	0.112	0.096	0.106	0.105	0.108	0.110	0.105
OH	3.070	3.046	3.003	3.073	3.229	3.119	3.119	3.024	3.082	3.172	3.019	3.053	3.002
Sum Cat#	19.542	19.518	19.537	19.567	19.508	19.542	19.540	19.532	19.540	19.589	19.587	19.553	19.584
XMg	0.70	0.70	0.69	0.69	0.69	0.69	0.70	0.70	0.70	0.70	0.69	0.69	0.70

Biotite Analyses by sample (recalculated to 100%), cations based on 22 (O) Oxygens.

Ultrapotassic 338z (con't)										
Label	Bt4	Bt5	Bt5	Bt5	Bt6	Bt6	Bt6	Bt6	Bt6	Bt6
	R2	R1	C	R2	R1	C1	C2	C3	C4	R2
SiO2	38.06	38.01	38.14	38.05	37.85	37.91	37.78	37.95	37.73	37.63
TiO2	3.34	3.66	3.65	3.61	3.61	3.61	3.61	3.63	3.56	3.52
Al2O3	16.61	16.52	16.40	16.42	16.62	16.45	16.56	16.53	16.41	16.62
Cr2O3	0.04	0.04	0.10	0.04	0.07	0.03	0.11	0.02	0.06	0.06
FeO	12.00	11.96	11.82	11.87	11.96	11.99	12.02	11.78	12.30	12.12
MnO	0.10	0.12	0.11	0.09	0.06	0.15	0.09	0.13	0.10	0.12
MgO	15.29	15.13	15.24	15.31	15.18	15.39	15.26	15.34	15.38	15.23
CaO	0.02	0.00	0.01	0.00	0.02	0.01	0.00	0.02	0.00	0.00
Na2O	0.10	0.12	0.11	0.10	0.15	0.13	0.10	0.12	0.13	0.11
K2O	9.92	9.86	9.87	10.00	10.00	9.86	9.96	9.98	9.82	10.07
NiO	0.03	0.07	0.01	0.03	0.00	0.00	0.01	0.00	0.03	0.05
F	1.85	1.66	1.67	1.41	1.53	1.70	1.66	1.81	1.47	1.36
Cl	0.41	0.44	0.52	0.47	0.48	0.44	0.44	0.44	0.45	0.44
H2O(c)	3.10	3.19	3.17	3.30	3.24	3.17	3.18	3.11	3.26	3.31
O=F	0.78	0.69	0.70	0.59	0.64	0.72	0.69	0.77	0.62	0.57
O=Cl	0.09	0.10	0.12	0.11	0.11	0.10	0.10	0.10	0.10	0.10
Sum Ox%	100	100	100	100	100	100	100	100	100	100
Si	5.585	5.578	5.593	5.583	5.559	5.565	5.551	5.569	5.547	5.536
Ti	0.369	0.404	0.403	0.399	0.398	0.398	0.399	0.401	0.394	0.389
Al/Al IV	2.415	2.422	2.407	2.417	2.441	2.435	2.449	2.431	2.453	2.464
Al VI	0.457	0.436	0.429	0.423	0.436	0.410	0.419	0.427	0.392	0.419
Cr	0.005	0.005	0.011	0.005	0.008	0.004	0.013	0.002	0.007	0.007
Fe2+	1.473	1.467	1.449	1.456	1.469	1.472	1.477	1.446	1.512	1.491
Mn2+	0.013	0.015	0.014	0.011	0.007	0.018	0.011	0.016	0.013	0.015
Mg	3.343	3.311	3.332	3.348	3.322	3.367	3.342	3.355	3.371	3.341
Ca	0.004	0.000	0.002	0.000	0.003	0.002	0.000	0.003	0.000	0.000
Na	0.029	0.036	0.032	0.030	0.044	0.038	0.030	0.033	0.038	0.031
K	1.856	1.846	1.847	1.870	1.872	1.846	1.866	1.867	1.843	1.890
Ni	0.003	0.008	0.001	0.003	0.000	0.000	0.001	0.000	0.003	0.006
F	0.861	0.770	0.774	0.655	0.710	0.790	0.771	0.843	0.683	0.635
Cl	0.103	0.110	0.129	0.117	0.120	0.109	0.111	0.110	0.111	0.110
OH	3.037	3.120	3.097	3.227	3.170	3.101	3.118	3.047	3.206	3.256
Sum Cat#	19.551	19.527	19.520	19.545	19.559	19.554	19.557	19.551	19.573	19.590
XMg	0.69	0.69	0.70	0.70	0.69	0.70	0.69	0.70	0.69	0.69

Biotite Analyses by sample (recalculated to 100%), cations based on 22 (O) Oxygens.

Ultrapotassic 209-2														
Label	*Bt7	*Bt8	*Bt1	*Bt1	*Bt2	*Bt2	*Bt3	*Bt3	*Bt3	*Bt4	*Bt4	*Bt4	*Bt4	8Bt5
	C	C	R1	C	R1	C	R1	R1	C	R1	C	C2	R2	R1
SiO2	36.80	36.83	36.70	36.78	36.76	36.90	36.73	36.91	36.93	36.64	36.89	36.77	36.70	36.82
TiO2	4.27	4.82	4.79	4.85	4.95	4.92	4.73	4.73	4.80	4.79	4.69	4.74	4.67	4.62
Al2O3	14.95	14.97	15.23	15.10	14.97	15.03	15.25	15.03	14.98	15.19	15.30	15.06	15.31	14.82
Cr2O3	0.04	0.05	0.02	0.02	0.05	0.03	0.00	0.03	0.08	0.03	0.05	0.00	0.04	0.02
FeO	17.91	18.05	17.73	17.79	17.88	17.81	17.66	17.85	17.85	17.98	17.67	17.93	17.81	17.93
MnO	0.06	0.01	0.10	0.03	0.06	0.07	0.02	0.05	0.03	0.03	0.04	0.04	0.01	0.06
MgO	12.78	11.96	11.93	12.09	12.02	11.89	12.04	11.92	12.01	12.04	12.10	12.04	12.06	12.51
CaO	0.03	0.03	0.02	0.02	0.00	0.01	0.02	0.02	0.00	0.01	0.01	0.02	0.01	0.02
Na2O	0.16	0.18	0.20	0.14	0.20	0.20	0.21	0.19	0.11	0.19	0.12	0.14	0.15	0.21
K2O	8.66	8.77	8.93	8.82	8.80	8.86	9.00	8.90	8.86	8.77	8.78	8.87	8.81	8.64
NiO	0.00	0.00	0.03	0.04	0.01	0.00	0.01	0.03	0.00	0.00	0.00	0.03	0.07	0.00
F	1.48	1.52	1.48	1.47	1.15	1.26	1.55	1.34	1.48	1.56	1.39	1.57	1.70	1.68
Cl	0.36	0.36	0.34	0.35	0.36	0.34	0.39	0.36	0.38	0.34	0.38	0.38	0.36	0.37
H2O(c)	3.19	3.17	3.19	3.20	3.35	3.31	3.15	3.25	3.20	3.15	3.24	3.14	3.08	3.10
O=F	0.62	0.64	0.62	0.62	0.48	0.53	0.66	0.57	0.62	0.66	0.59	0.66	0.71	0.70
O=Cl	0.08	0.08	0.07	0.08	0.08	0.07	0.08	0.08	0.08	0.08	0.08	0.08	0.08	0.08
Sum Ox%	100	100	100	100	100	100	100	100	100	100	100	100	100	100
Si	5.534	5.543	5.523	5.530	5.531	5.548	5.526	5.553	5.555	5.515	5.539	5.536	5.519	5.539
Ti	0.482	0.545	0.542	0.549	0.560	0.557	0.535	0.536	0.542	0.542	0.529	0.536	0.528	0.523
Al/Al IV	2.466	2.457	2.477	2.470	2.469	2.452	2.474	2.447	2.445	2.485	2.461	2.464	2.481	2.461
Al VI	0.184	0.200	0.224	0.205	0.187	0.210	0.230	0.220	0.210	0.210	0.247	0.209	0.234	0.166
Cr	0.005	0.006	0.003	0.002	0.006	0.004	0.000	0.004	0.010	0.004	0.007	0.000	0.005	0.003
Fe2+	2.252	2.272	2.231	2.237	2.250	2.238	2.222	2.247	2.245	2.263	2.219	2.257	2.240	2.256
Mn2+	0.008	0.002	0.013	0.004	0.008	0.009	0.003	0.007	0.004	0.004	0.005	0.006	0.001	0.007
Mg	2.864	2.682	2.676	2.709	2.694	2.666	2.700	2.675	2.692	2.700	2.708	2.703	2.704	2.805
Ca	0.006	0.005	0.003	0.003	0.001	0.001	0.003	0.003	0.000	0.002	0.002	0.004	0.002	0.003
Na	0.045	0.052	0.058	0.044	0.057	0.056	0.060	0.054	0.033	0.054	0.035	0.043	0.045	0.060
K	1.662	1.684	1.714	1.691	1.689	1.698	1.727	1.708	1.701	1.683	1.681	1.703	1.691	1.659
Ni	0.000	0.000	0.004	0.005	0.001	0.000	0.001	0.004	0.000	0.000	0.000	0.004	0.009	0.000
F	0.704	0.724	0.709	0.701	0.550	0.599	0.740	0.637	0.700	0.743	0.661	0.744	0.808	0.795
Cl	0.093	0.092	0.087	0.090	0.092	0.086	0.098	0.093	0.097	0.088	0.097	0.097	0.092	0.094
OH	3.204	3.184	3.204	3.209	3.358	3.314	3.162	3.270	3.203	3.170	3.242	3.159	3.100	3.110
Sum Cat#	19.510	19.449	19.469	19.449	19.451	19.440	19.481	19.457	19.437	19.462	19.433	19.464	19.460	19.482
XMg	0.56	0.54	0.55	0.55	0.55	0.54	0.55	0.54	0.55	0.54	0.55	0.55	0.55	0.55

Biotite Analyses by sample (recalculated to 100%), cations based on 22 (O) Oxygens.

Ultrapotassic 209-2 (Con't)								Ultrapotassic 361z											
Label	*Bt5 C	*Bt5 C2	*Bt5 C3	*Bt5 C4	*Bt5 R2	*Bt6 C	*Bt6 R	Label	Bt1 R1	Bt1 C	Bt1 R2	Bt2 R1	Bt2 C	Bt2 C2	Bt2 R2	Bt3 R1	Bt3 C	Bt3 R2	Bt4 R1
SiO2	36.75	36.77	37.09	37.02	36.85	36.94	36.49	SiO2	36.95	36.89	36.73	37.03	37.11	36.97	36.96	37.14	37.06	36.85	36.98
TiO2	4.88	4.92	4.78	4.84	4.81	4.77	4.74	TiO2	4.36	4.38	4.58	5.18	5.15	5.15	5.16	5.23	5.32	5.27	5.13
Al2O3	14.96	15.01	14.79	14.83	15.05	15.06	15.20	Al2O3	14.76	14.78	14.63	14.21	14.34	14.38	14.24	14.07	14.16	14.12	14.32
Cr2O3	0.04	0.02	0.04	0.00	0.02	0.01	0.06	Cr2O3	0.11	0.09	0.11	0.07	0.08	0.06	0.11	0.06	0.08	0.05	0.06
FeO	17.72	17.75	17.51	17.67	17.65	17.43	17.72	FeO	18.53	18.19	18.66	17.31	17.25	17.38	17.47	17.64	17.42	17.79	17.59
MnO	0.10	0.05	0.09	0.02	0.02	0.05	0.05	MnO	0.09	0.10	0.11	0.13	0.11	0.11	0.15	0.17	0.13	0.12	0.14
MgO	12.20	12.03	12.23	12.19	12.19	12.29	12.32	MgO	11.19	11.34	11.25	11.94	11.97	11.80	11.86	11.69	11.70	11.74	11.75
CaO	0.00	0.02	0.01	0.00	0.01	0.03	0.02	CaO	0.00	0.00	0.00	0.02	0.00	0.00	0.00	0.00	0.01	0.02	0.03
Na2O	0.14	0.16	0.13	0.16	0.17	0.14	0.15	Na2O	0.09	0.07	0.12	0.15	0.06	0.11	0.09	0.09	0.13	0.09	0.13
K2O	8.89	8.96	8.96	8.96	8.87	8.90	8.97	K2O	9.68	9.89	9.60	9.71	9.65	9.79	9.69	9.71	9.65	9.69	9.64
NiO	0.00	0.00	0.03	0.00	0.02	0.04	0.00	NiO	0.00	0.01	0.00	0.00	0.01	0.00	0.01	0.02	0.04	0.04	0.01
F	1.35	1.47	1.34	1.35	1.86	1.42	1.09	F	0.98	1.24	1.10	1.00	1.20	1.01	1.03	0.84	1.49	1.04	1.10
Cl	0.34	0.34	0.36	0.34	0.33	0.37	0.34	Cl	0.34	0.32	0.28	0.28	0.32	0.29	0.33	0.28	0.33	0.30	0.30
H2O(c)	3.26	3.20	3.26	3.26	3.02	3.23	3.38	H2O(c)	3.41	3.29	3.37	3.43	3.33	3.42	3.40	3.50	3.18	3.40	3.38
O=F	0.57	0.62	0.56	0.57	0.78	0.60	0.46	O=F	0.41	0.53	0.46	0.43	0.50	0.43	0.43	0.36	0.63	0.44	0.46
O=Cl	0.07	0.08	0.08	0.07	0.07	0.08	0.07	O=Cl	0.08	0.07	0.06	0.06	0.07	0.07	0.08	0.06	0.08	0.07	0.07
Sum Ox%	100	100	100	100	100	100	100	Sum Ox%	100	100	100	100	100	100	100	100	100	100	100
Si	5.529	5.533	5.574	5.565	5.540	5.547	5.492	Si	5.598	5.590	5.571	5.586	5.592	5.581	5.582	5.609	5.596	5.573	5.584
Ti	0.552	0.557	0.540	0.547	0.544	0.538	0.536	Ti	0.496	0.499	0.522	0.588	0.583	0.584	0.586	0.594	0.605	0.599	0.583
Al/Al IV	2.471	2.467	2.426	2.435	2.460	2.453	2.508	Al/Al IV	2.402	2.410	2.429	2.414	2.408	2.419	2.418	2.391	2.404	2.427	2.416
Al VI	0.182	0.195	0.194	0.192	0.205	0.212	0.189	Al VI	0.235	0.229	0.186	0.113	0.139	0.138	0.116	0.113	0.116	0.091	0.132
Cr	0.005	0.002	0.004	0.000	0.002	0.001	0.007	Cr	0.013	0.010	0.013	0.009	0.010	0.008	0.013	0.007	0.010	0.006	0.007
Fe2+	2.229	2.233	2.200	2.221	2.219	2.189	2.231	Fe2+	2.349	2.306	2.367	2.185	2.175	2.194	2.206	2.227	2.199	2.250	2.221
Mn2+	0.013	0.007	0.012	0.003	0.002	0.007	0.007	Mn2+	0.012	0.013	0.014	0.016	0.013	0.015	0.020	0.022	0.016	0.015	0.018
Mg	2.736	2.699	2.739	2.730	2.732	2.752	2.764	Mg	2.528	2.563	2.544	2.686	2.690	2.656	2.670	2.630	2.632	2.647	2.643
Ca	0.000	0.003	0.002	0.000	0.001	0.005	0.002	Ca	0.000	0.000	0.000	0.003	0.000	0.000	0.000	0.000	0.002	0.003	0.005
Na	0.041	0.045	0.038	0.045	0.049	0.043	0.044	Na	0.028	0.020	0.034	0.044	0.017	0.032	0.027	0.025	0.039	0.026	0.037
K	1.706	1.721	1.719	1.718	1.702	1.705	1.723	K	1.871	1.911	1.857	1.869	1.854	1.886	1.866	1.870	1.860	1.871	1.857
Ni	0.000	0.000	0.003	0.000	0.002	0.004	0.000	Ni	0.000	0.001	0.000	0.001	0.001	0.000	0.001	0.002	0.004	0.005	0.001
F	0.640	0.698	0.635	0.639	0.887	0.675	0.519	F	0.469	0.595	0.523	0.480	0.570	0.483	0.490	0.404	0.712	0.496	0.526
Cl	0.087	0.088	0.092	0.086	0.083	0.096	0.087	Cl	0.087	0.084	0.071	0.071	0.081	0.075	0.085	0.071	0.086	0.076	0.077
OH	3.272	3.214	3.272	3.275	3.030	3.230	3.394	OH	3.444	3.321	3.405	3.449	3.350	3.442	3.425	3.525	3.203	3.428	3.398
Sum Cat#	19.464	19.461	19.452	19.456	19.459	19.456	19.503	Sum Cat#	19.530	19.552	19.538	19.515	19.482	19.511	19.505	19.490	19.483	19.514	19.503
XMg	0.55	0.55	0.56	0.55	0.55	0.56	0.55	XMg	0.52	0.53	0.52	0.55	0.55	0.55	0.55	0.54	0.55	0.54	0.54

Biotite Analyses by sample (recalculated to 100%), cations based on 22 (O) Oxygens.

Ultrapotassic 361z (Con't)								Ultrapotassic 404											
Label	Bt4 C	Bt4 R2	Bt5 R1	Bt5 C	Bt5 R2	Bt6 C	Bt6 R	Label	Bt1 R1	Bt1 C	Bt1 R2	Bt2 R	Bt2 C	Bt3 R1	Bt3 C	Bt3 R2	Bt4 R	Bt4 C	Bt5 C
SiO2	37.04	36.83	36.99	37.01	36.97	36.87	36.99	SiO2	37.77	38.18	38.05	38.35	37.98	38.15	37.90	38.06	38.00	37.77	37.95
TiO2	5.32	5.10	4.90	4.95	4.94	4.69	4.70	TiO2	4.38	4.19	4.37	4.04	4.06	4.23	4.26	4.14	4.12	4.16	4.38
Al2O3	14.31	14.22	14.36	14.29	14.25	14.25	14.32	Al2O3	14.70	14.53	14.26	14.67	14.54	14.88	14.80	14.76	14.81	14.71	14.57
Cr2O3	0.05	0.10	0.07	0.10	0.09	0.05	0.04	Cr2O3	0.02	0.00	0.06	0.01	0.07	0.08	0.05	0.08	0.04	0.06	0.04
FeO	17.41	17.84	17.59	17.61	17.96	18.46	18.56	FeO	15.51	15.33	15.54	15.11	15.39	14.79	14.85	15.06	15.30	15.49	15.50
MnO	0.11	0.15	0.22	0.17	0.15	0.15	0.13	MnO	0.06	0.08	0.07	0.11	0.07	0.03	0.09	0.08	0.12	0.07	0.07
MgO	11.70	11.66	11.82	11.67	11.61	11.33	11.30	MgO	13.83	13.99	13.87	14.03	14.10	13.90	14.14	13.91	13.81	13.83	13.79
CaO	0.03	0.03	0.02	0.00	0.01	0.00	0.01	CaO	0.04	0.02	0.05	0.01	0.01	0.06	0.01	0.03	0.04	0.02	0.00
Na2O	0.10	0.13	0.06	0.06	0.09	0.09	0.08	Na2O	0.24	0.16	0.17	0.15	0.15	0.15	0.16	0.16	0.14	0.12	0.14
K2O	9.69	9.69	9.70	9.82	9.67	9.83	9.68	K2O	9.14	9.21	9.27	9.16	9.32	9.34	9.44	9.41	9.32	9.49	9.29
NiO	0.00	0.00	0.02	0.05	0.06	0.04	0.00	NiO	0.00	0.01	0.00	0.03	0.00	0.02	0.00	0.00	0.00	0.00	0.00
F	1.02	1.29	1.23	1.39	0.86	1.34	0.83	F	1.47	1.47	1.31	1.45	1.51	1.55	1.23	1.33	1.28	1.20	1.34
Cl	0.29	0.28	0.29	0.31	0.29	0.31	0.27	Cl	0.23	0.21	0.28	0.23	0.23	0.25	0.24	0.25	0.25	0.25	0.18
H2O(c)	3.41	3.28	3.31	3.23	3.49	3.23	3.49	H2O(c)	3.27	3.29	3.33	3.29	3.26	3.25	3.39	3.35	3.37	3.39	3.35
O=F	0.43	0.54	0.52	0.58	0.36	0.56	0.35	O=F	0.62	0.62	0.55	0.61	0.63	0.65	0.52	0.56	0.53	0.51	0.56
O=Cl	0.07	0.06	0.07	0.07	0.07	0.07	0.06	O=Cl	0.05	0.05	0.06	0.05	0.05	0.06	0.05	0.06	0.06	0.06	0.04
Sum Ox%	100	100	100	100	100	100	100	Sum Ox%	100	100	100	100	100	100	100	100	100	100	100
Si	5.588	5.574	5.589	5.597	5.593	5.598	5.607	Si	5.619	5.669	5.665	5.686	5.650	5.656	5.625	5.654	5.648	5.626	5.643
Ti	0.603	0.581	0.557	0.563	0.562	0.536	0.536	Ti	0.490	0.469	0.489	0.451	0.454	0.472	0.476	0.463	0.460	0.466	0.490
Al/Al IV	2.412	2.426	2.411	2.403	2.407	2.402	2.393	Al/Al IV	2.381	2.331	2.335	2.314	2.350	2.344	2.375	2.346	2.352	2.374	2.357
Al VI	0.132	0.110	0.146	0.144	0.134	0.149	0.166	Al VI	0.195	0.212	0.167	0.248	0.199	0.257	0.214	0.238	0.242	0.207	0.197
Cr	0.006	0.012	0.008	0.012	0.011	0.005	0.005	Cr	0.002	0.000	0.007	0.002	0.008	0.010	0.006	0.009	0.005	0.007	0.005
Fe2+	2.196	2.259	2.222	2.227	2.272	2.344	2.351	Fe2+	1.930	1.903	1.934	1.873	1.915	1.834	1.844	1.871	1.902	1.930	1.928
Mn2+	0.015	0.019	0.028	0.021	0.019	0.019	0.016	Mn2+	0.008	0.010	0.009	0.014	0.009	0.004	0.011	0.010	0.015	0.009	0.008
Mg	2.630	2.631	2.661	2.631	2.617	2.564	2.553	Mg	3.068	3.097	3.076	3.100	3.126	3.071	3.130	3.079	3.059	3.072	3.057
Ca	0.005	0.004	0.003	0.000	0.002	0.000	0.002	Ca	0.007	0.003	0.007	0.001	0.001	0.010	0.002	0.005	0.006	0.003	0.001
Na	0.030	0.039	0.017	0.019	0.026	0.025	0.023	Na	0.071	0.048	0.048	0.045	0.043	0.045	0.045	0.045	0.041	0.035	0.041
K	1.865	1.871	1.870	1.894	1.867	1.905	1.872	K	1.735	1.745	1.760	1.733	1.770	1.766	1.788	1.782	1.767	1.803	1.762
Ni	0.000	0.000	0.003	0.006	0.007	0.005	0.000	Ni	0.000	0.001	0.000	0.004	0.000	0.003	0.000	0.000	0.000	0.000	0.000
F	0.488	0.616	0.589	0.665	0.409	0.643	0.400	F	0.692	0.690	0.615	0.680	0.708	0.724	0.577	0.625	0.600	0.566	0.627
Cl	0.075	0.070	0.075	0.078	0.074	0.080	0.070	Cl	0.058	0.053	0.071	0.057	0.059	0.064	0.060	0.064	0.064	0.064	0.046
OH	3.437	3.314	3.336	3.256	3.517	3.277	3.530	OH	3.250	3.256	3.314	3.262	3.233	3.212	3.363	3.311	3.336	3.370	3.327
Sum Cat#	19.482	19.526	19.515	19.517	19.516	19.552	19.523	Sum Cat#	19.505	19.487	19.496	19.470	19.524	19.472	19.517	19.501	19.497	19.533	19.488
XMg	0.55	0.54	0.55	0.54	0.54	0.52	0.52	XMg	0.61	0.62	0.61	0.62	0.62	0.63	0.63	0.62	0.62	0.61	0.61

Biotite Analyses by sample (recalculated to 100%), cations based on 22 (O) Oxygens.

Ultrapotassic 404 (Con't)								Ultrapotassic 408											
Label	Bt5 C	Bt5 R	Bt5 R	Bt6 R	Bt6 C	Bt7 R	Bt7 C	Label	Bt1 R	Bt1 C	Bt2 R	Bt2 C	Bt1 R2	Bt3 C	Bt3 R1	Bt4 R	Bt4 C	Bt5 R	Bt5 C
SiO2	37.73	37.68	37.66	37.99	37.63	37.84	37.99	SiO2	36.73	36.63	37.01	37.35	36.52	36.20	36.20	36.47	36.25	36.13	36.83
TiO2	4.36	4.43	4.30	4.26	4.24	4.27	4.30	TiO2	4.26	4.32	4.09	3.90	4.25	4.55	4.67	4.51	4.57	4.31	4.24
Al2O3	14.52	14.58	14.57	14.40	14.43	14.40	14.49	Al2O3	14.98	14.94	15.01	15.42	15.04	14.69	14.72	14.65	14.69	14.82	14.91
Cr2O3	0.07	0.05	0.08	0.03	0.06	0.05	0.04	Cr2O3	0.05	0.07	0.00	0.03	0.00	0.05	0.02	0.03	0.05	0.03	0.00
FeO	15.76	15.65	15.54	15.44	15.56	15.46	15.39	FeO	19.07	19.02	19.14	18.67	19.57	20.04	19.71	19.61	19.75	19.96	19.47
MnO	0.05	0.09	0.10	0.08	0.09	0.07	0.09	MnO	0.06	0.13	0.08	0.07	0.10	0.06	0.05	0.08	0.09	0.10	0.07
MgO	13.82	13.80	13.92	13.82	13.98	13.89	13.83	MgO	11.20	11.31	11.32	11.85	11.21	10.84	10.96	11.03	11.12	11.21	11.06
CaO	0.00	0.00	0.01	0.05	0.06	0.04	0.02	CaO	0.03	0.02	0.04	0.14	0.05	0.03	0.05	0.02	0.03	0.06	0.04
Na2O	0.11	0.09	0.15	0.15	0.20	0.17	0.16	Na2O	0.13	0.14	0.11	0.10	0.15	0.14	0.12	0.12	0.10	0.16	0.13
K2O	9.27	9.33	9.38	9.52	9.46	9.52	9.33	K2O	9.36	9.33	9.04	8.25	9.01	9.32	9.38	9.37	9.24	9.11	9.11
NiO	0.01	0.01	0.03	0.02	0.00	0.00	0.02	NiO	0.02	0.00	0.00	0.04	0.01	0.00	0.01	0.00	0.03	0.01	0.00
F	1.49	1.29	1.29	1.35	1.53	1.46	1.57	F	0.73	0.60	0.81	0.74	0.58	0.67	0.83	0.69	0.63	0.63	0.86
Cl	0.21	0.23	0.18	0.19	0.22	0.24	0.26	Cl	0.15	0.14	0.19	0.18	0.16	0.14	0.14	0.15	0.15	0.16	0.14
H2O(c)	3.27	3.35	3.36	3.34	3.24	3.26	3.22	H2O(c)	3.57	3.63	3.54	3.60	3.64	3.59	3.51	3.57	3.61	3.60	3.52
O=F	0.63	0.55	0.54	0.57	0.65	0.61	0.66	O=F	0.31	0.25	0.34	0.31	0.24	0.28	0.36	0.29	0.27	0.26	0.36
O=Cl	0.05	0.05	0.04	0.04	0.05	0.05	0.06	O=Cl	0.03	0.03	0.04	0.04	0.04	0.03	0.03	0.03	0.03	0.04	0.03
Sum Ox%	100	100	100	100	100	100	100	Sum Ox%	100	100	100	100	100	100	100	100	100	100	100
Si	5.623	5.615	5.612	5.658	5.616	5.641	5.654	Si	5.563	5.549	5.594	5.599	5.537	5.517	5.511	5.546	5.514	5.501	5.579
Ti	0.489	0.496	0.482	0.477	0.476	0.479	0.481	Ti	0.484	0.491	0.465	0.440	0.484	0.521	0.535	0.516	0.523	0.494	0.483
Al/Al IV	2.377	2.385	2.388	2.342	2.384	2.359	2.346	Al/Al IV	2.437	2.451	2.406	2.401	2.463	2.483	2.489	2.454	2.486	2.499	2.421
Al VI	0.173	0.176	0.171	0.184	0.153	0.171	0.195	Al VI	0.238	0.217	0.266	0.324	0.224	0.156	0.153	0.171	0.149	0.160	0.241
Cr	0.008	0.006	0.009	0.004	0.007	0.006	0.005	Cr	0.006	0.008	0.000	0.004	0.000	0.006	0.003	0.004	0.006	0.004	0.000
Fe2+	1.964	1.950	1.936	1.922	1.942	1.927	1.916	Fe2+	2.416	2.409	2.419	2.340	2.481	2.555	2.509	2.494	2.512	2.540	2.468
Mn2+	0.007	0.011	0.013	0.010	0.011	0.008	0.011	Mn2+	0.008	0.017	0.010	0.009	0.013	0.008	0.006	0.010	0.012	0.013	0.010
Mg	3.069	3.065	3.092	3.068	3.108	3.085	3.068	Mg	2.528	2.553	2.550	2.647	2.532	2.462	2.487	2.499	2.521	2.543	2.497
Ca	0.000	0.001	0.001	0.007	0.010	0.006	0.003	Ca	0.006	0.004	0.006	0.023	0.008	0.004	0.009	0.003	0.005	0.010	0.007
Na	0.033	0.026	0.045	0.043	0.058	0.048	0.047	Na	0.040	0.041	0.032	0.031	0.045	0.042	0.037	0.036	0.029	0.047	0.039
K	1.761	1.773	1.784	1.808	1.800	1.811	1.771	K	1.808	1.803	1.744	1.579	1.742	1.814	1.821	1.818	1.795	1.770	1.761
Ni	0.001	0.001	0.004	0.002	0.000	0.000	0.003	Ni	0.003	0.000	0.000	0.005	0.001	0.000	0.001	0.000	0.003	0.001	0.000
F	0.702	0.609	0.609	0.635	0.722	0.689	0.738	F	0.352	0.288	0.385	0.353	0.276	0.320	0.404	0.336	0.305	0.302	0.410
Cl	0.055	0.059	0.047	0.048	0.057	0.062	0.066	Cl	0.040	0.037	0.050	0.045	0.043	0.036	0.035	0.040	0.038	0.042	0.037
OH	3.243	3.332	3.344	3.316	3.220	3.250	3.196	OH	3.608	3.675	3.566	3.603	3.681	3.644	3.561	3.624	3.657	3.656	3.553
Sum Cat#	19.506	19.505	19.537	19.525	19.565	19.542	19.501	Sum Cat#	19.536	19.544	19.493	19.401	19.530	19.568	19.560	19.550	19.555	19.582	19.507
XMg	0.61	0.61	0.62	0.62	0.62	0.62	0.62	XMg	0.51	0.52	0.51	0.53	0.51	0.49	0.50	0.50	0.50	0.50	0.50

Biotite Analyses by sample (recalculated to 100%), cations based on 22 (O) Oxygens.

Ultrapotassic 398a																		
Label	Bt1	Bt1	Bt1	Bt2	Bt2	Bt2	Bt3	Bt3	Bt4	Bt4	Bt5	Bt5	Bt6	Bt6	Bt6	Bt7	Bt7	Bt7
	R1	C	R2	R1	C	R2	R	C	R	C	R	C	R1	C	R2	R1	C	R2
SiO2	38.07	38.24	38.09	38.23	38.09	37.91	37.95	37.87	38.08	38.23	38.03	38.13	38.18	37.94	38.22	37.97	37.98	38.15
TiO2	3.70	3.69	3.66	3.86	3.77	3.82	3.73	3.78	3.68	3.76	3.72	3.77	3.62	3.70	3.77	3.95	3.93	3.96
Al2O3	14.53	14.41	14.29	14.37	14.51	14.51	14.45	14.53	14.69	14.42	14.47	14.39	14.50	14.46	14.35	14.38	14.40	14.40
Cr2O3	0.13	0.12	0.10	0.13	0.17	0.17	0.13	0.17	0.14	0.19	0.15	0.12	0.16	0.15	0.15	0.16	0.18	0.18
FeO	14.26	14.11	14.51	14.25	14.04	14.22	14.45	14.29	14.13	14.30	14.39	14.07	14.21	14.44	14.29	14.33	14.37	14.15
MnO	0.10	0.12	0.14	0.08	0.12	0.13	0.13	0.13	0.13	0.11	0.08	0.11	0.08	0.13	0.14	0.11	0.13	0.13
MgO	15.06	15.13	15.12	15.06	15.16	15.18	15.25	15.12	15.16	14.96	15.02	15.12	15.10	15.11	14.83	15.09	14.89	14.96
CaO	0.01	0.02	0.03	0.02	0.01	0.01	0.02	0.03	0.00	0.00	0.05	0.08	0.00	0.00	0.00	0.02	0.04	0.00
Na2O	0.18	0.17	0.17	0.17	0.20	0.17	0.16	0.19	0.15	0.14	0.14	0.15	0.17	0.20	0.13	0.18	0.18	0.18
K2O	9.64	9.63	9.61	9.46	9.61	9.57	9.41	9.59	9.55	9.59	9.63	9.76	9.70	9.60	9.81	9.52	9.64	9.58
NiO	0.03	0.06	0.04	0.08	0.02	0.01	0.01	0.04	0.00	0.04	0.02	0.00	0.00	0.03	0.03	0.01	0.03	0.02
F	1.58	1.62	1.33	1.65	1.78	1.44	1.61	1.28	1.64	1.51	1.72	1.74	1.54	1.41	1.52	1.44	1.40	1.46
Cl	0.15	0.13	0.11	0.13	0.12	0.17	0.13	0.13	0.12	0.11	0.15	0.15	0.14	0.11	0.14	0.14	0.11	0.16
H2O(c)	3.26	3.24	3.38	3.24	3.18	3.32	3.25	3.40	3.24	3.31	3.19	3.18	3.28	3.34	3.28	3.33	3.35	3.32
O=F	0.67	0.69	0.56	0.70	0.75	0.61	0.67	0.53	0.69	0.64	0.72	0.73	0.65	0.59	0.64	0.60	0.58	0.61
O=Cl	0.03	0.03	0.02	0.03	0.03	0.04	0.03	0.03	0.03	0.02	0.03	0.03	0.03	0.03	0.03	0.03	0.02	0.04
Sum Ox%	100	100	100	100	100	100	100	100	100	100	100	100	100	100	100	100	100	100
Si	5.646	5.666	5.654	5.662	5.643	5.622	5.628	5.618	5.639	5.665	5.644	5.654	5.659	5.630	5.671	5.631	5.636	5.652
Ti	0.412	0.411	0.409	0.430	0.420	0.427	0.417	0.423	0.409	0.419	0.414	0.421	0.403	0.413	0.421	0.441	0.438	0.441
Al/Al IV	2.354	2.334	2.346	2.338	2.357	2.378	2.372	2.382	2.361	2.335	2.356	2.346	2.341	2.370	2.329	2.369	2.364	2.348
Al VI	0.185	0.183	0.155	0.171	0.177	0.157	0.154	0.157	0.202	0.183	0.175	0.169	0.191	0.160	0.181	0.144	0.155	0.167
Cr	0.015	0.014	0.012	0.015	0.020	0.021	0.016	0.020	0.016	0.023	0.017	0.015	0.020	0.018	0.018	0.019	0.022	0.021
Fe2+	1.769	1.748	1.801	1.764	1.739	1.764	1.792	1.773	1.748	1.771	1.786	1.745	1.761	1.792	1.774	1.778	1.784	1.754
Mn2+	0.013	0.016	0.018	0.010	0.015	0.016	0.017	0.016	0.017	0.014	0.011	0.014	0.011	0.016	0.018	0.013	0.016	0.016
Mg	3.328	3.342	3.344	3.323	3.348	3.355	3.370	3.345	3.345	3.304	3.323	3.340	3.336	3.343	3.281	3.336	3.294	3.305
Ca	0.002	0.003	0.005	0.003	0.002	0.002	0.004	0.005	0.000	0.000	0.008	0.013	0.000	0.000	0.000	0.003	0.006	0.000
Na	0.053	0.050	0.046	0.050	0.058	0.050	0.048	0.056	0.044	0.039	0.040	0.044	0.049	0.060	0.039	0.052	0.051	0.051
K	1.824	1.820	1.819	1.788	1.815	1.810	1.781	1.816	1.804	1.813	1.823	1.845	1.832	1.817	1.857	1.802	1.824	1.811
Ni	0.004	0.008	0.006	0.010	0.002	0.002	0.001	0.005	0.000	0.005	0.002	0.000	0.000	0.003	0.003	0.001	0.003	0.002
F	0.740	0.762	0.625	0.773	0.833	0.675	0.753	0.599	0.768	0.709	0.806	0.813	0.720	0.660	0.713	0.673	0.655	0.683
Cl	0.037	0.034	0.028	0.032	0.032	0.043	0.033	0.034	0.031	0.027	0.037	0.037	0.035	0.029	0.037	0.035	0.028	0.042
OH	3.222	3.204	3.347	3.196	3.136	3.282	3.213	3.367	3.201	3.264	3.157	3.149	3.244	3.311	3.250	3.291	3.317	3.275
Sum Cat#	19.604	19.593	19.613	19.565	19.597	19.604	19.599	19.615	19.586	19.572	19.599	19.605	19.603	19.622	19.591	19.589	19.593	19.569
XMg	0.65	0.66	0.65	0.65	0.66	0.66	0.65	0.65	0.66	0.65	0.65	0.66	0.66	0.65	0.65	0.65	0.65	0.65

Biotite Analyses by sample (recalculated to 100%), cations based on 22 (O) Oxygens.

Ultrapotassic 403											
Label	Bt1 C	Bt1 R	Bt2 C	Bt2 R	Bt3 C	Bt3 R	Bt4 C	Bt4 R	Bt5 C	Bt5 R	Bt3 R
SiO2	40.23	41.03	41.45	41.05	40.60	39.88	40.90	40.23	40.42	40.93	42.11
TiO2	2.62	2.12	1.91	2.42	2.66	2.95	2.49	2.73	2.73	2.52	2.12
Al2O3	12.44	12.37	12.37	12.02	12.11	12.02	11.64	12.19	11.66	11.71	11.73
Cr2O3	0.12	0.11	0.07	0.04	0.05	0.06	0.08	0.07	0.06	0.06	0.10
FeO	10.47	10.10	9.81	9.89	10.37	10.54	9.77	10.24	10.15	9.71	9.59
MnO	0.16	0.04	0.00	0.16	0.18	0.34	0.20	0.13	0.29	0.15	0.04
MgO	19.07	19.50	19.83	19.61	19.10	19.13	19.86	19.37	19.64	19.84	19.77
CaO	0.00	0.03	0.02	0.01	0.02	0.02	0.03	0.04	0.01	0.03	0.02
Na2O	0.05	0.10	0.07	0.02	0.07	0.08	0.07	0.03	0.05	0.08	0.05
K2O	10.29	9.95	9.89	10.15	10.33	10.42	10.28	10.36	10.46	10.34	9.88
NiO	0.02	0.09	0.04	0.07	0.02	0.06	0.17	0.07	0.04	0.10	0.00
F	3.50	3.67	3.23	3.56	3.43	3.36	3.55	3.65	3.49	3.43	3.65
Cl	0.08	0.12	0.13	0.13	0.10	0.10	0.07	0.12	0.12	0.11	0.12
H2O(c)	2.43	2.36	2.58	2.40	2.46	2.47	2.41	2.34	2.42	2.46	2.38
O=F	1.47	1.54	1.36	1.50	1.44	1.42	1.50	1.54	1.47	1.45	1.54
O=Cl	0.02	0.03	0.03	0.03	0.02	0.02	0.02	0.03	0.03	0.02	0.03
Sum Ox%	100	100	100	100	100	100	100	100	100	100	100
Si	5.882	5.964	6.003	5.971	5.930	5.852	5.961	5.882	5.914	5.961	6.088
Ti	0.288	0.233	0.207	0.266	0.292	0.326	0.273	0.299	0.299	0.276	0.230
Al/Al IV	2.118	2.036	1.997	2.029	2.070	2.077	1.999	2.100	2.010	2.012	1.912
Al VI	0.025	0.083	0.114	0.031	0.014	0.000	0.000	0.000	0.000	0.000	0.089
Cr	0.013	0.013	0.008	0.005	0.006	0.007	0.009	0.008	0.007	0.007	0.011
Fe2+	1.280	1.227	1.188	1.204	1.266	1.294	1.191	1.253	1.242	1.182	1.159
Mn2+	0.020	0.005	0.000	0.019	0.022	0.042	0.025	0.016	0.035	0.018	0.005
Mg	4.155	4.225	4.280	4.252	4.157	4.184	4.314	4.221	4.282	4.309	4.260
Ca	0.001	0.005	0.003	0.002	0.003	0.004	0.004	0.006	0.002	0.004	0.004
Na	0.016	0.027	0.021	0.005	0.020	0.022	0.019	0.009	0.014	0.023	0.014
K	1.920	1.845	1.827	1.882	1.924	1.951	1.911	1.933	1.951	1.920	1.822
Ni	0.002	0.010	0.005	0.008	0.002	0.007	0.020	0.008	0.005	0.012	0.000
F	1.617	1.686	1.477	1.638	1.585	1.558	1.636	1.689	1.615	1.580	1.673
Cl	0.019	0.030	0.033	0.033	0.024	0.025	0.019	0.029	0.030	0.026	0.030
OH	2.364	2.284	2.490	2.330	2.391	2.416	2.346	2.282	2.355	2.394	2.297
Sum Cat#	19.720	19.674	19.654	19.674	19.705	19.766	19.727	19.736	19.761	19.725	19.594
XMg	0.77	0.78	0.78	0.78	0.77	0.76	0.78	0.77	0.78	0.79	0.79

Feldspar Analyses by sample (recalculated to 100%), cations based on 8(O) Oxygens.

Terrane/Sample	GT 2000x										
Label	PI1 C	PI1 R	PI2 C	PI2 R	PI3 R	PI4 R	PI4 C	PI6 R	PI7 C	PI7 R	PI5 R
SiO2	58.39	60.63	58.37	58.69	58.61	58.77	59.03	59.27	58.96	59.12	59.01
Al2O3	26.35	25.06	26.73	26.24	26.38	26.20	26.07	25.97	26.06	25.76	26.00
Fe2O3	0.05	0.04	0.00	0.06	0.00	0.08	0.03	0.03	0.05	0.10	0.10
CaO	7.26	6.34	7.40	7.59	7.28	7.19	7.19	7.04	7.30	7.44	7.46
Na2O	7.69	7.74	7.30	7.22	7.49	7.56	7.46	7.56	7.41	7.40	7.23
K2O	0.25	0.19	0.19	0.20	0.23	0.19	0.22	0.13	0.22	0.19	0.19
Sum Ox%	100	100	100	100	100	100	100	100	100	100	100
Si	2.612	2.694	2.607	2.621	2.618	2.625	2.634	2.643	2.632	2.640	2.634
Al/Al IV	1.390	1.312	1.407	1.382	1.389	1.379	1.371	1.364	1.371	1.356	1.368
Al VI	0.000	0.000	0.000	0.000	0.000	0.000	0.000	0.000	0.000	0.000	0.000
Fe3+	0.002	0.001	0.000	0.002	0.000	0.003	0.001	0.001	0.002	0.003	0.003
Ca	0.348	0.302	0.354	0.363	0.349	0.344	0.344	0.336	0.349	0.356	0.357
Na	0.666	0.667	0.632	0.625	0.649	0.655	0.646	0.654	0.642	0.640	0.626
K	0.014	0.010	0.011	0.012	0.013	0.011	0.012	0.007	0.013	0.011	0.011
Sum Cat#	5.03	4.99	5.01	5.01	5.02	5.02	5.01	5.01	5.01	5.01	5.00
Ab	64.8	68.1	63.4	62.5	64.2	64.9	64.4	65.6	63.9	63.6	63.0
An	33.9	30.8	35.5	36.3	34.5	34.0	34.3	33.7	34.8	35.3	35.9
Or	1.4	1.1	1.1	1.2	1.3	1.1	1.2	0.7	1.3	1.1	1.1

Feldspar Analyses by sample (recalculated to 100%), cations based on 8(O) Oxygens.

GT 288d1												
Label	Pl1	Pl1	Pl1	Pl1	Pl2	Pl3	Pl3	Pl4	Pl4	Pl5	Pl6	Pl6
	C	C	R	C	R	C	C	C	R	C	C	R
SiO2	59.97	59.87	60.25	60.33	59.70	59.91	60.10	59.69	60.01	60.05	60.28	60.07
Al2O3	25.31	25.28	25.02	24.99	25.33	25.12	25.01	25.39	25.24	25.19	25.19	25.02
Fe2O3	0.03	0.05	0.05	0.05	0.10	0.15	0.09	0.06	0.08	0.05	0.00	0.13
CaO	6.77	6.93	6.66	6.54	7.00	7.02	6.68	6.95	6.75	6.92	6.80	6.76
Na2O	7.83	7.71	7.88	7.87	7.75	7.64	7.96	7.74	7.73	7.66	7.59	7.88
K2O	0.09	0.16	0.14	0.21	0.11	0.16	0.16	0.18	0.18	0.12	0.14	0.12
Sum Ox%	100	100	100	100	100	100	100	100	100	100	100	100
Si	2.671	2.668	2.683	2.686	2.662	2.671	2.679	2.662	2.673	2.675	2.682	2.677
Al/Al IV	1.328	1.328	1.313	1.311	1.332	1.320	1.314	1.335	1.325	1.322	1.321	1.314
Al VI	0.000	0.000	0.000	0.000	0.000	0.000	0.000	0.000	0.000	0.000	0.000	0.000
Fe3+	0.001	0.002	0.002	0.002	0.003	0.005	0.003	0.002	0.003	0.002	0.000	0.004
Ca	0.323	0.331	0.318	0.312	0.334	0.335	0.319	0.332	0.322	0.330	0.324	0.323
Na	0.676	0.666	0.681	0.680	0.670	0.661	0.688	0.669	0.668	0.661	0.654	0.682
K	0.005	0.009	0.008	0.012	0.006	0.009	0.009	0.010	0.010	0.007	0.008	0.007
Sum Cat#	5.01	5.01	5.00	5.00	5.01	5.00	5.01	5.01	5.00	5.00	4.99	5.01
Ab	67.3	66.2	67.7	67.7	66.3	65.7	67.7	66.1	66.8	66.2	66.3	67.4
An	32.2	32.9	31.6	31.1	33.1	33.4	31.4	32.9	32.2	33.1	32.9	31.9
Or	0.5	0.9	0.8	1.2	0.6	0.9	0.9	1.0	1.0	0.7	0.8	0.7

Feldspar Analyses by sample (recalculated to 100%), cations based on 8(O) Oxygens.

GT 474d																
Label	Pl1 C	Pl1 C	Pl1 R	Pl1 R	Pl2 C	Pl2 C	Pl2 R	Pl2 R	Pl3 C	Pl3 C	Pl3 R	Pl3 R	Pl4 R	Pl4 R	Pl4 C	Pl4 C
SiO2	63.68	63.91	63.86	63.95	63.41	63.25	63.05	63.14	63.61	64.02	63.33	63.57	63.81	63.78	63.59	63.69
Al2O3	22.91	22.77	22.77	22.67	22.90	23.06	23.09	22.99	22.86	22.78	22.93	22.89	22.61	22.79	22.83	22.84
Fe2O3	0.12	0.00	0.07	0.08	0.15	0.06	0.19	0.13	0.13	0.08	0.14	0.20	0.14	0.12	0.06	0.05
CaO	3.16	3.13	3.31	3.31	3.31	3.41	3.39	3.42	3.10	3.16	3.43	3.22	3.43	3.35	3.21	3.30
Na2O	9.64	9.60	9.51	9.58	9.67	9.57	9.65	9.75	9.67	9.33	9.57	9.42	9.46	9.46	9.72	9.55
K2O	0.49	0.59	0.48	0.41	0.56	0.65	0.63	0.57	0.62	0.63	0.60	0.70	0.54	0.50	0.59	0.57
Sum Ox%	100	100	100	100	100	100	100	100	100	100	100	100	100	100	100	100
Si	2.814	2.823	2.820	2.824	2.806	2.801	2.794	2.797	2.813	2.826	2.804	2.812	2.821	2.818	2.813	2.815
Al/Al IV	1.193	1.185	1.185	1.179	1.195	1.203	1.206	1.201	1.192	1.185	1.196	1.193	1.178	1.187	1.190	1.190
Al VI	0.000	0.000	0.000	0.000	0.000	0.000	0.000	0.000	0.000	0.000	0.000	0.000	0.000	0.000	0.000	0.000
Fe3+	0.004	0.000	0.002	0.003	0.005	0.002	0.006	0.005	0.004	0.003	0.005	0.007	0.005	0.004	0.002	0.002
Ca	0.150	0.148	0.157	0.157	0.157	0.162	0.161	0.163	0.147	0.149	0.163	0.152	0.162	0.159	0.152	0.156
Na	0.826	0.822	0.814	0.821	0.829	0.821	0.829	0.837	0.830	0.798	0.821	0.808	0.811	0.810	0.833	0.818
K	0.028	0.033	0.027	0.023	0.032	0.036	0.035	0.032	0.035	0.036	0.034	0.039	0.031	0.028	0.033	0.033
Sum Cat#	5.01	5.01	5.01	5.01	5.02	5.03	5.03	5.04	5.02	5.00	5.02	5.01	5.01	5.01	5.02	5.01
Ab	82.3	82.0	81.6	82.1	81.5	80.5	80.9	81.1	82.0	81.2	80.7	80.8	80.8	81.2	81.8	81.2
An	14.9	14.8	15.7	15.7	15.4	15.9	15.7	15.7	14.5	15.2	16.0	15.3	16.2	15.9	15.0	15.5
Or	2.8	3.3	2.7	2.3	3.1	3.6	3.4	3.1	3.5	3.6	3.3	3.9	3.1	2.8	3.3	3.2

Feldspar Analyses by sample (recalculated to 100%), cations based on 8(O) Oxygens.

GT 474d (Con't)								GT 481d											
Label	Pl5 C	Pl5 C	Pl5 R	Pl5 R	Ksp1 C	Ksp2 C	Ksp3 C	Label	Pl8 C	Pl8 C	Pl1 C	Pl1 C	Pl1 R	Pl1 R	Pl1 C	Pl2 R	Pl2 C	Pl3 C	Pl3 R
SiO2	63.92	63.63	63.50	63.56	64.10	63.80	64.02	SiO2	59.10	59.12	58.11	58.46	58.46	58.65	58.54	58.92	58.53	58.30	58.68
Al2O3	22.92	22.77	22.72	22.89	19.59	19.94	19.52	Al2O3	25.74	25.64	26.33	26.14	26.39	26.19	26.39	25.99	26.45	26.41	26.05
Fe2O3	0.07	0.10	0.10	0.13	0.11	0.06	0.10	Fe2O3	0.03	0.08	0.11	0.16	0.15	0.12	0.12	0.13	0.11	0.15	0.14
CaO	3.26	3.27	3.43	3.30	0.00	0.00	0.03	CaO	7.64	7.60	7.78	7.66	7.59	7.79	7.60	7.47	7.45	7.57	7.49
Na2O	9.31	9.70	9.70	9.57	1.06	0.79	0.97	Na2O	7.27	7.37	7.40	7.34	7.11	6.94	7.06	7.27	7.22	7.30	7.38
K2O	0.52	0.54	0.54	0.53	15.14	15.41	15.36	K2O	0.21	0.19	0.28	0.24	0.30	0.31	0.31	0.22	0.26	0.29	0.26
Sum Ox%	100	100	100	100	100	100	100	Sum Ox%	100	100	100	100	100	100	100	100	100	100	100
Si	2.821	2.814	2.811	2.811	2.953	2.941	2.953	Si	2.640	2.641	2.603	2.616	2.613	2.621	2.616	2.631	2.615	2.608	2.624
Al/Al IV	1.192	1.187	1.185	1.193	1.064	1.084	1.061	Al/Al IV	1.355	1.350	1.390	1.378	1.390	1.379	1.390	1.368	1.392	1.393	1.373
Al VI	0.000	0.000	0.000	0.000	0.000	0.000	0.000	Al VI	0.000	0.000	0.000	0.000	0.000	0.000	0.000	0.000	0.000	0.000	0.000
Fe3+	0.002	0.003	0.003	0.004	0.004	0.002	0.003	Fe3+	0.001	0.003	0.004	0.005	0.005	0.004	0.004	0.004	0.004	0.005	0.005
Ca	0.154	0.155	0.162	0.156	0.000	0.000	0.002	Ca	0.366	0.364	0.373	0.367	0.364	0.373	0.364	0.358	0.357	0.363	0.359
Na	0.797	0.832	0.832	0.821	0.094	0.070	0.086	Na	0.630	0.638	0.643	0.637	0.616	0.601	0.611	0.629	0.626	0.633	0.640
K	0.029	0.030	0.031	0.030	0.890	0.906	0.903	K	0.012	0.011	0.016	0.014	0.017	0.018	0.018	0.013	0.014	0.016	0.015
Sum Cat#	5.00	5.02	5.03	5.02	5.01	5.00	5.01	Sum Cat#	5.00	5.01	5.03	5.02	5.01	5.00	5.00	5.00	5.01	5.02	5.02
Ab	81.3	81.8	81.1	81.5	9.6	7.2	8.7	Ab	62.5	63.0	62.3	62.6	61.8	60.6	61.6	62.9	62.8	62.5	63.1
An	15.7	15.3	15.8	15.5	0.0	0.0	0.2	An	36.3	35.9	36.2	36.1	36.5	37.6	36.6	35.8	35.8	35.9	35.4
Or	3.0	3.0	3.0	3.0	90.4	92.8	91.2	Or	1.2	1.1	1.5	1.4	1.7	1.8	1.8	1.3	1.4	1.6	1.5

Feldspar Analyses by sample (recalculated to 100%), cations based on 8(O) Oxygens.

	GT 481d (Con't)									GT 486d									
Label	Pl4 R	Pl4 C	Pl5 R	Pl5 C	Pl6 C	Pl7 C	Pl7 R	Ksp1 C	Ksp1 C	Label	Pl1 C	Pl1 R	Pl2 C	Pl2 R	Pl2 C	Pl2 R	Pl2 R	Pl3 C	Pl3 R
SiO2	58.45	58.63	58.75	58.91	58.72	58.83	58.88	63.13	64.44	SiO2	59.69	59.64	59.51	59.49	59.42	59.54	59.60	59.82	59.81
Al2O3	26.51	26.31	26.03	25.78	26.12	26.17	26.11	20.33	19.14	Al2O3	25.77	25.65	25.81	25.57	25.76	25.58	25.67	25.38	25.52
Fe2O3	0.07	0.07	0.15	0.10	0.11	0.05	0.14	0.19	0.21	Fe2O3	0.10	0.16	0.00	0.08	0.08	0.08	0.09	0.08	0.04
CaO	7.44	7.36	7.47	7.58	7.59	7.46	7.44	0.05	0.06	CaO	6.63	6.61	6.62	6.71	6.60	6.75	6.59	6.56	6.60
Na2O	7.24	7.32	7.32	7.30	7.17	7.16	7.10	1.44	1.16	Na2O	7.57	7.70	7.79	7.95	7.82	7.84	7.81	7.85	7.79
K2O	0.30	0.32	0.28	0.34	0.29	0.33	0.33	14.85	14.99	K2O	0.24	0.24	0.27	0.19	0.31	0.21	0.23	0.30	0.24
Sum Ox%	100	100	100	100	100	100	100	100	100	Sum Ox%	100	100	100	100	100	100	100	100	100
Si	2.612	2.620	2.626	2.634	2.624	2.628	2.629	2.914	2.968	Si	2.658	2.658	2.653	2.654	2.651	2.656	2.657	2.667	2.665
Al/Al IV	1.396	1.385	1.371	1.359	1.376	1.377	1.374	1.106	1.038	Al/Al IV	1.352	1.347	1.356	1.345	1.355	1.345	1.348	1.334	1.340
Al VI	0.000	0.000	0.000	0.000	0.000	0.000	0.000	0.000	0.000	Al VI	0.000	0.000	0.000	0.000	0.000	0.000	0.000	0.000	0.000
Fe3+	0.003	0.002	0.005	0.003	0.004	0.002	0.005	0.007	0.007	Fe3+	0.003	0.006	0.000	0.003	0.003	0.003	0.003	0.003	0.001
Ca	0.356	0.352	0.358	0.363	0.363	0.357	0.356	0.003	0.003	Ca	0.316	0.316	0.316	0.321	0.315	0.322	0.315	0.314	0.315
Na	0.627	0.634	0.634	0.632	0.621	0.620	0.614	0.129	0.104	Na	0.654	0.665	0.673	0.688	0.677	0.679	0.675	0.678	0.672
K	0.017	0.018	0.016	0.019	0.016	0.019	0.019	0.874	0.881	K	0.014	0.014	0.015	0.010	0.018	0.012	0.013	0.017	0.014
Sum Cat#	5.01	5.01	5.01	5.01	5.01	5.00	5.00	5.03	5.00	Sum Cat#	5.00	5.01	5.01	5.02	5.02	5.02	5.01	5.01	5.01
Ab	62.7	63.1	62.9	62.3	62.1	62.3	62.1	12.8	10.5	Ab	66.4	66.9	67.0	67.5	67.0	67.0	67.3	67.2	67.2
An	35.6	35.1	35.5	35.8	36.3	35.9	36.0	0.3	0.3	An	32.2	31.7	31.5	31.5	31.2	31.8	31.4	31.1	31.5
Or	1.7	1.8	1.6	1.9	1.6	1.9	1.9	86.9	89.2	Or	1.4	1.4	1.5	1.0	1.8	1.2	1.3	1.7	1.4

Feldspar Analyses by sample (recalculated to 100%), cations based on 8(O) Oxygens.

GT 486d (Con't)										
Label	Pl3	Pl4	Pl4	Pl4	Pl5	Pl5	Pl5	Pl6	Pl6	Ksp1
	R	C	R	C	C	C	R	R	C	C
SiO2	59.53	59.67	59.89	59.77	59.80	59.70	59.51	59.34	59.37	64.70
Al2O3	25.64	25.45	25.50	25.78	25.55	25.73	25.88	25.82	25.71	18.79
Fe2O3	0.01	0.12	0.04	0.10	0.13	0.01	0.02	0.11	0.03	0.06
CaO	6.63	6.62	6.64	6.50	6.53	6.75	6.65	6.76	6.76	0.05
Na2O	7.88	7.77	7.60	7.55	7.68	7.56	7.79	7.69	7.87	1.21
K2O	0.31	0.35	0.32	0.30	0.31	0.26	0.16	0.28	0.25	15.19
Sum Ox%	100	100	100	100	100	100	100	100	100	100
Si	2.656	2.662	2.668	2.661	2.664	2.659	2.651	2.647	2.649	2.981
Al/Al IV	1.348	1.338	1.339	1.353	1.342	1.350	1.359	1.357	1.353	1.021
Al VI	0.000	0.000	0.000	0.000	0.000	0.000	0.000	0.000	0.000	0.000
Fe3+	0.000	0.004	0.001	0.003	0.004	0.000	0.001	0.004	0.001	0.002
Ca	0.317	0.317	0.317	0.310	0.312	0.322	0.317	0.323	0.323	0.003
Na	0.681	0.672	0.657	0.651	0.664	0.653	0.673	0.665	0.680	0.108
K	0.018	0.020	0.019	0.017	0.018	0.015	0.009	0.016	0.015	0.893
Sum Cat#	5.02	5.01	5.00	5.00	5.00	5.00	5.01	5.01	5.02	5.01
Ab	67.0	66.6	66.2	66.6	66.8	66.0	67.3	66.2	66.8	10.8
An	31.2	31.4	32.0	31.7	31.4	32.5	31.8	32.2	31.8	0.3
Or	1.8	2.0	1.9	1.7	1.8	1.5	0.9	1.6	1.4	89.0

Feldspar Analyses by sample (recalculated to 100%), cations based on 8 (O) Oxygens.

Terrane/ Sample	CD 209-1									CD 457										
Label	Pt1	Pt1	Pt2	Pt3	Pt4	Pt4	Pt5	Pt5	Pt6	Label	Pt1	Pt1	PL2	Pt2	Pt3	Pt3	Pt4	Pt4	Pt5	Pt5
	C	R	R	C	C	R	C	R	C		C	R	C	R	C	R	C	R	C	R
SiO2	48.51	47.51	48.24	48.42	49.14	48.46	48.12	48.56	47.11	SiO2	57.58	57.69	58.08	57.39	57.85	57.80	58.11	57.66	58.09	58.00
Al2O3	33.51	33.45	33.07	32.97	32.76	33.20	33.50	33.15	33.94	Al2O3	26.42	26.41	26.25	26.28	26.30	26.32	26.16	26.46	26.45	26.21
Fe2O3	0.04	0.16	0.28	0.06	0.06	0.10	0.08	0.14	0.13	Fe2O3	0.02	0.11	0.07	0.10	0.05	0.13	0.06	0.13	0.00	0.13
MgO	0.01	0.01	0.01	0.01	0.01	0.00	0.02	0.00	0.01	MgO	0.01	0.00	0.02	0.00	0.00	0.02	0.00	0.02	0.00	0.03
CaO	15.48	16.40	15.84	15.69	15.09	15.66	15.97	15.37	16.85	CaO	8.37	8.30	7.71	8.15	7.91	8.14	7.96	8.14	7.94	8.08
SrO	0.00	0.00	0.00	0.00	0.00	0.00	0.00	0.00	0.00	SrO	0.00	0.00	0.00	0.00	0.00	0.00	0.00	0.00	0.00	0.00
BaO	0.00	0.02	0.17	0.04	0.14	0.10	0.00	0.16	0.00	BaO	0.00	0.00	0.16	0.25	0.00	0.04	0.00	0.00	0.06	0.06
Na2O	2.35	2.23	2.19	2.58	2.69	2.38	2.19	2.45	1.80	Na2O	7.30	7.15	7.36	7.49	7.50	7.35	7.30	7.25	7.09	7.26
K2O	0.05	0.08	0.04	0.07	0.11	0.06	0.06	0.05	0.06	K2O	0.21	0.21	0.22	0.18	0.14	0.13	0.25	0.16	0.16	0.12
Rb2O	0.07	0.14	0.14	0.17	0.01	0.04	0.07	0.14	0.11	Rb2O	0.08	0.13	0.13	0.16	0.24	0.07	0.17	0.17	0.21	0.08
Sum Ox%	100	100	100	100	100	100	100	100	100	Sum Ox%	100	100	100	100	100	100	100	100	100	100
Si	2.215	2.182	2.211	2.218	2.244	2.217	2.202	2.222	2.163	Si	2.586	2.590	2.606	2.585	2.597	2.594	2.606	2.589	2.603	2.601
Al/Al IV	1.803	1.811	1.787	1.780	1.763	1.789	1.806	1.788	1.836	Al/Al IV	1.399	1.397	1.388	1.395	1.392	1.392	1.383	1.400	1.397	1.386
Al VI	0.000	0.000	0.000	0.000	0.000	0.000	0.000	0.000	0.000	Al VI	0.000	0.000	0.000	0.000	0.000	0.000	0.000	0.000	0.000	0.000
Fe3+	0.001	0.006	0.010	0.002	0.002	0.004	0.003	0.005	0.004	Fe3+	0.001	0.004	0.002	0.004	0.002	0.004	0.002	0.004	0.000	0.005
Mg	0.001	0.001	0.001	0.000	0.001	0.000	0.002	0.000	0.001	Mg	0.001	0.000	0.001	0.000	0.000	0.002	0.000	0.001	0.000	0.002
Ca	0.757	0.807	0.778	0.770	0.738	0.767	0.782	0.753	0.829	Ca	0.402	0.399	0.371	0.394	0.381	0.391	0.382	0.391	0.381	0.388
Sr	0.000	0.000	0.000	0.000	0.000	0.000	0.000	0.000	0.000	Sr	0.000	0.000	0.000	0.000	0.000	0.000	0.000	0.000	0.000	0.000
Ba	0.000	0.000	0.003	0.001	0.002	0.002	0.000	0.003	0.000	Ba	0.000	0.000	0.003	0.004	0.000	0.001	0.000	0.000	0.001	0.001
Na	0.207	0.198	0.195	0.229	0.237	0.211	0.194	0.217	0.160	Na	0.636	0.622	0.640	0.654	0.653	0.639	0.634	0.632	0.616	0.631
K	0.003	0.004	0.002	0.004	0.006	0.003	0.003	0.003	0.003	K	0.013	0.012	0.013	0.010	0.008	0.007	0.014	0.009	0.009	0.007
Rb	0.002	0.004	0.004	0.005	0.000	0.001	0.002	0.004	0.003	Rb	0.002	0.004	0.004	0.004	0.007	0.002	0.005	0.005	0.006	0.003
Sum Cat#	4.99	5.01	4.99	5.01	5.00	4.99	4.99	4.99	5.00	Sum Cat#	5.04	5.03	5.03	5.05	5.04	5.03	5.03	5.03	5.01	5.02
Ab	21.4	19.5	19.9	22.7	24.1	21.4	19.8	22.2	16.0	Ab	60.4	60.0	62.1	61.3	62.3	61.4	61.2	60.9	60.8	61.3
An	78.1	79.6	79.2	76.3	75.0	77.9	79.7	76.8	83.3	An	38.2	38.5	36.0	36.9	36.3	37.6	36.9	37.7	37.6	37.7
Or	0.3	0.4	0.3	0.4	0.6	0.3	0.3	0.3	0.3	Or	1.2	1.1	1.2	1.0	0.8	0.7	1.3	0.9	0.9	0.7

Feldspar Analyses by sample (recalculated to 100%), cations based on 8 (O) Oxygens.

CD 430										Ultrapotassic 338z										
Label	Pt1	Pt2	Pt2	Pt3	Pt3	Pt4	Pt4	Pt5	Pt5	Label	Pt1	Pt1	Pt1	Pt2	Pt2	Pt2	Pt2	Pt3	Pt3	Pt3
	R	C	R	C	R	C	R	C	R		R1	C	R2	R1	C1	C2	R2	R1	C	R2
SiO2	52.33	53.34	52.47	50.40	49.68	53.60	53.56	50.77	51.46	SiO2	59.54	59.54	59.36	59.70	59.36	59.65	59.33	59.70	59.49	60.05
Al2O3	29.98	29.34	29.49	31.14	31.60	29.31	29.37	31.02	30.27	Al2O3	26.37	26.16	26.33	26.21	26.17	26.31	26.52	26.22	26.30	26.13
Fe2O3	0.11	0.11	0.08	0.18	0.29	0.11	0.16	0.15	0.30	Fe2O3	0.00	0.02	0.02	0.00	0.00	0.02	0.02	0.01	0.02	0.03
MgO	0.02	0.00	0.01	0.00	0.02	0.00	0.00	0.01	0.05	MgO	0.01	0.00	0.00	0.00	0.03	0.03	0.00	0.00	0.00	0.01
CaO	12.18	11.61	12.35	13.78	14.54	11.34	11.54	13.73	13.26	CaO	6.67	6.65	6.54	6.59	6.63	6.58	6.69	6.63	6.83	6.50
SrO	0.00	0.00	0.00	0.00	0.00	0.00	0.00	0.00	0.00	SrO	0.00	0.00	0.00	0.00	0.00	0.00	0.00	0.00	0.00	0.00
BaO	0.27	0.00	0.00	0.10	0.08	0.00	0.00	0.12	0.00	BaO	0.00	0.24	0.32	0.18	0.42	0.00	0.14	0.02	0.02	0.00
Na2O	4.94	5.41	5.30	4.18	3.62	5.40	5.19	4.09	4.45	Na2O	7.11	7.17	7.14	7.04	7.10	7.19	7.01	7.21	7.05	7.04
K2O	0.08	0.09	0.11	0.07	0.06	0.11	0.11	0.07	0.09	K2O	0.18	0.22	0.20	0.23	0.23	0.22	0.28	0.13	0.22	0.26
Rb2O	0.08	0.10	0.20	0.15	0.11	0.13	0.05	0.05	0.13	Rb2O	0.12	0.00	0.09	0.04	0.06	0.00	0.02	0.08	0.06	0.00
Sum Ox%	100	100	100	100	100	100	100	100	100	Sum Ox%	100	100	100	100	100	100	100	100	100	100
Si	2.381	2.419	2.390	2.304	2.274	2.427	2.425	2.317	2.346	Si	2.648	2.651	2.646	2.655	2.648	2.650	2.640	2.654	2.647	2.665
Al/Al IV	1.607	1.568	1.582	1.677	1.705	1.565	1.567	1.668	1.627	Al/Al IV	1.382	1.373	1.383	1.374	1.376	1.378	1.391	1.373	1.379	1.366
Al VI	0.000	0.000	0.000	0.000	0.000	0.000	0.000	0.000	0.000	Al VI	0.000	0.000	0.000	0.000	0.000	0.000	0.000	0.000	0.000	0.000
Fe3+	0.004	0.004	0.003	0.006	0.010	0.004	0.006	0.005	0.010	Fe3+	0.000	0.001	0.001	0.000	0.000	0.001	0.001	0.000	0.001	0.001
Mg	0.001	0.000	0.001	0.000	0.001	0.000	0.000	0.001	0.004	Mg	0.000	0.000	0.000	0.000	0.002	0.002	0.000	0.000	0.000	0.001
Ca	0.593	0.564	0.603	0.675	0.713	0.550	0.560	0.671	0.647	Ca	0.318	0.317	0.312	0.314	0.317	0.314	0.319	0.316	0.326	0.309
Sr	0.000	0.000	0.000	0.000	0.000	0.000	0.000	0.000	0.000	Sr	0.000	0.000	0.000	0.000	0.000	0.000	0.000	0.000	0.000	0.000
Ba	0.005	0.000	0.000	0.002	0.001	0.000	0.000	0.002	0.000	Ba	0.000	0.004	0.006	0.003	0.007	0.000	0.002	0.000	0.000	0.000
Na	0.436	0.476	0.468	0.370	0.321	0.474	0.456	0.362	0.393	Na	0.613	0.619	0.617	0.607	0.614	0.620	0.605	0.622	0.608	0.606
K	0.005	0.005	0.006	0.004	0.004	0.006	0.006	0.004	0.005	K	0.010	0.012	0.011	0.013	0.013	0.013	0.016	0.007	0.012	0.015
Rb	0.002	0.003	0.006	0.005	0.003	0.004	0.001	0.002	0.004	Rb	0.003	0.000	0.003	0.001	0.002	0.000	0.001	0.002	0.002	0.000
Sum Cat#	5.04	5.04	5.06	5.04	5.03	5.03	5.02	5.03	5.04	Sum Cat#	4.98	4.98	4.98	4.97	4.98	4.98	4.98	4.98	4.97	4.96
Ab	41.8	45.4	43.2	35.1	30.8	45.8	44.6	34.8	37.4	Ab	64.9	65.0	65.0	64.7	64.4	65.5	64.2	65.6	64.1	65.2
An	57.0	53.8	55.7	63.9	68.4	53.2	54.7	64.5	61.7	An	33.6	33.3	32.9	33.5	33.3	33.1	33.8	33.3	34.3	33.2
Or	0.5	0.5	0.6	0.4	0.4	0.6	0.6	0.4	0.5	Or	1.1	1.3	1.2	1.4	1.4	1.3	1.7	0.8	1.3	1.6

Feldspar Analyses by sample (recalculated to 100%), cations based on 8 (O) Oxygens.

Ultrapotassic 338z (Con't)																				
Label	Pl4	Pl4	Pl4	Ksp1	Ksp1	Ksp2	Ksp2	Ksp2	Ksp2	Ksp3	Ksp3	Ksp3	Ksp4	Ksp4	Ksp4	Ksp5	Ksp5	Ksp5	Ksp5	Ksp5
	R1	C	R2	C	R	C	C	R	R	C	R	R	R1	C	R2	C	C	R	R	C
SiO2	59.76	59.48	59.58	63.11	63.61	64.08	63.80	63.67	63.37	63.54	63.54	63.34	63.65	63.98	63.49	63.31	63.40	63.24	63.51	63.94
Al2O3	26.08	26.22	26.34	20.22	20.19	19.81	19.76	20.08	20.11	20.02	20.08	20.12	20.20	19.72	19.68	20.18	20.22	20.04	20.44	19.95
Fe2O3	0.00	0.02	0.05	0.00	0.00	0.00	0.00	0.02	0.00	0.00	0.03	0.00	0.00	0.02	0.00	0.02	0.00	0.03	0.00	0.00
MgO	0.02	0.00	0.00	0.00	0.03	0.01	0.02	0.02	0.00	0.00	0.01	0.02	0.02	0.01	0.02	0.02	0.02	0.00	0.00	0.01
CaO	6.69	6.83	6.65	0.06	0.03	0.05	0.05	0.01	0.01	0.02	0.04	0.03	0.09	0.00	0.01	0.01	0.07	0.05	0.06	0.04
SrO	0.00	0.00	0.00	0.00	0.00	0.00	0.00	0.00	0.00	0.00	0.00	0.00	0.00	0.00	0.00	0.00	0.00	0.00	0.00	0.00
BaO	0.14	0.00	0.00	2.45	2.09	1.83	2.01	2.03	2.30	2.13	1.91	2.37	2.03	1.76	2.57	2.00	2.21	2.43	2.01	1.52
Na2O	7.01	7.12	7.10	1.85	2.03	1.89	1.94	1.77	1.96	1.81	1.86	1.85	2.11	1.67	1.72	1.77	1.86	1.95	2.09	1.82
K2O	0.21	0.27	0.21	12.32	12.02	12.34	12.42	12.42	12.25	12.47	12.53	12.27	11.90	12.84	12.52	12.70	12.20	12.27	11.89	12.72
Rb2O	0.08	0.07	0.07	0.00	0.00	0.00	0.00	0.00	0.00	0.00	0.00	0.00	0.00	0.00	0.00	0.00	0.00	0.00	0.00	0.00
Sum Ox%	100	100	100	100	100	100	100	100	100	100	100	100	100	100	100	100	100	100	100	100
Si	2.658	2.647	2.649	2.924	2.934	2.952	2.947	2.939	2.932	2.937	2.934	2.931	2.934	2.952	2.945	2.928	2.930	2.930	2.926	2.945
Al/Al IV	1.367	1.375	1.380	1.104	1.098	1.075	1.076	1.092	1.096	1.091	1.093	1.097	1.097	1.073	1.076	1.100	1.102	1.094	1.110	1.083
Al VI	0.000	0.000	0.000	0.000	0.000	0.000	0.000	0.000	0.000	0.000	0.000	0.000	0.000	0.000	0.000	0.000	0.000	0.000	0.000	0.000
Fe3+	0.000	0.001	0.002	0.000	0.000	0.000	0.000	0.001	0.000	0.000	0.001	0.000	0.000	0.001	0.000	0.001	0.000	0.001	0.000	0.000
Mg	0.001	0.000	0.000	0.000	0.002	0.001	0.001	0.001	0.000	0.000	0.001	0.001	0.001	0.001	0.001	0.001	0.001	0.000	0.000	0.001
Ca	0.319	0.325	0.317	0.003	0.001	0.002	0.003	0.000	0.001	0.001	0.002	0.002	0.005	0.000	0.001	0.001	0.004	0.002	0.003	0.002
Sr	0.000	0.000	0.000	0.000	0.000	0.000	0.000	0.000	0.000	0.000	0.000	0.000	0.000	0.000	0.000	0.000	0.000	0.000	0.000	0.000
Ba	0.002	0.000	0.000	0.044	0.038	0.033	0.036	0.037	0.042	0.039	0.034	0.043	0.037	0.032	0.047	0.036	0.040	0.044	0.036	0.027
Na	0.605	0.614	0.612	0.167	0.182	0.168	0.173	0.159	0.176	0.163	0.167	0.166	0.188	0.150	0.154	0.158	0.167	0.175	0.187	0.163
K	0.012	0.015	0.012	0.728	0.707	0.725	0.732	0.731	0.723	0.735	0.738	0.724	0.700	0.756	0.741	0.749	0.719	0.725	0.699	0.747
Rb	0.002	0.002	0.002	0.000	0.000	0.000	0.000	0.000	0.000	0.000	0.000	0.000	0.000	0.000	0.000	0.000	0.000	0.000	0.000	0.000
Sum Cat#	4.97	4.98	4.97	4.97	4.96	4.96	4.97	4.96	4.97	4.97	4.97	4.97	4.96	4.96	4.96	4.98	4.96	4.97	4.96	4.97
Ab	64.3	64.2	64.9	17.7	19.6	18.1	18.4	17.1	18.7	17.4	17.7	17.8	20.2	16.0	16.4	16.8	18.0	18.5	20.2	17.3
An	33.9	34.0	33.6	0.3	0.2	0.3	0.3	0.0	0.1	0.1	0.2	0.2	0.5	0.0	0.1	0.1	0.4	0.3	0.3	0.2
Or	1.3	1.6	1.3	77.3	76.2	78.1	77.5	78.9	76.8	78.4	78.4	77.5	75.3	80.6	78.6	79.3	77.4	76.6	75.6	79.6

Feldspar Analyses by sample (recalculated to 100%), cations based on 8 (O) Oxygens.

Ultrapotassic 209-2																
Label	P17	P11	P11	P11	P12	P12	P12	P13	P13	P13	P14	P14	P15	P15	P16	P16
	C	C	R	R	C	R	R	R	C	C	R	C	C	R	C	R
SiO2	49.23	50.37	49.28	49.55	49.67	50.80	47.96	47.30	47.60	48.29	48.77	48.84	50.99	50.45	49.43	49.79
Al2O3	33.04	32.32	32.81	32.78	32.57	32.01	33.77	34.25	34.04	33.72	33.43	33.40	32.00	32.10	32.77	32.57
Fe2O3	0.13	0.13	0.18	0.06	0.08	0.09	0.29	0.12	0.05	0.07	0.14	0.02	0.16	0.13	0.10	0.08
MgO	0.05	0.00	0.03	0.00	0.00	0.01	0.07	0.00	0.00	0.00	0.00	0.00	0.00	0.02	0.00	0.00
CaO	14.58	13.57	14.74	14.37	14.73	13.48	15.44	16.23	16.16	15.61	14.90	15.14	13.55	13.68	14.44	14.31
SrO	0.00	0.00	0.00	0.00	0.00	0.00	0.00	0.00	0.00	0.00	0.00	0.00	0.00	0.00	0.00	0.00
BaO	0.00	0.12	0.00	0.26	0.00	0.16	0.00	0.14	0.02	0.00	0.14	0.10	0.00	0.00	0.20	0.24
Na2O	2.84	3.30	2.76	2.77	2.88	3.28	2.25	1.86	1.88	2.11	2.43	2.41	3.12	3.41	2.88	2.88
K2O	0.07	0.14	0.06	0.10	0.05	0.06	0.08	0.10	0.08	0.07	0.09	0.08	0.15	0.10	0.09	0.12
Rb2O	0.06	0.05	0.12	0.08	0.01	0.12	0.14	0.00	0.17	0.12	0.08	0.00	0.02	0.11	0.08	0.00
Sum Ox%	100	100	100	100	100	100	100	100	100	100	100	100	100	100	100	100
Si	2.244	2.291	2.248	2.260	2.263	2.308	2.194	2.167	2.180	2.206	2.226	2.228	2.313	2.295	2.255	2.269
Al/Al IV	1.775	1.732	1.764	1.762	1.748	1.714	1.821	1.850	1.837	1.815	1.798	1.795	1.710	1.721	1.762	1.749
Al VI	0.000	0.000	0.000	0.000	0.000	0.000	0.000	0.000	0.000	0.000	0.000	0.000	0.000	0.000	0.000	0.000
Fe3+	0.005	0.004	0.006	0.002	0.003	0.003	0.010	0.004	0.002	0.003	0.005	0.001	0.005	0.005	0.003	0.003
Mg	0.003	0.000	0.002	0.000	0.000	0.001	0.005	0.000	0.000	0.000	0.000	0.000	0.000	0.001	0.000	0.000
Ca	0.712	0.661	0.720	0.702	0.719	0.656	0.757	0.796	0.793	0.764	0.729	0.740	0.658	0.667	0.706	0.699
Sr	0.000	0.000	0.000	0.000	0.000	0.000	0.000	0.000	0.000	0.000	0.000	0.000	0.000	0.000	0.000	0.000
Ba	0.000	0.002	0.000	0.005	0.000	0.003	0.000	0.003	0.000	0.000	0.003	0.002	0.000	0.000	0.004	0.004
Na	0.251	0.291	0.244	0.245	0.254	0.289	0.199	0.166	0.167	0.187	0.216	0.213	0.275	0.300	0.255	0.254
K	0.004	0.008	0.004	0.006	0.003	0.004	0.005	0.006	0.005	0.004	0.006	0.005	0.009	0.006	0.005	0.007
Rb	0.002	0.001	0.004	0.002	0.000	0.004	0.004	0.000	0.005	0.004	0.002	0.000	0.000	0.003	0.002	0.000
Sum Cat#	5.00	4.99	4.99	4.99	4.99	4.98	5.00	4.99	4.99	4.98	4.98	4.98	4.97	5.00	4.99	4.99
Ab	25.9	30.2	25.1	25.5	26.0	30.2	20.6	17.1	17.2	19.5	22.6	22.2	29.2	30.8	26.2	26.4
An	73.5	68.6	74.1	73.1	73.6	68.7	78.4	82.1	81.7	79.7	76.3	77.1	69.9	68.3	72.6	72.4
Or	0.4	0.9	0.4	0.6	0.3	0.4	0.5	0.6	0.5	0.4	0.6	0.5	0.9	0.6	0.5	0.7

Feldspar Analyses by sample (recalculated to 100%), cations based on 8 (O) Oxygens.

Ultrapotassic 361z																
Label	Ksp1 (Clast)							Ksp2	Ksp2	Ksp2	Ksp2	Ksp2	Ksp2	Ksp3	Ksp4	Ksp4
	R1	C1	C2	C3	C4	C5	R2	R1	C1	C2	C3	C4	R2	C	R	C
SiO2	63.61	63.16	63.70	63.76	64.15	63.73	63.49	63.00	63.36	63.12	63.21	63.10	62.57	62.86	63.08	62.77
Al2O3	19.05	19.07	19.07	18.86	18.72	18.83	19.16	19.11	19.10	18.95	18.96	19.01	18.99	19.05	18.97	18.93
Fe2O3	0.05	0.00	0.00	0.02	0.04	0.01	0.00	0.06	0.00	0.01	0.06	0.00	0.07	0.06	0.04	0.02
MgO	0.01	0.00	0.04	0.02	0.00	0.01	0.01	0.00	0.02	0.01	0.00	0.02	0.01	0.00	0.00	0.01
CaO	0.00	0.04	0.04	0.03	0.01	0.03	0.03	0.00	0.02	0.02	0.04	0.01	0.03	0.05	0.05	0.02
SrO	0.00	0.00	0.00	0.00	0.00	0.00	0.00	0.00	0.00	0.00	0.00	0.00	0.00	0.00	0.00	0.00
BaO	1.30	1.88	1.28	1.25	0.67	1.36	1.18	2.18	1.89	2.19	2.20	1.84	2.51	2.00	1.76	2.21
Na2O	1.26	1.30	1.33	1.27	1.40	1.25	1.33	1.13	1.13	1.20	1.12	1.20	1.12	1.02	1.12	1.03
K2O	14.72	14.55	14.54	14.79	15.01	14.79	14.79	14.53	14.49	14.50	14.42	14.84	14.72	14.95	15.00	15.01
Rb2O	0.00	0.00	0.00	0.00	0.00	0.00	0.00	0.00	0.00	0.00	0.00	0.00	0.00	0.00	0.00	0.00
Sum Ox%	100	100	100	100	100	100	100	100	100	100	100	100	100	100	100	100
Si	2.957	2.949	2.958	2.964	2.972	2.964	2.952	2.946	2.954	2.952	2.954	2.949	2.940	2.944	2.949	2.945
Al/Al IV	1.044	1.050	1.044	1.033	1.022	1.032	1.050	1.053	1.049	1.045	1.044	1.047	1.051	1.052	1.045	1.047
Al VI	0.000	0.000	0.000	0.000	0.000	0.000	0.000	0.000	0.000	0.000	0.000	0.000	0.000	0.000	0.000	0.000
Fe3+	0.002	0.000	0.000	0.001	0.001	0.000	0.000	0.002	0.000	0.000	0.002	0.000	0.002	0.002	0.002	0.001
Mg	0.001	0.000	0.003	0.001	0.000	0.001	0.001	0.000	0.001	0.001	0.000	0.001	0.001	0.000	0.000	0.000
Ca	0.000	0.002	0.002	0.002	0.001	0.002	0.001	0.000	0.001	0.001	0.002	0.000	0.001	0.003	0.003	0.001
Sr	0.000	0.000	0.000	0.000	0.000	0.000	0.000	0.000	0.000	0.000	0.000	0.000	0.000	0.000	0.000	0.000
Ba	0.024	0.034	0.023	0.023	0.012	0.025	0.022	0.040	0.034	0.040	0.040	0.034	0.046	0.037	0.032	0.041
Na	0.114	0.117	0.120	0.114	0.126	0.112	0.121	0.102	0.103	0.108	0.101	0.109	0.102	0.092	0.101	0.094
K	0.873	0.866	0.861	0.877	0.887	0.878	0.877	0.867	0.861	0.865	0.860	0.885	0.882	0.893	0.894	0.898
Rb	0.000	0.000	0.000	0.000	0.000	0.000	0.000	0.000	0.000	0.000	0.000	0.000	0.000	0.000	0.000	0.000
Sum Cat#	5.01	5.02	5.01	5.02	5.02	5.01	5.02	5.01	5.00	5.01	5.00	5.02	5.03	5.02	5.03	5.03
Ab	11.2	11.5	11.9	11.3	12.3	11.1	11.8	10.1	10.3	10.7	10.1	10.6	9.9	9.0	9.8	9.1
An	0.0	0.2	0.2	0.2	0.1	0.2	0.1	0.0	0.1	0.1	0.2	0.0	0.1	0.3	0.2	0.1
Or	86.4	84.9	85.6	86.3	86.5	86.4	85.9	85.9	86.2	85.3	85.7	86.1	85.5	87.1	86.8	86.9

Feldspar Analyses by sample (recalculated to 100%), cations based on 8 (O) Oxygens.

Ultrapotassic 361z (Con't)																			
Label	Ksp5	Ksp5	Ksp6	Ksp6	Ksp7	Ksp8	Ksp9	Pl1	Pl1	Pl2	Pl2	Pl3	Pl3	Pl4	Pl4	Pl5	Pl5	Pl6	Pl6
	R	C	R	C	R	C	C	C	R	C	R	C	R	R	C	C	R	C	R
SiO2	63.32	63.60	63.49	63.00	63.28	63.10	63.11	58.08	57.46	57.22	57.20	57.12	57.01	56.96	57.61	57.47	57.54	56.91	57.06
Al2O3	19.14	19.12	19.05	19.10	19.11	19.23	19.21	26.61	27.05	27.18	27.33	27.32	27.45	27.18	27.25	26.89	26.73	27.36	27.39
Fe2O3	0.06	0.02	0.08	0.03	0.06	0.01	0.04	0.07	0.09	0.11	0.05	0.01	0.06	0.10	0.03	0.04	0.09	0.10	0.08
MgO	0.01	0.01	0.00	0.00	0.00	0.00	0.02	0.02	0.00	0.01	0.00	0.00	0.00	0.00	0.01	0.01	0.03	0.00	0.04
CaO	0.00	0.02	0.01	0.03	0.00	0.03	0.01	8.11	8.52	8.69	8.77	8.96	8.91	8.94	8.63	8.76	8.52	9.00	8.99
SrO	0.00	0.00	0.00	0.00	0.00	0.00	0.00	0.00	0.00	0.00	0.00	0.00	0.00	0.00	0.00	0.00	0.00	0.00	0.00
BaO	1.64	1.53	1.82	1.93	1.72	2.12	1.67	0.06	0.06	0.00	0.00	0.08	0.00	0.00	0.00	0.00	0.32	0.00	0.00
Na2O	1.09	1.05	1.03	1.14	1.14	1.01	0.97	6.72	6.47	6.51	6.41	6.24	6.38	6.53	6.22	6.52	6.50	6.41	6.17
K2O	14.74	14.66	14.53	14.78	14.71	14.52	14.96	0.24	0.22	0.23	0.18	0.17	0.15	0.20	0.22	0.19	0.20	0.23	0.22
Rb2O	0.00	0.00	0.00	0.00	0.00	0.00	0.00	0.09	0.15	0.05	0.07	0.09	0.02	0.09	0.04	0.12	0.08	0.00	0.06
Sum Ox%	100	100	100	100	100	100	100	100	100	100	100	100	100	100	100	100	100	100	100
Si	2.951	2.958	2.958	2.946	2.951	2.947	2.945	2.600	2.576	2.566	2.564	2.562	2.556	2.558	2.577	2.577	2.583	2.554	2.558
Al/Al IV	1.052	1.048	1.046	1.052	1.050	1.059	1.057	1.404	1.429	1.437	1.443	1.444	1.450	1.439	1.436	1.421	1.415	1.447	1.447
Al VI	0.000	0.000	0.000	0.000	0.000	0.000	0.000	0.000	0.000	0.000	0.000	0.000	0.000	0.000	0.000	0.000	0.000	0.000	0.000
Fe3+	0.002	0.001	0.003	0.001	0.002	0.000	0.002	0.002	0.003	0.004	0.002	0.000	0.002	0.003	0.001	0.001	0.003	0.003	0.003
Mg	0.001	0.001	0.000	0.000	0.000	0.000	0.001	0.002	0.000	0.001	0.000	0.000	0.000	0.000	0.000	0.000	0.002	0.000	0.003
Ca	0.000	0.001	0.000	0.001	0.000	0.001	0.000	0.389	0.409	0.418	0.421	0.430	0.428	0.430	0.413	0.421	0.410	0.433	0.432
Sr	0.000	0.000	0.000	0.000	0.000	0.000	0.000	0.000	0.000	0.000	0.000	0.000	0.000	0.000	0.000	0.000	0.000	0.000	0.000
Ba	0.030	0.028	0.033	0.035	0.031	0.039	0.030	0.001	0.001	0.000	0.000	0.001	0.000	0.000	0.000	0.000	0.006	0.000	0.000
Na	0.098	0.094	0.093	0.103	0.103	0.092	0.087	0.584	0.563	0.566	0.557	0.543	0.555	0.569	0.539	0.567	0.566	0.558	0.537
K	0.876	0.869	0.863	0.882	0.875	0.865	0.891	0.014	0.012	0.013	0.010	0.009	0.008	0.012	0.013	0.011	0.011	0.013	0.012
Rb	0.000	0.000	0.000	0.000	0.000	0.000	0.000	0.003	0.004	0.002	0.002	0.003	0.001	0.002	0.001	0.003	0.002	0.000	0.002
Sum Cat#	5.01	5.00	5.00	5.02	5.01	5.00	5.02	5.00	5.00	5.00	5.00	4.99	5.00	5.01	4.98	5.00	5.00	5.01	4.99
Ab	9.8	9.5	9.4	10.1	10.2	9.2	8.7	59.0	56.9	56.7	56.2	55.0	55.9	56.2	55.8	56.6	56.9	55.6	54.6
An	0.0	0.1	0.0	0.1	0.0	0.1	0.0	39.3	41.4	41.9	42.5	43.6	43.2	42.5	42.8	42.0	41.2	43.1	43.9
Or	87.2	87.6	87.3	86.3	86.7	86.8	88.3	1.4	1.2	1.3	1.0	0.9	0.9	1.1	1.3	1.1	1.1	1.3	1.3

Feldspar Analyses by sample (recalculated to 100%), cations based on 8 (O) Oxygens.

Ultrapotassic 404											Ultrapotassic 408										
Label	Pl1 C	Pl1 R	Pl2 C	Pl2 R	Pl3 C	Pl3 R	Pl4 C	Pl4 R	Pl5 C	Pl5 R	Label	Pl5 C	Pl5 R	Pl3 C	Pl4 C	Pl4 R	Pl6 C	Pl6 R	Pl7 C	Pl7 R	Pl7 C
SiO2	46.60	47.15	49.61	48.50	49.20	48.72	48.93	47.96	49.46	48.19	SiO2	56.39	56.90	56.31	56.67	56.55	56.84	56.23	56.40	55.85	56.16
Al2O3	34.51	34.27	32.86	33.55	32.79	33.26	33.27	33.85	32.94	33.57	Al2O3	27.68	27.64	27.89	27.60	27.46	27.52	27.74	27.99	27.96	27.70
Fe2O3	0.09	0.17	0.08	0.06	0.01	0.11	0.06	0.10	0.08	0.11	Fe2O3	0.05	0.03	0.05	0.07	0.10	0.00	0.16	0.07	0.03	0.09
MgO	0.00	0.00	0.00	0.01	0.01	0.03	0.01	0.02	0.00	0.00	MgO	0.00	0.01	0.00	0.01	0.00	0.01	0.00	0.00	0.03	0.00
CaO	16.95	16.22	14.78	15.41	14.73	15.33	15.09	15.77	14.54	15.84	CaO	9.37	9.22	9.43	9.27	9.28	9.46	9.54	9.42	9.61	9.45
SrO	0.00	0.00	0.00	0.00	0.00	0.00	0.00	0.00	0.00	0.00	SrO	0.00	0.00	0.00	0.00	0.00	0.00	0.00	0.00	0.00	0.00
BaO	0.00	0.14	0.02	0.08	0.34	0.00	0.10	0.06	0.00	0.00	BaO	0.31	0.04	0.00	0.12	0.12	0.00	0.04	0.00	0.33	0.14
Na2O	1.67	1.91	2.52	2.29	2.69	2.39	2.45	2.01	2.83	2.15	Na2O	6.07	5.94	6.07	6.08	6.23	6.03	6.07	5.93	5.96	6.16
K2O	0.05	0.06	0.06	0.04	0.09	0.06	0.04	0.05	0.05	0.03	K2O	0.11	0.15	0.12	0.12	0.09	0.14	0.11	0.14	0.11	0.13
Rb2O	0.13	0.08	0.07	0.08	0.14	0.10	0.05	0.17	0.10	0.11	Rb2O	0.02	0.07	0.13	0.06	0.18	0.00	0.10	0.04	0.12	0.16
Sum Ox%	100	100	100	100	100	100	100	100	100	100	Sum Ox%	100	100	100	100	100	100	100	100	100	100
Si	2.141	2.163	2.258	2.215	2.249	2.224	2.232	2.194	2.253	2.203	Si	2.536	2.550	2.530	2.544	2.543	2.549	2.528	2.530	2.517	2.528
Al/Al IV	1.868	1.852	1.763	1.805	1.766	1.790	1.789	1.825	1.769	1.809	Al/Al IV	1.467	1.460	1.476	1.460	1.455	1.454	1.470	1.480	1.485	1.470
Al VI	0.000	0.000	0.000	0.000	0.000	0.000	0.000	0.000	0.000	0.000	Al VI	0.000	0.000	0.000	0.000	0.000	0.000	0.000	0.000	0.000	0.000
Fe3+	0.003	0.006	0.003	0.002	0.000	0.004	0.002	0.003	0.003	0.004	Fe3+	0.002	0.001	0.002	0.002	0.003	0.000	0.005	0.002	0.001	0.003
Mg	0.000	0.000	0.000	0.000	0.000	0.002	0.001	0.002	0.000	0.000	Mg	0.000	0.001	0.000	0.000	0.000	0.001	0.000	0.000	0.002	0.000
Ca	0.834	0.797	0.721	0.754	0.722	0.750	0.738	0.773	0.710	0.776	Ca	0.452	0.443	0.454	0.446	0.447	0.454	0.459	0.453	0.464	0.456
Sr	0.000	0.000	0.000	0.000	0.000	0.000	0.000	0.000	0.000	0.000	Sr	0.000	0.000	0.000	0.000	0.000	0.000	0.000	0.000	0.000	0.000
Ba	0.000	0.003	0.000	0.001	0.006	0.000	0.002	0.001	0.000	0.000	Ba	0.006	0.001	0.000	0.002	0.002	0.000	0.001	0.000	0.006	0.002
Na	0.149	0.170	0.222	0.203	0.238	0.211	0.217	0.179	0.250	0.190	Na	0.529	0.516	0.529	0.529	0.543	0.524	0.530	0.516	0.521	0.538
K	0.003	0.004	0.003	0.002	0.005	0.003	0.002	0.003	0.003	0.002	K	0.006	0.008	0.007	0.007	0.005	0.008	0.006	0.008	0.006	0.007
Rb	0.004	0.002	0.002	0.002	0.004	0.003	0.002	0.005	0.003	0.003	Rb	0.001	0.002	0.004	0.002	0.005	0.000	0.003	0.001	0.004	0.004
Sum Cat#	5.00	5.00	4.97	4.99	4.99	4.99	4.98	4.99	4.99	4.99	Sum Cat#	5.00	4.98	5.00	4.99	5.00	4.99	5.00	4.99	5.01	5.01
Ab	15.0	17.4	23.4	21.1	24.4	21.8	22.6	18.6	25.9	19.6	Ab	53.3	53.2	53.2	53.7	54.2	53.1	53.0	52.8	52.1	53.4
An	84.3	81.7	76.0	78.3	74.0	77.5	76.8	80.5	73.5	79.9	An	45.5	45.7	45.7	45.2	44.6	46.1	46.0	46.3	46.4	45.2
Or	0.3	0.4	0.4	0.2	0.5	0.4	0.2	0.3	0.3	0.2	Or	0.6	0.9	0.7	0.7	0.5	0.8	0.6	0.8	0.6	0.7

Feldspar Analyses by sample (recalculated to 100%), cations based on 8 (O) Oxygens.

Ultrapotassic 398a																					
Label	Ksp1	Ksp1	KSp2	Ksp3	Ksp3	Ksp4	Ksp4	Ksp4	Ksp5	Ksp5	Ksp6	Pl1	Pl1	Pl2	Pl2	Pl3	Pl3	Pl4	Pl4	Pl5	Pl5
	C	R	C	C	R	C	R	R	C	R	C	C	R	C	R	C	R	C	R	C	R
SiO2	60.45	60.36	60.89	61.01	60.80	60.75	60.38	60.53	61.12	60.18	61.13	56.08	55.30	56.26	56.26	56.27	55.60	56.40	55.49	56.18	55.24
Al2O3	20.14	20.24	19.88	19.91	19.87	19.78	20.14	19.81	19.80	20.43	20.00	28.40	28.04	28.32	28.43	28.23	28.55	28.20	28.49	28.08	28.51
Fe2O3	0.06	0.13	0.05	0.00	0.10	0.04	0.07	0.04	0.02	0.10	0.00	0.10	0.04	0.00	0.08	0.10	0.03	0.09	0.03	0.11	0.16
MgO	0.03	0.00	0.01	0.00	0.01	0.00	0.00	0.00	0.00	0.00	0.01	0.00	0.02	0.02	0.01	0.00	0.02	0.00	0.03	0.03	0.00
CaO	0.03	0.05	0.01	0.00	0.00	0.04	0.02	0.01	0.61	0.00	0.00	9.30	10.37	9.42	9.52	9.27	9.95	9.18	9.96	9.54	9.96
SrO	0.00	0.00	0.00	0.00	0.00	0.00	0.00	0.00	0.00	0.00	0.00	0.00	0.00	0.00	0.00	0.00	0.00	0.00	0.00	0.00	0.00
BaO	5.63	6.22	5.47	5.52	5.60	5.52	5.67	6.32	5.15	5.87	5.31	0.00	0.12	0.06	0.00	0.06	0.02	0.06	0.00	0.12	0.33
Na2O	1.76	1.78	1.58	1.72	1.62	1.80	1.81	1.68	1.81	1.78	1.66	5.94	5.80	5.70	5.55	5.77	5.60	5.87	5.79	5.73	5.61
K2O	11.91	11.21	12.10	11.83	11.98	12.07	11.91	11.61	11.49	11.64	11.89	0.17	0.18	0.17	0.16	0.16	0.13	0.14	0.14	0.15	0.17
Rb2O	0.00	0.00	0.00	0.00	0.00	0.00	0.00	0.00	0.00	0.00	0.00	0.01	0.13	0.06	0.01	0.12	0.09	0.06	0.09	0.07	0.00
Sum Ox%	100	100	100	100	100	100	100	100	100	100	100	100	100	100	100	100	100	100	100	100	100
Si	2.876	2.874	2.893	2.895	2.891	2.890	2.875	2.888	2.893	2.865	2.895	2.516	2.497	2.523	2.521	2.525	2.499	2.529	2.497	2.524	2.491
Al/Al IV	1.129	1.136	1.113	1.114	1.113	1.109	1.130	1.114	1.105	1.146	1.116	1.502	1.492	1.497	1.501	1.493	1.513	1.490	1.510	1.486	1.515
Al VI	0.000	0.000	0.000	0.000	0.000	0.000	0.000	0.000	0.000	0.000	0.000	0.000	0.000	0.000	0.000	0.000	0.000	0.000	0.000	0.000	0.000
Fe3+	0.002	0.005	0.002	0.000	0.004	0.002	0.002	0.002	0.001	0.004	0.000	0.003	0.001	0.000	0.003	0.004	0.001	0.003	0.001	0.004	0.006
Mg	0.002	0.000	0.001	0.000	0.001	0.000	0.000	0.000	0.000	0.000	0.001	0.000	0.002	0.001	0.000	0.000	0.001	0.000	0.002	0.002	0.000
Ca	0.002	0.002	0.000	0.000	0.000	0.002	0.001	0.001	0.031	0.000	0.000	0.447	0.502	0.453	0.457	0.446	0.479	0.441	0.480	0.459	0.481
Sr	0.000	0.000	0.000	0.000	0.000	0.000	0.000	0.000	0.000	0.000	0.000	0.000	0.000	0.000	0.000	0.000	0.000	0.000	0.000	0.000	0.000
Ba	0.105	0.116	0.102	0.103	0.104	0.103	0.106	0.118	0.096	0.109	0.099	0.000	0.002	0.001	0.000	0.001	0.000	0.001	0.000	0.002	0.006
Na	0.162	0.164	0.145	0.159	0.150	0.166	0.167	0.156	0.166	0.164	0.152	0.516	0.507	0.496	0.483	0.502	0.488	0.511	0.505	0.499	0.491
K	0.722	0.681	0.733	0.716	0.726	0.732	0.724	0.707	0.694	0.707	0.719	0.010	0.010	0.010	0.009	0.009	0.008	0.008	0.008	0.009	0.010
Rb	0.000	0.000	0.000	0.000	0.000	0.000	0.000	0.000	0.000	0.000	0.000	0.000	0.004	0.002	0.000	0.003	0.003	0.002	0.003	0.002	0.000
Sum Cat#	5.00	4.98	4.99	4.99	4.99	5.00	5.01	4.99	4.98	5.00	4.98	5.00	5.02	4.98	4.97	4.98	4.99	4.99	5.01	4.99	5.00
Ab	16.4	17.0	14.8	16.2	15.3	16.6	16.7	15.9	16.8	16.8	15.7	53.1	49.5	51.6	50.9	52.2	49.9	53.0	50.7	51.4	49.7
An	0.2	0.2	0.0	0.0	0.0	0.2	0.1	0.1	3.1	0.0	0.0	45.9	49.0	47.1	48.1	46.4	49.0	45.8	48.2	47.3	48.7
Or	72.9	70.7	74.8	73.3	74.1	73.0	72.6	72.0	70.4	72.1	74.1	1.0	1.0	1.0	0.9	1.0	0.8	0.8	0.8	0.9	1.0

Feldspar Analyses by sample (recalculated to 100%), cations based on 8 (O) Oxygens.

Ultrapotassic 398a (Con't)						Ultrapotassic 403											
Label	Pl6	Pl6	Pl7	Pl7	Pl8	Label	Ksp1	Ksp1	Ksp2	Ksp2	Ksp3	Ksp3	Ksp4	Ksp4	Ksp5	Ksp5	Ksp6	Ksp6
	C	R	C	R	C		C	R	C	R	C	R	C	R	C	R	C	R
SiO2	55.96	55.45	55.70	55.14	44.51	SiO2	63.71	63.07	63.97	63.93	63.74	63.74	63.07	63.37	63.19	62.11	63.58	63.13
Al2O3	28.37	28.48	28.61	28.59	35.22	Al2O3	18.40	18.98	18.50	18.64	18.54	18.66	18.98	18.74	18.90	19.06	18.76	18.84
Fe2O3	0.03	0.19	0.08	0.06	0.52	Fe2O3	0.01	0.06	0.10	0.13	0.06	0.06	0.01	0.15	0.00	0.00	0.06	0.00
MgO	0.00	0.03	0.00	0.00	0.04	MgO	0	0	0	0	0	0	0	0	0	0	0	0
CaO	9.83	9.66	9.64	10.08	19.01	CaO	0.88	0.85	0.79	0.86	0.84	0.78	0.84	0.85	0.72	1.26	0.58	0.94
SrO	0.00	0.00	0.00	0.00	0.00	SrO	0.00	0.11	0.00	0.00	0.00	0.00	0.05	0.00	0.00	0.21	0.00	0.00
BaO	0.00	0.32	0.06	0.00	0.13	BaO	1.27	1.60	1.17	1.01	1.48	1.35	1.67	1.10	1.57	2.48	1.27	1.56
Na2O	5.63	5.59	5.66	5.86	0.49	Na2O	0.66	0.60	0.51	0.56	0.54	0.60	0.61	0.65	0.61	0.68	0.72	0.63
K2O	0.17	0.19	0.14	0.14	0.01	K2O	15.07	14.74	14.97	14.86	14.81	14.82	14.76	15.14	15.03	14.22	15.02	14.89
Rb2O	0.03	0.08	0.09	0.12	0.07	Rb2O	0	0	0	0	0	0	0	0	0	0	0	0
Sum Ox%	100	100	100	100	100	Sum Ox%	100	100	100	100	100	100	100	100	100	100	100	100
Si	2.512	2.498	2.503	2.485	2.060	Si	2.969	2.945	2.974	2.968	2.969	2.966	2.945	2.953	2.950	2.921	2.961	2.948
Al/Al IV	1.501	1.513	1.515	1.519	1.921	Al/Al IV	1.011	1.044	1.013	1.020	1.018	1.023	1.045	1.029	1.040	1.057	1.030	1.037
Al VI	0.000	0.000	0.000	0.000	0.000	Al VI	0.000	0.000	0.000	0.000	0.000	0.000	0.000	0.000	0.000	0.000	0.000	0.000
Fe3+	0.001	0.007	0.003	0.002	0.018	Fe3+	0.000	0.002	0.003	0.004	0.002	0.002	0.000	0.005	0.000	0.000	0.002	0.000
	0.000	0.002	0.000	0.000	0.003													
Ca	0.473	0.466	0.464	0.487	0.943	Ca	0.044	0.042	0.040	0.043	0.042	0.039	0.042	0.042	0.036	0.063	0.029	0.047
Sr	0.000	0.000	0.000	0.000	0.000	Sr	0.000	0.003	0.000	0.000	0.000	0.000	0.001	0.000	0.000	0.006	0.000	0.000
Ba	0.000	0.006	0.001	0.000	0.002	Ba	0.023	0.029	0.021	0.018	0.027	0.025	0.031	0.020	0.029	0.046	0.023	0.029
Na	0.490	0.488	0.493	0.513	0.044	Na	0.060	0.054	0.046	0.051	0.048	0.055	0.056	0.059	0.055	0.062	0.065	0.057
K	0.010	0.011	0.008	0.008	0.000	K	0.896	0.878	0.888	0.880	0.880	0.880	0.879	0.900	0.895	0.853	0.892	0.887
	0.001	0.002	0.003	0.004	0.002													
Sum Cat#	4.99	4.99	4.99	5.02	4.99	Sum Cat#	5.00	5.00	4.99	4.99	4.99	4.99	5.00	5.01	5.01	5.01	5.00	5.01
Ab	50.3	50.1	50.9	50.7	4.4	Ab	5.9	5.4	4.6	5.1	4.9	5.5	5.5	5.7	5.4	6.0	6.4	5.6
An	48.6	47.9	47.9	48.1	95.1	An	4.3	4.2	4.0	4.3	4.2	3.9	4.1	4.1	3.5	6.2	2.9	4.6
Or	1.0	1.1	0.9	0.8	0.0	Or	87.5	87.3	89.3	88.7	88.3	88.2	87.2	88.1	88.2	82.9	88.4	86.9

Pyroxene Analyses by sample (recalculated to 100%), cations based on 6 (O) Oxygens.

Terrane/Sample	GT 2000x							GT 288d1			GT 486d						
Label	Cpx1	Cpx2	Cpx5	Cpx6	Cpx7	Cpx8		Cpx2	Cpx3	Label	Cpx1	Cpx2	Cpx3	Cpx4	Cpx5	Cpx6	Cpx7
	C	C	R	C	C	R	Label	R	C		R	C	C	C	C	C	C
SiO2	53.63	53.08	53.45	53.94	53.14	53.55	SiO2	52.89	53.82	SiO2	52.17	52.44	52.18	52.40	52.42	52.20	52.33
TiO2	0.06	0.10	0.11	0.06	0.10	0.07	TiO2	0.11	0.04	TiO2	0.15	0.17	0.19	0.12	0.15	0.16	0.15
Al2O3	1.70	2.42	1.81	1.35	1.89	1.73	Al2O3	2.77	1.64	Al2O3	2.94	3.10	3.39	2.79	2.84	3.27	3.21
Cr2O3	0.16	0.08	0.05	0.07	0.13	0.08	Cr2O3	0.05	0.01	Cr2O3	0.08	0.04	0.08	0.02	0.03	0.02	0.00
Fe2O3	0.00	0.00	0.00	0.00	0.00	0.00	Fe2O3	0.00	0.00	Fe2O3	0.00	0.00	0.00	0.00	0.00	0.00	0.00
FeO	7.11	7.64	6.79	6.55	6.97	7.21	FeO	7.46	6.61	FeO	8.60	8.65	9.18	8.49	8.83	8.76	8.91
MnO	0.39	0.29	0.35	0.31	0.27	0.31	MnO	0.36	0.32	MnO	0.40	0.35	0.42	0.41	0.37	0.35	0.36
MgO	13.95	13.68	14.38	14.51	14.21	14.10	MgO	13.93	14.73	MgO	12.99	13.11	12.61	13.09	13.04	12.97	12.96
CaO	22.99	22.72	23.05	23.21	23.29	22.94	CaO	22.42	22.85	CaO	22.66	22.15	21.94	22.66	22.31	22.26	22.09
Sum Ox%	100	100	100	100	100	100	Sum Ox%	100	100	Sum Ox%	100	100	100	100	100	100	100
Si	1.983	1.965	1.974	1.989	1.967	1.980	Si	1.956	1.983	Si	1.944	1.949	1.944	1.951	1.952	1.942	1.947
Ti	0.002	0.003	0.003	0.002	0.003	0.002	Ti	0.003	0.001	Ti	0.004	0.005	0.005	0.003	0.004	0.004	0.004
Al/Al IV	0.017	0.035	0.026	0.011	0.033	0.020	Al/Al IV	0.044	0.017	Al/Al IV	0.056	0.051	0.056	0.049	0.048	0.058	0.053
Al VI	0.057	0.071	0.053	0.048	0.049	0.056	Al VI	0.077	0.054	Al VI	0.073	0.084	0.092	0.073	0.076	0.086	0.087
Cr	0.005	0.002	0.001	0.002	0.004	0.002	Cr	0.002	0.000	Cr	0.003	0.001	0.003	0.001	0.001	0.001	0.000
Fe3+	0.000	0.000	0.000	0.000	0.000	0.000	Fe3+	0.000	0.000	Fe3+	0.000	0.000	0.000	0.000	0.000	0.000	0.000
Fe2+	0.220	0.237	0.210	0.202	0.216	0.223	Fe2+	0.231	0.204	Fe2+	0.268	0.269	0.286	0.264	0.275	0.273	0.277
Mn2+	0.012	0.009	0.011	0.010	0.008	0.010	Mn2+	0.011	0.010	Mn2+	0.013	0.011	0.013	0.013	0.012	0.011	0.011
Mg	0.769	0.755	0.792	0.798	0.784	0.777	Mg	0.768	0.809	Mg	0.721	0.726	0.700	0.726	0.724	0.719	0.719
Ca	0.911	0.901	0.912	0.917	0.924	0.909	Ca	0.889	0.902	Ca	0.905	0.882	0.876	0.904	0.890	0.887	0.880
Sum Cat#	3.98	3.98	3.98	3.98	3.99	3.98	Sum Cat#	3.98	3.98	Sum Cat#	3.99	3.98	3.98	3.98	3.98	3.98	3.98
Wo(Ca)	47.95	47.61	47.66	47.86	48.02	47.61	Wo(Ca)	47.08	47.12	Wo(Ca)	47.76	46.98	47.03	47.71	47.12	47.21	46.92
En(Mg)	40.47	39.88	41.38	41.61	40.76	40.72	En(Mg)	40.69	42.25	En(Mg)	38.08	38.70	37.62	38.35	38.32	38.28	38.30
Fs(Fe2+)	11.57	12.51	10.96	10.54	11.21	11.67	Fs(Fe2+)	12.23	10.63	Fs(Fe2+)	14.16	14.32	15.36	13.95	14.56	14.51	14.78
XMg	0.78	0.76	0.79	0.80	0.78	0.78	XMg	0.77	0.80	XMg	0.73	0.73	0.71	0.73	0.73	0.73	0.72

Pyroxene Analyses by sample (recalculated to 100%), cations based on 6 (O) Oxygens.

	GT 474d																	
Label	Cpx1	Cpx2	*Cpx2	Cpx3	Cpx3	Cpx4	*Cpx4	*Cpx5	Cpx5	Cpx6	Cpx6	Cpx6	Cpx6	Cpx6	Cpx7	Cpx8	*Cpx9	*Cpx9
	C	C	C	C	R	R	R	R	R	C	C	R	C	R	C	C	R	R
SiO2	53.05	53.14	53.11	52.89	53.25	53.16	52.89	53.30	53.58	53.35	53.32	52.76	52.79	52.75	52.97	52.89	52.83	52.85
TiO2	0.21	0.18	0.23	0.21	0.19	0.20	0.15	0.15	0.15	0.15	0.19	0.22	0.17	0.19	0.19	0.18	0.22	0.22
Al2O3	2.27	2.19	2.20	2.32	2.07	2.13	2.12	2.01	2.07	2.16	2.26	2.20	2.21	2.33	2.22	2.05	2.11	2.21
Cr2O3	0.03	0.04	0.00	0.01	0.00	0.00	0.02	0.00	0.01	0.04	0.01	0.02	0.02	0.00	0.00	0.01	0.03	0.00
Fe2O3	0.00	0.00	0.00	0.00	0.00	0.00	0.00	0.00	0.00	0.00	0.00	0.00	0.00	0.00	0.00	0.00	0.00	0.00
FeO	11.15	10.87	10.71	10.80	10.51	10.63	12.40	10.25	10.22	10.49	9.99	11.04	10.38	10.94	10.71	10.26	10.68	11.23
MnO	0.53	0.46	0.50	0.51	0.54	0.51	0.61	0.53	0.55	0.58	0.55	0.54	0.64	0.54	0.55	0.61	0.55	0.52
MgO	12.34	12.26	12.31	12.13	12.47	12.25	12.61	12.67	12.41	12.39	12.37	12.49	12.57	12.14	12.19	12.81	12.57	12.28
CaO	20.42	20.86	20.94	21.13	20.97	21.10	19.20	21.07	21.02	20.83	21.33	20.72	21.21	21.11	21.17	21.21	21.03	20.69
Sum Ox%	100	100	100	100	100	100	100	100	100	100	100	100	100	100	100	100	100	100
Si	1.983	1.986	1.984	1.979	1.987	1.986	1.983	1.988	1.996	1.990	1.987	1.975	1.974	1.975	1.981	1.976	1.976	1.979
Ti	0.006	0.005	0.006	0.006	0.005	0.006	0.004	0.004	0.004	0.004	0.005	0.006	0.005	0.005	0.005	0.005	0.006	0.006
Al/Al IV	0.017	0.014	0.016	0.021	0.013	0.014	0.017	0.012	0.004	0.010	0.013	0.025	0.026	0.025	0.019	0.024	0.024	0.021
Al VI	0.083	0.082	0.081	0.081	0.079	0.080	0.076	0.076	0.086	0.085	0.086	0.072	0.072	0.078	0.079	0.067	0.069	0.077
Cr	0.001	0.001	0.000	0.000	0.000	0.000	0.001	0.000	0.000	0.001	0.000	0.001	0.001	0.000	0.000	0.000	0.001	0.000
Fe3+	0.000	0.000	0.000	0.000	0.000	0.000	0.000	0.000	0.000	0.000	0.000	0.000	0.000	0.000	0.000	0.000	0.000	0.000
Fe2+	0.349	0.340	0.335	0.338	0.328	0.332	0.389	0.320	0.318	0.327	0.311	0.346	0.325	0.343	0.335	0.321	0.334	0.352
Mn2+	0.017	0.015	0.016	0.016	0.017	0.016	0.019	0.017	0.017	0.018	0.017	0.017	0.020	0.017	0.017	0.019	0.017	0.017
Mg	0.688	0.683	0.685	0.676	0.694	0.683	0.705	0.704	0.689	0.689	0.687	0.697	0.700	0.678	0.680	0.713	0.701	0.686
Ca	0.818	0.835	0.838	0.847	0.838	0.845	0.771	0.842	0.839	0.833	0.852	0.831	0.850	0.847	0.848	0.849	0.843	0.830
Sum Cat#	3.96	3.96	3.96	3.96	3.96	3.96	3.97	3.96	3.96	3.96	3.96	3.97	3.97	3.97	3.97	3.97	3.97	3.97
Wo(Ca)	44.11	44.96	45.10	45.51	45.07	45.42	41.36	45.12	45.43	45.04	46.04	44.35	45.32	45.35	45.52	45.09	44.89	44.45
En(Mg)	37.09	36.75	36.89	36.33	37.30	36.70	37.80	37.75	37.34	37.26	37.14	37.19	37.35	36.30	36.49	37.88	37.32	36.72
Fs(Fe2+)	18.80	18.29	18.01	18.16	17.63	17.87	20.84	17.13	17.23	17.70	16.82	18.46	17.32	18.35	17.99	17.03	17.79	18.83
XMg	0.66	0.67	0.67	0.67	0.68	0.67	0.65	0.69	0.68	0.68	0.69	0.67	0.68	0.66	0.67	0.69	0.68	0.66

Pyroxene Analyses by sample (recalculated to 100%), cations based on 6 (O) Oxygens.

	GT 481d																
Label	Cpx1 C	Cpx1 R	Cpx1 R	Cpx2 C	Cpx2 R	Cpx3 C	Cpx3 R	Cpx4 R	Cpx4 C	Cpx4 C	Cpx5 R	Cpx5 C	Cpx3 C	Cpx3 C	Cpx6 C	Cpx6 R	Cpx6 C
SiO2	51.08	51.62	53.21	51.41	51.54	52.03	51.77	51.81	51.22	51.45	52.81	53.05	51.66	52.26	392.90	52.71	52.68
TiO2	0.32	0.26	0.09	0.31	0.27	0.20	0.21	0.24	0.30	0.25	0.11	0.09	0.22	0.15	0.76	0.08	0.10
Al2O3	4.02	3.57	1.58	3.66	3.54	2.98	3.17	3.45	3.76	3.78	2.05	1.75	3.02	2.49	13.05	1.75	1.89
Cr2O3	0.00	0.01	0.00	0.01	0.00	0.00	0.00	0.00	0.00	0.02	0.01	0.00	0.05	0.00	0.00	0.04	0.02
Fe2O3	0.00	0.00	0.00	0.00	0.00	0.00	0.00	0.00	0.00	0.00	0.00	0.00	0.00	0.00	0.00	0.00	0.00
FeO	10.47	10.33	8.93	10.73	10.47	10.04	10.42	10.38	10.57	10.63	9.54	9.22	9.95	9.67	67.79	9.28	9.63
MnO	0.42	0.46	0.44	0.50	0.44	0.44	0.45	0.45	0.46	0.49	0.43	0.46	0.42	0.46	3.28	0.38	0.48
MgO	11.91	11.99	13.65	12.23	12.33	12.50	12.56	12.41	12.06	11.89	13.29	13.46	12.54	12.65	100.00	13.53	13.35
CaO	21.78	21.76	22.11	21.14	21.42	21.81	21.41	21.27	21.64	21.50	21.76	21.97	22.13	22.31	100.00	22.24	21.85
Sum Ox%	100	100	100	100	100	100	100	100	100	100	100	100	100	100	678	100	100
Si	1.916	1.934	1.980	1.927	1.930	1.946	1.939	1.938	1.922	1.929	1.970	1.977	1.936	1.955	1.978	1.967	1.968
Ti	0.009	0.007	0.003	0.009	0.008	0.006	0.006	0.007	0.008	0.007	0.003	0.003	0.006	0.004	0.003	0.002	0.003
Al/Al IV	0.084	0.066	0.020	0.073	0.070	0.054	0.061	0.062	0.078	0.071	0.030	0.023	0.064	0.045	0.022	0.033	0.032
Al VI	0.094	0.091	0.050	0.089	0.086	0.078	0.079	0.090	0.088	0.096	0.060	0.053	0.069	0.065	0.056	0.044	0.051
Cr	0.000	0.000	0.000	0.000	0.000	0.000	0.000	0.000	0.000	0.001	0.000	0.000	0.002	0.000	0.000	0.001	0.000
Fe3+	0.000	0.000	0.000	0.000	0.000	0.000	0.000	0.000	0.000	0.000	0.000	0.000	0.000	0.000	0.000	0.000	0.000
Fe2+	0.328	0.324	0.278	0.336	0.328	0.314	0.327	0.325	0.332	0.333	0.298	0.287	0.312	0.303	0.285	0.290	0.300
Mn2+	0.013	0.015	0.014	0.016	0.014	0.014	0.014	0.014	0.015	0.015	0.013	0.014	0.013	0.015	0.014	0.012	0.015
Mg	0.666	0.670	0.757	0.684	0.688	0.697	0.701	0.692	0.675	0.664	0.739	0.748	0.700	0.705	0.750	0.752	0.743
Ca	0.875	0.874	0.882	0.849	0.860	0.874	0.859	0.852	0.870	0.864	0.869	0.877	0.889	0.894	0.872	0.889	0.875
Sum Cat#	3.99	3.98	3.98	3.98	3.98	3.98	3.99	3.98	3.99	3.98	3.98	3.98	3.99	3.99	3.98	3.99	3.99
Wo(Ca)	46.83	46.79	46.01	45.43	45.82	46.36	45.53	45.61	46.36	46.40	45.62	45.87	46.75	47.02	45.71	46.05	45.60
En(Mg)	35.60	35.88	39.49	36.58	36.70	36.97	37.16	37.03	35.96	35.69	38.76	39.11	36.84	37.07	39.33	38.96	38.73
Fs(Fe2+)	17.57	17.33	14.50	17.99	17.49	16.67	17.31	17.36	17.68	17.90	15.62	15.02	16.40	15.92	14.96	15.00	15.67
XMg	0.67	0.67	0.73	0.67	0.68	0.69	0.68	0.68	0.67	0.67	0.71	0.72	0.69	0.70	0.72	0.72	0.71

Pyroxene Analyses by sample (recalculated to 100%), cations based on 6 (O) Oxygens.

	CD 209-1																		
Label	Opx1	Opx1	Opx2	Opx4	Opx4	Opx5	Opx5	Cpx1	Cpx1	Cpx2	Cpx2	Cpx3	Cpx3	Cpx3	Cpx3	Cpx4	Cpx4	Cpx5
	C	R	R	C	R	C	R	C	C	C	C	C	R	R	R	C	C	C
SiO2	50.41	50.43	51.58	51.18	51.61	51.19	51.19	52.61	52.15	52.66	53.21	52.37	51.91	52.67	52.50	52.30	52.78	53.00
TiO2	0.09	0.11	0.06	0.12	0.11	0.10	0.05	0.12	0.29	0.18	0.14	0.21	0.41	0.18	0.29	0.08	0.24	0.10
Al2O3	0.74	0.89	0.78	0.88	0.80	0.91	0.84	0.84	1.52	1.16	0.81	1.25	2.14	1.41	1.75	0.90	1.28	0.74
Cr2O3	0.07	0.06	0.07	0.04	0.09	0.10	0.04	0.12	0.19	0.09	0.11	0.08	0.07	0.00	0.09	0.09	0.12	0.11
Fe2O3(c)	3.13	3.08	0.43	1.35	0.45	1.37	1.57	0.23	0.00	0.00	0.00	0.00	0.00	0.00	0.00	0.82	0.00	0.00
FeO(c)	25.72	25.39	27.35	26.33	27.04	26.21	26.33	10.35	10.27	10.33	9.77	10.47	11.73	10.52	10.79	9.32	10.33	10.47
MnO	0.48	0.51	0.55	0.63	0.45	0.54	0.57	0.21	0.24	0.20	0.26	0.31	0.28	0.32	0.35	0.27	0.20	0.22
MgO	18.66	18.91	18.52	18.80	18.77	18.90	18.89	13.86	13.29	13.31	13.45	12.88	13.12	13.16	12.75	13.21	13.15	12.96
CaO	0.70	0.63	0.65	0.66	0.68	0.67	0.52	21.66	22.06	22.08	22.26	22.45	20.35	21.74	21.47	22.99	21.93	22.39
Sum Ox%	100	100	100	100	100	100	100	100	100	100	100	100	100	100	100	100	100	100
Si	1.934	1.931	1.973	1.956	1.971	1.955	1.957	1.973	1.957	1.974	1.989	1.969	1.950	1.974	1.969	1.965	1.977	1.989
Ti	0.003	0.003	0.002	0.004	0.003	0.003	0.001	0.003	0.008	0.005	0.004	0.006	0.012	0.005	0.008	0.002	0.007	0.003
Al/Al IV	0.033	0.040	0.027	0.040	0.029	0.041	0.038	0.027	0.043	0.026	0.011	0.031	0.050	0.026	0.031	0.035	0.023	0.011
Al VI	0.000	0.000	0.008	0.000	0.007	0.000	0.000	0.010	0.025	0.025	0.025	0.024	0.045	0.036	0.047	0.004	0.033	0.022
Cr	0.002	0.002	0.002	0.001	0.003	0.003	0.001	0.003	0.005	0.003	0.003	0.003	0.002	0.000	0.003	0.003	0.004	0.003
Fe3+	0.090	0.089	0.013	0.039	0.013	0.039	0.045	0.006	0.000	0.000	0.000	0.000	0.000	0.000	0.000	0.023	0.000	0.000
Fe2+	0.825	0.813	0.875	0.842	0.864	0.837	0.842	0.325	0.322	0.324	0.305	0.329	0.369	0.330	0.338	0.293	0.323	0.329
Mn2+	0.016	0.016	0.018	0.020	0.015	0.017	0.019	0.007	0.008	0.006	0.008	0.010	0.009	0.010	0.011	0.009	0.006	0.007
Mg	1.067	1.079	1.056	1.071	1.068	1.076	1.076	0.774	0.743	0.744	0.750	0.722	0.734	0.735	0.713	0.740	0.734	0.725
Ca	0.029	0.026	0.027	0.027	0.028	0.027	0.022	0.871	0.887	0.887	0.892	0.904	0.819	0.873	0.863	0.926	0.880	0.900
Sum Cat#	4.000	4.000	4.000	4.000	4.000	4.000	4.000	4.000	3.998	3.994	3.987	3.997	3.990	3.990	3.983	4.000	3.987	3.990
Wo(Ca)	1.51	1.35	1.37	1.39	1.42	1.41	1.11	44.20	45.42	45.37	45.81	46.26	42.62	45.05	45.08	47.26	45.43	46.08
En(Mg)	55.55	56.26	53.94	55.22	54.50	55.45	55.49	39.32	38.08	38.05	38.51	36.91	38.20	37.94	37.25	37.79	37.87	37.10
Fs(Fe2+)	42.94	42.39	44.69	43.39	44.08	43.14	43.40	16.48	16.51	16.58	15.68	16.83	19.18	17.01	17.67	14.96	16.70	16.82
XMg	0.56	0.57	0.55	0.56	0.55	0.56	0.56	0.71	0.70	0.70	0.71	0.69	0.67	0.69	0.68	0.72	0.69	0.69

Pyroxene Analyses by sample (recalculated to 100%), cations based on 6 (O) Oxygens.

	CD 457					CD 430							
Label	Opx2	Opx3	Opx3	Opx5	Label	Opx5	Cpx1	Cpx2	Cpx2	Cpx3	Cpx4	Cpx4	Cpx5
	R	C	R	C		C	C	C	R	C	C	R	R
SiO2	49.48	49.68	49.93	49.66	SiO2	51.75	49.76	50.75	50.41	50.40	50.04	50.52	50.57
TiO2	0.14	0.07	0.08	0.07	TiO2	0.17	0.62	0.53	0.65	0.54	0.63	0.61	0.56
Al2O3	0.72	0.60	0.65	0.76	Al2O3	1.76	4.24	3.70	4.12	4.15	4.29	4.27	3.90
Cr2O3	0.08	0.00	0.00	0.04	Cr2O3	0.01	0.13	0.04	0.03	0.07	0.00	0.00	0.05
Fe2O3(c)	1.47	1.32	0.59	0.96	Fe2O3(c)	1.29	1.37	0.29	0.23	0.06	0.69	0.00	0.15
FeO(c)	32.61	32.98	33.63	33.47	FeO(c)	22.31	8.28	8.72	8.81	10.20	9.54	9.40	9.29
MnO	0.81	0.62	0.62	0.69	MnO	0.64	0.19	0.18	0.26	0.26	0.28	0.25	0.29
MgO	14.05	13.94	13.84	13.73	MgO	21.61	12.42	12.81	12.60	12.59	12.63	12.36	12.60
CaO	0.64	0.80	0.67	0.64	CaO	0.44	22.99	22.99	22.89	21.74	21.90	22.57	22.59
Sum Ox%	100	100	100	100	Sum Ox%	100	100	100	100	100	100	100	100
Si	1.956	1.964	1.974	1.965	Si	1.938	1.867	1.899	1.887	1.891	1.878	1.892	1.895
Ti	0.004	0.002	0.003	0.002	Ti	0.005	0.018	0.015	0.018	0.015	0.018	0.017	0.016
Al/Al IV	0.033	0.028	0.026	0.035	Al/Al IV	0.062	0.133	0.101	0.113	0.109	0.122	0.108	0.105
Al VI	0.000	0.000	0.004	0.001	Al VI	0.015	0.055	0.062	0.069	0.075	0.068	0.080	0.067
Cr	0.002	0.000	0.000	0.001	Cr	0.000	0.004	0.001	0.001	0.002	0.000	0.000	0.002
Fe3+	0.044	0.039	0.017	0.029	Fe3+	0.036	0.039	0.008	0.006	0.002	0.020	0.000	0.004
Fe2+	1.078	1.090	1.112	1.108	Fe2+	0.699	0.260	0.273	0.276	0.320	0.299	0.295	0.291
Mn2+	0.027	0.021	0.021	0.023	Mn2+	0.020	0.006	0.005	0.008	0.008	0.009	0.008	0.009
Mg	0.828	0.822	0.816	0.810	Mg	1.206	0.695	0.714	0.703	0.704	0.706	0.690	0.703
Ca	0.027	0.034	0.028	0.027	Ca	0.018	0.924	0.921	0.918	0.874	0.881	0.906	0.907
Sum Cat#	4.000	4.000	4.000	4.000	Sum Cat#	4.000	4.000	4.000	4.000	4.000	4.000	3.996	4.000
Wo(Ca)	1.42	1.74	1.45	1.38	Wo(Ca)	0.93	49.20	48.28	48.40	46.04	46.70	47.92	47.71
En(Mg)	42.82	42.23	41.71	41.65	En(Mg)	62.73	36.97	37.43	37.06	37.11	37.44	36.50	36.99
Fs(Fe2+)	55.76	56.04	56.84	56.97	Fs(Fe2+)	36.34	13.83	14.29	14.55	16.86	15.87	15.58	15.31
XMg	0.43	0.43	0.42	0.42	XMg	0.63	0.73	0.72	0.72	0.69	0.70	0.70	0.71

Pyroxene Analyses by sample (recalculated to 100%), cations based on 6 (O) Oxygens.

	Ultrapotassic 361z																				
Label	Cpx7 C	Cpx1 C	Cpx1 C	Cpx1 C	Cpx1 R	Cpx2 R1	Cpx2 C1	Cpx2 C2	Cpx2 C3	Cpx2 C4	Cpx2 R2	Cpx3 R	Cpx3 C	Cpx3 R	Cpx4 R1	Cpx4 C1	Cpx4 C2	Cpx4 R2	Cpx5 R	Cpx5 C	Cpx5 R
SiO2	52.42	52.55	49.95	52.79	53.00	51.87	52.01	52.05	52.29	52.09	52.00	51.82	51.63	51.82	52.33	52.50	52.83	51.01	52.70	52.66	52.28
TiO2	0.12	0.14	0.26	0.06	0.04	0.24	0.21	0.26	0.25	0.21	0.19	0.18	0.21	0.21	0.21	0.12	0.17	0.23	0.19	0.18	0.26
Al2O3	1.37	1.19	5.50	0.79	0.55	1.34	1.54	1.38	1.42	1.37	1.31	1.38	1.47	1.38	1.26	1.23	1.11	2.78	1.24	1.42	1.44
Cr2O3	0.00	0.00	0.06	0.00	0.05	0.10	0.06	0.00	0.01	0.03	0.02	0.04	0.00	0.03	0.05	0.02	0.00	0.00	0.00	0.00	0.04
Fe2O3(c)	0.00	0.00	0.00	0.00	0.00	0.00	0.00	0.00	0.00	0.00	0.00	0.01	0.07	0.00	0.00	0.00	0.00	0.80	0.00	0.00	0.00
FeO(c)	11.79	11.72	13.14	11.76	11.22	14.10	11.99	12.43	11.73	11.98	12.08	11.56	12.87	12.50	11.80	11.10	10.66	11.88	12.19	11.37	11.58
MnO	0.54	0.53	0.40	0.37	0.42	0.67	0.48	0.53	0.50	0.39	0.44	0.47	0.46	0.48	0.52	0.49	0.49	0.35	0.43	0.43	0.50
MgO	11.59	11.56	11.70	11.64	11.86	11.83	11.65	11.83	11.64	11.60	11.93	11.66	11.92	11.79	12.20	12.23	12.14	13.54	11.77	11.71	11.70
CaO	22.18	22.31	18.99	22.58	22.85	19.84	22.07	21.51	22.17	22.33	22.02	22.89	21.35	21.79	21.63	22.32	22.60	19.39	21.48	22.23	22.17
Sum Ox%	100	100	100	100	100	100	100	100	100	100	100	100	100	100	100	100	100	100	100	100	100
Si	1.981	1.985	1.882	1.995	2.000	1.972	1.968	1.971	1.976	1.972	1.969	1.963	1.960	1.965	1.976	1.978	1.987	1.920	1.989	1.984	1.974
Ti	0.003	0.004	0.007	0.002	0.001	0.007	0.006	0.008	0.007	0.006	0.005	0.005	0.006	0.006	0.006	0.003	0.005	0.006	0.005	0.005	0.008
Al/Al IV	0.019	0.015	0.118	0.005	0.000	0.028	0.032	0.029	0.024	0.028	0.031	0.037	0.040	0.035	0.024	0.022	0.013	0.080	0.011	0.016	0.026
Al VI	0.042	0.038	0.127	0.030	0.024	0.032	0.037	0.032	0.039	0.033	0.027	0.025	0.026	0.027	0.032	0.033	0.036	0.044	0.044	0.047	0.039
Cr	0.000	0.000	0.002	0.000	0.002	0.003	0.002	0.000	0.000	0.001	0.001	0.001	0.000	0.001	0.001	0.001	0.000	0.000	0.000	0.000	0.001
Fe3+	0.000	0.000	0.000	0.000	0.000	0.000	0.000	0.000	0.000	0.000	0.000	0.000	0.002	0.000	0.000	0.000	0.000	0.023	0.000	0.000	0.000
Fe2+	0.373	0.370	0.414	0.372	0.354	0.448	0.379	0.394	0.371	0.380	0.382	0.366	0.409	0.396	0.372	0.350	0.336	0.374	0.385	0.358	0.366
Mn2+	0.017	0.017	0.013	0.012	0.013	0.022	0.015	0.017	0.016	0.012	0.014	0.015	0.015	0.015	0.017	0.016	0.016	0.011	0.014	0.014	0.016
Mg	0.653	0.651	0.657	0.655	0.667	0.670	0.657	0.667	0.656	0.655	0.673	0.658	0.674	0.666	0.686	0.687	0.681	0.759	0.662	0.658	0.659
Ca	0.898	0.903	0.767	0.914	0.924	0.808	0.895	0.873	0.897	0.905	0.893	0.929	0.868	0.885	0.875	0.901	0.911	0.782	0.869	0.898	0.897
Sum Cat#	3.985	3.984	3.987	3.986	3.986	3.990	3.991	3.991	3.986	3.991	3.996	4.000	4.000	3.998	3.990	3.991	3.984	4.000	3.978	3.979	3.985
Wo(Ca)	46.69	46.93	41.70	47.10	47.49	41.94	46.32	45.13	46.64	46.68	45.85	47.56	44.50	45.45	45.25	46.50	47.27	40.82	45.36	46.91	46.68
En(Mg)	33.94	33.82	35.76	33.76	34.30	34.79	34.04	34.52	34.08	33.75	34.53	33.70	34.56	34.21	35.50	35.45	35.32	39.65	34.56	34.37	34.28
Fs(Fe2+)	19.37	19.25	22.54	19.14	18.22	23.26	19.64	20.35	19.28	19.57	19.62	18.74	20.94	20.34	19.26	18.05	17.41	19.53	20.09	18.72	19.04
XMg	0.64	0.64	0.61	0.64	0.65	0.60	0.63	0.63	0.64	0.63	0.64	0.64	0.62	0.63	0.65	0.66	0.67	0.67	0.63	0.65	0.64

Pyroxene Analyses by sample (recalculated to 100%), cations based on 6 (O) Oxygens.

	Ultrapotassic 404																		
Label	Cpx1 R	Cpx1 C	Cpx1 R	Cpx1 C	Cpx1 R	Cpx2 R	Cpx2 R	Cpx2 C	Cpx2 C	Cpx2 R	Cpx2 C	Cpx3 C	Cpx3 R	Cpx3 C	Cpx3 R	Cpx3 C	Cpx3 R	Cpx4 R	Cpx5 R
SiO2	55.22	53.03	52.16	52.41	52.80	52.46	52.56	52.40	52.09	52.73	51.98	52.35	52.25	52.84	52.94	52.56	52.49	52.80	52.51
TiO2	0.27	0.07	0.18	0.16	0.16	0.19	0.22	0.15	0.27	0.09	0.20	0.17	0.19	0.15	0.09	0.16	0.13	0.15	0.27
Al2O3	1.38	0.49	1.17	1.07	1.20	1.08	1.19	1.10	1.39	0.52	1.14	1.03	1.03	0.68	0.68	0.87	0.94	0.89	1.62
Cr2O3	0.02	0.05	0.07	0.00	0.00	0.00	0.01	0.01	0.05	0.05	0.01	0.05	0.03	0.00	0.00	0.00	0.03	0.00	0.07
Fe2O3(c)	0.00	0.00	0.27	0.31	0.00	0.02	0.00	0.00	0.00	0.06	1.00	0.31	0.58	0.00	0.00	0.20	0.23	0.00	0.00
FeO(c)	15.19	10.33	10.65	9.50	10.33	9.83	11.20	10.38	11.72	10.03	9.12	9.80	9.98	9.59	10.60	9.68	9.92	9.87	9.26
MnO	0.58	0.38	0.37	0.31	0.36	0.43	0.28	0.46	0.48	0.40	0.42	0.39	0.31	0.45	0.42	0.39	0.42	0.34	0.35
MgO	16.16	12.96	12.97	13.09	13.68	13.08	13.08	12.74	13.12	12.83	13.02	13.08	13.42	13.33	13.02	13.19	13.22	13.26	14.06
CaO	11.18	22.69	22.16	23.15	21.44	22.89	21.45	22.75	20.86	23.28	23.10	22.82	22.20	22.96	22.25	22.96	22.63	22.70	21.88
Sum Ox%	100	100	100	100	100	100	100	100	100	100	100	100	100	100	100	100	100	100	100
Si	2.038	1.993	1.964	1.967	1.976	1.971	1.975	1.972	1.963	1.984	1.955	1.967	1.963	1.982	1.989	1.973	1.972	1.980	1.959
Ti	0.008	0.002	0.005	0.005	0.005	0.005	0.006	0.004	0.008	0.003	0.006	0.005	0.006	0.004	0.003	0.005	0.004	0.004	0.007
Al/Al IV	0.000	0.007	0.036	0.033	0.024	0.029	0.025	0.028	0.037	0.016	0.045	0.033	0.037	0.018	0.011	0.027	0.028	0.020	0.041
Al VI	0.060	0.014	0.016	0.014	0.030	0.018	0.028	0.021	0.025	0.007	0.005	0.013	0.009	0.012	0.019	0.012	0.013	0.019	0.030
Cr	0.001	0.002	0.002	0.000	0.000	0.000	0.000	0.000	0.001	0.002	0.000	0.001	0.001	0.000	0.000	0.000	0.001	0.000	0.002
Fe3+	0.000	0.000	0.008	0.009	0.000	0.001	0.000	0.000	0.000	0.002	0.028	0.009	0.016	0.000	0.000	0.006	0.006	0.000	0.000
Fe2+	0.469	0.325	0.336	0.298	0.324	0.309	0.352	0.327	0.369	0.316	0.287	0.308	0.314	0.301	0.333	0.304	0.312	0.309	0.289
Mn2+	0.018	0.012	0.012	0.010	0.011	0.014	0.009	0.015	0.015	0.013	0.013	0.012	0.010	0.014	0.013	0.012	0.013	0.011	0.011
Mg	0.889	0.726	0.728	0.733	0.763	0.732	0.733	0.715	0.737	0.719	0.729	0.733	0.752	0.745	0.729	0.738	0.740	0.741	0.782
Ca	0.442	0.913	0.894	0.931	0.860	0.921	0.863	0.917	0.842	0.939	0.931	0.919	0.893	0.922	0.896	0.923	0.911	0.912	0.875
Sum Cat#	3.924	3.994	4.000	4.000	3.992	4.000	3.992	3.999	3.998	4.000	4.000	4.000	4.000	3.999	3.993	4.000	4.000	3.996	3.997
Wo(Ca)	24.56	46.50	45.67	47.45	44.17	46.95	44.32	46.83	43.23	47.56	47.81	46.89	45.62	46.86	45.74	46.98	46.41	46.48	44.95
En(Mg)	49.40	36.96	37.19	37.34	39.21	37.31	37.61	36.50	37.81	36.45	37.47	37.39	38.38	37.86	37.26	37.55	37.71	37.76	40.19
Fs(Fe2+)	26.04	16.54	17.14	15.21	16.62	15.74	18.07	16.68	18.96	15.99	14.72	15.72	16.01	15.28	17.00	15.48	15.88	15.77	14.85
XMg	0.66	0.69	0.69	0.71	0.70	0.70	0.68	0.69	0.67	0.70	0.72	0.70	0.71	0.71	0.69	0.71	0.70	0.71	0.73

Pyroxene Analyses by sample (recalculated to 100%), cations based on 6 (O) Oxygens.

Ultrapotassic 408																					
Label	Opx1 R	Opx1 C	Opx1 C	Opx2 C	Opx2 C	Opx2 R	Opx3 R	Opx3 C	Opx3 R	Opx3 C	Opx4 R	Opx4 C	Opx4 C	Cpx1 R	Cpx1 C	Cpx1 C	Cpx1 R	Cpx2 R	Cpx2 C	Cpx2 R	Cpx2 C
SiO2	50.60	50.22	50.59	50.50	50.78	50.23	50.07	50.21	50.14	49.94	49.96	50.57	50.56	51.89	51.95	51.92	52.03	52.34	52.14	52.11	52.71
TiO2	0.10	0.08	0.13	0.10	0.06	0.12	0.11	0.08	0.13	0.09	0.16	0.16	0.09	0.24	0.18	0.07	0.07	0.19	0.04	0.17	0.07
Al2O3	0.55	0.51	0.60	0.66	0.39	0.63	0.58	0.61	0.66	0.65	0.71	0.62	0.52	1.20	1.18	0.58	0.64	1.07	0.59	1.11	0.60
Cr2O3	0.02	0.00	0.01	0.02	0.01	0.03	0.03	0.04	0.00	0.04	0.00	0.08	0.04	0.04	0.00	0.00	0.02	0.04	0.07	0.04	0.00
Fe2O3(c)	0.21	1.00	0.28	0.58	0.10	1.07	1.36	0.78	0.79	1.50	1.41	0.53	0.40	0.00	0.00	0.83	0.43	0.00	0.04	0.00	0.00
FeO(c)	31.62	31.55	31.49	31.11	31.84	30.99	31.05	31.80	31.84	31.06	30.89	30.50	31.53	13.49	12.91	11.77	12.26	12.25	12.70	12.66	11.86
MnO	0.96	0.94	0.82	0.81	0.91	0.87	0.90	0.98	0.93	0.90	0.75	0.83	0.94	0.34	0.31	0.48	0.37	0.30	0.43	0.37	0.36
MgO	15.17	15.03	15.33	15.47	15.28	15.38	15.25	14.92	14.81	15.13	15.14	15.68	15.31	11.61	11.49	11.73	11.67	11.66	11.41	11.63	11.94
CaO	0.76	0.65	0.76	0.76	0.62	0.68	0.64	0.57	0.69	0.69	0.97	1.04	0.60	21.18	21.96	22.63	22.50	22.15	22.56	21.90	22.46
Sum Ox%	100	100	100	100	100	100	100	100	100	100	100	100	100	100	100	100	100	100	100	100	100
Si	1.981	1.971	1.978	1.973	1.987	1.966	1.963	1.971	1.969	1.960	1.958	1.972	1.979	1.972	1.973	1.973	1.977	1.981	1.984	1.976	1.993
Ti	0.003	0.002	0.004	0.003	0.002	0.003	0.003	0.002	0.004	0.003	0.005	0.005	0.003	0.007	0.005	0.002	0.002	0.006	0.001	0.005	0.002
Al/Al IV	0.019	0.024	0.022	0.027	0.013	0.029	0.027	0.028	0.031	0.030	0.033	0.028	0.021	0.028	0.027	0.026	0.023	0.019	0.016	0.024	0.007
Al VI	0.006	0.000	0.005	0.003	0.005	0.000	0.000	0.000	0.000	0.000	0.000	0.000	0.002	0.025	0.026	0.000	0.006	0.029	0.010	0.026	0.020
Cr	0.001	0.000	0.000	0.001	0.000	0.001	0.001	0.001	0.000	0.001	0.000	0.003	0.001	0.001	0.000	0.000	0.000	0.001	0.002	0.001	0.000
Fe3+	0.006	0.030	0.008	0.017	0.003	0.032	0.040	0.023	0.023	0.044	0.042	0.015	0.012	0.000	0.000	0.024	0.012	0.000	0.001	0.000	0.000
Fe2+	1.035	1.036	1.030	1.017	1.042	1.014	1.018	1.044	1.046	1.019	1.013	0.995	1.032	0.429	0.410	0.374	0.390	0.388	0.404	0.401	0.375
Mn2+	0.032	0.031	0.027	0.027	0.030	0.029	0.030	0.033	0.031	0.030	0.025	0.027	0.031	0.011	0.010	0.016	0.012	0.009	0.014	0.012	0.012
Mg	0.885	0.879	0.894	0.901	0.891	0.897	0.891	0.873	0.867	0.884	0.885	0.911	0.893	0.658	0.651	0.664	0.661	0.658	0.647	0.657	0.673
Ca	0.032	0.027	0.032	0.032	0.026	0.029	0.027	0.024	0.029	0.029	0.040	0.043	0.025	0.862	0.893	0.921	0.916	0.898	0.920	0.890	0.910
Sum Cat#	4.000	4.000	4.000	4.000	4.000	4.000	4.000	4.000	4.000	4.000	4.000	4.000	4.000	3.994	3.995	4.000	4.000	3.989	4.000	3.993	3.991
Wo(Ca)	1.65	1.40	1.63	1.63	1.32	1.47	1.40	1.24	1.50	1.50	2.09	2.23	1.29	44.24	45.72	47.02	46.58	46.20	46.66	45.67	46.49
En(Mg)	45.32	45.26	45.71	46.22	45.50	46.25	46.02	44.97	44.65	45.77	45.66	46.75	45.81	33.76	33.30	33.90	33.61	33.84	32.84	33.73	34.36
Fs(Fe2+)	53.03	53.34	52.66	52.14	53.19	52.28	52.58	53.79	53.86	52.73	52.26	51.02	52.90	22.00	20.98	19.08	19.81	19.96	20.50	20.60	19.15
XMg	0.46	0.46	0.47	0.47	0.46	0.47	0.47	0.46	0.45	0.47	0.47	0.48	0.46	0.61	0.61	0.64	0.63	0.63	0.62	0.62	0.64

Pyroxene Analyses by sample (recalculated to 100%), cations based on 6 (O) Oxygens.

Ultrapotassic 408 (Con't)					Ultrapotassic 398a											
Label	Cpx3 C	Cpx3 C	Cpx3 R	Label	Cpx8 C	Cpx9 C	Cpx2 R	Cpx2 C	Cpx3 C	Cpx3 R	Cpx4 R	Cpx5 R	Cpx6 C	Cpx6 R	Cpx7 C	Cpx7 R
SiO2	51.57	51.58	51.83	SiO2	52.22	53.14	52.60	52.65	52.43	52.16	52.19	52.45	52.86	52.87	52.59	52.44
TiO2	0.27	0.31	0.26	TiO2	0.11	0.07	0.10	0.08	0.06	0.11	0.05	0.11	0.11	0.11	0.09	0.16
Al2O3	1.37	1.51	1.16	Al2O3	1.31	0.77	1.08	0.61	1.06	1.10	0.82	1.11	1.09	0.87	0.87	0.99
Cr2O3	0.07	0.00	0.02	Cr2O3	0.06	0.12	0.20	0.07	0.04	0.05	0.06	0.07	0.02	0.00	0.10	0.12
Fe2O3(c)	0.00	0.00	0.00	Fe2O3(c)	0.40	0.00	0.00	0.67	0.38	0.86	1.49	0.46	0.00	0.00	0.23	0.28
FeO(c)	14.25	13.31	13.19	FeO(c)	9.68	9.84	9.90	9.02	9.97	9.64	8.57	8.91	9.79	9.61	9.74	9.41
MnO	0.29	0.41	0.30	MnO	0.49	0.42	0.49	0.40	0.44	0.50	0.51	0.37	0.30	0.55	0.45	0.43
MgO	11.67	11.60	11.58	MgO	13.19	13.51	13.48	13.76	13.41	13.47	13.66	13.50	13.51	13.39	13.47	13.33
CaO	20.50	21.27	21.65	CaO	22.53	22.12	22.14	22.71	22.20	22.10	22.66	23.01	22.33	22.59	22.45	22.82
Sum Ox%	100	100	100	Sum Ox%	100	100	100	100	100	100	100	100	100	100	100	100
Si	1.964	1.960	1.970	Si	1.961	1.989	1.972	1.973	1.969	1.960	1.959	1.965	1.978	1.981	1.974	1.967
Ti	0.008	0.009	0.007	Ti	0.003	0.002	0.003	0.002	0.002	0.003	0.001	0.003	0.003	0.003	0.003	0.005
Al/Al IV	0.036	0.040	0.030	Al/Al IV	0.039	0.011	0.028	0.027	0.031	0.040	0.036	0.035	0.022	0.019	0.026	0.033
Al VI	0.025	0.028	0.022	Al VI	0.019	0.023	0.020	0.001	0.016	0.008	0.000	0.014	0.026	0.019	0.012	0.012
Cr	0.002	0.000	0.000	Cr	0.002	0.004	0.006	0.002	0.001	0.002	0.002	0.002	0.000	0.000	0.003	0.004
Fe3+	0.000	0.000	0.000	Fe3+	0.011	0.000	0.000	0.019	0.011	0.024	0.042	0.013	0.000	0.000	0.006	0.008
Fe2+	0.454	0.423	0.419	Fe2+	0.304	0.308	0.311	0.283	0.313	0.303	0.269	0.279	0.306	0.301	0.306	0.295
Mn2+	0.010	0.013	0.010	Mn2+	0.016	0.013	0.016	0.013	0.014	0.016	0.016	0.012	0.010	0.017	0.014	0.014
Mg	0.662	0.657	0.656	Mg	0.739	0.754	0.754	0.768	0.751	0.754	0.764	0.754	0.754	0.748	0.753	0.746
Ca	0.836	0.866	0.882	Ca	0.906	0.887	0.890	0.912	0.893	0.890	0.911	0.923	0.896	0.907	0.903	0.917
Sum Cat#	3.997	3.997	3.997	Sum Cat#	4.000	3.990	3.998	4.000	4.000	4.000	4.000	4.000	3.995	3.996	4.000	4.000
Wo(Ca)	42.85	44.49	45.05	Wo(Ca)	46.50	45.50	45.54	46.46	45.64	45.71	46.87	47.21	45.79	46.38	46.01	46.85
En(Mg)	33.92	33.76	33.53	En(Mg)	37.90	38.69	38.57	39.14	38.37	38.73	39.29	38.54	38.55	38.22	38.40	38.08
Fs(Fe2+)	23.24	21.75	21.43	Fs(Fe2+)	15.60	15.81	15.90	14.41	16.00	15.57	13.85	14.25	15.66	15.40	15.58	15.08
XMg	0.59	0.61	0.61	XMg	0.71	0.71	0.71	0.73	0.71	0.71	0.74	0.73	0.71	0.71	0.71	0.72

Garnet Analyses by sample (recalculated to 100%), cations based on 12 (O) Oxygens.

Terrane/ Sample	CD 457														
Label	Grt1	Grt1	Grt1	Grt1	Grt2	Grt2	Grt3	Grt3	Grt7	Grt4	Grt4	Grt5	Grt5	Grt6	Grt6
	R1	C1	C2	R2	R	C	C	R	C	R	C	R	C	C	R
SiO2	37.34	37.70	37.89	37.62	37.53	37.77	37.73	37.75	37.57	37.73	37.54	37.70	37.69	37.90	37.76
TiO2	0.06	0.09	0.05	0.04	0.05	0.02	0.09	0.10	0.08	0.05	0.07	0.06	0.03	0.04	0.04
Al2O3	21.91	21.79	21.48	21.60	21.54	21.22	21.53	21.74	21.38	21.59	21.39	21.51	21.13	21.54	21.47
Cr2O3	0.01	0.00	0.00	0.05	0.05	0.06	0.07	0.04	0.06	0.01	0.00	0.02	0.01	0.05	0.00
Fe2O3(c)	0.16	0.00	0.00	0.00	0.09	0.00	0.00	0.00	0.02	0.00	0.40	0.00	0.22	0.00	0.00
FeO	29.53	29.19	29.55	29.80	29.80	29.95	29.41	29.52	30.06	29.54	29.39	30.00	30.09	29.53	29.90
MnO	1.83	1.66	1.68	1.74	1.87	1.74	1.73	1.68	1.77	1.68	1.82	1.79	1.59	1.62	1.73
MgO	3.19	3.52	3.40	3.12	3.15	3.15	3.42	3.13	3.04	3.25	3.34	2.99	3.13	3.30	3.03
CaO	5.97	6.05	5.94	6.04	5.93	6.08	6.03	6.05	6.03	6.13	8.05	5.91	6.10	6.02	6.08
Sum Ox%	100	100	100	100	100	100	100	100	100	100	100	100	100	100	100
Si	2.965	2.984	3.003	2.988	2.984	3.004	2.991	2.992	2.990	2.993	2.983	2.997	3.000	3.003	3.001
Ti	0.004	0.005	0.003	0.002	0.003	0.001	0.006	0.006	0.005	0.003	0.004	0.004	0.002	0.003	0.002
Al/Al IV	0.035	0.016	0.000	0.012	0.016	0.000	0.009	0.008	0.010	0.007	0.017	0.003	0.000	0.000	0.000
Al VI	2.017	2.017	2.007	2.011	2.002	1.990	2.004	2.024	1.995	2.012	1.986	2.012	1.982	2.011	2.011
Cr	0.001	0.000	0.000	0.003	0.003	0.004	0.004	0.002	0.004	0.001	0.000	0.001	0.001	0.003	0.000
Fe3+	0.010	0.000	0.000	0.000	0.005	0.000	0.000	0.000	0.001	0.000	0.024	0.000	0.013	0.000	0.000
Fe2+	1.961	1.932	1.959	1.980	1.982	1.992	1.950	1.957	2.000	1.960	1.953	1.995	2.003	1.957	1.987
Mn2+	0.123	0.111	0.113	0.117	0.126	0.117	0.116	0.113	0.119	0.113	0.123	0.121	0.107	0.108	0.116
Mg	0.377	0.415	0.401	0.369	0.374	0.374	0.403	0.370	0.361	0.385	0.396	0.354	0.371	0.391	0.358
Ca	0.508	0.514	0.504	0.515	0.505	0.518	0.512	0.514	0.514	0.521	0.515	0.503	0.520	0.511	0.517
Sum Cat#	8.000	7.994	7.990	7.997	8.000	7.999	7.995	7.985	8.000	7.994	8.000	7.991	8.000	7.987	7.992
Pyrope	12.71	13.96	13.47	12.40	12.51	12.45	13.53	12.51	12.04	12.93	13.24	11.90	12.37	13.17	12.02
Almandin	66.05	65.02	65.79	66.43	66.35	66.38	65.42	66.25	66.80	65.79	65.40	67.10	66.72	65.95	66.72
Spessartine	4.15	3.74	3.80	3.91	4.22	3.91	3.89	3.84	3.99	3.79	4.11	4.08	3.57	3.65	3.89
Andradite	0.48	0.00	0.00	0.00	0.26	0.00	0.00	0.00	0.07	0.00	1.19	0.00	0.64	0.00	0.00
Uvarovite	0.05	0.00	0.00	0.16	0.16	0.19	0.21	0.11	0.19	0.05	0.00	0.07	0.04	0.16	0.00
Grossulaire	16.57	17.28	16.94	17.10	16.50	17.08	16.96	17.28	16.92	17.45	16.07	16.86	16.66	17.07	17.37
XMg	0.16	0.18	0.17	0.16	0.16	0.16	0.17	0.16	0.15	0.16	0.17	0.15	0.16	0.17	0.15

Apatite Analyses by sample (recalculated to 100%), cations based on 25 (O) Oxygens.

Terrane/ Sample	Ultrapotassic 338z														
Label	Apt1 C	Apt1 R	Apt2 R1	Apt2 C1	Apt2 R2	Apt3 R1	Apt3 C	Apt3 R2	Apt4 R1	Apt4 C1	Apt4 C2	Apt4 R2	Apt5 R1	Apt5 C1	Apt5 C2
SiO2	0.12	0.11	0.13	0.03	0.05	0.08	0.36	0.09	0.09	0.09	0.06	0.03	0.06	0.10	0.07
CaO	54.25	53.22	53.04	53.65	53.61	53.56	53.40	53.47	53.71	53.56	53.61	53.07	53.39	52.89	53.14
P2O5	41.21	42.08	42.33	41.97	41.93	41.93	41.72	42.08	41.91	41.81	41.76	42.30	41.91	42.86	42.22
SrO	0.71	0.62	0.68	0.67	0.64	0.70	0.68	0.60	0.72	0.74	0.71	0.70	0.69	0.64	0.71
F	5.39	5.70	5.40	5.17	5.46	5.51	5.76	5.52	5.35	5.68	5.81	5.82	5.88	5.25	5.70
Cl	0.77	0.88	0.89	0.68	0.79	0.69	0.65	0.71	0.61	0.66	0.65	0.68	0.71	0.60	0.73
H2O(c)	0.00	0.00	0.00	0.00	0.00	0.00	0.00	0.00	0.00	0.00	0.00	0.00	0.00	0.00	0.00
O=F	2.26	2.40	2.27	2.18	2.30	2.32	2.42	2.33	2.26	2.39	2.45	2.45	2.47	2.21	2.40
O=Cl	0.17	0.20	0.20	0.20	0.18	0.15	0.14	0.16	0.14	0.15	0.15	0.15	0.16	0.14	0.17
Sum Ox%	100.00	100.00	100.00	100.00	100.00	100.00	100.00	100.00	100.00	100.00	100.00	100.00	100.00	100.00	100.00
Si	0.020	0.018	0.023	0.005	0.008	0.012	0.063	0.017	0.014	0.015	0.010	0.005	0.009	0.017	0.011
Ca	9.953	9.720	9.660	9.790	9.792	9.780	9.755	9.749	9.797	9.795	9.811	9.678	9.768	9.575	9.693
P	5.974	6.073	6.091	6.053	6.052	6.051	6.021	6.063	6.041	6.040	6.040	6.097	6.058	6.131	6.086
Sr	0.071	0.061	0.067	0.066	0.064	0.069	0.067	0.060	0.071	0.073	0.070	0.069	0.068	0.063	0.070
F	2.915	3.073	2.904	2.781	2.945	2.969	3.103	2.969	2.882	3.068	3.137	3.133	3.176	2.802	3.070
Cl	0.224	0.253	0.258	0.255	0.228	0.200	0.189	0.203	0.178	0.193	0.191	0.195	0.206	0.173	0.211
OH	0.000	0.000	0.000	0.000	0.000	0.000	0.000	0.000	0.000	0.000	0.000	0.000	0.000	0.000	0.000
Sum Cat#	19.157	19.198	19.002	18.951	19.088	19.081	19.197	19.061	18.984	19.185	19.258	19.178	19.285	18.761	19.141

Apatite Analyses by sample (recalculated to 100%), cations based on 25 (O) Oxygens.

Ultrapotassic 338z (Con't)						Ultrapotassic 361z						
Label	Apt5	Apt6	Apt6	Apt6	Apt6	Label	Apt6	Apt1	Apt2	Apt3	Apt4	Apt5
	R2	R1	C1	C2	R2		C	C	C	C	C	C
SiO2	0.02	0.06	0.07	0.08	0.12	SiO2	0.45	0.42	0.26	0.35	0.23	0.37
CaO	54.05	53.48	53.82	52.87	53.50	CaO	55.43	56.20	56.08	55.42	55.76	55.10
P2O5	41.51	41.68	41.64	42.10	41.63	P2O5	41.42	41.25	41.48	42.04	41.80	42.23
SrO	0.66	0.64	0.67	0.67	0.75	SrO	0.64	0.10	0.13	0.14	0.18	0.21
F	5.55	6.31	5.57	6.46	5.92	F	1.92	1.73	1.54	1.62	1.64	1.77
Cl	0.71	0.64	0.73	0.70	0.74	Cl	0.16	0.14	0.23	0.19	0.16	0.24
H2O(c)	0.00	0.00	0.00	0.00	0.00	H2O(c)	0.82	0.92	0.99	0.97	0.97	0.89
O=F	2.34	2.65	2.34	2.72	2.49	O=F	0.81	0.73	0.65	0.68	0.69	0.75
O=Cl	0.16	0.14	0.16	0.16	0.17	O=Cl	0.04	0.03	0.05	0.04	0.04	0.06
Sum Ox%	100.00	100.00	100.00	100.00	100.00	Sum Ox%	100.00	100.00	100.00	100.00	100.00	100.00
Si	0.004	0.010	0.012	0.015	0.021	Si	0.077	0.070	0.043	0.058	0.038	0.062
Ca	9.903	9.812	9.851	9.678	9.807	Ca	10.009	10.144	10.118	9.955	10.039	9.886
P	6.009	6.042	6.023	6.090	6.031	P	5.910	5.883	5.914	5.966	5.947	5.988
Sr	0.066	0.063	0.067	0.066	0.074	Sr	0.063	0.009	0.013	0.014	0.017	0.020
F	3.003	3.417	3.012	3.492	3.202	F	1.026	0.922	0.822	0.858	0.872	0.939
Cl	0.205	0.187	0.213	0.202	0.214	Cl	0.046	0.041	0.065	0.053	0.046	0.070
OH	0.000	0.000	0.000	0.000	0.000	OH	0.929	1.037	1.114	1.089	1.083	0.991
Sum Cat#	19.190	19.531	19.178	19.543	19.350	Sum Cat#	18.059	18.106	18.087	17.993	18.041	17.956

Apatite Analyses by sample (recalculated to 100%), cations based on 25 (O) Oxygens.

	Ultrapotassic 209-2						Ultrapotassic 404								
Label	Apt1 C	Ap2 C	Ap3 C	Ap4 C	Ap5 C	Label	Apt6 .	Apt5	Apt1 C	Apt1 R	Apt2 C	Apt2 R	Apt3 C	Apt4 C	Apt4 C
SiO2	0.40	0.44	0.49	0.40	0.42	SiO2	0.22	0.39	0.34	0.31	0.51	0.44	0.43	0.33	0.38
CaO	55.21	55.46	55.30	55.01	55.36	CaO	54.54	55.35	55.90	55.36	55.09	55.39	55.35	55.14	55.61
P2O5	41.58	41.35	41.46	41.78	41.34	P2O5	41.94	41.79	41.26	41.77	41.87	41.66	41.69	42.08	41.53
SrO	0.77	0.67	0.69	0.74	0.80	SrO	0.95	0.38	0.45	0.47	0.42	0.40	0.49	0.38	0.38
F	1.74	1.75	1.69	1.72	1.89	F	1.62	1.92	1.81	2.05	1.80	1.87	1.56	1.63	1.78
Cl	0.18	0.20	0.18	0.21	0.21	Cl	0.77	0.19	0.17	0.20	0.23	0.23	0.19	0.19	0.22
H2O(c)	0.91	0.90	0.93	0.92	0.83	H2O(c)	0.82	0.83	0.87	0.76	0.87	0.84	1.00	0.97	0.88
O=F	0.74	0.74	0.71	0.73	0.80	O=F	0.68	0.81	0.77	0.86	0.76	0.79	0.66	0.69	0.75
O=Cl	0.04	0.05	0.04	0.05	0.05	O=Cl	0.17	0.05	0.04	0.05	0.05	0.05	0.05	0.04	0.05
Sum Ox%	100.00	100.00	100.00	100.00	100.00	Sum Ox%	100.00	100.00	100.00	100.00	100.00	100.00	100.00	100.00	100.00
Si	0.067	0.073	0.083	0.067	0.070	Si	0.037	0.066	0.056	0.051	0.085	0.075	0.073	0.057	0.065
Ca	9.967	10.024	9.983	9.917	10.012	Ca	9.859	9.967	10.107	9.979	9.910	9.982	9.972	9.909	10.033
P	5.930	5.905	5.914	5.951	5.907	P	5.990	5.946	5.895	5.949	5.951	5.932	5.934	5.976	5.920
Sr	0.075	0.066	0.068	0.072	0.078	Sr	0.093	0.036	0.044	0.046	0.042	0.039	0.047	0.037	0.038
F	0.928	0.934	0.900	0.916	1.009	F	0.860	1.022	0.970	1.092	0.954	0.994	0.830	0.867	0.947
Cl	0.051	0.057	0.053	0.058	0.059	Cl	0.221	0.056	0.049	0.056	0.066	0.066	0.055	0.054	0.062
OH	1.021	1.009	1.047	1.026	0.932	OH	0.919	0.923	0.982	0.851	0.980	0.939	1.115	1.079	0.991
Sum Cat#	18.038	18.069	18.047	18.007	18.069	Sum Cat#	17.979	18.015	18.102	18.025	17.988	18.027	18.026	17.979	18.055

Apatite Analyses by sample (recalculated to 100%), cations based on 25 (O) Oxygens.

	Ultrapotassic 408						Ultrapotassic 398a			
Label	Apt1 C	Apt2 C	Apt3 C	Apt4 C	Apt5 C	Label	Apt1 C	Apt2 C	Apt3 C	Apt4 C
SiO2	0.39	0.36	0.22	0.38	0.36	SiO2	0.21	0.32	0.34	0.23
CaO	55.40	55.50	55.53	56.05	55.53	CaO	55.52	55.54	55.19	55.57
P2O5	42.14	42.05	42.12	41.45	42.02	P2O5	41.77	41.61	42.01	41.81
SrO	0.04	0.08	0.10	0.10	0.06	SrO	0.47	0.50	0.44	0.37
F	1.67	1.75	1.64	1.77	1.76	F	1.88	1.85	1.67	1.75
Cl	0.13	0.09	0.13	0.13	0.12	Cl	0.12	0.13	0.11	0.10
H2O(c)	0.97	0.94	0.97	0.91	0.92	H2O(c)	0.86	0.87	0.96	0.93
O=F	0.71	0.73	0.70	0.75	0.74	O=F	0.80	0.78	0.71	0.74
O=Cl	0.03	0.02	0.03	0.03	0.03	O=Cl	0.03	0.03	0.03	0.02
Sum Ox%	100.00	100.00	100.00	100.00	100.00	Sum Ox%	100.00	100.00	100.00	100.00
Si	0.066	0.060	0.037	0.063	0.060	Si	0.035	0.053	0.058	0.039
Ca	9.936	9.963	9.974	10.104	9.972	Ca	10.010	10.018	9.922	10.009
P	5.971	5.964	5.977	5.905	5.961	P	5.950	5.931	5.968	5.951
Sr	0.004	0.007	0.009	0.009	0.005	Sr	0.045	0.048	0.043	0.036
F	0.884	0.927	0.872	0.944	0.933	F	1.003	0.985	0.890	0.932
Cl	0.039	0.024	0.039	0.039	0.033	Cl	0.034	0.039	0.032	0.026
OH	1.077	1.049	1.090	1.016	1.034	OH	0.963	0.976	1.078	1.042
Sum Cat#	17.977	17.994	17.997	18.080	17.999	Sum Cat#	18.040	18.050	17.991	18.035

Apatite Analyses by sample (recalculated to 100%), cations based on 25 (O) Oxygens.

Ultrapotassic 403								
Label	Apt1	Apt2	Apt3	Apt1	Apt2	Apt4	Apt5	Apt6
	C	C	C	C	C	C	C	C
SiO2	-	-	-	-	-	-	-	-
CaO	56.14	55.75	54.07	54.13	54.10	54.18	53.46	53.38
P2O5	42.02	42.42	40.31	40.08	40.34	40.08	40.68	40.50
SrO	0.00	0.00	3.82	3.98	3.76	3.96	4.06	4.33
F	0.00	0.00	0.00	0.00	0.00	0.00	0.00	0.00
Cl	0.10	0.08	0.11	0.11	0.12	0.08	0.12	0.11
H2O(c)	1.76	1.77	1.72	1.72	1.72	1.72	1.72	1.72
O=F	0.00	0.00	0.00	0.00	0.00	0.00	0.00	0.00
O=Cl	0.02	0.02	0.03	0.02	0.03	0.02	0.03	0.02
Sum Ox%	100.00	100.00	100.00	100.00	100.00	100.00	100.00	100.00
Si	-	-	-	-	-	-	-	-
Ca	10.087	9.987	9.958	9.991	9.959	9.997	9.827	9.832
P	5.965	6.005	5.864	5.845	5.866	5.843	5.908	5.894
Sr	0.000	0.000	0.381	0.398	0.375	0.396	0.404	0.432
F	0.000	0.000	0.000	0.000	0.000	0.000	0.000	0.000
Cl	0.029	0.023	0.031	0.031	0.035	0.024	0.032	0.030
OH	1.971	1.976	1.968	1.969	1.964	1.976	1.967	1.970
Sum Cat#	18.052	17.992	18.203	18.233	18.200	18.236	18.138	18.159

Opaque Analyses by sample (recalculated 100%), cations based on 4 (O) Oxygens.

	CD 209-1							CD 457					
Label	Ilm1 C	Ilm2 C	Ilm3 C	Ilm4 C	Ilm5 C	Ilm6 C	Label	Ilm1 C	Ilm2 C	Ilm3 C	Ilm4 C	Ilm5 C
SiO2	0.02	0.01	0.01	0.01	0.01	0.01	SiO2	0.00	0.00	0.01	0.01	0.01
TiO2	52.47	52.56	51.71	52.44	51.98	51.37	TiO2	53.20	52.87	52.84	52.58	52.40
Al2O3	0.10	0.05	0.07	0.07	0.09	0.07	Al2O3	0.04	0.03	0.03	0.02	0.04
Cr2O3	0.14	0.10	0.10	0.09	0.16	0.11	Cr2O3	0.00	0.04	0.03	0.03	0.00
Fe2O3(c)	0.17	0.85	2.47	0.80	1.97	2.38	Fe2O3(c)	0.00	0.00	0.00	0.39	0.54
FeO(c)	46.08	44.75	43.91	45.34	44.05	45.39	FeO(c)	45.73	46.28	46.40	46.02	46.38
MnO	0.91	0.56	0.58	0.53	0.46	0.47	MnO	0.56	0.53	0.45	0.54	0.48
MgO	0.10	1.08	1.13	0.72	1.25	0.19	MgO	0.47	0.25	0.18	0.40	0.14
NiO	0.01	0.05	0.00	0.00	0.01	0.00	NiO	0.00	0.00	0.06	0.02	0.01
Sum Ox%	100.00	100.00	100.00	100.00	100.00	100.00	Sum Ox%	100.00	100.00	100.00	100.00	100.00
Si	0.000	0.000	0.000	0.000	0.000	0.000	Si	0.000	0.000	0.000	0.000	0.000
Ti	0.995	0.990	0.974	0.990	0.978	0.975	Ti	1.004	1.001	1.001	0.996	0.994
Al/Al IV	0.000	0.000	0.000	0.000	0.000	0.000	Al/Al IV	0.000	0.000	0.000	0.000	0.000
Al VI	0.003	0.002	0.002	0.002	0.003	0.002	Al VI	0.001	0.001	0.001	0.001	0.001
Cr	0.003	0.002	0.002	0.002	0.003	0.002	Cr	0.000	0.001	0.001	0.001	0.000
Fe3+	0.003	0.016	0.047	0.015	0.037	0.045	Fe3+	0.000	0.000	0.000	0.007	0.010
Fe2+	0.972	0.937	0.920	0.952	0.922	0.958	Fe2+	0.960	0.974	0.978	0.969	0.979
Mn2+	0.019	0.012	0.012	0.011	0.010	0.010	Mn2+	0.012	0.011	0.010	0.012	0.010
Mg	0.004	0.040	0.042	0.027	0.047	0.007	Mg	0.018	0.009	0.007	0.015	0.005
Ni	0.000	0.001	0.000	0.000	0.000	0.000	Ni	0.000	0.000	0.001	0.000	0.000
Sum Cat#	2.000	2.000	2.000	2.000	2.000	2.000	Sum Cat#	1.995	1.998	1.998	2.000	2.000
Ilmenite	97.47	93.98	92.21	95.41	92.47	96.03	Ilmenite	97.02	97.94	98.37	96.98	97.94
Geikielite	0.41	4.04	4.24	2.73	4.68	0.71	Geikielite	1.78	0.92	0.67	1.49	0.51
Pyrophanite	1.95	1.17	1.23	1.11	0.99	1.00	Pyrophanite	1.20	1.14	0.96	1.17	1.04
Hematite	0.16	0.81	2.33	0.75	1.87	2.26	Hematite	0.00	0.00	0.00	0.36	0.51
XMg	0.00	0.04	0.04	0.03	0.05	0.01	XMg	0.02	0.01	0.01	0.02	0.01

Opaque Analyses by sample (recalculated 100%), cations based on 4 (O) Oxygens.

	CD 430								Ultrapotassic 209-2							
Label	Ilm1	Ilm2	Ilm2	Ilm3	Ilm3	Ilm5	Ilm1	Label	Ilm7	Ilm1	Ilm2	Ilm3	Ilm4	Ilm5	Ilm6
	C	C	C	C	C	C	C		C	C	C	C	C	C	C
SiO2	0.00	0.00	0.00	0.00	0.00	0.00	0.00	SiO2	0.00	0.00	0.00	0.00	0.01	0.00	0.00
TiO2	36.41	41.29	49.35	46.79	52.76	52.82	14.66	TiO2	52.86	53.14	53.55	53.07	53.04	53.24	53.16
Al2O3	0.07	0.11	0.04	0.04	0.02	0.04	0.15	Al2O3	0.03	0.05	0.05	0.01	0.03	0.04	0.02
Cr2O3	0.12	0.11	0.11	0.09	0.05	0.10	0.29	Cr2O3	0.02	0.00	0.00	0.01	0.03	0.06	0.00
Fe2O3(c)	31.03	21.90	6.85	11.08	0.00	0.00	71.81	Fe2O3(c)	0.00	0.00	0.00	0.00	0.00	0.00	0.00
FeO(c)	31.66	35.53	42.49	41.73	46.52	46.47	12.89	FeO(c)	46.11	45.57	45.16	45.43	45.88	45.77	45.53
MnO	0.22	0.32	0.27	0.18	0.44	0.42	0.03	MnO	0.85	1.06	1.07	1.14	0.85	0.73	0.93
MgO	0.46	0.68	0.90	0.10	0.16	0.15	0.13	MgO	0.11	0.12	0.17	0.30	0.16	0.14	0.28
NiO	0.05	0.07	0.00	0.02	0.05	0.00	0.03	NiO	0.02	0.05	0.00	0.04	0.00	0.00	0.06
Sum Ox%	100.00	100.00	100.00	100.00	100.00	100.00	100.00	Sum Ox%	100.00	100.00	100.00	100.00	100.00	100.00	100.00
Si	0.000	0.000	0.000	0.000	0.000	0.000	0.000	Si	0.000	0.000	0.000	0.000	0.000	0.000	0.000
Ti	0.699	0.788	0.933	0.893	1.000	1.001	0.288	Ti	1.002	1.005	1.010	1.004	1.004	1.007	1.005
Al/Al IV	0.000	0.000	0.000	0.000	0.000	0.000	0.000	Al/Al IV	0.000	0.000	0.000	0.000	0.000	0.000	0.000
Al VI	0.002	0.003	0.001	0.001	0.001	0.001	0.005	Al VI	0.001	0.002	0.001	0.000	0.001	0.001	0.001
Cr	0.002	0.002	0.002	0.002	0.001	0.002	0.006	Cr	0.000	0.000	0.000	0.000	0.001	0.001	0.000
Fe3+	0.596	0.418	0.130	0.211	0.000	0.000	1.413	Fe3+	0.000	0.000	0.000	0.000	0.000	0.000	0.000
Fe2+	0.676	0.754	0.894	0.885	0.981	0.979	0.282	Fe2+	0.972	0.959	0.948	0.955	0.966	0.962	0.957
Mn2+	0.005	0.007	0.006	0.004	0.009	0.009	0.001	Mn2+	0.018	0.023	0.023	0.024	0.018	0.016	0.020
Mg	0.018	0.026	0.034	0.004	0.006	0.005	0.005	Mg	0.004	0.005	0.006	0.011	0.006	0.005	0.011
Ni	0.001	0.001	0.000	0.000	0.001	0.000	0.001	Ni	0.000	0.001	0.000	0.001	0.000	0.000	0.001
Sum Cat#	2.000	2.000	2.000	2.000	1.999	1.998	2.000	Sum Cat#	1.998	1.994	1.989	1.996	1.995	1.992	1.995
Ilmenite	67.85	75.74	89.55	88.68	98.44	98.54	28.37	Ilmenite	97.75	97.25	97.01	96.41	97.57	97.89	96.92
Geikielite	1.77	2.58	3.39	0.36	0.61	0.55	0.49	Geikielite	0.44	0.47	0.65	1.15	0.60	0.52	1.08
Pyrophanite	0.46	0.68	0.58	0.38	0.95	0.91	0.07	Pyrophanite	1.82	2.28	2.34	2.44	1.83	1.59	2.00
Hematite	29.92	21.00	6.49	10.59	0.00	0.00	71.07	Hematite	0.00	0.00	0.00	0.00	0.00	0.00	0.00
XMg	0.03	0.03	0.04	0.00	0.01	0.01	0.02	XMg	0.00	0.01	0.01	0.01	0.01	0.01	0.01

Opaque Analyses by sample (recalculated 100%), cations based on 4 (O) Oxygens.

Ultrapotassic 404								Ultrapotassic 408							
Label	Ilm1 C	Ilm2 C	Ilm3 C	Ilm4 C	Ilm5 C	Ilm6 C	4Ilm7 C	Label	Ilm1 C	Ilm2 C	Ilm3 C	Ilm4 C	Ilm5 C	Ilm6 C	Ilm7 C
SiO2	0.00	0.00	0.00	0.01	0.00	0.00	0.01	SiO2	0.00	0.00	0.00	0.01	0.01	0.00	0.00
TiO2	53.19	52.72	52.85	53.60	53.17	52.91	53.17	TiO2	53.30	53.87	53.23	52.39	52.71	52.63	52.85
Al2O3	0.03	0.03	0.05	0.02	0.03	0.01	0.03	Al2O3	0.05	0.02	0.00	0.03	0.03	0.03	0.03
Cr2O3	0.00	0.04	0.12	0.00	0.00	0.00	0.00	Cr2O3	0.01	0.00	0.05	0.00	0.00	0.00	0.00
Fe2O3(c)	0.00	0.07	0.00	0.00	0.00	0.00	0.00	Fe2O3(c)	0.00	0.00	0.00	0.68	0.08	0.25	0.00
FeO(c)	45.65	46.00	45.90	45.00	45.27	45.33	45.35	FeO(c)	45.41	44.98	45.62	45.63	46.00	45.84	46.14
MnO	0.91	0.81	0.76	1.01	1.11	1.26	1.11	MnO	0.88	0.90	0.94	0.97	0.91	0.94	0.82
MgO	0.18	0.33	0.28	0.34	0.41	0.46	0.33	MgO	0.32	0.16	0.13	0.29	0.27	0.29	0.15
NiO	0.04	0.01	0.04	0.02	0.00	0.03	0.00	NiO	0.02	0.08	0.04	0.00	0.00	0.03	0.01
Sum Ox%	100.00	100.00	100.00	100.00	100.00	100.00	100.00	Sum Ox%	100.00	100.00	100.00	100.00	100.00	100.00	100.00
Si	0.000	0.000	0.000	0.000	0.000	0.000	0.000	Si	0.000	0.000	0.000	0.000	0.000	0.000	0.000
Ti	1.006	0.999	1.000	1.010	1.004	1.001	1.005	Ti	1.006	1.015	1.007	0.993	0.999	0.997	1.001
Al/Al IV	0.000	0.000	0.000	0.000	0.000	0.000	0.000	Al/Al IV	0.000	0.000	0.000	0.000	0.000	0.000	0.000
Al VI	0.001	0.001	0.001	0.001	0.001	0.000	0.001	Al VI	0.001	0.001	0.000	0.001	0.001	0.001	0.001
Cr	0.000	0.001	0.002	0.000	0.000	0.000	0.000	Cr	0.000	0.000	0.001	0.000	0.000	0.000	0.000
Fe3+	0.000	0.001	0.000	0.000	0.000	0.000	0.000	Fe3+	0.000	0.000	0.000	0.013	0.001	0.005	0.000
Fe2+	0.960	0.969	0.966	0.943	0.951	0.953	0.953	Fe2+	0.954	0.942	0.960	0.962	0.969	0.966	0.972
Mn2+	0.019	0.017	0.016	0.021	0.024	0.027	0.024	Mn2+	0.019	0.019	0.020	0.021	0.019	0.020	0.018
Mg	0.007	0.012	0.011	0.013	0.015	0.017	0.012	Mg	0.012	0.006	0.005	0.011	0.010	0.011	0.006
Ni	0.001	0.000	0.001	0.000	0.000	0.001	0.000	Ni	0.000	0.002	0.001	0.000	0.000	0.001	0.000
Sum Cat#	1.994	2.000	1.998	1.989	1.995	1.999	1.995	Sum Cat#	1.993	1.985	1.993	2.000	2.000	2.000	1.998
Ilmenite	97.36	97.01	97.29	96.54	96.05	95.59	96.36	Ilmenite	96.89	97.41	97.49	96.20	96.97	96.69	97.68
Geikielite	0.69	1.21	1.06	1.28	1.57	1.72	1.26	Geikielite	1.21	0.63	0.48	1.08	1.01	1.08	0.55
Pyrophanite	1.96	1.72	1.65	2.18	2.39	2.70	2.39	Pyrophanite	1.91	1.96	2.02	2.08	1.95	1.99	1.77
Hematite	0.00	0.06	0.00	0.00	0.00	0.00	0.00	Hematite	0.00	0.00	0.00	0.64	0.07	0.24	0.00
XMg	0.01	0.01	0.01	0.01	0.02	0.02	0.01	XMg	0.01	0.01	0.01	0.01	0.01	0.01	0.01